

11-8-2018

Secure Large Scale Penetration of Electric Vehicles in the Power Grid

Abla Hariri

Florida International University, ahari001@fiu.edu

Follow this and additional works at: <https://digitalcommons.fiu.edu/etd>



Part of the [Computer and Systems Architecture Commons](#), and the [Electrical and Electronics Commons](#)

Recommended Citation

Hariri, Abla, "Secure Large Scale Penetration of Electric Vehicles in the Power Grid" (2018). *FIU Electronic Theses and Dissertations*. 3848.

<https://digitalcommons.fiu.edu/etd/3848>

This work is brought to you for free and open access by the University Graduate School at FIU Digital Commons. It has been accepted for inclusion in FIU Electronic Theses and Dissertations by an authorized administrator of FIU Digital Commons. For more information, please contact dcc@fiu.edu.

FLORIDA INTERNATIONAL UNIVERSITY

Miami, Florida

SECURE LARGE SCALE PENETRATION OF ELECTRIC VEHICLES IN THE
POWER GRID

A dissertation submitted in partial fulfillment of

the requirements for the degree of

DOCTOR OF PHILOSOPHY

in

ELECTRICAL ENGINEERING

by

Abla Hariri

2018

To: Dean John L. Volakis
College of Engineering and Computing

This dissertation, written by Abla Hariri, and entitled Secure Large Scale Penetration of Electric Vehicles in the Power Grid, having been approved in respect to style and intellectual content, is referred to you for judgment.

We have read this dissertation and recommend that it be approved.

Kemal Akkaya

Berrin Tansel

Sakhrat Khizroev

Osama Mohammed, Major Professor

Date of Defense: November 8, 2018

The dissertation of Abla Hariri is approved.

Dean John L. Volakis
College of Engineering and Computing

Andrés G. Gil
Vice President for Research and Economic Development
and Dean of the University Graduate School

Florida International University, 2018

© Copyright 2018 by Abla Hariri

All rights reserved.

DEDICATION

I dedicate this dissertation to my own support system:

My loving and forever supporting parents, Omar and Zahra,

My beloved and inspiring siblings, Mariam and Mohammad,

and My late grandfather, Mohammad Burji, for everything he was to me.

ACKNOWLEDGMENTS

This dissertation would not have been possible without the help, support, and dedication of my major advisor, Prof. Osama Mohammed. I wish to express my gratitude to Professor Mohammed, for his guidance and encouragement during my graduate study. His continuous guidance and suggestions have always been very useful for me, and I am grateful for working at the FIU Energy Systems Research Laboratory (ESRL). At the ESRL, I found all the equipment and facilities I needed to undergo my research and experimentally verify my results. Working in this laboratory and under Prof. Mohammed's supervision has always pushed me to do and be at a higher professional level. Professor Mohammed has been an endless source of technical knowledge and directions with new ideas that has let me grow professionally and made development of this research successful.

I would also like to thank my dissertation committee members Professor Kemal Akkaya, Professor Sakhrat Khirzoev, and Professor Berrin Tansel for their insightful comments and constructive suggestions in the review of my research proposal and dissertation.

I would like to acknowledge the research support provided to me from the Department of Electrical and Computer Engineering at Florida International University, in addition to the doctoral dissertation year fellowship (DYF) from FIU graduate school during the last year of my study.

Thanks are also due to all the member scholars at the Energy Systems Research Laboratory, whose discussions, contributions, and assistance helped me achieve my research goals. I am also grateful to the FIU community and department staff.

ABSTRACT OF THE DISSERTATION
SECURE LARGE SCALE PENETRATION OF ELECTRIC VEHICLES IN THE
POWER GRID

by

Abla Hariri

Florida International University, 2018

Miami, Florida

Professor Osama Mohammed, Major Professor

As part of the approaches used to meet climate goals set by international environmental agreements, policies are being applied worldwide for promoting the uptake of Electric Vehicles (EV)s. The resulting increase in EV sales and the accompanying expansion in the EV charging infrastructure carry along many challenges, mostly infrastructure-related. A pressing need arises to strengthen the power grid to handle and better manage the electricity demand by this mobile and geo-distributed load. Because the levels of penetration of EVs in the power grid have recently started increasing with the increase in EV sales, the real-time management of en-route EVs, before they connect to the grid, is quite recent and not many research works can be found in the literature covering this topic comprehensively. In this dissertation, advances and novel ideas are developed and presented, seizing the opportunities lying in this mobile load and addressing various challenges that arise in the application of public charging for EVs.

A Bilateral Decision Support System (BDSS) is developed here for the management of en-route EVs. The BDSS is a middleware-based MAS that achieves a win-win situation for the EVs and the power grid. In this framework, the two are complementary

in a way that the desired benefit of one cannot be achieved without attaining that of the other. A Fuzzy Logic based on-board module is developed for supporting the decision of the EV as to which charging station to charge at. GPU computing is used in the higher-end agents to handle the big amount of data resulting in such a large scale system with mobile and geo-distributed nodes. Cyber security risks that threaten the BDSS are assessed and measures are applied to revoke possible attacks. Furthermore, the Collective Distribution of Mobile Loads (CDML), a service with ancillary potential to the power system, is developed. It comprises a system-level optimization. In this service, the EVs requesting a public charging session are collectively redistributed onto charging stations with the objective of achieving the optimal and secure operation of the power system by reducing active power losses in normal conditions and mitigating line congestions in contingency conditions. The CDML uses the BDSS as an industrially viable tool to achieve the outcomes of the optimization in real time. By participating in this service, the EV is considered as an interacting node in the system-wide communication platform, providing both enhanced self-convenience in terms of access to public chargers, and contribution to the collective effort of providing benefit to the power system under the large scale uptake of EVs.

On the EV charger level, several advantages have been reported favoring wireless charging of EVs over wired charging. Given that, new techniques are presented that facilitate the optimization of the magnetic link of wireless EV chargers while considering international EMC standards.

The original techniques and developments presented in this dissertation were experimentally verified at the Energy Systems Research Laboratory at FIU.

TABLE OF CONTENTS

CHAPTER	PAGE
Chapter 1 Introduction and Literature Survey	1
1.1 History and Types of EVs and Electric Vehicle Supply Equipment	1
1.1.1 Brief History	1
1.1.2 Types of EVs.....	2
1.1.2.1 Hybrid Electric Vehicles (HEVs)	3
1.1.2.2 Plug-in Hybrid Electric Vehicles (PHEVs)	3
1.1.2.3 Battery Electric Vehicles (BEVs)	3
1.1.3 Electric Vehicle Supply Equipment (EVSE)	3
1.1.3.1 Plug-in Charging.....	4
1.1.3.2 Wireless Charging.....	5
1.2 Anti-Electric Vehicle Arguments and Refutations	6
1.2.1 Power System and Environment Standpoint.....	7
1.2.2 Consumer Standpoint.....	10
1.2.2.1 Range Anxiety and Charging Speed	10
1.2.2.2 Availability of and Access to Public Charging Stations.....	10

1.3	Motivations for fostering the uptake of a large number of EVs	11
1.3.1	Attempts for making the experience more convenient	13
1.3.1.1	Power system operators’ standpoint	13
1.3.1.2	Consumer standpoint	13
1.4	Problem Statement	14
1.5	Research Objectives	16
1.6	Original contribution and significance.....	17
1.7	Dissertation organization	18
Chapter 2 Standards and Enabling Communication Technologies Involved in the Management of Electric Vehicles		22
2.1	Introduction.....	22
2.2	At the Premises of the Electric Vehicle Charging Station.....	23
2.2.1	Electric Vehicle – Electric Vehicle Supply Equipment.....	24
2.2.2	Electric Vehicle Supply Equipment – Energy Management Unit	25
2.2.3	Energy Management Unit – Grid Control Center.....	26
2.3	Control Center to Mobile Electric Vehicles.....	27
2.4	Inter-Control Center.....	29

2.5	Summary	30
Chapter 3 Middleware-based Communication Platform for Smart Grid Decentralized Applications		32
3.1	Introduction.....	32
3.2	Middleware for the communication in a Multi-Agent System	32
3.3	Data Sharing Structure in DDS.....	37
3.4	Application 1: DDS-based Multi-Agent System for Market Operation in a Multi-Microgrid Environment	39
3.4.1	Application description.....	39
3.4.2	System Description	40
3.5	Application 2: A Decentralized Multi-Agent System for Management of En Route Electric Vehicles	44
3.5.1	Application Description.....	45
3.5.2	System Description	46
3.6	Conclusion	48
Chapter 4 Intelligent Fuzzy Logic Based On-board Module for Guiding the Electric Vehicles to Charging Stations		49
4.1	Introduction.....	49
4.2	Motivations	49

4.3	Fuzzy Logic	51
4.4	Design of the On-board Module	51
4.5	Module's platform	58
4.6	Case Studies	58
4.7	Summary	60
Chapter 5 A Bilateral Decision Support Platform for Public Charging of Connected Electric Vehicles		62
5.1	Introduction.....	62
5.2	Need and Scope.....	67
5.3	Model and Communication Scheme	69
5.1.1	On-board Module / EV Agent.....	74
5.1.2	EVCS Agent.....	74
5.1.3	VB Agent	74
5.1.3.1	Distinction among the Price Vectors: BPV, CPV, OPV.....	77
5.1.3.2	Stage 1.....	78
5.1.3.3	Stage 2.....	80
5.1.3.4	Stage 3.....	81

5.1.3.5	Stage 4.....	81
5.1.3.6	Stage 5.....	82
5.1.4	HL Agent	82
5.2	The Bilateral Decision Support Platform- Hardware Setup Implementation	82
5.3	Use Cases and Results	83
5.3.1	Decision Support on the EV Side: Evaluation of the On-Board EV Decision Support Module	85
5.3.1.1	Case 1 (VB1).....	87
5.3.1.2	Case 2 (VB2).....	87
5.3.1.3	Case 3 (VB3).....	87
5.3.1.4	Case 4 (VB4).....	87
5.3.2	Decision Support on the Power System side: Evaluation to the VBA Price-Based Strategy	89
5.4	Conclusion	91
5.5	Public Charging Infrastructure – System of Systems	91
Chapter 6 Collective Distribution of Mobile Loads for Optimal and Secure Operation of Power Systems.....		
6.1	Introduction and Literature Review	95
6.1.1	Impacts of the large-scale penetration of EVs on the grid.....	96

6.1.2	Proposed Solutions.....	97
6.1.2.1	Solutions in the Planning Phase.....	97
6.1.2.2	Solutions in the Operation Phase.....	98
6.1.2.3	Vehicle Routing Problems of EVs.....	99
6.1.3	EVs as Enabling Technologies to Ancillary Services.....	99
6.1.4	The Proposed Method and its Ancillary Service Potential.....	101
6.2	Collective Distribution of Mobile Loads Using the Bilateral Decision Support System.....	103
6.2.1	CDML Stage 1.....	106
6.2.2	CDML Stage 2.....	108
6.2.3	CDML Stage 3.....	108
6.2.4	VBA Logic.....	109
6.2.5	Non-discriminatory Approach to fulfilling the EV requests.....	110
6.3	The Optimization.....	110
6.3.1	Particle Swarm Optimization.....	112
6.3.2	Normal Conditions.....	113
6.3.3	N-1 Contingencies.....	114

6.4	Case Studies and Results	115
6.4.1	Modified IEEE 14-bus System, Normal Conditions.....	116
6.4.2	Modified IEEE 14-bus System, Contingency Conditions	119
6.4.3	Experiment: 8 Bus System.....	121
6.5	Prospects for Commercialization of the CDML and Future Work.....	126
6.6	Conclusion	129
Chapter 7 Advanced Computing for Real-time Handling of Big-Data that is associated with the Management of a Large Number of Electric Vehicles		
7.1	Introduction.....	130
7.2	Supervisory Management of Large Electric Vehicle Fleet: A Big Data Issue	132
7.3	GPU Parallelization Using CUDA Computing Environment.....	137
7.4	Three-Stage CPU-GPU Coordinated Computing	141
7.5	Data Sets and Results.....	143
7.6	Conclusion	146
Chapter 8 Cyber Security Measures for Securing the developed System-Level Data Sharing Platform		
8.1	Introduction.....	147
8.1.1	Cryptography	148

8.1.2	Security Goals achieved by Cryptography	150
8.1.2.1	Confidentiality	150
8.1.2.2	Integrity.....	151
8.1.2.3	Availability	151
8.1.2.4	Other Goals	151
8.1.3	Example Security Attacks.....	152
8.1.3.1	Man-in-the-middle (MITM) attack.....	152
8.1.3.2	Denial-of-service (DoS) attack	154
8.1.4	Cyber Security Threat Sources and Risk Management	156
8.1.4.1	Insiders.....	156
8.1.4.2	Outsiders	156
8.1.4.3	Cyber Security Risk Management	157
8.2	Threat Scenarios in the proposed communication infrastructure for the EV public charging application.....	158
8.2.1	Unauthorized subscription	159
8.2.2	Unauthorized publication.....	159
8.2.3	Tampering and Replay.....	160

8.3	Security measures taken to secure the BDSS	160
8.3.1	Configuring and Deploying Security Measures.....	160
8.3.2	Authentication.....	162
8.3.2.1	Identity CA Certificate.....	163
8.3.2.2	Private Key.....	163
8.3.2.3	Identity Certificate	163
8.3.3	Access Control.....	163
8.3.3.1	Permissions CA certificate.....	164
8.3.3.2	The Domain governance signed by the Permissions CA.....	164
8.3.3.3	The DomainParticipant permissions signed by the Permissions CA	169
8.3.3.4	Vehicle Access Control with the Web Integration Service	170
8.3.4	Penetration Testing	171
8.3.4.1	Authentication.....	171
8.3.4.2	Access control.....	172
8.3.4.3	An EV using a wrong API Key.....	172
8.4	Summary	173

Chapter 9	Wireless Power Transfer for Electric Vehicle Charging Applications, Part I	174
9.1	Performance Evaluation of a Wireless Power Transfer System using Coupled 3D Finite Element-Circuit Model	174
9.1.1	Wireless Power Transfer Modeling	175
9.1.1.1	Equivalent Lumped Parameter Circuit Modeling	175
9.1.1.2	3DFEA Modeling	177
9.1.2	The Finite Element and Matlab Script	177
9.1.3	Results and Verification	179
9.1.3.1	3DFE Model Results and Validation	179
9.1.3.2	3DFEA-MatLab Script Results	181
9.1.3.3	Verification of the Script	183
9.1.4	Concluding the study	184
9.2	An Iterative Design Approach for Shielding of WPT Systems in Electric Vehicle Charging Applications	184
9.2.1	The WPT System Model	186
9.2.1.1	FEA Model	186
9.2.1.2	Equivalent Circuit and Current Calculation	187
9.2.2	Iterative Design Process	189

9.2.2.1	Process Description.....	189
9.2.2.2	Levels of Charging.....	192
9.2.2.3	Results.....	193
9.2.3	Concluding the study	194
Chapter 10	Wireless Power Transfer for Electric Vehicle Charging Applications, Part II	195
10.1	A Computational Approach for a Wireless Power Transfer Link Design Optimization Considering Electromagnetic Compatibility	195
10.1.1	Description and Modeling of the WPTL	197
10.1.2	The 3DFE Design and Lumped Circuit Model.....	199
10.1.3	The EM-AI Optimization Approach	202
10.1.3.1	The FE-MATLAB Script.....	202
10.1.3.2	NNs and GA Optimization.....	203
10.1.4	Optimization Results.....	205
10.1.5	Concluding the study	206
10.2	An Integrated Characterization Model and Multi-Objective Optimization for the Design of an EV Charger’s Circular Wireless Power Transfer Pads.....	206
10.2.1	The Analytical Model	208
10.2.1.1	Self-Inductance of the Coil	210

10.2.1.2	Resistance of the Coil	212
10.2.1.3	Coupling Inductance of the Two Coils	212
10.2.2	Multi-Objective Optimization Methodology	213
10.2.2.1	Objective Functions	214
10.2.2.2	Decision Variables	215
10.2.2.3	Constraints	215
10.2.3	Concluding the study	218
Chapter 11	Conclusions and Future Works	219
11.1	Conclusions.....	219
11.2	Future Works	223
Appendix	227
LIST OF REFERENCES	230
VITA	247

LIST OF TABLES

TABLE	PAGE
Table 3-1 Application Protocols Comparative Table	34
Table 3-2 DDS Performance for 32 Byte Message Size (1000Msgs/s).....	38
Table 4-1 Fuzzy Logic Controller Parameters.....	55
Table 4-2 Case Studies Results.....	59
Table 5-1 Literature Review on Vehicle Routing Problems of EVs	63
Table 5-2 CPVS given 3 EVCSs (1,2,3), and Discretization Level=3 (A,B,C)	78
Table 5-3 Inputs and outputs of the FLM in the presented case studies.....	86
Table 6-1 N-1 Contingency	120
Table 6-2 N-3 Contingency	120
Table 6-3 Average Percentage Loss Reduction in Each Run Period.....	126
Table 7-1 Response time in CPU approach vs. GPU approach.....	145
Table 9-1 Verification of Several of the Simulated Points.....	184
Table 9-2 Operating Load Parameters	188
Table 9-3 Equivalent Circuit Characteristics of the Initial Pad Design.....	188

Table 9-4 Recorded Magnetic Field Levels Through the Iterative Process of Changing the Shield Radius and Fixing the Shield Thickness	193
Table 9-5 Recorded Magnetic Field Levels Through the Iterative Process of Changing the Shield Thickness and Fixing the Shield Radius	194
Table 10-1 NN prediction vs. FEA Solution	204
Table 10-2 Comparison Of Computational Time For The EM-AI Design Optimization Approach With And Without NN Utilization	205
Table 10-3 GA result.	206
Table 10-4 Comparison between Characterization Results from the Analytical and FEA Model.....	210
Table 10-5 Nomenclature of the symbols used in the equations	211

LIST OF FIGURES

FIGURE	PAGE
Figure 1.1 State-by-state UCS map in reports of (a) 2012 and (b) 2014	9
Figure 2.1 Standards and enabling technologies for the first communications category in the application of public charging of EVs	24
Figure 2.2 Conceptual figure of the communication between the mobile EVs and a head-end grid CC	28
Figure 2.3 Conceptual figure of the communication among several head-end grid CCs	30
Figure 3.1 DDS Communication framework for the MAS using RTPS.	41
Figure 3.2 DDS-Based Decentralized MAS Configuration for the Application of the Management of En Route Electric Vehicles	46
Figure 4.1 A screenshot from one of the services that help find public charging stations.	50
Figure 4.2 Map showing the driving routes between 2 EVs and 3 EVCSs.	52
Figure 4.3 Feature vectors of 3 distinct EVCSs as perceived by 2 distinct EVs.	52
Figure 4.4 Flowchart of EV Agent Controller Logic.....	53
Figure 4.5 Triangular membership functions of the 4 inputs to the fuzzy logic controller.	55
Figure 4.6 (a) triangular membership functions of the SoC input, (b) each membership function: low (blue), medium (red), and high (green), independently plotted.	56

Figure 4.7 Snapshot from the log file showing the distance in miles and time in minutes from an EV to an EVCS.....	57
Figure 4.8 Testing module board interfaced with commercial GPS module.....	58
Figure 4.9 EV and EVCSs assumed locations in the case studies.....	59
Figure 5.1 Vision - Communication among the involved stakeholders.....	67
Figure 5.2 Hierarchical architecture of the proposed multi-agent system.....	69
Figure 5.3 (a) DDS Network Architecture; (b) Flow of Information and Logical Relation between the Agents.....	70
Figure 5.4 EV agent / on-board module, and its interaction with the application's global dataspace.....	72
Figure 5.5 Stages of the VBA strategy.....	76
Figure 5.6 Price vector elements' correspondence to EVCSs.....	77
Figure 5.7 The 2 rounds of stage 2 of the VBA strategy.....	79
Figure 5.8 BDSS Platform (a) EVCS Agents; (b) VBAs and HLA (c) EV Agents.....	84
Figure 5.9 Labelled screenshot from the RTI Connex DDS View software to obtain a full view of the system during experiment.....	85
Figure 5.10 Map showing the VBs, EVCSs, and EVs in the presented case study.....	86
Figure 5.11 Screenshot of the Wireshark showing the packets being sent from and to the EV, with HTTP POST and GET, as an RTI DDS participant with Publisher and Subscriber.....	88
Figure 5.12 Illustration of the case study.....	89

Figure 5.13 Percentage of power consumption to the power set points at the EVCSs.....	90
Figure 5.14 BDSS extension – System of Systems	94
Figure 6.1 Conceptual figure of the platform showing the interaction of the power system optimizer agent.....	104
Figure 6.2 BDSS as a tool for achieving the CDML.	105
Figure 6.3 Flowchart highlighting the higher level power system optimization as it relates to the BDSS platform.....	107
Figure 6.4 Flowchart of VBA algorithm, that is highlighted in black in Figure 6.3.	108
Figure 6.5 Single line diagram of the modified IEEE 14-bus system.	116
Figure 6.6 (a) Initial & (b) Optimal Distribution of the EVs onto the EVCSs, in all Periods between (a) hours 0 – 6, (b) hours 6 – 12, (c) hours 12 – 18, (d) hours 18 – 24.....	118
Figure 6.7 (a) Losses with the Initial Distribution vs with the Optimal Distribution, and (b) Percentage loss reduction in all Periods.	119
Figure 6.8 (a) FIU Smart Grid Testbed view (b) Single line diagram of the experimental 8-bus system.....	123
Figure 6.9 Labview Interface	124
Figure 6.10 The different (a) Generation and (b) Load in Initial and Optimal Distributions, for all six periods.....	125
Figure 6.11 (a) Sum of generation and of load in initial and in optimal distribution, (b) Losses in the Initial vs Optimal distribution, for all six periods.	126
Figure 7.1 Supervisory Management of Large Number of EVs.	136

Figure 7.2 GPU Grid building blocks.....	137
Figure 7.3 The sequence of steps on the host and device parts of the application code.	138
Figure 7.4 The three stage coordinated computing between CPU and GPU.....	140
Figure 7.5 The grid dimensions in each stage.....	142
Figure 7.6 Runtime of application in CPU and GPU environments.....	144
Figure 7.7 Geo-distributed EVs in a Virtual Block.	144
Figure 8.1 The CIA triad.....	150
Figure 8.2 Threat Scenarios	158
Figure 8.3 Configuring and Deploying DDS Secure.	161
Figure 8.4 Creating and Listing the API keys for the Remote Client Applications	171
Figure 8.5 System's Response to Using a Wrong Private Key.....	171
Figure 8.6 System's Response to Using an Altered Permissions File	172
Figure 8.7 Access Denied for Unregistered API key.....	172
Figure 9.1 Electric Circuit of the WPT system.....	176
Figure 9.2 The 3DFE coils coupled with an electric circuit	177
Figure 9.3 Platform interface methodology MATLAB and FEA.....	179
Figure 9.4 Magnetic Field Plots from 3DFEA Using Slices	180

Figure 9.5 Magnetic field density magnitude (a) along line P ₁ (b) along line P ₂ (c) along line P ₃	180
Figure 9.6 Simulink and FEA model results (a) input voltage (V) (b) primary coil current (A) (a) output voltage (V) (b) secondary coil current (A)	181
Figure 9.7 (a) Efficiency versus number of turns at different distances; (b) Efficiency versus Turns Ratio N ₁ =5 N ₂ =variable at different distances; (c) Efficiency versus Turns Ratio N ₁ =variable N ₂ =5 at different distances; (d) Efficiency versus Coil Gauges at different distances.	182
Figure 9.8 Color Map Showing the Magnetic Field Density B for the Initial WPT Pad Design	187
Figure 9.9 WPT Equivalent Circuit	187
Figure 9.10 Flowchart for the iterative approach for optimal design of shielding layer.	189
Figure 9.11 Magnetic Flux Density B in uT Along Line V in the Initial and the Final WPT Pads Design	192
Figure 9.12 Magnetic Flux Density B in uT Along Line H in the Initial WPT Pads Design	192
Figure 10.1 Electric circuit model and the 3DFE domain of the WPTL	197
Figure 10.2 EM Model of the WPTL, top right: experimental platform.	200
Figure 10.3 (a) Field Distribution of the WPTL; (b) Evaluation Locations; (c) Magnetic field density, B, in Tesla along lines 1 and 2, for both the optimum (Opt) and a non-optimum (non-Opt) combination of parameters, compared with the ICNIRP standard reference level.....	201
Figure 10.4 Optimization Procedure.....	204

Figure 10.5 Left: 3D model of WPT Pads; Right: A 2D Axisymmetric Model showing the coils sandwiched between core and shielding layers.	208
Figure 10.6 The spiral windings i and j between the two layers of the core	211
Figure 10.7 A zoom in view on the Ferrite core center area.....	216
Figure 10.8 Optimization results (a) Pareto front (b) evaluated transferred power for each individual in the Pareto front.	217

LIST OF ACRONYMS

ACL	Access Control List
BDSS	Bilateral Decision Support System
BPV	base price vector
CA	certificate authority
CC	Control Center
CDML	Collective Distribution of Mobile Loads
CPO	Charging Point Operator
CPU	central processing unit
CPV	candidate price vector
DDoS	distributed denial-of-service
DDS	Data Distribution Service
DESS	Distributed Energy Storage System
DoS	denial-of-service
EMC	Electromagnetic Compatibility
EMU	Energy Management Unit

ESP	Energy Service Provider
ESR	equivalent series resistance
EV	Electric Vehicle
EVCS	Electric Vehicle Charging Station
EVSE	Electric Vehicle Supply Equipment
EVSP	electric vehicle service provider
FEA	Finite Element Analysis
FL	fuzzy logic
FLC	Fuzzy Logic Controller
FLM	fuzzy logic module
FV	feature vector
GA	Genetic Algorithm
GPU	graphics processing unit
HLA	higher-level agent
HTTP	Hypertext Transfer Protocol
ICNIRP	International Commission on Non-Ionizing Radiation Protection

LUT	lookup table
MAS	multi-agent system
MITM	man-in-the-middle
NN	Neural Network
OPV	optimum price vector
PKC	public key cryptography
PSA	power system agent
PSO	Particle swarm optimization
QoS	Quality of Service
RTPS	Real-Time Publish-Subscribe
SAE	Society of Automotive Engineers
SC	supercharger
SoC	state of charge
TCP	Transmission Control Protocol
UDP	User Datagram Protocol
UL	upper limit

VB	virtual block
VBA	virtual block agent
VRP	Vehicle Routing Problem
WIS	Web Integration Service
WPT	wireless power transfer
WPTL	wireless power transfer link

Chapter 1 Introduction and Literature Survey

1.1 History and Types of EVs and Electric Vehicle Supply Equipment

1.1.1 Brief History

The early rise of the concept of an electric vehicle (EV) dates back to the 1800s [1]. Back then, electric cars outsold their internal combustion counterparts. Thomas Edison, the most famous US inventor, had partnered with Henry Ford, the founder of the Ford Motor Company, for the production of low-cost EVs. However, shortly after, many developments contributed to the decline of EVs, including better roads and the discovery of cheap Texas crude oil. By 1935, all EVs disappeared. The oil prices soared again, accompanied by gasoline shortages, peaking in 1973 with the Arab Oil Embargo. In response, the U.S. looked for ways to lower its dependence on foreign oil. In 1976, the U.S. congress passed the Electric and Hybrid Vehicle Research, Development, and Demonstration Act, to support R&D in EVs. However, EVs produced in the 1970s had limited performance, with low maximum speeds and range, causing a decline in interest in EVs in the following years. In the 1990s, new Acts, like the Clean Air Act Amendment and the Energy Policy Act, were passed in the U.S., renewing interest in EVs. As a result, automakers began working on EVs, achieving better speeds and performance.

Two main events have boosted the interest in EVs and EVs' production to the levels that we witness today. Along with rising concerns about environmental pollution from the transportation sector, the world's first mass-produced hybrid EV, the Toyota Prius, was produced in 1997 in Japan, becoming the best-selling hybrid worldwide. Also, in 2006,

Tesla Motors, a Silicon Valley startup, started producing a luxury electric sports car that could go an unprecedented 200+ miles on a single charge.

Late in 2010, the first plug-in hybrid, the Chevy Volt, was released in the U.S. market. Around the same time of the year, the all-electric Nissan LEAF was released. With many other automakers manufacturing more EVs, the EV owners faced a problem of chargers' availability. For that, and to promote deployment of EVs, the Department of Energy passed the American Recovery and Reinvestment Act (ARRA), in which it funded projects that lead to the deployment of a nation-wide charging infrastructure. With additional and continuous installations of chargers by private enterprise groups and automakers, today's total of public EV chargers plummeted. Also, new battery technology is being developed and deployed in the newly-introduced EVs in the market. Those improvements on the battery side not only improve the plug-in EV's range, but also reduce the overall costs of EVs, increasing their affordability.

As the governmental support has backed the manufacturing and deployment of EVs and contributed to the positive progress in terms of EV charging infrastructure deployment, it becomes obvious that the future of EVs is directly dependent on governmental policies.

1.1.2 Types of EVs

When grouped by the degree to which they use electricity as their energy source, EVs can be classified into three categories: The Hybrid Electric Vehicles (HEVs), Plug-in Hybrid Electric Vehicles (PHEVs), and Battery Electric Vehicles (BEVs).

1.1.2.1 Hybrid Electric Vehicles (HEVs)

Those EVs drive system comprises both a gasoline engine and an electric motor. The electric energy is generated by “regenerative braking”, an energy recovery mechanism that recaptures much of the car's kinetic energy and convert it into electricity. They do not have the capacity to connect to the grid to get any of its electrical energy from it.

1.1.2.2 Plug-in Hybrid Electric Vehicles (PHEVs)

Plug-in hybrids (PHEVs) are considered as a variant from the HEVs in that they can be plugged into the power grid to charge their battery. They still use regenerative braking as another electric energy source and fuel as the source to power their internal combustion engine. The capacity that they have to connect to the grid to get electrical energy from it makes them realize more savings in fuel costs than HEVs.

1.1.2.3 Battery Electric Vehicles (BEVs)

A battery electric vehicle (BEV) does not use the support of a traditional internal combustion engine, but only of an electric motor and battery. They must be connected to the grid as an external source of electricity to recharge the battery. BEVs also use regenerative braking as an additional source of electricity. The electricity is stored in onboard high-capacity battery packs, for use to run the vehicle when driving.

1.1.3 Electric Vehicle Supply Equipment (EVSE)

EVs that have the capacity to connect to the grid to charge their batteries receive the electrical energy from the grid through Electric Vehicle Supply Equipment (EVSE)s, which are also known as charging points.

The term EVSE defines all kinds of equipment and accessories used to supply electricity to EVs. In most cases, the battery charger is on-board the vehicle. The EVSE simply regulates the flow of AC power to the EV charger. In DC charging, the EVSE equipment directly charges the batteries, the battery charger being off-board.

The EVSE can comprise a physical connector or a wireless but electrical connection. Plug-in EVSEs can be categorized into levels 1, 2, and 3, based on the various charging rates. Wireless charging is an alternative form of EVSE that provides more convenience to the EV owner. It can be further categorized into stationary wireless charging and dynamic wireless charging. The duration for charging depends on the type and level of the EVSE connector, the type and capacity of the battery, and the rating of the battery charger.

1.1.3.1 Plug-in Charging

Plug-in EVSEs are categorized according to the charging rates of the EVs. According to the Society of Automotive Engineers (SAE), there are three defined levels: Level 1, Level 2, and DC charging.

Level 1 charging EVSE connectors do not require the installation of any additional equipment and are popular for residential use, because they are connectors that plug into ordinary household outlets (120 V), typically providing a charging rate of 1.9 kW.

DC Fast Charging is the fastest type of charging currently available. There are different levels of DC Fast Chargers that provide charging rates ranging between 36 kW and 240 kW. Because of their high power, they are typically not suitable for residential charging. They are usually installed in public Electric Vehicle Charging Stations (EVCS)s. The fast

charging provided by those EVSEs make it practical for EV drivers to drive beyond an EV's single-charge range in one day. In those, the charger is off-board and the direct current (DC) is delivered directly to the battery.

Level 2 EVSEs sit between the slow and cheap Level 1 charging and the DC Fast Charging stations. They supply 240V, with typical charging rates of 19.2 kW, and are the most commonly installed today.

1.1.3.2 Wireless Charging

In most industrial wireless charging applications like EV charging, phone charging, and charging of artificial cardiac pacemakers, inductive coupling is used. Resonant inductive coupling is used to increase transmission range.

The concept of inductive coupling is simple. When a current flows through a coil, a magnetic field is generated around it. If another coil is placed in proximity of the first coil, a voltage will be induced across it. If the secondary circuit is closed with a battery load connected, a current will flow, charging the battery.

In EV charging applications, the secondary (receiving) coil is fixed permanently beneath the car. Its design is customized according to the battery size and the type of car. The primary (transmitting) coil is embedded in a floor-mounted enclosure. It is usually designed to detect if there is a magnetic object present on or near the pad to stop the charging process so as to prevent a fire or any kind of short-circuit hazard.

Wireless charging of EVs can operate in stationary or dynamic settings. Charging in stationary settings is when an EV parks above a floor-mounted pad to charge while it is

parked and not being driven. Charging in dynamic settings is when an EV charges while it is in motion. The idea is to have charging pads installed at specific distance intervals, so that when the vehicle is being driven on a highway or a street, the secondary (receiving) coil that is fixed in the car passes above the pads and charges along the way.

Several automakers of EVs provide positioning systems in stationary wireless charging systems to guide the driver to park in such a way to have the secondary coil aligned with the primary. Furthermore, different designs of the coils have been proposed in the literature in order to increase the tolerance to misalignments, both in stationary and in dynamic wireless charging.

Several advantages have been reported and discussed [2], [3] favoring wireless charging of EV batteries over wired charging. Some of those are:

1. Ease of use: the operator can't forget to plug in, or be exposed to unfavorable weather in order to recharge the battery.
2. Safety advantages: safe power transfer in any weather, with no exposed or loose terminals or potential for electrocution or tripping.
3. Any premature disconnection is harmless with wireless charging as it does not cause physical damage.

1.2 Anti-Electric Vehicle Arguments and Refutations

Although EVs reduce dependence on petroleum, provide a cheaper solution to transportation, and create new advanced industries and job opportunities that enhance economic prosperity, a lot of consumers and auto manufacturers are still reluctant to

embrace EVs. Their arguments can be grouped into those from a power system and environment standpoint and those from a standpoint related to customer convenience.

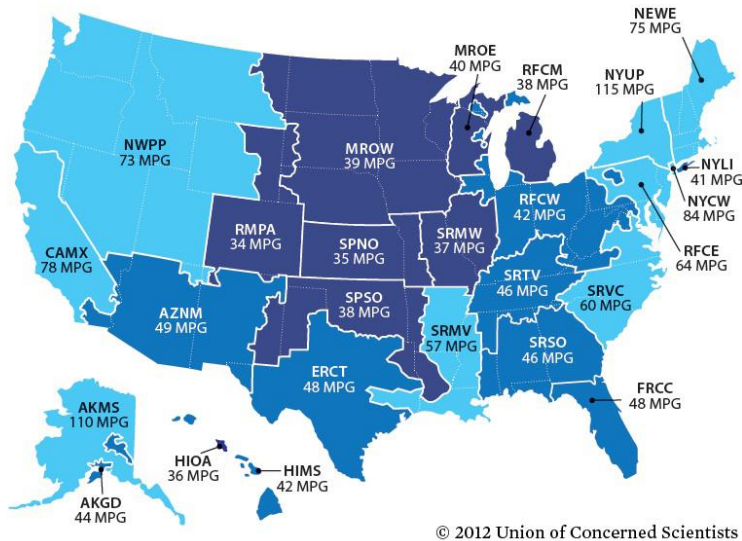
1.2.1 Power System and Environment Standpoint

The argument is that EVs are just as polluting as gas-powered vehicles because they consume electricity produced from coal plants, that does generate global warming emissions. This argument gets debunked when considering the shift towards a greener grid. With the increase in renewable energy resources such as solar, wind, and hydro, the grid is getting cleaner, continuously emphasizing the advantages that result from the shift towards EVs' in the transportation sector. The amount of emissions resulting from the addition of large-scale EV charging then depends on the used mix of energy sources to power the region's electricity grid. For example, coal power plants produce nearly twice the global warming emissions of natural gas power plants. Renewable sources produce virtually no emissions.

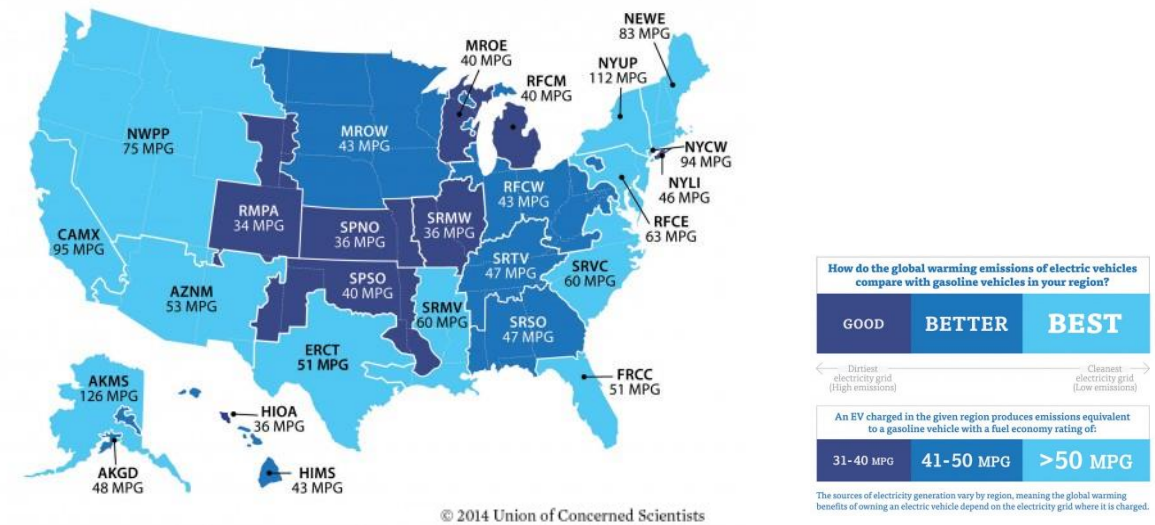
To evaluate those average emissions, a report [4] by the Union of Concerned Scientists (UCS) compared the global warming emissions from EVs charged from the power grid with those from gasoline-powered vehicles in the US. It found that even in regions where the electricity grid is primarily dependent on coal, EVs produce lower global warming emissions than the average compact gasoline-powered vehicle (with a fuel economy of 27 miles per gallon). This report also indicated that EVs charged entirely from renewable sources produce no global warming emissions. For providing a reasonable estimate of how much of improvement EVs provide over gas-powered vehicles in different regions, the UCS applied a state-by-state study, based on the analysis presented in [5], given the

regional average mix of energy sources used and the average emissions intensity (global warming pollution per unit of electricity) over the course of the year 2009, and the average BEV efficiency for model year 2011. The study performed for this report found that an EV charged in any given region produces emissions equivalent to a gasoline vehicle with a fuel economy rating of 31 miles per gallon (MPG) and higher. The report then classified those with equivalency to [31-40 MPG] to be as “Good,” [41-50 MPG] as “Better,” and [>50 MPG] as “Best.” Based on this categorization, the report found that nearly 45% of the Americans live in the “best” regions, 38% live in “better” areas, and 17% reside in “good” regions.

Furthermore, an updated study based on the 2014 data showed an improvement in many states, given the fact that the grid became much greener by the time. Figure 1.1 shows the state-by-state improvements comparison between 2009 and 2014, according to the UCS study.



(a)



(b)

Figure 1.1 State-by-state UCS map in reports of (a) 2012 and (b) 2014

1.2.2 Consumer Standpoint

1.2.2.1 Range Anxiety and Charging Speed

Range Anxiety is a phenomenon where EV owners are in constant fear of having their EV battery running out of charge while driving. Many believe that this is one important barrier that keeps them from owning an EV. This argument also makes many believe that EVs will not proliferate beyond a certain limit. However, the fast charging infrastructure that is being developed and expanded is already reducing the “range anxiety” of EV owners, because of the direct relationship between the speed of charging and convenience levels for consumers.

An important example is the endeavors of Tesla, an EV and EVSE manufacturer, that is not only continuously expanding its charging network around the US, but also increasing the charging rates at its DC fast charging “superchargers” (SC)s [6]. Moreover, currently, there are extensive research efforts that are focused on developing extreme fast charging technologies [7].

1.2.2.2 Availability of and Access to Public Charging Stations

Not everyone nowadays has the luxury of charging an EV at home. Many park their vehicles on the street or in public parkings. For that, the charging infrastructure of today ranges from household sockets to chargers at public charging stations. The chargers at one of the newest charging stations introduced by Tesla [8] for “urban” charging involve superchargers of dedicated 72 kW capacity to charge a single vehicle each. Those SCs aim at people living in the city and who do not have the possibility to charge at home.

Another issue that consumers of EVs face, and that supports the range anxiety phenomenon, is the shortage of public EVCSs. This sometimes forces an EV owner to drive a long distance to charge their vehicle. Also and unfortunately, access to those stations is not always fast. Given the shortage of their number translated by a small EV/EVSE ratio [9], long queues form at public EVCSs [10]. As part of its vision, Tesla has announced and already embarked on a plan to double its charging network around the US. In addition, it has built large charging stations in the US and China [11], comprising several dozens of superchargers.

An example of successfully handling this issue is the public charging infrastructure expansion in Estonia [12]. They have a nationwide coverage of EVCSs, the network consisting of many fast charging stations installed along highways at a minimum distance of 40-60 km. A similar successful expansion in the US is the West Coast Electric Highway, where public EVCSs have been installed at 25-mile intervals extending from Ashland in the south to Cottage Grove on Interstate 5 in Oregon [13]. This project has installed DC fast chargers and level 2 chargers.

1.3 Motivations for fostering the uptake of a large number of EVs

In the pursuit of restricting global warming emissions, global and collective efforts are being made in the form of international agreements and policy measures. The main international comprehensive climate agreement made in this context is the Paris Agreement. It is an agreement made within the United Nations Framework Convention on Climate Change (UNFCCC), and it deals with greenhouse-gas-emissions mitigation, adaptation, and finance. Under the Paris Agreement, each country shall determine, plan,

and regularly report on the contribution that it undertakes in order to mitigate global warming.

The main aim of the Paris Agreement is limiting the increase in the global average temperature to below 2 °C, which would significantly reduce the risks and impacts of climate change. Several technologies that can contribute to this goal were identified and a comprehensive assessment of where they are today and where they need to be was performed. This assessment is called “Tracking Clean Energy Progress (TCEP),” and it is performed by the International Energy Agency (IEA), a Paris-based autonomous intergovernmental organization established in the framework of the Organization for Economic Co-operation and Development (OECD) in 1974 in the wake of the 1973 oil crisis. The IEA uses a Sustainable Development Scenario (SDS), a pathway to reach the Paris Agreement well below 2°C climate goal.

Among the identified supporting technologies are EVs, that help decarbonize the transport sector. According to the IEA’s TCEP assessment, some of the identified technologies have made excellent progress in 2017, particularly solar photovoltaics, LEDs and EVs [14]. The other technologies are not on track. With important policy announcements in major global regions made in 2017, EV sales accelerated worldwide, fostering the uptake of EVs to exceed 3 million [15].

According to one of IEA’s scenarios that is based on proposed policies, and that describes a future energy system that would limit average global temperature increases to 2°C by 2050, the transport sector can contribute to 21% of the overall CO₂ reductions by that year.

Given those numbers, it can be seen that environmental goals can be strongly supported through the accelerated electrification of the transportation sector, thus establishing a solid motivation to invest in EV-related research and impose suitable policy measures to drive the large scale uptake of EVs.

1.3.1 Attempts for making the experience more convenient

1.3.1.1 Power system operators' standpoint

From the power system operators' standpoint, several platforms and services have been presented in literature for using EVs towards ancillary services, organizing the large scale penetration of EVs in the power grid, and shaving off the undesired associated effects.

Many of those presented services are portrayed in the contexts of demand response programs or coordination of charging at EVCSs. Several studies apply vehicle-to-grid and vehicle-to-vehicle approaches to fully utilize the flexibility of this energy storage system.

However, because the levels of penetration of EVs in the power grid have been recently increasing with the increase in EV sales, the real-time management of en-route EVs is quite recent and not many research works can be found in the literature covering this topic comprehensively, the thing which makes it one main research objective of this dissertation.

1.3.1.2 Consumer standpoint

Extensive research is being focused on applying technologies and investigating combined efforts from interdisciplinary fields that could be used towards realizing smarter cities and communities, providing extra levels of convenience for citizens and contributing to the global efforts to a cleaner environment.

Among the attempts for providing a more convenient experience to the consumer of EVs are both the expansion of public charging infrastructure and the design of wireless (stationary and dynamic) charging pads that support a safe and fast charging experience that is comparable to the DC plugin charging. Many challenges accompany those attempts, including interoperability challenges and the need for designs that are compliant with communication and Electromagnetic Compatibility (EMC) standards.

1.4 Problem Statement

To meet the Paris Agreement climate goal explained in section 1.3, member countries are applying policies that foster the identified technologies by the IEA. Among those policies are many financial incentives that are succeeding in escalating the uptake of EVs. The increase in EV sales and the accompanying expansion in the EV charging infrastructure carry along many challenges. All anti-electric vehicle arguments, some of which are explained in section 1.2, prove that the largest challenge to a larger uptake of EVs is infrastructure-related. A very important challenge is the need to ensure the availability of and to facilitate the access to public EVCSs. Another infrastructure challenge is the need to strengthen the power grid to handle and better manage the electricity demand by this mobile and geo-distributed load, both in the design and operation phases. Also, there is a need for deploying EVSEs that support faster charging, both wired and wireless, and/or manufacturing batteries that provide extended range of driving on a single-charge. Directing efforts towards a more optimal and secure infrastructure network is indispensable for fostering the uptake of EVs, ultimately leading to reaching the worldwide climate change goals.

The work presented in this dissertation provides solutions to those challenges, thus contributing to a better EV charging infrastructure network. The presented studies can be grouped into two main thrusts: the real-time management of en-route EVs to better manage connections to the power grid (whether wired or wireless connections), and the design optimization of wireless chargers of EVs considering compliance with EMC standards.

In the first thrust, the feasibility and robustness of a service with ancillary service potential that could help the power system handle and better manage the electricity demand by the EVs is investigated. For that, a connectivity platform is presented that connects EVs, public EVCSs, and utility operators in a pursuit to organize the large-scale connections of EVs as mobile and geo-distributed loads to the power system, to achieve an optimal and secure operation of the power system. When building this platform, several challenges arise and are addressed sequentially in the chapters of this dissertation. Some of those are the need for processing the big data that arises in real-time, the cyber-security threats that accompany this framework, and the on-board module that would participate in such a service while assisting the EV drivers in routing them to the EVCS that would be best for their energy status at the time of the request.

The second thrust towards a stronger infrastructure for EV charging is on the device-level of the wireless chargers for EVs. In this work, several studies are performed on optimizing the design of the wireless pads in EV chargers, considering compliance with EMC standards.

1.5 Research Objectives

In this dissertation, several contributions from different angles are made to support the efforts to enhance the EV charging infrastructure and the effects of charging on the power system. The objectives of this dissertation can be summarized as the following:

- Investigate the communication links and the enabling technologies that are related to the management of EVs in the public charging category and the feasibility of the use of a system-wide multi-agent system (MAS) to facilitate this real-time application.
- Design an on-board system that would render the vehicle an interacting node within a system-wide communication platform to provide enhanced self-convenience in terms of access to public chargers, while simultaneously being part of the collective effort to provide benefit to the power system under the large scale uptake of EVs.
- Examine the validity of a bilateral decision support system, the two sides being the EV and the power grid, examine its prospects, and explore its ability to provide advantage to both simultaneously.
- Investigate the ancillary service potential of real-time collective redistribution of en-route EVs, using a developed system-level communication platform.
- Explore new and effective techniques that facilitate the optimization of the efficiency of the magnetic part of wireless EVSEs, while considering and abiding by international safety standards.

1.6 Original contribution and significance

The studies and solutions presented in this dissertation contribute to a seamless transition into the vision of cities dominated by EVs and their charging infrastructure.

Because the levels of penetration of EVs in the power grid has been recently increasing with the increase in EV sales, the real-time management of en-route EVs is quite recent and not many research works can be found in the literature covering this topic comprehensively. Regarding this aspect of the work, advances and novel ideas are presented in this dissertation, addressing the various challenges that arise in this application.

On a different scale, the component level, new and effective techniques that facilitate the optimization of the efficiency of the magnetic part of wireless EVSEs are presented. Those methods consider international EMC standards.

The original contributions and studies of this dissertation can be summarized as following:

- Present a middleware-based multi-agent system to facilitate the real-time management of en route EVs. The communication between the EVs and the control centers in this system were tested in real-time.
- Design an artificial intelligence based on-board system that renders the EV an interacting node in the system-wide communication platform, providing both enhanced self-convenience in terms of access to public chargers and

contribution to the collective effort of providing benefit to the power system under the large scale uptake of EVs.

- Examine and sequentially address the challenges accompanying the developed bilateral decision support system.
- Investigate the ancillary service potential of real-time collective redistribution of en-route EVs, using a developed system-level communication platform.
- Present new and effective techniques that facilitate the optimization of the efficiency of the magnetic part of wireless EVSEs, while considering and abiding by international safety standards.

1.7 Dissertation organization

This dissertation is organized in eleven chapters, including this chapter, which introduces the general contributions of this dissertation.

Chapter 2 assesses the communication links and the enabling technologies that are related to the management of EVs in the public charging category. We conclude the chapter by proposing to link all levels into one correlated connectivity platform. The recommendation drawn is used to architect the system proposed for achieving the collective benefit of all involved entities, as will be seen in later chapters.

Chapter 3 discusses the advantages of using a MAS, an automated system composed of several intelligent pieces of software, each interfaced with a different participant, and all working together in a message-sharing communication scheme to facilitate a designed

system-level operation. In this chapter, and following the drawn conclusions of Chapter 2, a middleware is used to apply the MAS's approach.

In chapter 4, the details of an intelligent fuzzy logic (FL) based on-board module that is developed to guide EVs to EVCSs are presented. The motivations behind developing this automated on-board module, as it relates to the solutions provided in this dissertation to the public charging category, are discussed first. Then, a brief overview on FL is presented, followed by the details of the design of the fuzzy logic module (FLM) presented here. The module's platform is then explained, with the results of four case studies to test the module.

Chapter 5 presents the communication scheme of the proposed framework: the Bilateral Decision Support System (BDSS), with the two sides being the EV and the power grid. The credibility of using the communication middleware and means are experimentally verified on a group of connected vehicles communicating with a higher-end server in case studies in the results section. This is important as the communication requirements and the deployed system imposes important constraints that need to be studied. The effectiveness of the developed approach is strictly contingent on the deployable communication system that helps achieve it.

Chapter 6 introduces the service of "Collective Distribution of Mobile Loads," a service with ancillary service potential that achieves an optimal and secure operation of the power system under normal and contingency conditions. It comprises a real-time system-level optimization for the collective redistribution of EVs onto EVCSs using the BDSS platform that is presented in details in chapter 5. The hypothesis is validated by means of several

case studies in simulation on an IEEE 14-bus system, and an experiment is applied on an 8-bus system in a reconfigured laboratory-scale power system testbed.

Chapter 7 introduces a solution to the big data issue that arises when introducing a cognitive price-based strategy of the a higher-end agent that is presented in chapter 5. It also lays the foundation for the application of Graphics Processing Unit (GPU) computing for the deployment of such large scale real-time management systems that alternatively could have been confronted with the hurdle of the big data processing requirement.

Chapter 8 lays out the measures taken to secure the communications in the BDSS that was introduced in the previous chapters. As the BDSS system scope expands, security becomes a concern. Before getting into the security configuration of the application, a discussion on cryptography and its security goals, examples of security attacks and cyber security threat sources and risk management are presented. Then, possible threat scenarios in the application of the BDSS are elaborated upon, and the security measures taken are explained, providing details on the format and the content of the configuration files used.

Chapters 9 and 10 present different studies applied in the wireless power transfer (WPT) for the application of EV charging.

In chapter 9, the first case study presented comprises a numerical technique that involves coupling electromagnetic field analysis and an electric circuit simulation. This coupled model is utilized to evaluate the WPT system's efficiency and performance of different designs by varying a number of design variables. A MATLAB-FEA routine is developed, serving as an interface from which the changes to the Finite Element Analysis

(FEA) model and the circuit parameters are applied. Then the results from the FEA model are compared with a mathematical model's results for validation. The second case study applies a design approach for a shield for the coils of a WPT system to comply with safety standards. This study proposes an iterative approach for selecting a shield radius and thickness for a given WPT system, using Finite Elements Analysis, which ensures a safe level of EMI that is compliant with the International Commission on Non-Ionizing Radiation Protection (ICNIRP) standard, while minimizing the cost and weight of the system.

In chapter 10, the first case study presented, the numerical approach of coupled 3DFE and circuit theory, was used to provide an accurate solution for both efficiency calculations and for minimizing the field signature around the Wireless Power Transfer Link (WPTL). As the presented design optimization process requires utilizing a large number of iterations, each of which requires 3DFE analysis, Artificial Neural Networks (NNs) were developed, trained, and used to significantly reduce the computational effort. A Genetic Algorithm (GA) based process was utilized to optimize the considered design parameters of the WPTL system. The objective of the optimization is to maximize the WPTL efficiency and minimize the field signature around it. A constraint function was applied to the output power of the system.

Chapter 11 provides a summary of the dissertation outcomes, the significance of this research, and recommendations for future work related to its topic.

Appendix I provides a table of the FL rules of the on-board module presented in chapter 4.

Chapter 2 Standards and Enabling Communication Technologies Involved in the Management of Electric Vehicles

2.1 Introduction

The charging of EVs can be categorized into residential, public, and commercial settings. The charging infrastructure at home brings convenience but cannot be the only choice for consumers to charge their vehicles, as not everyone has the luxury of having private parking at home. In addition to residential chargers, EVSE is usually installed at workplaces, universities, and businesses for boosting convenience levels of employees, students, and customers, respectively. The infrastructure encompassing those fall under the “commercial” category. Lastly, networks of public EVSE are installed at several locations for consumers who want to charge on the go. For some, this would be their only option. For others, like taxi-sharing fleets or those who travel a long distance by car, public charging will most likely be needed while one is away from home. The work in this dissertation mainly focuses on the management of EVs that seek public charging and provides a framework for collectively redistributing them onto the public EVCSs by rerouting them, hereby offering a powerful service with ancillary potential to the power system. Work is done on securing the proposed framework against access by non-authentic nodes.

Before proposing a connectivity framework that provides those benefits, it is essential to first assess the communication links and the enabling technologies that are related to the management of EVs in the public charging category. This can be further categorized into three groups; the first group encompasses the communications that involve entities at the

premises of the EVCS; i.e. the communication between the EVs and EVSEs, between the EVSEs and the EVCS's Energy Management Unit (EMU), and between the grid's control center (CC) and the EVCS's EMU. The second is the communication between the mobile EVs and a head-end CC, and the third is the communications among the CCs.

In this chapter, we discuss the enabling technologies in each of those groups, giving example systems in where those are used. We conclude the chapter by proposing to use a technology that would link all levels into one correlated connectivity platform. The recommendation drawn is used to architect the system proposed for achieving the collective benefit of all involved entities, as will be seen in later chapters.

2.2 At the Premises of the Electric Vehicle Charging Station

In the first category, communications inside the EVCS involve that between the EVs and the EVSE, and that between the various EVSEs and the EVCS's EMU. Then, an elaboration on the technologies that facilitate this type of communications and the standards being set to organize this is presented. Furthermore, a discussion is presented on the communication between the EMU and any head-end CC that reaches out to all EVCSs and EVs to participate in their management. In this section, and after laying out the technologies being used, the requirements of any system that encompasses all the categories are outlined. The acceptable time ranges that the communication in those categories should happen are shown in Figure 2.1.

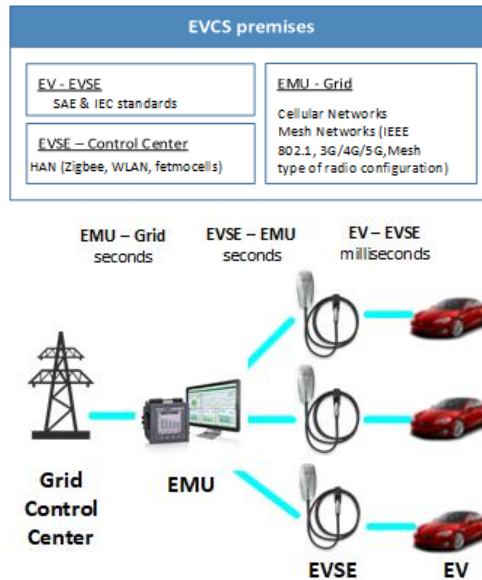


Figure 2.1 Standards and enabling technologies for the first communications category in the application of public charging of EVs

2.2.1 Electric Vehicle – Electric Vehicle Supply Equipment

Communication between the EV and the EVSE at the EVCS is necessary to monitor and manage the energy transfer, billing information, and authorizations. The SAE and the International Electrotechnical Commission (IEC) are defining several standards that set the rules for developed technologies (SAE J2293, J2836/1, J2836/2, J2836/3, J2847/1, J2847/2, J2847/3, J2931/1, J2931/2, IEC 61851-23, and IEC 61851-24) [16]. Each of those standards defines rules that optimize the power and communication implementations of a given aspect of the EV-EVSE interactions.

SAE J2293 establishes requirements for EVs and the off-board EVSEs used to transfer electrical energy to an EV from an Electric Utility Power System in North America. This standard also defines the physical requirements for the channels used to transfer the power and communicate information between the EV and the EVSE.

SAE J2836/1 presents use cases that identify the equipment and interactions to support AC or DC energy transfer for PEVs. SAE J2836/2 presents use cases and general information for communication between PEVs and the DC Off-board chargers. SAE J2836/3 presents use cases for a PEV communicating with an Energy Management System (EMS) as a Distributed Energy Resource (DER).

SAE J2847/1 establishes specifications for the communication between PEVs and the electric power grid, for energy transfer and other applications. SAE J2847/2 establishes specifications for the communication between PEVs and the DC off-board chargers.

SAE J2931/1 outlines the requirements for communication between PEVs, the EVSE, the utility or service provider, the Energy Services Interface (ESI), the AMI and the HAN. SAE J2931/2 defines the requirements for physical layer communications between the EV and the EVSE.

IEC 61851-23 and IEC 61851-24 provide the general requirements for the control communication between an EV and a DC EVSE.

2.2.2 Electric Vehicle Supply Equipment – Energy Management Unit

The EVSE can connect to the EVCS's EMU via HAN. The technologies used for HAN could be ZigBee, 802.11-based wireless local area network (WLAN), or femtocells. This is similar to the connectivity between the appliances at a home and the smart meter of an AMI.

2.2.3 Energy Management Unit – Grid Control Center

The EVCS's EMU acts as a gateway of the EVCS to the head-end grid CC. The EMU has to be equipped with two-way communication for data exchange. In this application, an example of the type of information that is needed from the EVCSs is their availabilities in terms of unoccupied chargers. This piece of information has to be updated every time a charger becomes available, because an EV has disconnected, or gets occupied, by an incoming EV. Other pieces of information to be shared by the EVCS are the price of charging, the types of chargers, available rates of charging, etc. Moreover, the head-end CC will need to convey some pieces of information to the EVCS, such as the information of EVs that are routed to it, new pricing signals, and others.

This can be seen as analogous to the smart meter application. An advanced metering infrastructure (AMI) enables two-way communications between end-customers and the utility company. An AMI is usually deployed to improve energy management of neighborhoods, detect power outages, enable remote load disconnection, and reduce the operation cost by transmitting accurate real-time consumption data to the utility, which can be extended down to each smart appliance. The electricity smart meter is a digital device installed at the customers' premises to collect time-based consumption data. They consist of an analog front-end, a digital processor, and a communication interface. The latter is essential for facilitating the information exchange with the utility, on one side, or the customer Home Area Network (HAN), on the other. The most common network interfaces with the utility side are radio frequency (RF), power line communication (PLC), broadband over power line (BPL), and cellular networks. For the HAN-side communication, Wi-Fi

and ZigBee wireless network are utilized to connect with the customers' devices and systems.

Those technologies can also be used towards the application at hand. Furthermore, to add an interoperability feature, the EMU, which serves as the EVCS's gateway, can share its data with a middleware layer, of which all participating EVCSs are joining members.

2.3 Control Center to Mobile Electric Vehicles

Regarding the second category, i.e. the communication between the CC and the mobile EVs, we consider the IEEE P2030 Guide [17] that presents possible communication interfaces with all smart grid end-use applications. In this guide, the communication with the EV when it is mobile is addressed in CT18 of the communications technology (CT) interoperability architectural perspective. Tackling the direct communications path/link between the mobile EV and a head-end software, it conveys that the wireless service provider (WSP) could use 3G/GSM, 4G/LTE™/WiMAX, or satellite transponder technology inside the vehicle as the means to communicate. In addition, the guide states that an EV can afford to have a few seconds of latency to retrieve location, pricing, and availability information. WiMAX and 4G have the required capabilities to handle the transmission of such data [16]. In addition, mobile data service based on 4G LTE is becoming more popular with the global LTE connections, reaching 2.5 billion at the end of the third quarter of 2017 [18]. Hence, 4G/LTE can provide a ubiquitous communication for EVs.

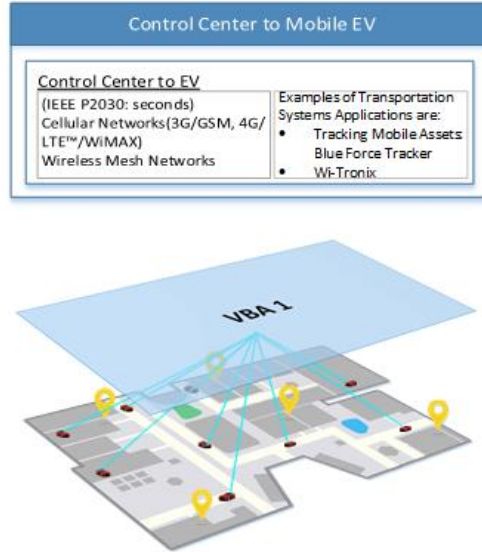


Figure 2.2 Conceptual figure of the communication between the mobile EVs and a head-end grid CC

Figure 2.2 shows a conceptual figure of the communication between the mobile EVs and a head-end grid CC. The expected number of nodes to which the head-end CC needs to connect depends on how large the network of the EVCSs is, how large the geographical area of which the CC is appointed the task of management is, and how many EVs are in that area. For this reason, and with the foreseen exponential rise in the uptake of EVs and the accompanying construction of the public charging infrastructure, the system must be designed to service thousands of EVs and a large network of EVCSs. Alternatively, it should have an easily scalable design to handle the ever-expanding network.

The latency issue is of great importance here, and its significance stems from the desire to have the data that the CCs convey to the EVCSs reach all the nodes in short periods, typically within a few seconds. This is needed to keep pace with the highly volatile number of incoming and outgoing EVs at the EVCS, which is translated as a feature of dynamism to the chargers being engaged and released. As the population of nodes increases, the

number of messages being sent in a point-to-point messaging scheme will multiply proportionally, straining the system within this very short window. This hinders the deployment of such a management framework on a large-scale. For that, a publish-subscribe messaging scheme is highly preferred.

2.4 Inter-Control Center

In the last category, the CCs will need to communicate among themselves to better optimize the distribution of the EVs onto the EVCSs, as well as share information regarding EVs moving from one area controlled by one CC into another. Depending on the CCs' assignments based on the service areas and their geographical locations, several of those might be residing on one server; so they will need to communicate over a shared memory transport. This is because a shared memory transport is a strategy that supports fast communication among processes within a single multi-core hardware host computer.

In other cases, the CCs might need to communicate with CCs of neighboring areas residing on different servers that might be at the same or different physical locations. Hence the need for a Transmission Control Protocol (TCP) transport over Local Area Network (LAN) or Wide Area Network (WAN), respectively. For information exchange among CCs over WAN, the IEC 60870- 6/TASE.2 Standard, also known as ICCP (Inter-Control Centre Communications Protocol) [19] is used by utilities. Figure 2.3 shows a conceptual figure of the communication among several head-end grid CCs.

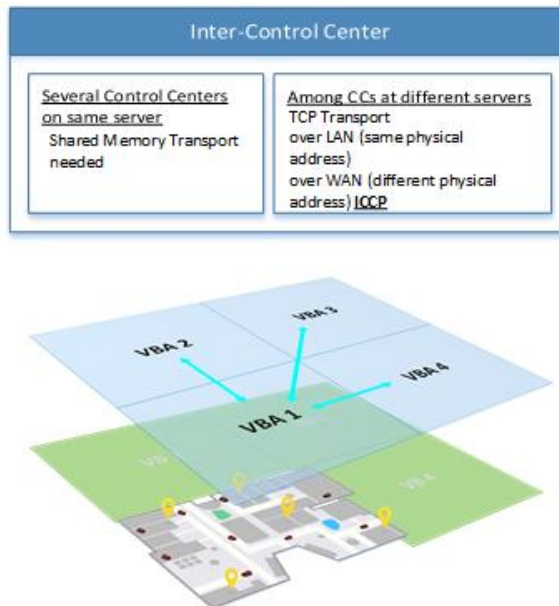


Figure 2.3 Conceptual figure of the communication among several head-end grid CCs

2.5 Summary

Briefing the requirements for these three categories, high data rate, wide coverage and scalability, high throughput, Quality of Service (QoS) support, and support of different transport protocols, are needed to support this application involving the mobility aspect.

The challenges faced in this application can be addressed by deploying a suitable middleware. A middleware is a software layer that sits between applications and the objects' operating system, network or hardware, thus serving as a reliable platform for communication among things with different interfaces, operating systems, and architectures. The used middleware should provide a framework or an environment that enables two applications to negotiate and exchange data in a distributed system, without being directly connected, and should also be capable of facilitating the communication and data sharing between applications running on one or more machine(s).

In the next chapter, several messaging middlewares are compared based on features related to smart grid applications. Two smart grid applications are presented, the most suitable middleware is chosen in each, and the system is built with that middleware.

Chapter 3 Middleware-based Communication Platform for Smart Grid

Decentralized Applications

3.1 Introduction

The current shift towards a smart grid brings along the management of distributed entities, applied through diverse operation and control schemes. For that, the Multi-agent system (MAS)'s approach is followed to facilitate several applications that integrate local, remote, stationary, and mobile participants. A MAS is an automated system composed of several intelligent pieces of software, each interfaced with a different entity, and all working together in a message-sharing communication scheme to facilitate a designed system-level operation. In this work, and following the drawn conclusions in Chapter 2, a middleware is used to apply the MAS's approach.

3.2 Middleware for the communication in a Multi-Agent System

A middleware is an intermediate layer that sits between applications and the objects' operating systems to facilitate communication among applications with different interfaces, operating systems, and architectures.

When it comes to choosing the middleware technology to use, there are broad alternatives of products that provide solutions for different applications. Generally speaking, the used middleware should provide an environment that enables two applications to negotiate and exchange data in a distributed system, without being directly connected, and should also be capable of facilitating the communication and data sharing between applications running on one or more machine(s). It is important to assess the needs

in the application at hand and undergo a detailed comparison of features among middlewares to choose the most suitable.

The middleware layer integrates two or more distributed software applications, allowing them to exchange data via various communication devices. Just like an operating system is a software that facilitates the usability of the hardware, a middleware is a software that facilitates the programmability of a distributed system. When a heterogeneous operation is required, a middleware adds a facilitating layer of interoperability to make programming the distributed system much easier.

It is important to first apply a thorough assessment of the candidate middlewares for the application at hand. Because of that, a comparison among several application layer protocols for messaging middlewares is presented here. Different groups, like the World Wide Web Consortium (W3C), Internet Engineering Task Force (IETF), EPCglobal, and IEEE, have worked to provide protocols in support of the distributed applications like those in IoT [20]. Table 3-1 provides a brief comparison between some of the most popular application protocols defined by these groups : the Data Distribution Service (DDS), the Constrained Application Protocol (CoAP), the Message Queue Telemetry Transport (MQTT), the Advanced Message Queuing Protocol (AMQP), the eXtensible Messaging and Presence Protocol (XMPP), and the Hypertext Transfer Protocol (HTTP). Critical features that should be considered when choosing the protocol include mainly the transport on which the protocols work, the messaging model and resource discovery that would facilitate or hinder scalability, tolerance to fault as a reliability metric, and support to QoS

policies for accurate data management. All these are significant features to meet the requirements of the MASs for distributed applications.

Table 3-1 Application Protocols Comparative Table

	Transport		Messaging Model	Resource Discovery	Immunity to SPoF	Failover and high availability	QoS Support
	UDP	TCP					
DDS	✓	✓	PS / RR	✓	Decentralized - No SPoF	Automatic failover via owner strength	✓
CoAP	✓	✗	RR	✓	CS - SPoF	IS	✓
MQTT	✗	✓	PS	✗	Broker - SPoF	IS	✓
AMQP	✗	✓	P2P	✗	Broker - SPoF	IS	✓
XMPP	✗	✓	PS / RR	✓	CS - SPoF	IS	✗
HTTP	✗	✓	RR	✗	CS - No SPoF	IS	✗

* PS: Publish Subscribe

* RR: Request Reply

* P2P: Peer to peer

* CS: Client-Server

* SPoF: Single Point of Failure

* IS: Implementation Specific

With regards to the transport protocol, TCP and UDP are protocols of the transport layer, the fourth layer in the OSI model. They are both protocols for sending packets over the Internet. Being the most commonly used protocol on the internet, the TCP is a reliable and connection-oriented protocol, in which an acknowledgment is awaited from the remote system to confirm receipt of packets once sent. On the other hand, the User Datagram Protocol (UDP) is a connectionless protocol that trades the reliability of TCP with speed of communication. In this protocol, packets are sent to the recipient without waiting to make sure if they were received. The elimination of this back-and-forth communication makes the communication between computers faster. This is used when speed is preferred over reliability of the connection.

While most of the compared messaging protocols work on top of the TCP transport protocol, CoAP works on top of UDP, utilizing less data overhead in applications where there is no need for connecting with remote locations. DDS is the only protocol among those compared that works on top of both UDP and TCP, providing an extra level of flexibility. This creates the perfect environment to design and operate scalable systems that encompass local and remote nodes.

Furthermore, there are three types of messaging models: The Request-Reply (RR), the Peer-to-peer (P2P), and the Publish/Subscribe (PS). Request-response is a simple messaging pattern in which the application that makes the request waits for the remote system to receive and process this request, and then returns a message in response.

Peer-to-peer messaging eliminates the need for a central server, which would otherwise act as a single point of failure. Each new “peer,” a participant in the network, connects to a few others, to organize its operation without the need for harmony with the operation of others.

In the Publish–subscribe messaging pattern, senders of messages, called publishers, do not specify to which receivers, called subscribers, their messages are being sent. The published messages are categorized into classes without prior knowledge of which subscribers, if any, there may be to those messages.

Another attribute that some middlewares have and others don’t is resource discovery. In this process, the middleware would determine which resource in the computational grid

is the best candidate to complete a given job in the shortest amount of time, with the most efficient use of resources, and at the minimum cost.

As for whether the application of the middleware will cause the system to be vulnerable to a single point of failure (SPoF), this is dictated by the used messaging model. That is, if the messaging model is based on the client-server pattern, the server acts as this SPoF. Some middlewares do not follow a client-server messaging model but rely on a broker, an intermediary computer program module that translates a message from the formal messaging protocol of the sender to the formal messaging protocol of the receiver. This broker also makes the distributed system vulnerable to a SPoF. The DDS is the only application protocol among the ones being compared here that is decentralized and is not susceptible to a SPoF. In addition, DDS provides an automatic failover service when the highest strength writer fails, like when it loses liveness, misses a deadline, or stops writing for example. This renders the application built with DDS a more reliable one.

Finally, some of the protocols being compared provide QoS support, and others don't. In contrast to other publish-subscribe application protocols, DDS is based on a reliable broker-less architecture, uses multicasting with flexibility of transport choice of UDP or TCP, and supports resource discovery. Also, DDS provides the developer with a wide variety of QoS policies that help in monitoring moving assets over wireless networks. Some QoS policies also facilitate the discovery of joining participants and maintain connection during lapses in service, such as the case when a train goes through a tunnel for a few minutes.

Because of those combined qualifications of DDS against the other application protocols, and its superiority in terms of suitability to the application of MASs in the smart grid, it is chosen for the two applications being presented in this chapter.

3.3 Data Sharing Structure in DDS

The data-centric publish subscribe model of the DDS middleware establishes the concept of a “global data space” that is accessible to all interested applications. Publishers are applications that contribute information to this data space, and subscribers are applications that acquire information from it. Each time a publisher posts new data into this “global data space,” the middleware propagates this information to all interested subscribers.

In addition, DDS provides a rich set of services, making distributed applications built with DDS much more manageable. Among those services is a DDS Web Integration Service (WIS), which is deployed as a gateway for the external requests from any remote nodes that are in the form of HTTP client applications. Those requests are issued in an HTTP-request format, and this service translates the communicated data to the DDS data format and vice versa, thus facilitating access to the global data space.

A benchmark performance test is presented in [21] to prove the real-time performance required by the DDS communication middleware in a practical system. Table 3-2 is presented here for the convenience of the reader. The benchmark test shows that the DDS can achieve 1000 messages/sec with a maximum 0.385 ms latency, proving suitable for providing scalability to the real-time applications presented in this chapter.

Table 3-2 DDS Performance for 32 Byte Message Size (1000Msgs/s)

Test Type	QoS	Avg. Latency (μ s)	Max Latency (μ s)	90%<t(μ s)
Unicast	Best Effort	243	336	269
Multicast	Best Effort	270	385	306

Because the DDS meets many challenging requirements, it is used across a wide variety of applications in different industries. A significant example of such real-world implemented frameworks is that of Volkswagen Smart Cars for driver assistance and integrated safety in the transportation industry. RTI Connex DDS integrates several subsystems like sensors, laser range finders, and video to assist safe operation. Another outstanding example where DDS is used is that of DocBox, an innovative clinical process management solution to improve medical safety, in the medical industry.

Two example MASs built with the RTI Connex DDS are presented in this chapter. The first, a DDS-based MAS for market operation in a multi-microgrid environment, is presented in section 3.4. The second, a DDS-based connectivity platform for the management of public charging of EVs, is presented in section 3.5. The description of the application and the MAS design are presented. It is interesting to note that although those are two separate MAS examples, they could be seamlessly integrated and their interdependencies, if any, considered easily. This is because they are designed and built using DDS, which provides a rich set of services, among which are a “web-integration service” and a “routing service,” that facilitate the bridging of applications across a LAN or a WAN.

3.4 Application 1: DDS-based Multi-Agent System for Market Operation in a Multi-Microgrid Environment

In the application of multi-microgrid market analysis, data needs to be communicated back and forth among all the microgrid entities to reach a good system forecast, apply a fair auction, and then announce back the winning loads and energy sources that will change from bidders to actual participants in the next period market.

To release the complexity and combine the several interlinked market analysis processes in a systematic and fair system, a reliable MAS is presented. This MAS facilitates the communication of the results among the several microgrids in which a hierarchical and distributed optimization is applied.

Because of the superiority of the DDS over the other messaging middlewares compared in this chapter, and to address the pressing scalability requirement of the application at hand, DDS is used in the design of this MAS.

3.4.1 Application description

This MAS is applied towards a multi-microgrid market analysis application. In this application, an approach that involves both game-theory and stochastic hierarchical optimization algorithms is followed. This approach is tailored to achieve the optimal operation of microgrids in distribution systems, where rapid load variations occur.

The DDS-based MAS of this application is structured to support a three-level market framework [22]. The first level comprises a game-theoretic double auction mechanism for a day-ahead market. Optimal rescheduling is applied in the second level for an hour-ahead

market, and an inter-microgrid reverse auction model is applied in the third level, for a real-time market. The objective of the optimization algorithm is to reduce the dependency of the microgrids on the network in the grid-connected mode or the need to shed load in the islanded mode. It is applied in a hierarchical structure to minimize the optimization solution time. With this approach, all the microgrids' capabilities, including load demand Response and rescheduling of resources, are considered in all three market levels.

3.4.2 System Description

The proposed framework consists of a Load agent, a Generation agent, a Distributed Energy Storage System (DESS) agent, and a Local Market Agent, in each microgrid. In addition to those, a General Market Agent, reaching over to all microgrids, is part of this MAS. The processes are sorted into three stages: Day Ahead, Hour Ahead, and Real-Time markets. Figure 3.1 presents the built DDS-based MAS for this application. It shows the connectivity among those agents in the three levels, and in a three-microgrid environment. In Figure 3.1, the load agent is referred to as LA, the generation agent as GA, the DESS agent as DA, the local market agent as LMA, and the general market agent as GMA.

First, and in the Day Ahead stage, the Load, Generation, and DESS Agents collect the data from the loads, generators, and DESSs in the microgrid, respectively, and publish them to the appropriate topics. The LMA subscribes to those topics to receive this data. With this collected data, the LMA runs the double auction and decides on the winning participants and the losing bidders. It then publishes the results to the corresponding topics, to which the Load, Generation, and DESS Agents subscribe.

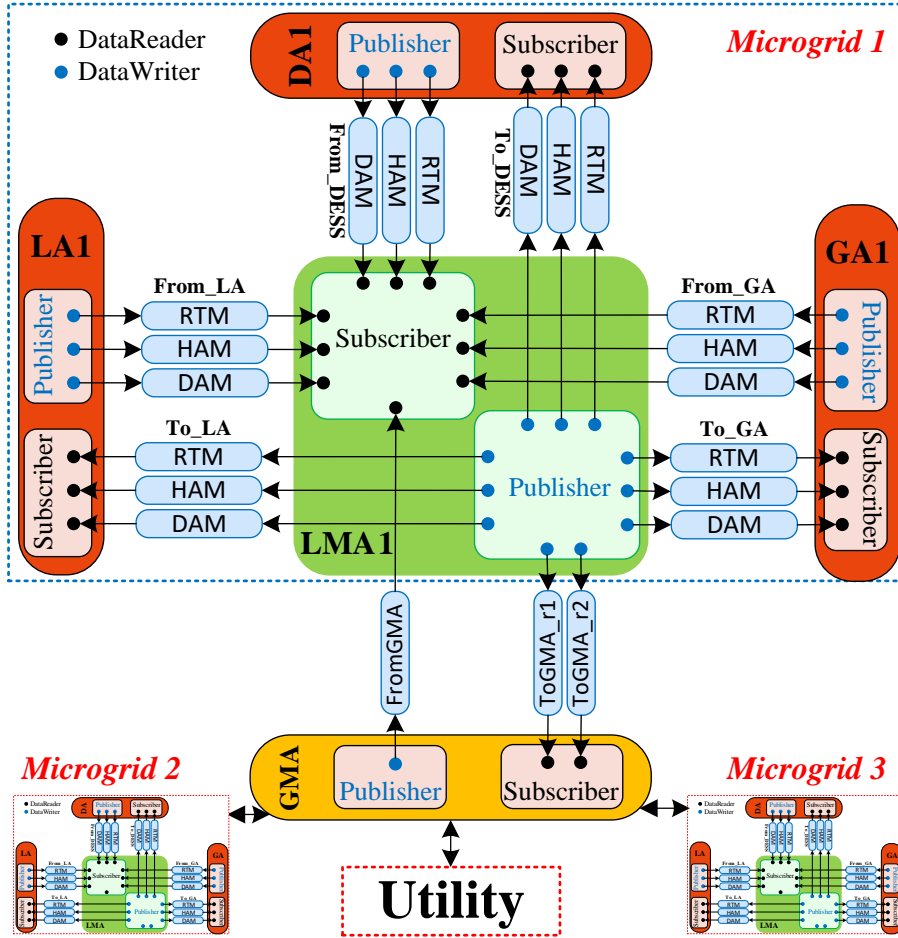


Figure 3.1 DDS Communication framework for the MAS using RTPS.

With the result of the auction, the Load, Generation, and DESS agents are now ready to participate in the Hour Ahead stage. In this stage, they calculate their readiness to participate in the Demand Response program in the hour-ahead market. They then announce their readiness to the appropriate topics. The LMA then subscribes to this information and uses it as an input to its optimization algorithm. The objective of this optimization is to calculate the new set-point for each winning participant. The output of the optimization is communicated back to the Load, Generation, and DESS agents.

With this data, the Load, Generation, and DESS agents are now ready for the Real-time stage, in which they calculate and announce their readiness to participate in the Demand Response program in the real-time market. Inside each microgrid, this data is collected by the LMA, which then runs the optimization for calculating the new set-point for each participant. This time, the output of the optimization applied by each of the three LMAs is used by the GMA to decide on the amount of power needed from each microgrid, if any. The decision of the GMA is then communicated to the LMAs, which again runs an optimization to arrive at the final set-point of each market participant. Finally, the LMAs convey the new set-points to the Load, Generation, and DESS agents and their final payment.

The agents were simulated on separate networks to emulate the real-world environment, in which each agent will be embedded at a remote location. The LMAs of all three microgrids were simulated on a computer connected to the FIU Smart Grid Testbed network. In addition, the GMA was simulated on another computer connected to that same network. The Load agents of all the microgrids were simulated on one computer. The Generation agents of all microgrids were simulated on another computer, which was connected to a different network. Additionally, the DESS agents were simulated on a different computer, also connected to a different internet network. The data was communicated over WAN by means of an HTTP-to-DDS translation capability service called the “web-integration service”.

In each microgrid, and for each of the Load, Generation, and DESS agents, six topics are identified. As can be seen in Figure 3.1, three of those are used for the data to be sent

from the agent, and the other three are used for the data to be sent to the agent. They are also categorized based on the three stages identified earlier: day ahead market (DAM), hour ahead market (HAM), and real-time market (RTM).

In microgrid 1, for example, the subscriber of the LMA reads the data from the topics that are labelled with “From” and that are associated with each of the Load, Generation, and DESS agents.

The DDS subscriber of the LMA has a data reader for each topic it needs to read from, but for the sake of simplifying the figure, only three data readers are shown. Similarly, the DDS publisher of the LMA has a data writer for each topic it needs to write to.

As can be seen in **Error! Reference source not found.**, the publisher of the Generation Agent writes to the following topics: *From_GA:DAM*, *From_GA:HAM*, and *From_GA:RTM*. The subscriber reads from: *To_GA:DAM*, *To_GA:HAM*, and *To_GA:RTM*.

The publisher of the Load Agent writes to the following topics: *From_LA:DAM*, *From_LA:HAM*, and *From_LA:RTM*. The subscriber reads from: *To_LA:DAM*, *To_LA:HAM*, and *To_LA:RTM*.

The publisher of the DESS Agent writes to the following topics: *From_DESS:DAM*, *From_DESS:HAM*, and *From_DESS:RTM*. The subscriber reads from: *To_DESS:DAM*, *To_DESS:HAM*, and *To_DESS:RTM*.

The publisher of the Local Market Agent writes to the following topics: *To_GA:DAM*, *To_GA:HAM*, *To_GA:RTM*, *To_LA:DAM*, *To_LA:HAM*, *To_LA:RTM*, *To_DESS:DAM*,

To_DESS:HAM, To_DESS:RTM, ToGMA_r1, and ToGMA_r2. The subscriber reads from: *From_GA:DAM, From_GA:HAM, From_GA:RTM, From_LA:DAM, From_LA:HAM, From_LA:RTM, From_DESS:DAM, From_DESS:HAM, From_DESS:RTM,* and *FromGMA.*

The publisher of the General Market Agent (GMA) writes to the topic *FromGMA*. The subscriber reads from: *ToGMA_r1* and *ToGMA_r2*.

The Load, Generation, DESS, and LMA agents, their associated topics, and the communication among them is replicated in each microgrid in the system. It is also important to note that the use of the publish-subscribe communication protocol has greatly facilitated the scalability of the system.

3.5 Application 2: A Decentralized Multi-Agent System for Management of En Route Electric Vehicles

In the specific application of managing a large fleet of EVs to organize their connection to the grid, a need arises to route those EVs to the most suitable EVCSs in their vicinity. A decentralized DDS-based MAS that links the EVs and EVCSs in real-time, while the EVs are en route, is presented.

Deploying a MAS for this purpose will help enhance the smart grid operation by providing benefits to all the involved entities: the EV, the EVCSs, and the grid. The EV will be routed to the most suitable EVCS according to its status and preferences. On the other hand, the EVCS will be able to enhance the dispatch of its energy resources, whether from generators, renewable energy resources, or energy storage systems, thus reinforcing

the overall purpose of serving the incoming vehicles requesting charge. As for the provided benefit to the operation of the grid, the extra awareness and visualization of the system status ultimately helps in achieving better control at both secondary and tertiary levels. While this section presents an additional example of using the DDS middleware for building an MAS for the application of routing of EVs to EVCSs, chapters 4 and 5 present an in-depth analysis that focuses on a raised hypothesis, the data sharing scheme of the MAS, and use cases presented to validate the hypothesis.

3.5.1 Application Description

The developed MAS is deployed into a rerouting plan of the en route EVs to the most suitable EVCSs based on price, State of Charge (SoC), and distance and time considerations.

The presented MAS framework consists of an EV agent, an EVCS agent, and a higher-level agent to manage the interactions between the different entities involved, as shown in Figure 3.2. Each of those agents is designed to share only the needed information to make the objective achievable.

When the vehicle's driver requests a charge or when the EV agent is aware that the SoC is low, the EV agent, which resides in the EV, takes an array of parameters as input, processes it through a pre-designed controller, and draws a conclusion on the most suitable EVCS to head to and charge the vehicle.

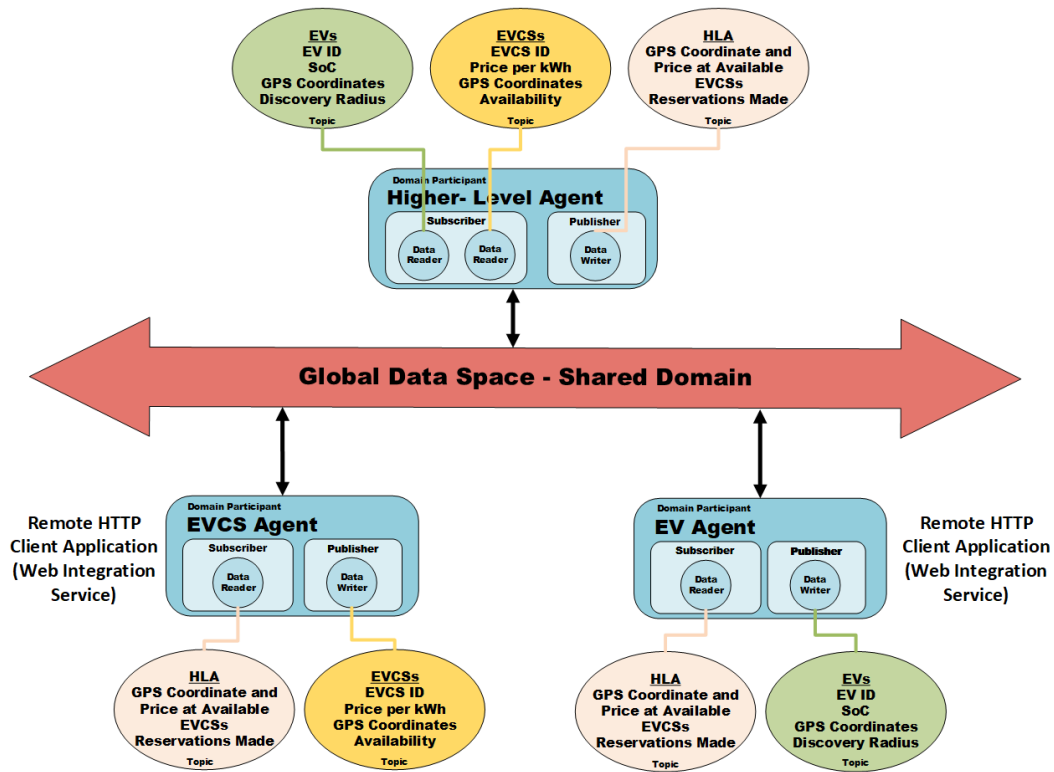


Figure 3.2 DDS-Based Decentralized MAS Configuration for the Application of the Management of En Route Electric Vehicles

3.5.2 System Description

As can be seen from Figure 3.2, the application involves a global data space which is shared between all agents. For the EV agent and the EVCS agent, which are at remote geographically distributed locations, to contribute to this shared global data space, they publish and subscribe to the information as HTTP client applications. An RTI Connexx DDS-based web-integration service is used to translate the contributed and retrieved information from HTTP format to DDS format and vice versa. Three topics are created for this application: *EVs* (in green), *EVCSs* (in yellow), and *HLA* (in pink). Each EV publishes its data to the topic *EVs*. Similarly, each EVCS publishes its data to the topic *EVCSs*. The higher-level agent subscribes to these two topics and sorts the data according to the EVs' and EVCSs'

unique IDs. It then publishes the data required by the EV agent to the topic *HLA*. The EV agent subscribes to topic *HLA* and executes its control logic accordingly.

It then issues a recommendation to the driver or takes the decision and changes route, in the case of an autonomous vehicle. In the design of the EV agent, the array of parameters considered is: the vehicle's SoC, the distance and time to the EVCSs that show readiness for service, and the price in cents per kWh for charging the vehicle in each of those EVCSs. In addition, the EV agent needs to share some of its information with other agents before it is able to receive the needed information about the available EVCSs. Those parameters that the EV agent needs to send are: the unique EV ID, the current EV's GPS coordinates, and a discovery radius to search for available EVCSs around it.

To get the array of information which is needed for the conclusion to be made ready, the other two aforementioned agents are involved in this strongly-correlated message-sharing system.

Each EVCS will have an EVCS agent interfacing with its main CC for obtaining information and sharing it with the proper MAS entities. This agent also receives messages to schedule charging for incoming vehicles and thus updates its state. This agent is designed to share the EVCS ID, the current price per kWh of charging, the GPS coordinates of the EVCS, and the current availability of chargers in this particular EVCS.

As for the higher-level agent, it is designed to receive the GPS coordinates shared by the EV agents and the EVCS agents, in addition to the discovery radius shared by the EV agent. It then searches for the EVCSs that are within this radius. Once it has found a number

of EVCSs in the discovery radius, it looks at which EVCS agents have shared their availability and willingness to accept incoming EVs to use their charging infrastructure. It then shares the GPS coordinates of those EVCSs, together with the price of charging at each of them, with the agent residing in the vehicle requesting a charge. The EV agent then has the array of information ready and can process it to draw a conclusion on the most suitable EVCS to go to. The EV agent's control logic is explained in Chapter 4, and case studies are applied to test the robustness of this on-board module. After the decision is made by the EV agent, a notification is made to the higher-level agent on the EVCS to which it will head. The higher-level agent will inform the EVCS agent of the incoming EV, to reserve the energy and get ready to serve the vehicle upon its arrival.

3.6 Conclusion

In this chapter, a comparison among several messaging middlewares was presented. The DDS middleware was found to be superior to the others under comparison because of supporting many attributes, like relying on a decentralized broker-less architecture, using multicasting with flexibility of transport choice of UDP or TCP, supporting resource discovery, and providing a wide variety of QoS policies that help in monitoring moving assets over wireless networks. Two MASs using this middleware in smart grid applications were presented; one for the application of energy and power markets in a multi-microgrid environment, and the other for the application of the management of en route EVs. In each application, the design of the system was presented, along with the individual agents, topics, and the messaging scheme followed in each MAS.

Chapter 4 Intelligent Fuzzy Logic Based On-board Module for Guiding the Electric Vehicles to Charging Stations

4.1 Introduction

When addressing the application of public charging of EVs, it is important to look at the logistics of how EVs are guided to public EVCSs. That is because this guidance not only provides a needed level of convenience to EV owners but also can be used for rerouting purposes, when this module participates in a bigger connectivity platform.

For those reasons, an intelligent fuzzy logic (FL) based on-board module is developed to guide EVs to EVCSs that have unoccupied chargers at the time the driver requests a public charging session. The motivations behind developing this automated on-board module, as it relates to the solutions provided in this dissertation to the public charging, are discussed first. Then, a brief overview on FL is presented, followed by the details of the design of the fuzzy logic module (FLM) presented here. The module's platform is then explained, with the results of four case studies to test the module.

4.2 Motivations

With the present technologies, to find a public charger when in need, the EV owner would have to first log onto an online tool that would show all the EVCSs on a map. Some examples of those services are the Plugshare app [23], Open Charge Map service [24], ChargeHub website [25], and Chargemap app [26]. Furthermore, electric vehicle manufacturers and electric vehicle service providers (EVSP)s like Tesla, FLO, and Chargepoint offer their own maps for customers. Figure 4.1 shows a screenshot of a map

from the Plugshare website, as an example of those services. To decide on which public EVCS to head to, the driver would then assess the available alternatives to choose the optimal decision for his/her EV's welfare and his/her time and other preferences. Despite this assessment, the chargers located by the EV driver might be occupied by the time they arrive there. To address this, an automated on-board module that operates as a decision-support module for the EV was necessary. It processes all the available alternatives, and raises a recommendation for the EV driver as to which EVCS to go to.

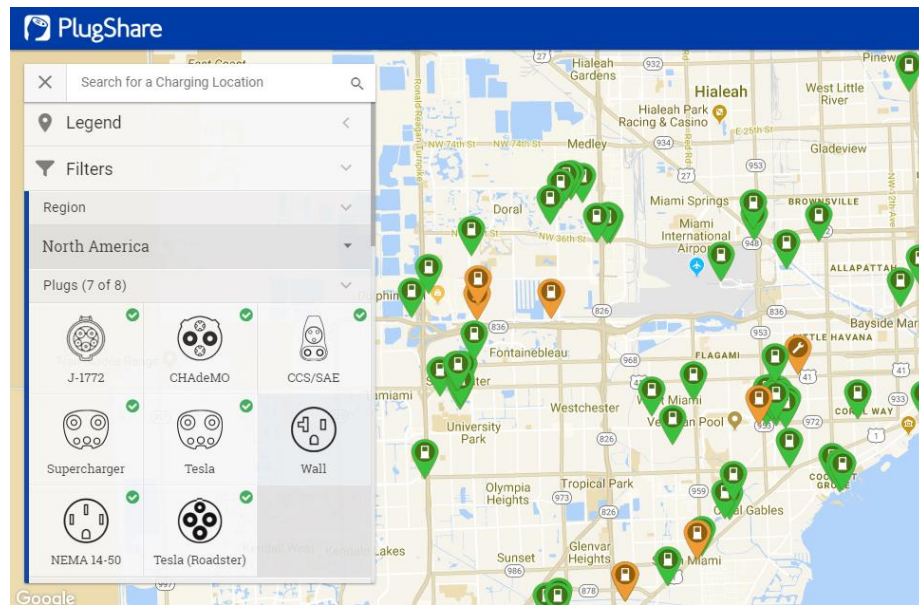


Figure 4.1 A screenshot from one of the services that help find public charging stations.

This module is used in a large-scale connectivity platform encompassing EVCSs and head-end CCs to provide benefits to all involved entities in the application of public charging. This large-scale connectivity will be introduced in chapter 5.

4.3 Fuzzy Logic

The main concept in FL is that an object does not belong to a single set totally; instead, it is allowed partial belonging to different subsets of the universal set. Partial belonging to a set can be described numerically by a membership function which assumes values between 0 and 1. In other words, membership functions are the building blocks of the fuzzy set theory.

In fuzzification, each piece of input data is converted to degrees of membership by a lookup in one or more several membership functions [27]. When all rules are evaluated, the output of the FLM is defuzzified to obtain a single crisp value that represents the action to be taken in controlling the process.

4.4 Design of the On-board Module

This on-board module is a fuzzy controller based on the Sugeno-like model. It takes a Feature Vector (FV) of each EVCS, in addition to the EV battery's SoC, as inputs. It then processes those and outputs a recommendation on the most suitable EVCS for the EV to head to and charge at. A FV of the EVCS consists of the price in cents per kWh of charging in that particular EVCS, the distance from the current location of the vehicle to the EVCS, and the time needed to reach it.

One EVCS can have more than one FV, because the latter corresponds to how the EVCS is perceived by the EV. Given that each EV has different GPS coordinates, the dtCS and ttCS parameters of the FV will be different for the same EVCS from the perspective of two different EVs, or more. Figure 4.2 shows a simple map with 2 EVs and 3 EVCSs, and the driving route from each EV to each EVCS. The differentiation of the FVs

corresponding to those 3 EVCSs as perceived by the 2 EVs is depicted in Figure 4.3. This figure illustrates the FVs of the 3 distinct EVCSs: EVCS1, EVCS2, and EVCS3 as perceived by 2 distinct EVs: EV1 and EV2. Each FV is illustrated above the pointer between the EV and the EVCS.

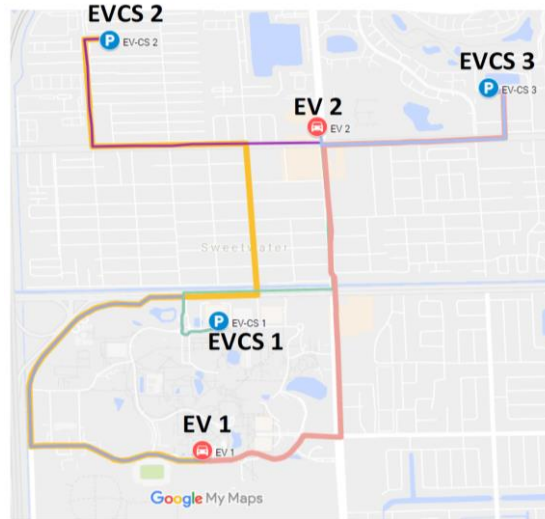


Figure 4.2 Map showing the driving routes between 2 EVs and 3 EVCSs.

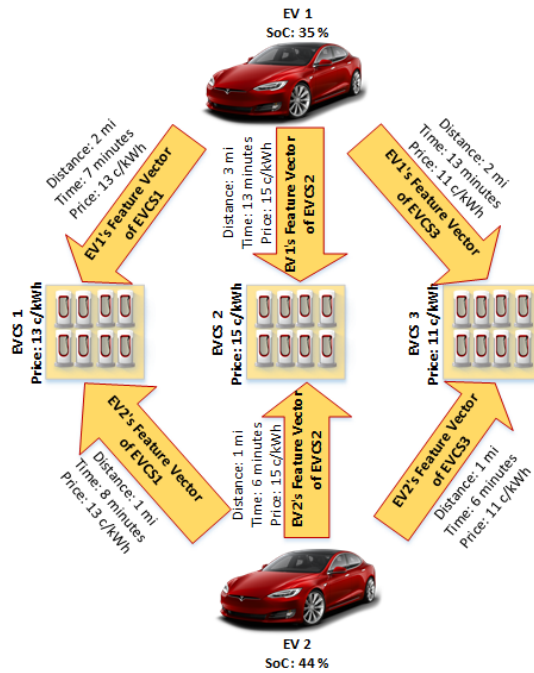


Figure 4.3 Feature vectors of 3 distinct EVCSs as perceived by 2 distinct EVs.

The on-board module is designed to obtain certain characteristics of the EVCSs that it needs to assess by issuing HTTP requests to a global data space where the information of those EVCSs reside. The needed characteristics to be obtained by the on-board module about the EVCSs include the GPS locations, the availability, and the price of charging at those EVCSs.

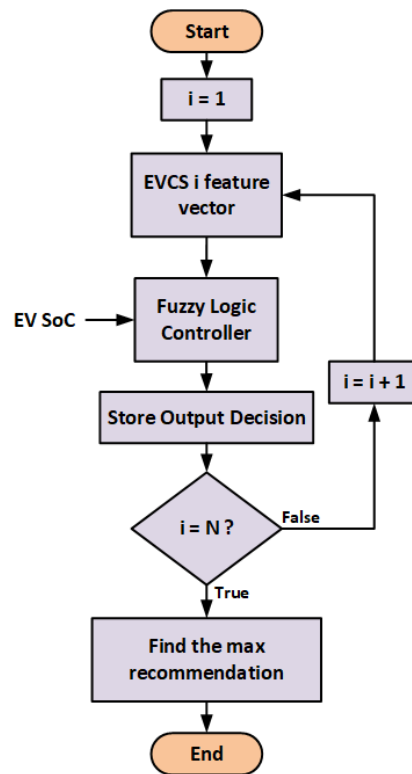


Figure 4.4 Flowchart of EV Agent Controller Logic.

The EVCSs' FVs received by the EV agent are processed as shown in the flowchart of Figure 4.4. In each iteration from one to N, where N is the total number of EVCSs discovered, the FLM produces a percentage recommendation representing how likely this EVCS will satisfy the vehicle's need. The decision of the fuzzy controller is based on several rule surfaces composed of a set of 72 logic rules. The FL rules of this on-board

module for recommending EVCSs in response to public charging requests are given in Appendix 1. The rules are defined for every combination of levels of the four input variables. The output recommendation levels for each set of inputs are values of 0%, 25%, 50%, 75%, and 100% for “do not recommend,” “poorly recommend,” “ok,” “recommend,” and “highly recommend,” respectively.

When the EV module needs to make a decision, it considers four inputs: the battery’s state of charge (SoC), the distance to be driven to the EVCS (dtCS), the time needed to arrive at the EVCS (ttCS), and the price of charging at that EVCS (pCS). In fuzzification, each piece of input data is converted to degrees of membership by a lookup in one or more several membership functions. Each input here (SoC, dtCS, ttCS, and pCS) is considered to have three triangular membership functions (Low, Medium, and High). For an input x , equation (4-1) is used to evaluate the membership to a subset. This equation represents a triangular membership function.

$$f(x) = \max\left(\min\left(\frac{x-a}{b-a}, \frac{c-x}{c-b}\right), 0\right) \quad (4-1)$$

where a , b , and c , are the vertices of the triangular membership function.

Initially, the assumed low (L), medium (M), and high (H) range categories of the input variables are:

SoC:	L = [0, 0.4];	M = [0.3, 0.7];	H = [0.6, 1].
dtCS:	L = [0, 4];	M = [1, 9];	H = [6, 10].
ttCS:	L = [0, 8];	M = [2, 20];	H = [8, 18].
pCS:	L = [6, 14];	M = [12, 18];	H = [16, 24].

It is noteworthy that the ranges of the first three inputs (SoC, dtCS, and ttCS) all start from 0. This means that for the Low (blue) membership function: $a = 0$ and $b = 0$ at the same time. This would lead to a 0 in the denominator of $f(x)$ at any instance of an input. To avoid this, a value is selected for a that is less than zero. We set $a = -c$ to achieve symmetry around the origin without affecting the calculation. The same approach is applied to the high membership function of the SoC input. The a , b , and c parameters of each of the four inputs are presented in Table 4-1 and in Figure 4.5. The exceptions discussed here are highlighted in Table 4-1.

Table 4-1 Fuzzy Logic Controller Parameters.

	SoC (%) /100			dtCS (miles)			ttCS (min)			pCS (c/kWh)		
	L	M	H	L	M	H	L	M	H	L	M	H
a	-4	.3	.6	-4	1	6	-8	2	8	6	12	16
b	0	.5	1	0	5	10	0	10	18	10	15	20
c	.4	.7	1.4	4	9	14	8	20	28	14	18	24

*L: low; M: medium; H: high

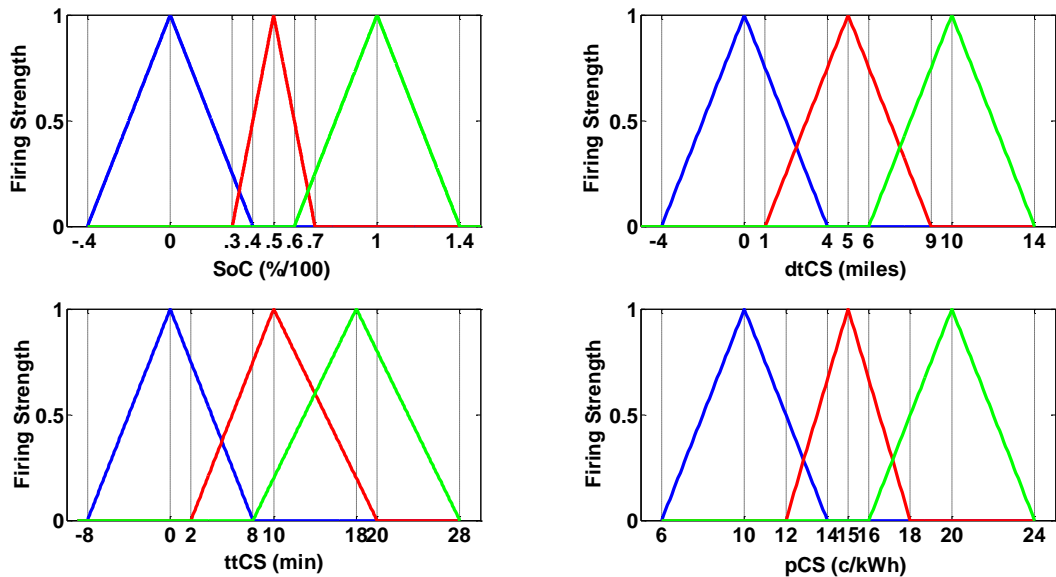


Figure 4.5 Triangular membership functions of the 4 inputs to the fuzzy logic controller.

Figure 4.6 (a) shows an example of the 3 overlapping triangular membership functions of the SoC input. Figure 4.6 (b) shows each membership function: low (blue), medium (red), and high (green), independently plotted, with the vertices of each labelled.

After the FVs are processed through the membership functions, the output of the FLM is defuzzified based on the weighted sum Sugeno technique, following equation (4-2):

$$output = \frac{\sum w_i x_i}{\sum w_i} \quad (4-2)$$

where w_i is the i^{th} rule firing strength and x_i is the defined decision corresponding to that rule. The output of the controller is a crisp value corresponding to the recommendation of going to EVCS x .

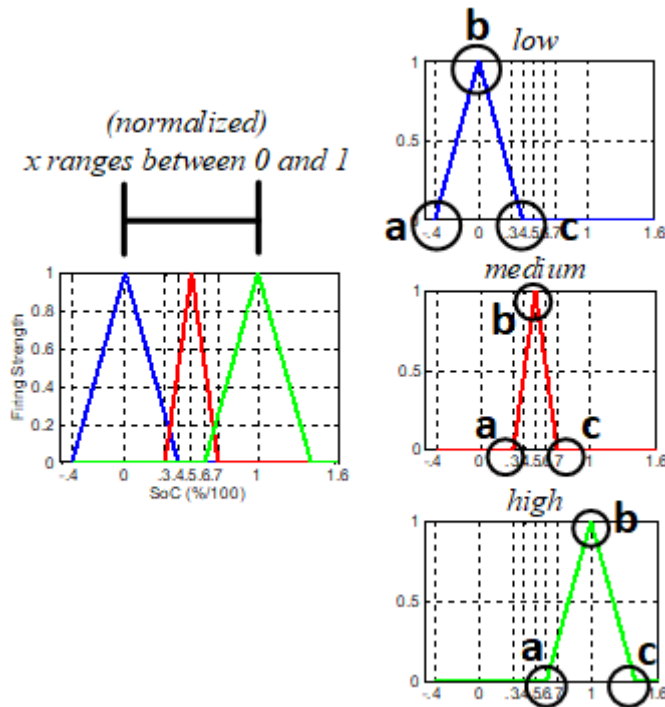


Figure 4.6 (a) triangular membership functions of the SoC input, (b) each membership function: low (blue), medium (red), and high (green), independently plotted.

The on-board module is designed to assess all the alternatives of the EVCSs, raising a recommendation on each one, and issue the highest achieved recommendation to the EV driver or, in case of a self-driving vehicle, drive there.

To obtain the dtCS and ttCS corresponding to the individual EVCSs in each FV, the traffic status at the time of the request is considered. In this work, this is done by means of the Google Maps Distance Matrix API [28]. This tool provides a way through HTTP to obtain the distance and time of driving between two points. It is used here to obtain the driving distance and time between the EV and the individual EVCSs. When the request for charging is issued by the driver, the GPS coordinates of the EV are obtained by means of a GPS module. This location and the retrieved GPS coordinates of the EVCS are put in the HTTP URL of the Distance Matrix API as the origin and destination, respectively. The HTTP request is issued and the response is analyzed to obtain the distance in miles and the time in minutes to arrive at the individual EVCSs. A screenshot from the log file showing the distance in miles and time in minutes from an EV to an EVCS is shown in Figure 4.7.

```
abla@abla-OptiPlex-9020:~/Desktop/GetDuration/objs/x64Linux3gcc4.8.2$ ./url_V1_publisher
RTI Data Distribution Service Research License issued to Florida International University -
Use only.
Expires on 17-nov-2017 See www.rti.com for more information.
Writing urlFile, count 0
{
  "destination_addresses" : [ "E Campus Cir, Miami, FL 33174, USA" ],
  "origin_addresses" : [ "755 NW 72nd Ave, Miami, FL 33126, USA" ],
  "rows" : [
    {
      "elements" : [
        {
          "distance" : {
            "text" : "7.3 mi",
            "value" : 11746
          },
          "duration" : {
            "text" : "14 mins",
            "value" : 851
          },
          "status" : "OK"
        }
      ]
    }
  ],
  "status" : "OK"
}
```

Figure 4.7 Snapshot from the log file showing the distance in miles and time in minutes from an EV to an EVCS

4.5 Module's platform

The module is developed as an HTTP client application that is cross-compiled to be embedded onto an ARM-processor microcontroller that is interfaced with a commercial serial GPS module. Figure 4.8 shows a picture of the testing module. This module is configured to connect to a 4G-LTE hotspot of the connected vehicle that it was tested in. To emulate the input needed from the EV, the SoC was hardcoded in the EV Agents.



Figure 4.8 Testing module board interfaced with commercial GPS module.

4.6 Case Studies

A case study in which four vehicles are routed to different EVCSs within their vicinity in Miami-Dade County. All vehicles and EVCS locations were added to the map in vital public locations. Figure 4.9 illustrates a map showing the locations of the EVs and the EVCSs in those case studies.

Each of the four vehicles shown on the map was assumed to have a certain SoC, shown in Table 4-2, and each EVCS was assumed to have a certain price of charging. Those EVCSs are assumed to have unoccupied chargers that are ready to service incoming EVs. The assumed SoC and prices were assigned to test the trustworthiness of the EV agent controller to give the best recommendation. The results are shown in Table 4-2.

Table 4-2 Case Studies Results

EVCS	Price (c/kWh)	EV 1			EV 2			EV 3			EV 4		
		Distance (mi)	Time (min)	Recommendation (%)	Distance (mi)	Time (min)	Recommendation (%)	Distance (mi)	Time (min)	Recommendation (%)	Distance (mi)	Time (min)	Recommendation (%)
1	19	7.2	16	8.47	5.9	19	0	3.3	11	25	5.4	15	50
2	15	2.1	10	59.77	1.7	9	63.33	5.1	15	50	7.2	17	0
3	13	1.6	10	71.79	4.4	12	35.82	7.3	14	57.21	9.4	16	0
4	10	0.9	6	89.98	2.5	13	58.33	4.6	16	75	7.2	17	0
5	11	1.5	9	79.3	2.9	14	50.83	4.9	16	75	7.4	16	0
6	17	4.9	10	22.86	3.6	14	15.15	1.9	10	49.47	5.1	12	50

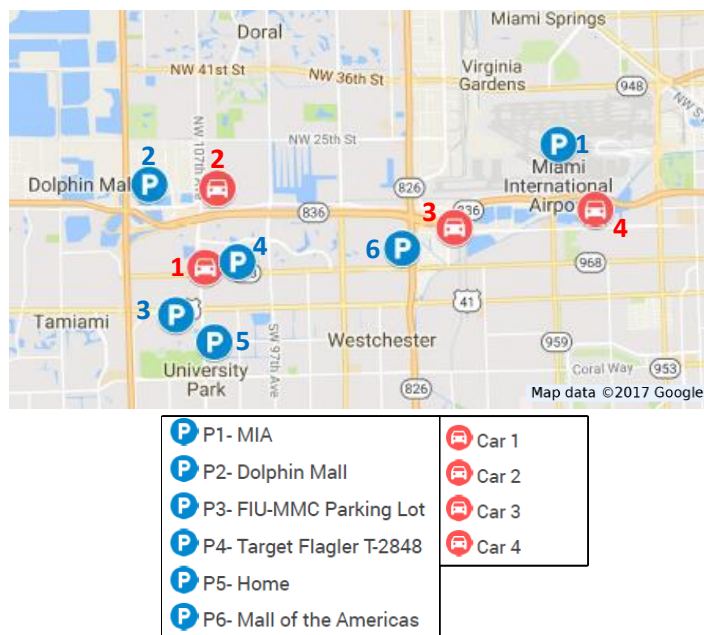


Figure 4.9 EV and EVCSs assumed locations in the case studies.

As reported in Table 4-2:

- EV 1 had an SoC of 65%. The highest recommendation was to EVCS 4, the EVCS with the lowest price and the closest in terms of distance and time.
- In the case of EV 2, the controller’s highest recommendation was to EVCS 2, the EVCS closest to the EV in terms of distance and time, although it was not the

cheapest, with a price of 15 cents per kWh. This is plausible, as the SoC of this EV was 45%, which necessitates charging as soon as possible.

- As for EV 3, which had an SoC of 77% at the time of issuing the charging request, the controller's highest recommendation was to charge in EVCS 4, the EVCS that offers the cheapest service, although it wasn't the closest. This is because the vehicle's SoC wasn't critical.
- EV 4 had a very low SoC of 21%, which led the controller to route it to the closest EVCS, no matter the price.

It is noteworthy to mention that in the cases of EV 3 and EV 4, the controller produced the same value of the recommendation to 2 EVCSs (EVCS 4 and EVCS 5 for EV 3, and EVCS 1 and EVCS 6 for EV 2) because there was a very small difference in the FVs of those EVCSs.

4.7 Summary

In this chapter, the motivations for developing an automated and intelligent on-board module, as it relates to the solutions provided in this dissertation to the application of public charging, are first discussed. The details of its design, in addition to case studies where this module proves valuable were presented. The system's case study results showed that the designed on-board module gives trustworthy rerouting recommendations to the drivers.

This type of guidance not only provides convenience to EV owners when in need of a public charging session, but also can be used for purposes that contribute to the welfare of the power system when this module participates in a bigger connectivity platform. This

other benefit is addressed in a system introduced in a Bilateral Decision Support System that encompasses EVs and power grid control centers. The details of this system are presented in chapter 5.

Chapter 5 A Bilateral Decision Support Platform for Public Charging of Connected Electric Vehicles

5.1 Introduction

To meet the new deadlines set by many governments for automakers to end the sale of new internal combustion engine vehicles, giant vehicle manufacturers have recently announced their commitment to the all-electric vision by 2030. Also, global companies have joined an international coalition initiative, EV100, in which they commit to transitioning their owned large fleet of internal combustion engine vehicles to an all-Electric Vehicle fleet and installing EVSE at their premises. Tesla, one of the largest automakers and EVSPs, has announced it is building EVCSs with tens of superchargers (SC)s [29], with the largest being a 50-stall station in Shanghai and others in Beijing and the USA. In addition, it is building Gigafactories specialized in manufacturing lithium-ion batteries to “supply enough batteries to support Tesla’s projected vehicle demand [30].” These infrastructure developments reflect a mass rollout of EV uptake, partially in response to government incentives. At this stage, there is a pressing need for presenting solutions to set the rules that seamlessly organize this expansion and its effect on the power system.

Fast charging and extreme fast charging [31] of EVs will affect the reliability of the power system as this large number of connected EVs will act as a bulk load that introduces a significant stochasticity in terms of their distribution upon public EVCSs.

Table 5-1 Literature Review on Vehicle Routing Problems of EVs

Ref. #	Offline Planning	Online Routing	Power Network			Considering Real-time Traffic	EV Owner Benefit	Comm. Infrastructure
			OPA	RTP	PS			
[32]	x	✓	x	✓	✓	✓	✓	x
[33]	✓	x	x	x	✓	x	✓	x
[34]	✓	x	x	x	x	x	✓	x
[35]	x	✓	✓	x	x	x	✓	x
[36]	x	✓	x	✓	x	✓	✓	x
[37]	x	✓	x	x	x	✓	✓	x
[38]	✓	x	x	✓	x	✓	✓	x
[39]	x	✓	x	x	x	✓	✓	x

* OPA: Optimal Power allocation

* RTP: Real-Time Pricing

* PS: Peak Shaving

In fact, there are several works in literature that address the impact of the large scale penetration of EVs on the reliability of the power grid [40], [41], [42]. Studies on the redistribution of this large fleet of EVs onto the EVCSs [32] have proven enhancements in system status and reduced values of losses. For this reason, the Vehicle Routing Problem (VRP) which has been well established in the literature for fuel-based vehicles, is being revisited with EVs. In fact, the limitation on their mileage range and frequent recharging needs make legacy VRP solutions unsuitable for battery-powered EVs. In Table 5-1, we summarize a review on some of the works in literature involving VRP, showing what aspects or combinations of them each paper addresses.

In [32], a hierarchical game approach is followed. It comprises a competition among the EVCSs and an evolutionary algorithm for the EV strategies in choosing the EVCSs. Pricing strategies obtained from a non-cooperative game are used to attract EVs to charge at off-peak hours. Hence the work applies a real-time pricing (RTP) strategy to achieve peak shaving (PS). The authors indicate the use of an EV navigation system, but do not

address the requirements of the communication infrastructure. The work in [33] translates the VRP problem into a traveling salesman problem, with the main objective of optimizing the EV route before it starts its trip. The impact of EV charging on the power distribution system is studied under the electricity market time-of-use (TOU) price, with the objective of achieving PS. This is an offline VRP of transport distribution EVs. The authors do not tackle the communication means for their proposed solution to the VRP. In [34], a differential evolution algorithm for solving a VRP is presented. The effect on the power system is not considered in this solution to the VRP, and the communication infrastructure that is needed for successfully achieving this VRP is not tackled. The work in [35] proposes an optimal power allocation (OPA) scheme that allocates power from the grid to energy storage systems at a network of EVCSs, as well as applies routing to customers to the EVCSs based on the decision of a central authority. Furthermore, the authors discuss the need for quantifying the impact of communications on the network's operations, but do not present the communication protocols and means that achieve their VRP. In [36], a two-stage optimization problem is used to solve the optimal power flow and the VRP. The approach followed for the VRP is a least cost routing strategy that minimizes the transportation cost for the EVs. This approach uses the manipulated locational margin prices for applying an RTP incentive strategy. The two-way communication between the EVs and the EVCSs is referred to, but the communication infrastructure needed for the achieving this VRP is not presented. The approach to solving the VRP in [37] is an implementation of a software agent embedded in the navigation system of the EV. Delays at EVCSs are minimized by means of the communication between this agent and the other EV agents. The designed embedded agent is based on probabilistic information. It

optimizes the policy of the EV using the intentions of other EVs. This solution to the VRP is solely concerned with minimizing the delays at EVCSs, and it does not consider the power system's status. Moreover, the communication system and protocols to achieve this solution are not presented. Dynamic location-based electricity pricing is considered in [38] for the EV owner to pick a travel path. The use of the RTP was to show the importance of considering the coupled operation of the power system and the transportation system when solving a VRP. The scheme to solve the VRP is based on finding optimal paths on an extended transportation graph. The problem formulated in [38] does not address the communication architecture needed to deploy the proposed system. In [39], a delegate MAS, which is a software representation of the real environment, is used to route vehicles to fast charging stations that are along their route. EV agents continuously communicate their intentions to EVCS agents through the presented delegate MAS approach. Reference [39] did not take into account the effect of the routing algorithm on the power system network. Also, authors in [39] did not discuss the communication network and protocol requirements to implement their system.

As discussed and as indicated in Table 5-1, none of the aforementioned papers address the communication requirements for the successful implementation of the routing systems and the necessary protocols. There remains a strong need for a correlated automated communication-based solution that provides a win-win situation by supporting the two decisions of the EV and the power system simultaneously. With this gap in mind, a detailed hierarchical MAS is proposed, with a communication scheme that reroutes EVs to EVCSs for the bilateral benefit of the EVs and the power grid. The platform is a bilateral decision

support system (BDSS), with the two sides being the EV and the power grid. In the context of this BDSS, the city is recognized as a collection of discrete geographical areas, each called a virtual block (VB), and the agent responsible of management in this area is called the virtual block agent (VBA).

On the EV side of the BDSS, the logic of the on-board module is based on an automated expert system (i.e. fuzzy logic). The contribution on the power system side of the BDSS is in the logic of the mid-level agent, the VBA. The proposed logic of the VBA is a novel price-based strategy that aims to redistribute the EVs to meet power set points while satisfying the EVs' preferences. The building block of this strategy is FL based as well. The benefit to the EVCSs is considered implicitly because the EVCSs communicate their availability, every time it is changed. The logic of all the involved participants are correlated by means of the proposed MAS.

Equally important is the fact that the BDSS presented in this chapter is achieved by means of a communication model and scheme that is designed and hardware-tested. The effectiveness of the proposed framework and the credibility of using the communication middleware and means are experimentally verified on a group of connected vehicles communicating with a higher-end server, as will be shown later in the results. This is important as the communication requirements and the deployed system imposes important constraints that need to be studied. The effectiveness of the developed approach is strictly contingent on the deployable communication system that helps achieve it. This is an important contribution of the work presented in this chapter to the literature on VRPs for EVs. Test results show that the implemented agents transmit and receive information

complying with the aims of the framework, and that the system realizes all the functions required and works stably in real-time.

5.2 Need and Scope

An EVSP is a provider of an infrastructure network of publicly accessible EVCSs, each involving several chargers, known as EVSE, and managed by an EMU located at the EVCS's premises, as depicted in Figure 5.1. Some EVSPs might be regulated by utilities or Energy Service Providers (ESPs), but are not necessarily that way. And one city might encompass several EVSP networks. The ESPs can coordinate with control centers of the different EVSPs to visualize the status of their managed EVCSs and to achieve the EV redistribution that enhances the power system status, while helping them deploy their resources for maximum gain. A supervisory higher-end management system issues the power set points of the EVCSs in a way that is optimal for the power system. The details of this higher-end management system is presented in chapter 6. An ESP personnel would

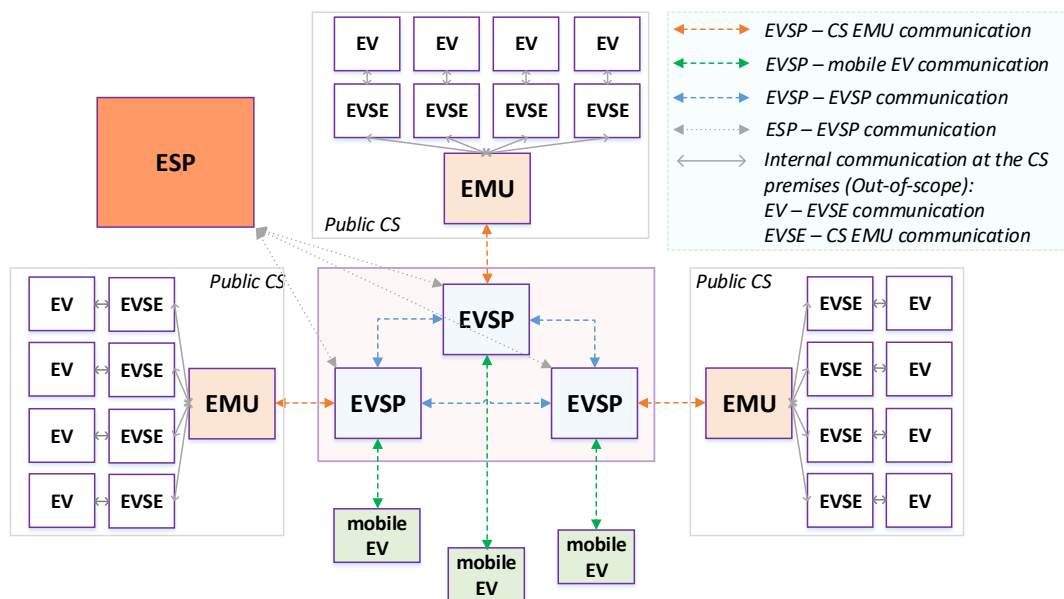


Figure 5.1 Vision - Communication among the involved stakeholders.

need to collect data and negotiate with other ESPs' personnel to make the decisions that will subsequently unfold as benefits to release the stresses from the utilities' power infrastructure, while respecting the individual EVCSs benefits. Those are complex decisions, and would require long intervals for operators to communicate and agree on strategies. For this reason, an intelligent automated MAS is required. As mentioned before, in this work, the city is recognized as a collection of discrete geographical areas, and a higher-end agent is appointed the task of decision-support of the ESP operating in that area. Each of those higher-end agents is designed to have a price-based strategy that would help achieve the optimum distribution of the EVs onto the EVCSs. After applying its strategy, it would then reach out to the EMUs of the EVCSs to notify them of the price change and to the geo-distributed EVs requesting charge to convey to them the new prices. The on-board module developed and presented in chapter 4 would then respond by issuing a recommendation to the EV driver on which EVCS to go to.

The vision is to have the stakeholders, mainly the ESPs, the EVSPs, the EV owners, and the manufacturers of EVs, cooperate to deploy this correlated and all-inclusive framework to trade the unilateral discriminatory benefits with the combined benefit of all. At the heart of such frameworks lies information and communication technologies to support, control, and manage energy transfer between vehicles and the power grid. Figure 5.1 depicts a representation of the communication links among those stakeholders to facilitate such a framework. The communication needs of this framework were discussed

in chapter 2, and the choice of the middleware and used protocols were presented and justified in chapter 3.

5.3 Model and Communication Scheme

The proposed framework is devised in the form of a decentralized hierarchical MAS. Each EV and EVCS is equipped with an intelligent agent. The EV agent is the on-board module presented in detail in chapter 4. The city in this work is recognized as a collection of discrete geographical areas, here called VBs. The higher-end agent that is appointed the task of decision-support of the ESP for each VB is the VBA. These agents, shown in red and blue circles respectively, on the map in the first (green) layer of VBs in Figure 5.2, interact with a VBA, in the second (blue) layer, responsible for managing all charging requests within their VB, and with a higher-level agent (HLA) in the third (purple) layer that reaches out to all VBAs.

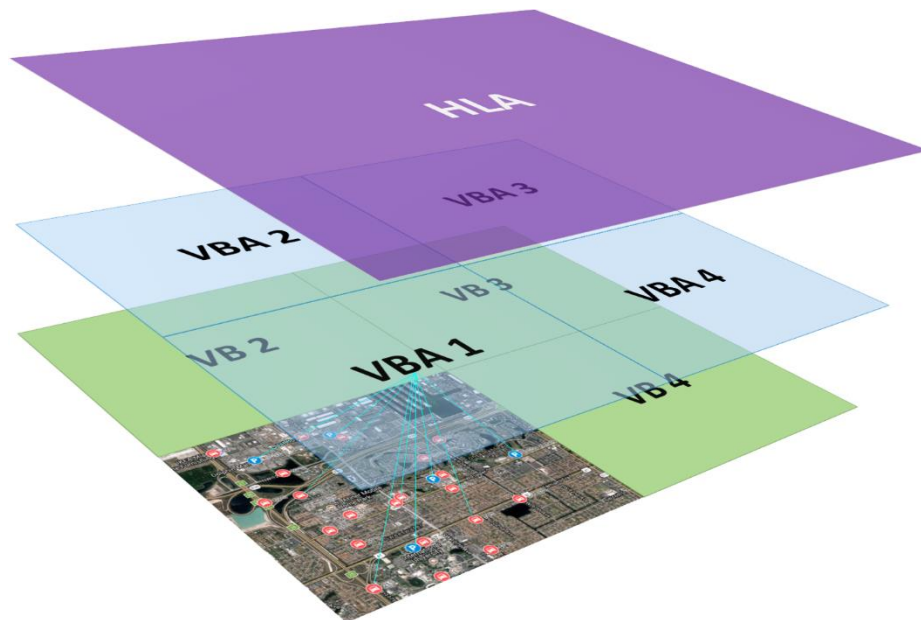
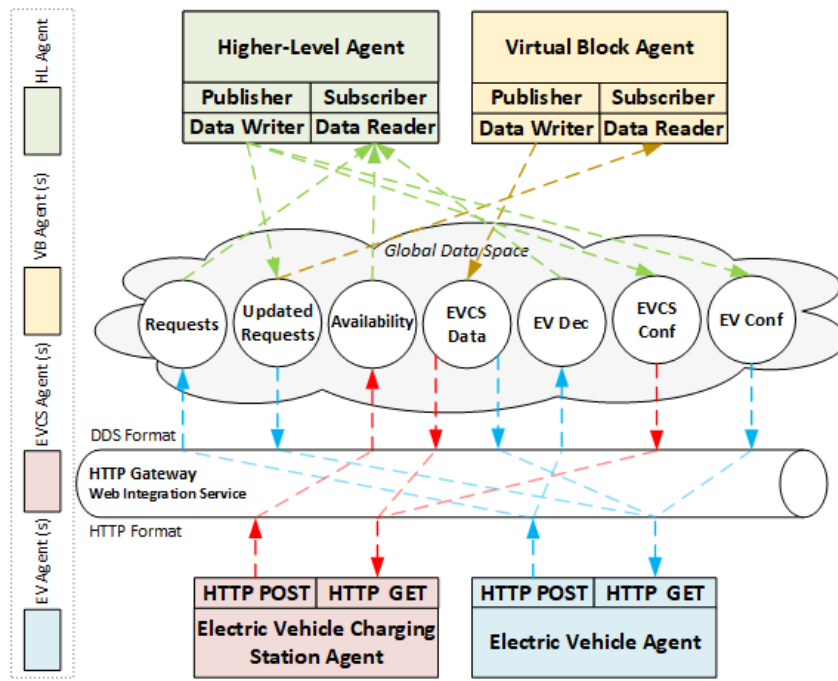
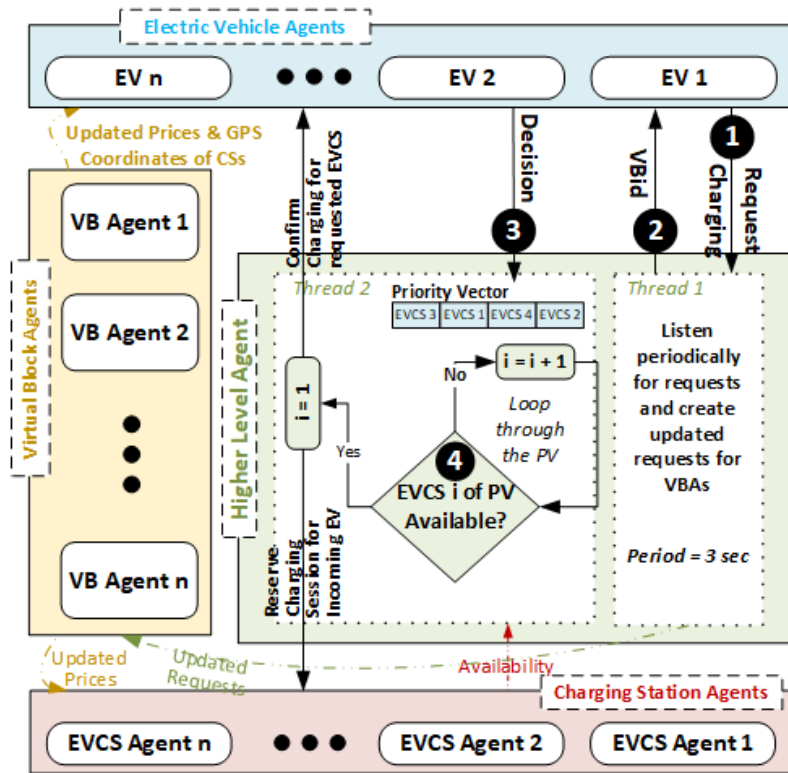


Figure 5.2 Hierarchical architecture of the proposed multi-agent system



(a)



(b)

Figure 5.3 (a) DDS Network Architecture; (b) Flow of Information and Logical Relation between the Agents

Figure 5.3 (a) and (b) are complimentary. Figure 5.3 (a) shows the DDS global dataspace that is accessed by the involved agents. The circles in this dataspace represent the topics. Each topic provides an identifier to some data items within the global data space. This topic has a name, a data-type, and a QoS profile related to the data itself. The arrows connecting the agents to these topics in the dataspace represent the contributions to and the data-retrievals from them by the publishers and subscribers of the involved agents, respectively. Figure 5.3 (b) shows the flow of information between the various agents. There are 4 types of agents: The EV Agents (Blue), the EVCS Agents (Red), the VBAs (Yellow), and the HLA (Green). The steps of communication between the HLA and the EV Agent are numbered 1 to 4 in Figure 5.3 (b) and are explained in more details in this section. Furthermore, Figure 5.4 depicts steps a, b, c, d, e, f that occur between step 2 and step 3 of Figure 5.3.

Step 1: First, the publisher of the EV Agent, issues a charging request by writing to the *Requests* topic. In this request, each EV Agent sends both its GPS coordinates and its EV ID for future communication with it. The subscriber of the HLA periodically retrieves all the requests from the *Requests* topic.

Step 2: The HLA then refers each EV Agent to the VBA responsible for its area. Now that each EV agent is aware of the VBA it is in, its subscriber will retrieve the data from the *EVCS Data* topic that is labelled with that particular VB id. In other words, the EV agent uses a content-based subscription to filter out only the information of interest, i.e. the data of the EVCSs that are in the VB in which the EV lies. The information it retrieves comprises the price of charging and the GPS location of each EVCS. This data is

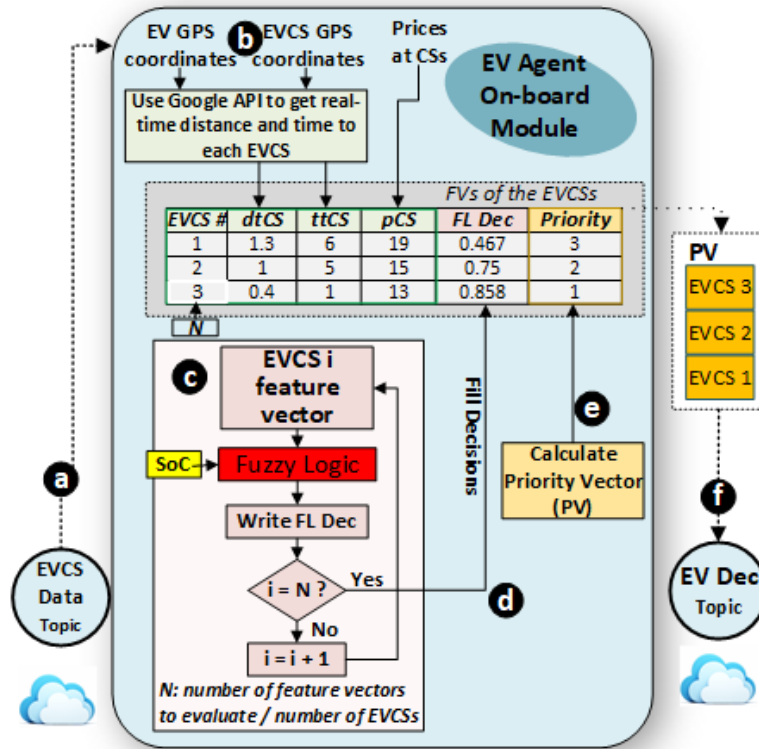


Figure 5.4 EV agent / on-board module, and its interaction with the application's global dataspace

continuously being published to the *EVCS Data* topic by the VBAs, with keyed instances. The VBA's subscriber continuously listens to the *Updated Requests* topic, and uses the VB ID as a content-based filter to filter out only the requests coming from the VB it manages.

It then modifies the price of charging based on its real-time price-based strategy, which will be explained in section 0.

Step 3: As depicted in Figure 5.4, and after receiving all the required data (step a), each EV Agent creates an FV for each EVCS in its VB (step b). The FV comprises 1) the dtCS, 2) the ttCS, and 3) the pCS. The EV Agent processes its FVs through an FLM that also considers the SoC of the battery as a fourth input (step c). It comes up with a priority index

associated with each EVCS on how likely it would recommend this EVCS to the driver (steps d & e).

The logic of this on-board module, the EV Agent, is based on a set of rules that was explained in detail in chapter 4. The EV agent will then publish these priorities in the form of a priority vector to the *EVDec* topic (step f). At this stage, the HLA's subscriber retrieves the decisions of the EV Agents from the *EVDec* topic, as depicted in step 3 of Figure 5.3 (b). The HLA's subscriber also retrieves the information about the availability of chargers and stalls at the EVCSs from the *Availability* topic. The EVCS Agents' publishers periodically publish their status to this topic.

Step 4: For each EV that has published its decision (i.e. its PV), the HLA assesses the first EVCS in the EV's PV decision against the availabilities to evaluate whether a charging session could be granted for this EV at that EVCS or not. If it finds it fulfillable, the HLA confirms to the EV and the corresponding EVCS by publishing the confirmation to the *EVConf* and *EVCSConf* topics, respectively. However, if the HLA finds that the requested EVCS cannot accommodate more charging sessions, it considers the next priority in the PV.

Step 5: This process continues until the HLA confirms to the EV on one EVCS and reserves a charging session for it. If none of the EVCSs are available within the EV Agent's VB, the HLA will refer the EV Agent to a neighboring VB or will ask it to wait, depending on the criticality of its SoC.

5.1.1 On-board Module / EV Agent

The FLM, that was explained in detail in chapter 4, is used for this application in specific. It is to be noted that this FLM takes into account the dtCS and ttCS corresponding to the individual EVCSs, based on the traffic status at the time of the request. In this work, this is done by means of the Google Maps Distance Matrix API. The FLM processes each FV through a set of membership functions. The output of the controller is a crisp value corresponding to the recommendation of going to EVCS x. Once the EV Agent reads a confirmation, it informs the EV driver or drives there, in case of a self-driving vehicle.

5.1.2 EVCS Agent

Being interfaced with the EMU of the EVCS, the EVCS Agent continuously monitors the availability of chargers and the power generation of any distributed generation at the EVCS premises. With every update, it publishes the new information to the *Availability* topic. The subscriber of the *EVCS Agent* is always listening to the *EVCS Data* topic to receive any updates in prices, communicated by the VBA. If it does, it relays this information to the EMU to update the internal transactions of the chargers that are not reserved yet. In addition, the EVCS Agent's subscriber continuously listens to the *EVCS Conf* topic and receives the IDs of the EVs that are heading to this EVCS. The EVCS Agent relays this information to the EMU to reserve a charging session.

5.1.3 VB Agent

The VBA obtains the power set points from a higher-end energy management system (EMS). The full details of this EMS are explained in chapter 6. The developed strategy of the VBA is a new intelligent price-based real-time strategy [43]. What makes it different

is the pre-cognitive feature that makes a robust and more confident decision in the real-time dynamic pricing at the EVCSs. The objective of this strategy is to change the distribution of the EVs in order to meet preset power load distribution at dispersed EVCSs. The strategy presented considers the interdependency of the prices between the different EVCSs, by controlling them from an agent reaching out to all EVCSs simultaneously. This is needed because the manipulated variables (the prices at different EVCSs confined in a geographical area) are inherently interdependent, considering the correlation between the different charging prices and the distribution of the EVs.

The VBA's role is to change the prices of charging at the EVCSs in a way to redistribute the EVs in a manner that meets those power set points. The VBA also identifies the price range at each EVCS within its service territory depending on input from the contracts with the EVSPs. It needs to "perceive", "contemplate" and draw a conclusion comprising the optimum price vector (OPV) that it observes will achieve this goal. We use the expressions "to maximize" and "perceives" because the output will be a recommendation to the EV driver, and not an infliction. Some drivers might have enough time and decide to diverge from the recommendation.

The VBA acquires a precognitive ability by means of a dynamically changing layer of duplicate FLMs. It uses this ability to come up with an action that will influence the EV agents requesting charge to raise the recommendations that it wants them to raise, in the same way that a mentalist influences an audience to think the way he wants them to, without forcing them to it.

When an EV agent's request is handed on from the HLA to the VBA, the VBA prepares a FLM as a duplicate to the one in the EV agent that requested the charge. In this duplicate module, the first, second and third inputs are ready at the time of its creation, as the EV's SoC and GPS location are passed on with the request from the EV agent to the HLA, which subsequently passes them on to the corresponding VBA. The locations of the EVCSs in the VB of the corresponding VBA are pre-known by the VBA. The fourth input (price of charging at the EVCS) is the manipulated variable by the VBA's algorithm. To attract more EVs to the EVCSs where more EVs can be accommodated, the VBA needs to decrease the price at those and vice versa. For every candidate price vector (CPV), constituting a specific combination of prices at the EVCSs, there will be a different distribution of the EVs on the EVCSs. It is the VBA's role to intelligently and in real-time decide on the OPV which will eventually lead to the optimum distribution of the EVs on the EVCSs. When the VBA runs

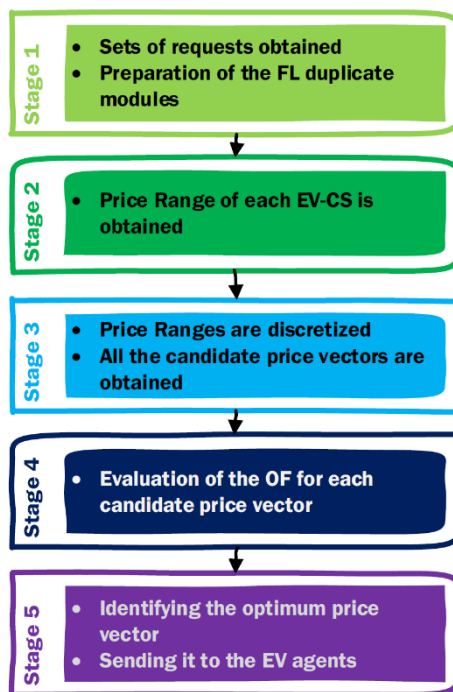


Figure 5.5 Stages of the VBA strategy

its algorithm, using this layer of duplicate FLMs, and finds the OPV, it sends it out to the EV agents that requested the charge.

Figure 5.5 shows the different stages of the cognitive algorithm of the VBA.

5.1.3.1 Distinction among the Price Vectors: BPV, CPV, OPV

Highlighting the difference among the vectors: the base price vector (BPV), the candidate price vector (CPV), and the optimum price vector (OPV) is key to reinforce the understanding of the VBA strategy. Figure 5.6 shows the elements of a price vector.

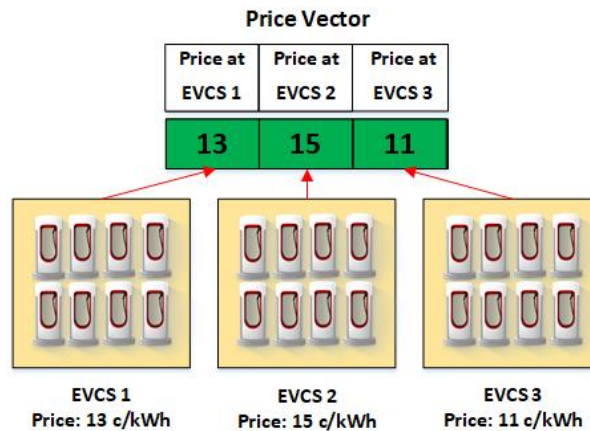


Figure 5.6 Price vector elements' correspondence to EVCSs.

The BPV is a base price vector, with all its elements as the base price, that is the state price of charging. For example, if the state price for charging at the EVCSs is 13 c/kWh and the number of EVCSs is 3, the BPV will be: [13,13,13].

The CPV is a candidate price vector. The VBA would process all possible combinations of prices, where each combination is a CPV. For example, if there are 3 EVCSs and the price ranges are discretized into 3 prices each, and knowing that those prices are

independent (repetition is possible), using the multiplication rule counting technique, the number of CPVs is: $3 \times 3 \times 3 = 3^3 = 27$. In other words, if:

- EVCS 1 can have one of the following prices [P1_a ;P1_b; P1_c],
- EVCS 1 can have one of the following prices [P2_a; P2_b; P2_c],
- EVCS 3 can have one of the following prices [P3_a; P3_b; P3_c],

then there will be 27 possible combinations of prices, i.e. 27 CPVs. Those are shown in Table 5-2.

Table 5-2 CPVS given 3 EVCSs (1,2,3), and Discretization Level=3 (A,B,C)

1	2	3	4	5	6	7	8	9
P1_a								
P2_a	P2_a	P2_a	P2_b	P2_b	P2_b	P2_c	P2_c	P2_c
P3_a	P3_b	P3_c	P3_a	P3_b	P3_c	P3_a	P3_b	P3_c
10	11	12	13	14	15	16	17	18
P1_b								
P2_a	P2_a	P2_a	P2_b	P2_b	P2_b	P2_c	P2_c	P2_c
P3_a	P3_b	P3_c	P3_a	P3_b	P3_c	P3_a	P3_b	P3_c
19	20	21	22	23	24	25	26	27
P1_c								
P2_a	P2_a	P2_a	P2_b	P2_b	P2_b	P2_c	P2_c	P2_c
P3_a	P3_b	P3_c	P3_a	P3_b	P3_c	P3_a	P3_b	P3_c

Then, the VBA processes all CPVs, and finds the one OPV. The OPV is the price vector among the 27 CPVs that would maximize the VBA’s chance of success at distributing the EVs on the different EVCSs in a way that meets the power set points in the EVCSs.

5.1.3.2 Stage 1

In the first stage of the VBA strategy, it receives from the HLA the input requests in the VB that it manages. It then prepares the FL duplicate module for each EV agent that requested a charging session.

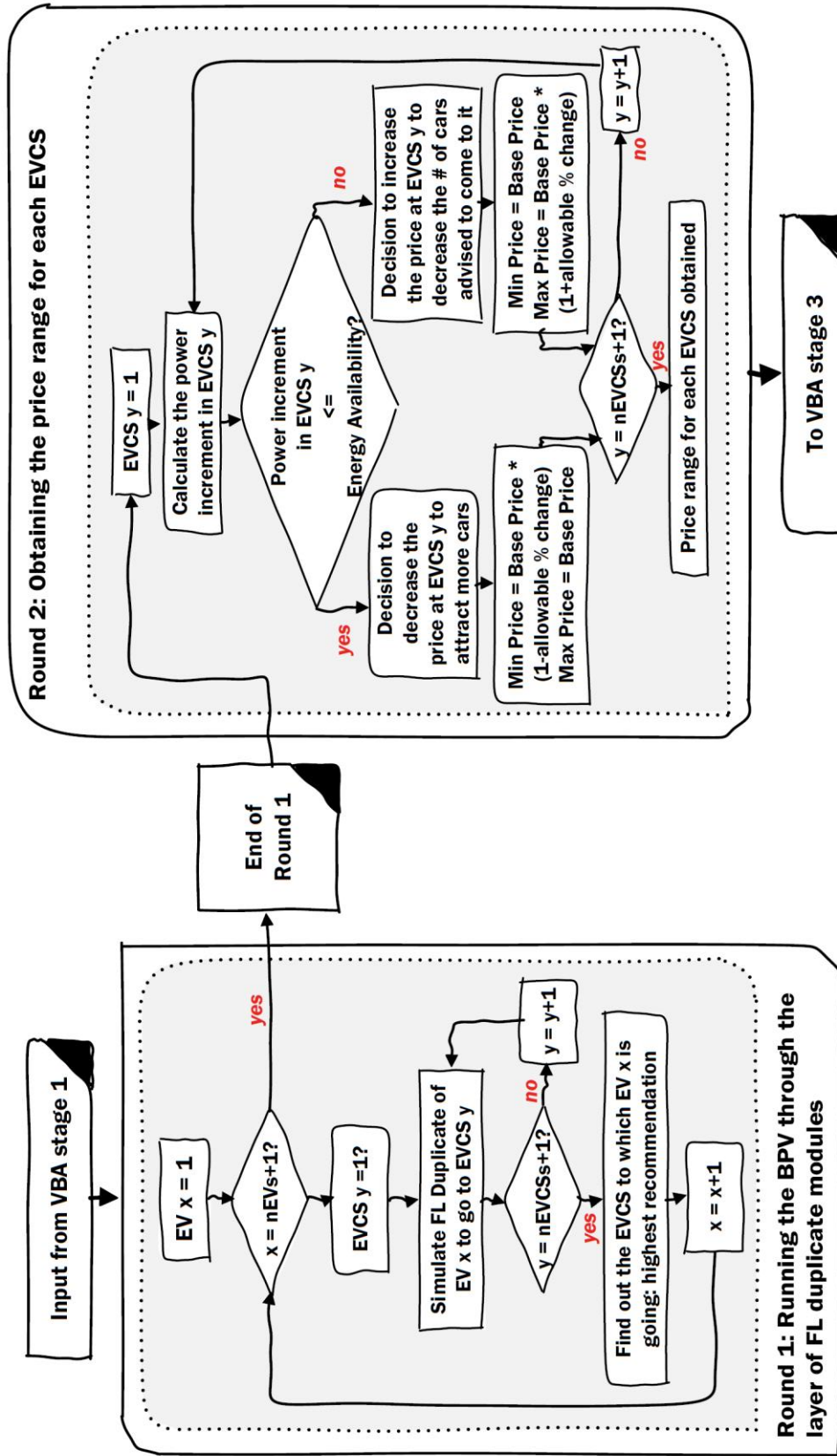


Figure 5.7 The 2 rounds of stage 2 of the VBA strategy

5.1.3.3 Stage 2

The flowchart of Figure 5.7 presents the details of stage 2 of the VBA's algorithm, in which it decides on the price range (for each EVCS) that it must discretize. This stage is made up of 2 rounds, as depicted in the flowchart.

The VBA will run the first round by running the BPV, which reflects the same price (state price) for all EVCSs in the VB. In other words, if the state price for charging at the EVCSs is 13 c/kWh and the number of EVCSs is 6, the base price vector will be: [13,13,13,13,13,13]. At this stage the fourth input to the FL duplicate module (the price of charging at the EVCS) is the same for the EVCSs. However, each duplicate FLM still has to run several times, since the second and third input of the fuzzy logic controller (FLC) is different for each EVCS. This is because the EVs are not at an equal driving distance and time from all EVCSs. Each duplicate FLM will output 1 recommendation. So the first round of stage 2 covers the step of running the BPV through the layer of FL duplicate modules.

In round 2 of stage 2, the recommendations resulting from round 1 are aggregated to find the power increment in each EVCS. The load distribution that results is compared to the anticipated distribution, and a decision is taken on whether to decrease or increase the price at the individual EVCSs. If for an EVCS x , the EVs expected to arrive for charging are more than what it can accommodate, the minimum, P_{x_min} , of the interval [P_{x_min} P_{x_max}], is set as the base price, because the aim is to increase the price at this EVCS so as to discourage the EV agents from raising the recommendations to go to this EVCS. If the result of aggregation shows that the number of EVs expected to arrive at an EVCS are

less than what it can accommodate, the maximum, P_{x_max} , of the interval $[P_{x_min}, P_{x_max}]$, is set as the base price, because the aim is to decrease the price so as to encourage the EV agents to raise the recommendations to go to this EVCS.

The allowable price variation range is assumed to be based on a contract done with the individual EVCS operators. In this work, this is a +/- 30% fixed percentage of the state price.

5.1.3.4 Stage 3

In this stage, the price ranges (for each EVCS), as obtained from stage 2, are discretized, and all the CPVs are obtained.

5.1.3.5 Stage 4

The VBA's logic is devised to have a pre-cognitive feature with the price at the individual EVCSs as the manipulated variable. The individual manipulated variables are combined into a vector, comprising the price of charging at the EVCSs in the corresponding VB. To attract more EVs to the EVCSs where more EVs can be accommodated, the VBA decreases the price at those and vice versa. For each CPV, there will be a different distribution of the EVs onto the EVCSs. The VBA decides which of the CPVs is the OPV that will eventually lead to the optimum load distribution. When the VBA receives the requests, it creates a layer of duplicate modules of the FLMs of the requesting EV agents. This layer is simulated for each CPV, the output recommendations are aggregated to obtain the distribution of the EVs on the EVCS, and the objective function (OF) for each CPV is evaluated. This strategy gives the VBA a "cognitive feature" that allows it to know how the EVs will react to the different CPVs. In this strategy, the objective function $f(x)$ to be

minimized is defined in equation (5-1) as the distance between the two vectors: power distribution vector, PD(x), where x is the CPV, and the anticipated power distribution vector, APD. nCSs is the number of EVCSs that this VB is managing.

$$f(x) = \sqrt{\sum_{i=1}^{nCSs} (PD_i(x) - APD_i)^2} \quad (5-1)$$

5.1.3.6 Stage 5

The OPV is identified and then sent to the EV and EVCS agents.

5.1.4 HL Agent

As shown in Figure 5.3, the HLA is coded into two parallel threads. The two threads are depicted inside the HLA in Figure 5.3 (b). The publishing and subscription to and from the data space's topics is depicted in Figure 5.3 (a). In the first thread, the subscriber of the HLA continuously listens to the EV requests for charging in the *Requests* topic. This thread processes these requests and identifies in which VB each EV request is, and then publishes this information to the *Updated Requests* topic.

In the parallel thread, the subscriber of the HLA continuously listens to both the *EV Dec* and the *Availability* topics. This thread then prioritizes the EV published decisions based on the criticality of the SoC of the EVs and decides on which EVCS the EV may go to, depending on the availability at the corresponding EVCS.

5.2 The Bilateral Decision Support Platform- Hardware Setup Implementation

Sixteen interactive agents were coded and compiled, and the system was divided into a software platform correlated with a hardware platform. The former consists of 11 pieces

of code, representing the EVCS Agents of the use case that is explained in section 5.3, compiled and simulated on a Linux operating system desktop. In order to emulate the remote status of each of those 11 EVCS Agents, the GPS coordinates of each EVCS was hardcoded in the agent. Figure 5.8 (a) shows the simulation of the 11 EVCS Agents during the experiment. The hardware platform consists of 4 VBAs and 1 HLA, shown in Figure 5.8 (b), each being a cross-compiled executable embedded onto an ARM- processor microcontroller. The hardware platform also includes three on-board modules representing the EV Agents. Each of those modules is developed as an HTTP application embedded onto an ARM-processor microcontroller, interfaced with a commercial serial GPS module, and connected to a 4G-LTE hotspot of the connected vehicle (Figure 5.8 (c)). To emulate the EV input needed, the SoC was hardcoded in the EV Agents.

5.3 Use Cases and Results

The effectiveness of the proposed bilateral decision support framework is demonstrated by presenting price-based case studies from two complementary perspectives: 1) The on-board decision support module to choose the optimal EVCS in favor of the EVs status, and 2) The electric power grid decision support by means of the VBA pricing strategy to redistribute the load demand onto the EVCSs.

A full view of the system during experiment is presented in Figure 5.9. With the participants operating, a screenshot is taken from the RTI Connex DDS View software.

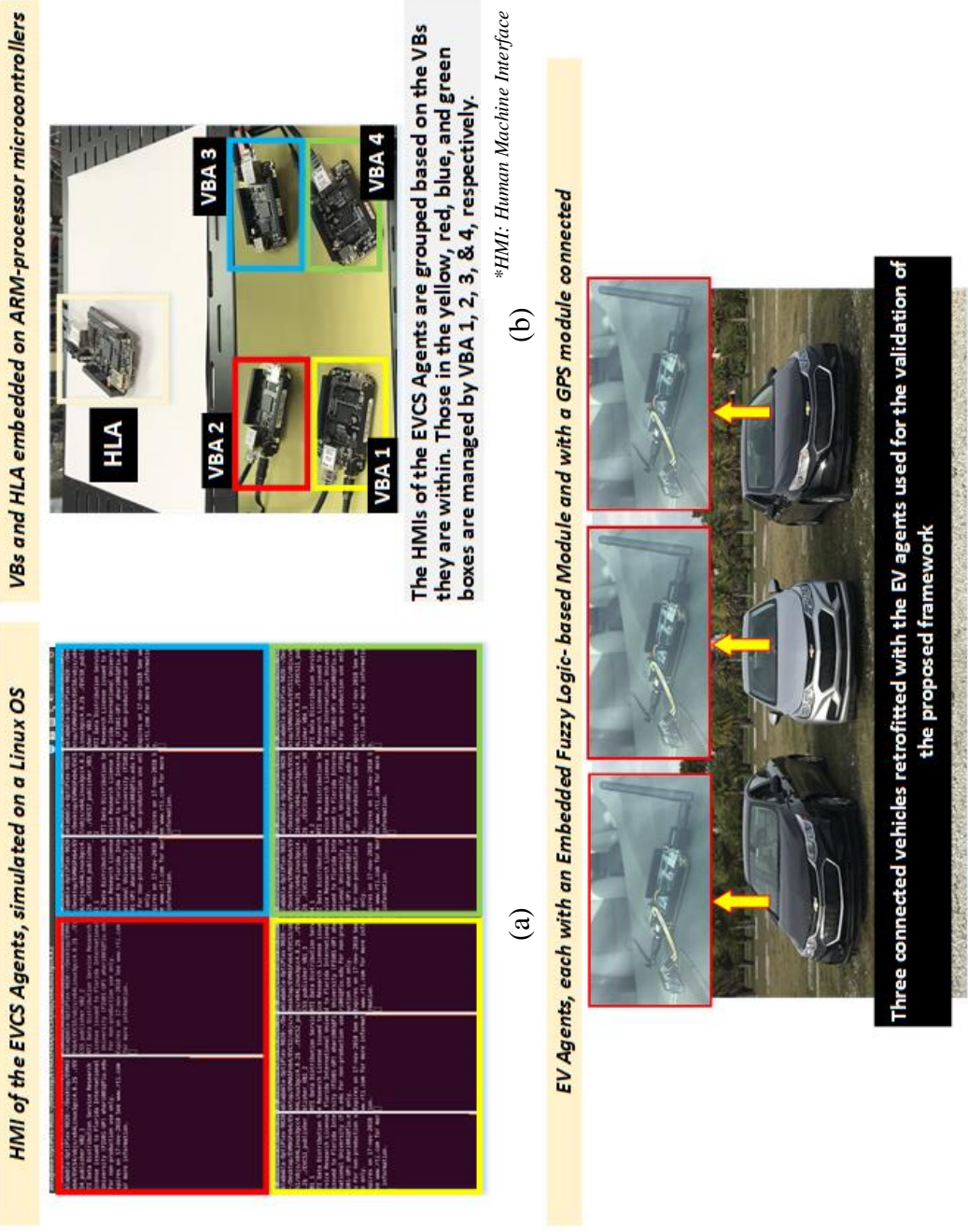


Figure 5.8 BDSS Platform (a) EVCS Agents; (b) VBAs and HLA (c) EV Agents

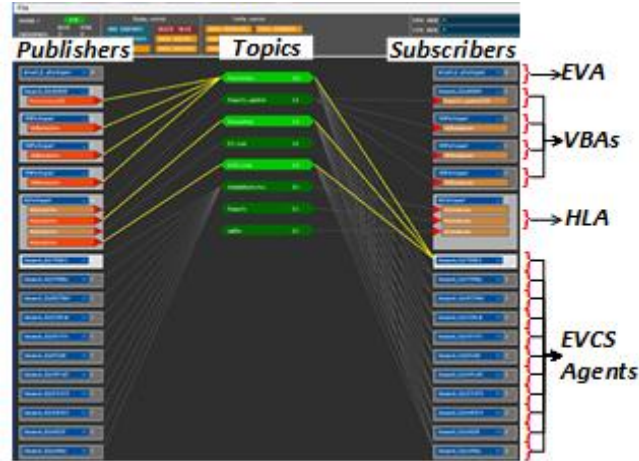


Figure 5.9 Labelled screenshot from the RTI Connex DDS View software to obtain a full view of the system during experiment.

The screenshot is labelled to show the publishers and the subscribers of the different participants, as well as the topics in the global dataspace. The EVA, the 4 VBAs, the HLA, and the 11 EVCSs, are labelled.

5.3.1 Decision Support on the EV Side: Evaluation of the On-Board EV Decision Support Module

To corroborate the robustness of the on-board module's response to different scenarios, 4 VBs were defined in the area of Miami-Dade County, as shown in Figure 5.10. Four EV requests for charging were issued, each from a different VB. Two or three EVCSs were defined in each VB. The locations of those EVCSs are selected to be in public parking garages, shopping plazas, and university campus garages. Figure 5.10 marks the 4 EVs, the 11 EVCSs, and the 4 VBs on the map. Also, the GPS coordinates of the VB boundaries are identified. The EVs' locations marked on the map represent the location at which they issued the request for charging from. The connected cars, retrofitted with the on-board module, roamed around the 4 VBs.

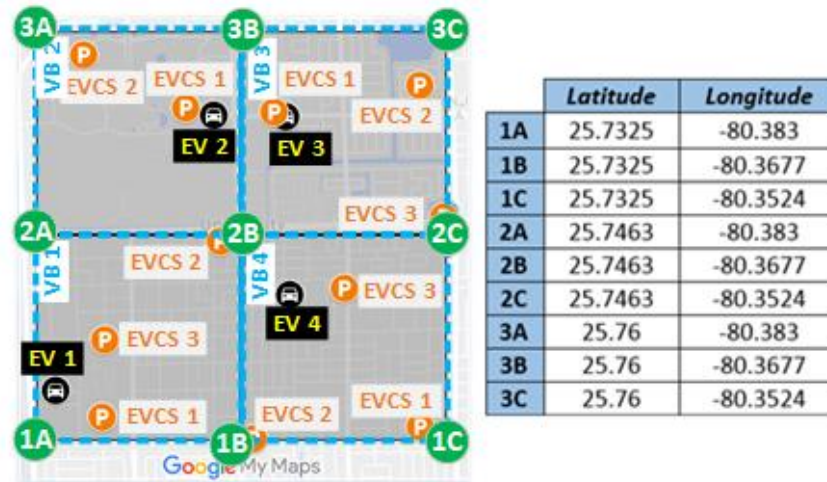


Figure 5.10 Map showing the VBs, EVCSs, and EVs in the presented case study

Table 5-3 shows the input parameters for the on-board module in the 4 case studies, the calculated dtCS and ttCS, and the output results of the FLM. The recommendations given by the FLM to the driver are the EVCSs highlighted in yellow.

Table 5-3 Inputs and outputs of the FLM in the presented case studies

EV #, SoC	EV GPS coord.	EVCS #	GPS coord.	dtCS	ttCS	pCS	FLM result
1, 70%	25.73589, -80.38164	1	25.73411, -80.37817	0.6	5	13	0.858
		2	25.74591, -80.36935	1.6	5	13	0.833
		3	25.73931, -80.37799	0.5	3	13	0.858
2, 85%	25.7544, -80.36986	1	25.75488, -80.37193	0.1	1	19	0.25
		2	25.75844, -80.37957	1.1	6	10	0.994
3, 20%	25.75429, -80.36448	1	25.7546, -80.36536	0.2	1	19	1
		2	25.75641, -80.35446	1.1	4	14	0.65
		3	25.74754, -80.35269	1.2	4	14	0.636
4, 55%	25.74233, -80.36419	1	25.73346, -80.35442	1.3	6	19	0.467
		2	25.73264, -80.36689	1	5	15	0.75
		3	25.74277, -80.36008	0.4	1	13	0.858

5.3.1.1 Case 1 (VB1)

The prices at all the 3 EVCSs in VB1 are set at the Florida state price of supercharging [44], that is, all EVCS have a charging price of 0.13 \$/kWh. Also, the FLM perceives a high SoC (70%). Therefore, the only two parameters governing the decision of the FLM are the dtCS and ttCS. Thus, the FLM will decide to go to the closest in terms of time and distance, i.e. EVCS3.

5.3.1.2 Case 2 (VB2)

In this case, the price of charging at EVCS1 is 0.19 \$/kWh, representing a high price rate, whereas at EVCS2 the price of charging is 0.10 \$/kWh, representing a low price rate. Also, the FLM perceives a high SoC (85%). Despite the fact that EVCS1 is closer to EV2 than EVCS2 in terms of distance and time, the on-board module recommends going to EVCS2, which is the EVCS with lower price. It is important to mention here that this is viable since we are assuming the 6 min ttCS2 is within the driver's preset time preference.

5.3.1.3 Case 3 (VB3)

The price at EVCS1 is set at 0.19 \$/kWh, which is higher than that of EVCS2 and EVCS3 (0.14 \$/kWh each). The SoC of EV3 is 20%. Although the prices at EVCSs 2 and 3 are lower than that at EVCS1, the on-board module recommends going to EVCS 1, the closest EVCS in terms of distance and time because it senses that the SoC is critical, being 20%.

5.3.1.4 Case 4 (VB4)

In this case, the prices at the 3 EVCSs are set to be at three levels: low (0.13 \$/kWh), medium (0.15 \$/kWh), and high (0.19 \$/kWh). The SoC of EV4 is 55%. Therefore, the

FLM recommends going to EVCS3, the one with lowest price and the closest in terms of distance and time.

The results of these 4 case studies demonstrate that the decision-support task of the on-board module works as anticipated, in favor of the EV status. To further illustrate the participation of the EV on-board module in the framework, a screenshot is taken from Wireshark, a packet analyzer software [45], when the EV request is issued. Figure 5.11 depicts this, showing the packets being sent from and to the EV, with the HTTP methods POST and GET, respectively. The details of each packet are highlighted, showing the request URL, showing that the EV participates in the framework as an RTI DDS participant with a publisher and a subscriber.

Moreover, the seamless integration between the power grid’s decision-support that is achieved by means of the VBA’s logic, on one hand, and the EV decision-support that is achieved by means of the EV Agent’s logic, on the other hand, is demonstrated in the case study presented below.

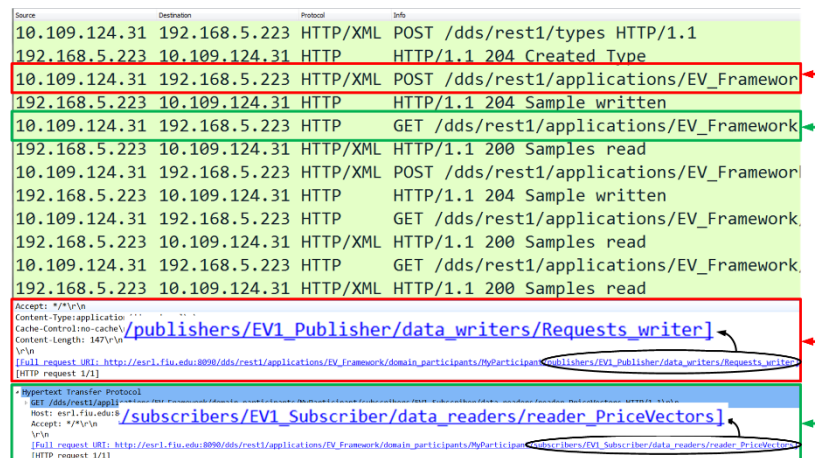


Figure 5.11 Screenshot of the Wireshark showing the packets being sent from and to the EV, with HTTP POST and GET, as an RTI DDS participant with Publisher and Subscriber.

5.3.2 Decision Support on the Power System side: Evaluation to the VBA Price-Based Strategy

To evaluate the validity of the VBA strategy in supporting the power system by meeting the set points provided to it, a case study is applied, where 21 EVs and 6 EVCSs are located in one VB. Figure 5.12 shows a Google Maps screenshot of the EVs and EVCSs in the one VB for this case study, the red showing the EVs and the blue showing the EVCSs. The EVs' SoC are chosen to be in the range of 20% and 80%, and the EV batteries are assumed to be of 100kWh capacity each. All EVCSs are assumed to accommodate only SCs, with the sharing charging rate of 60kW per charging vehicle (120 kW per SC) [44], in this study. For this reason, the power set points are assumed as increments of 60 kW. The BPV is chosen to be the Florida state price of supercharging at the time this study was conducted

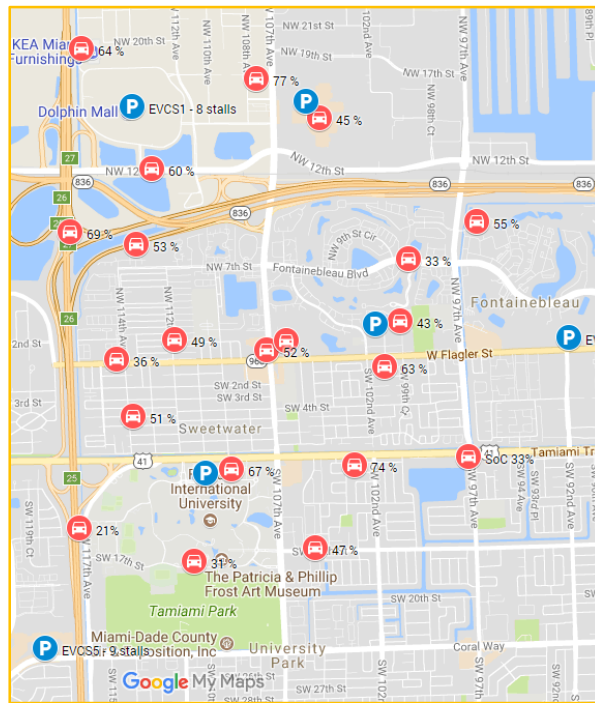


Figure 5.12 Illustration of the case study

[44], that is 0.13 \$/kWh. It is assumed that we can change the price by $\pm 30\%$ for each EVCS.

The VBA applies its strategy by looping through the CPVs, evaluating the distribution of the EVs in response to each CPV, and deciding on the OPV that if issued, will lead to the anticipated distribution of the EVs onto the EVCSs to meet the power set points.

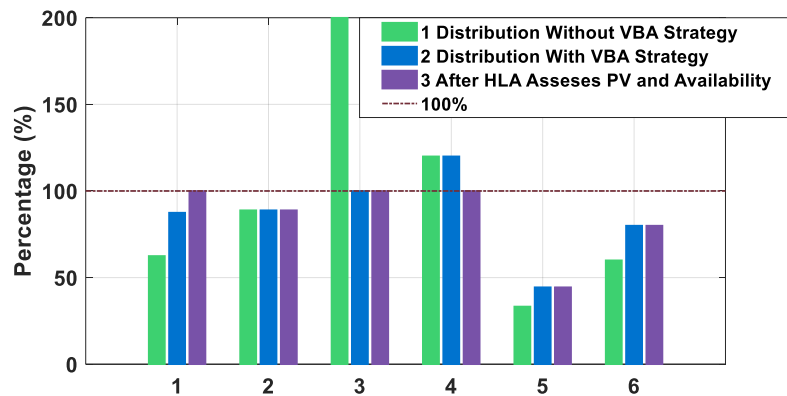


Figure 5.13 Percentage of power consumption to the power set points at the EVCSs.

Figure 5.13 shows the percentage of power consumption to the anticipated power set points at all EVCSs, before and after applying the VBA strategy. The green bars and blue bars represent the EVCS's percentages resulting from the distribution of the EVs after responding to the BPV and the OPV, respectively. This improvement in the percentages reflects the success of the redistribution of the EVs by the VBA's cognitive strategy. However, in EVCS4, the percentage remains at 120%, and was not reduced to 100%. In this case, one of the EVs that has claimed EVCS4 as the highest priority in its PV will not be accommodated. So, when the HLA prioritizes those requests and assesses the availability at that EVCS, it finds out that this EV cannot be accommodated. As a result, it assesses the subsequent EVCS priority in the PV issued by that EV to the *EV Dec* topic.

The HLA continues and loops through the PV until it finds a EVCS that can accommodate this EV. In this case, the second EVCS in this EV's PV is EVCS1. The HLA finds out that this EVCS1 can accommodate this EV. The new distribution is evaluated, and the purple bars reflect the results. The results show further improvement in the percentages for EVCS4 and EVCS1.

5.4 Conclusion

This chapter presented a decentralized hierarchical MAS that serves the purpose of a bilateral decision support framework for the application of public charging of connected EVs. The effectiveness of the proposed framework is demonstrated by presenting price-based case studies from two complementary perspectives: 1) The on-board decision support module to choose the optimal EVCS in favor of the EVs status, and 2) the electric power grid decision support by means of the logic of a higher-end agent to redistribute the EVs onto the EVCSs.

The results proved that given a power distribution that could be provided by means of a higher-end optimization or energy management system, the bilateral decision support framework achieves the anticipated win-win situation for the EVs and the power grid. In this framework, the two are complementary in a way that the desired benefit to one cannot be achieved without attaining that of the other.

5.5 Public Charging Infrastructure – System of Systems

The work in [46] considers the optimal operation inside a PV-augmented EVCS that is equipped with a BESS. A MOOP is applied to maximize the revenue of the EVCS owner, while minimizing the BESS capacity fading. The MOOP was applied with the constraints

of the the power fluctuations limits imposed by the hosting grid at the point of common coupling (PCC).

The MAS of the BDSS developed and presented in this chapter was extended to include a MAS at each public charging station with the EVCS's EMU acting as a gateway to the global databus of the BDSS. This renders the extended BDSS an interconnected system of systems, adding an extra layer of autonomy to the application at hand. This EVCS's EMU can be used as a gateway of the EVCS to contribute and retrieve information, to and from the higher level domains, regarding the availability in terms of chargers, willingness to accept more EVs, and information of incoming EVs. MOOPs like that in [46] can be extended to include an objective of identifying the optimum number of EV chargers to be deployed at a certain time, while considering the fluctuations at the PCC, the BESS fading, and the PV intermittency.

Figure 5.14 shows the architecture of this system of systems, showing three levels. Level 1 is that of the BDSS databus, the domain which en route EVs join to issue their charging requests and retrieve guidance. The higher-end agents of the BDSS, the VBA and the HLA, are also participants of this domain. Level 2 is the databus of the EVCS domain. All agents at the premises of the EVCS contribute and retrieve information to and from a dedicated databus for this domain. The participant agents in this domain are those of the EVSEs installed at this EVCS, the PV system, and the BESS. The EVCS's EMU serves as the gateway of the EVCS domain to the higher level, level 1. The next level is the EVSE domain, referred to as Level 3 in Figure 5.14. The participants of this domain are the EVSEs and the EVs connected to them. The information contributed to and retrived from this databus involve that of deployment information of the EVSEs.

In this architecture, the power system operator is connected to the databuses of levels 1 and 2. This is needed for applying the BDSS in a way to enhance the power system operation. An example of a power system optimization that uses the BDSS and contributes information to its databus is presented in a service in Chapter 6.

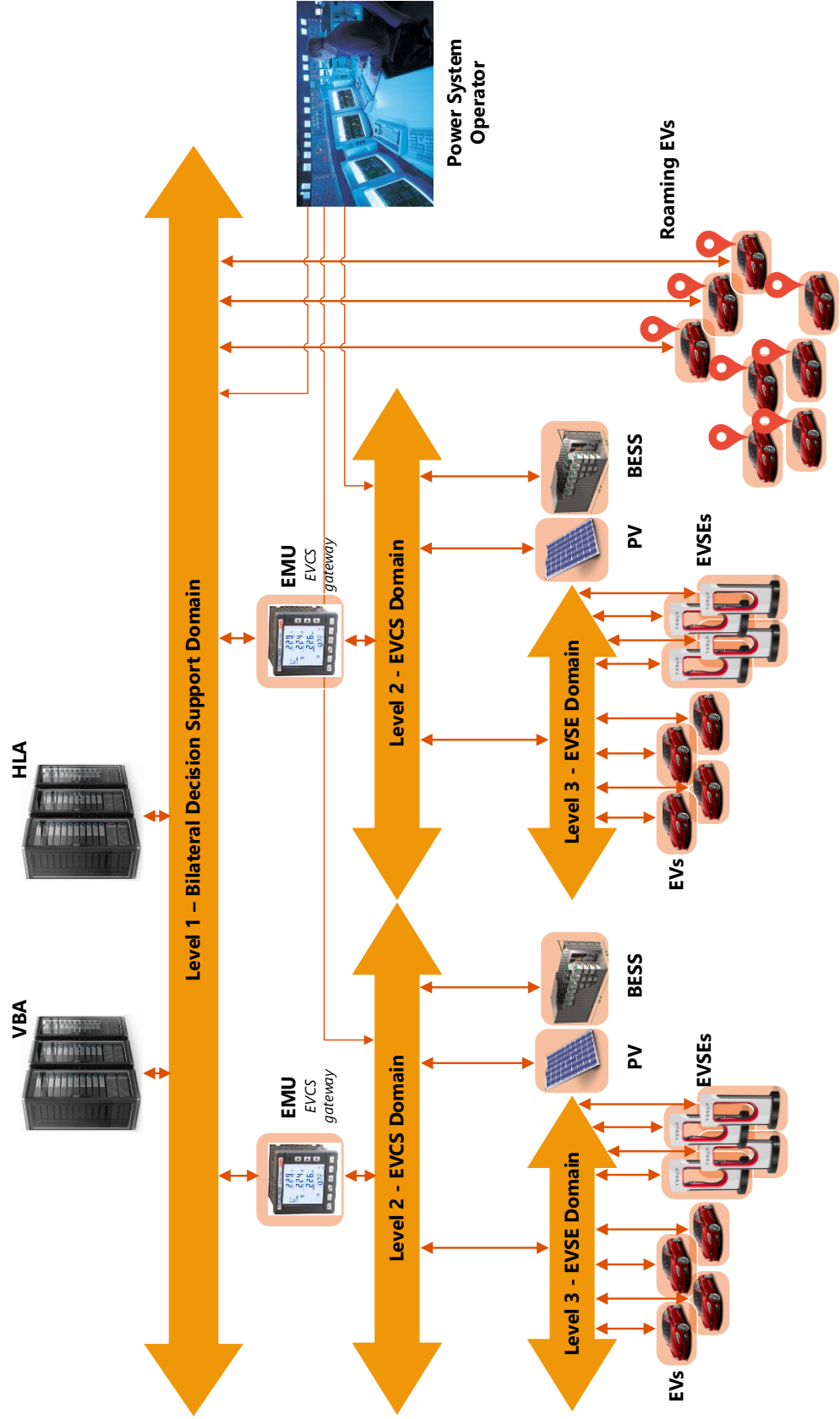


Figure 5.14 BDSS extension – System of Systems

Chapter 6 Collective Distribution of Mobile Loads for Optimal and Secure Operation of Power Systems

6.1 Introduction and Literature Review

In the post-contingency events in power systems, changes in the flows on the transmission lines remaining connected to the system can cause voltage limit violations, system frequency fluctuations, and dynamic problems with the generation output. It is the Independent System Operator (ISO)'s role to maintain the secure operation of the power system as an overriding factor [29]. Secondly, and within the constraints of the secure operation, the ISO aims at achieving the most economical operation of the power system at any given time. Power system security involves the deployment of support services, called ancillary services, designed to keep the system operating when contingency scenarios occur. Those ancillary services comprise of agreements between energy providers and/or consumers on one hand and the ISO on the other. The services typically fall into three categories: Regulation and Frequency Response, Spinning Reserves, and Non-Spinning Reserves [47]. Some of those services are invoked in both normal and contingency conditions. Others are designed for contingency conditions only. They can be further categorized based on their time response, where some are expected to respond within seconds and others within minutes. Some examples of ancillary services in deregulated energy markets are reactive power support [48] for maintaining voltage stability and primary and secondary frequency control. According to [49], the value of frequency regulation has reached a high value compared to other ancillary services, with a maximum value of \$200/kW-year. Furthermore, the real-time congestion management is

an ancillary service defined and utilized in [50], [51] which runs a separate energy market for participants to mitigate the congestion in the power system economically. In addition, demand response is a method that is ideally suited for providing ancillary services to the grid. Consumers react to price signals, shifting their load from peak-load conditions to off-peak or light-load conditions to reduce their energy costs. This provides several benefits to the power system.

6.1.1 Impacts of the large-scale penetration of EVs on the grid

Several studies in literature have assessed the effects that the large scale penetration of EVs have on the power grid. For example, the work in [52] examined the impacts of PEVs charging on a medium voltage distribution network in Bosnia and Herzegovina. Simulations were done to assess the effects of PEV charging on voltage profiles, energy losses, and the violations of network operational constraints. The analysis showed increase of the peak load, increase in energy losses, and overload of distribution transformers. The work suggested regulating the time and duration of the PEV charging to mitigate the negative impacts. Reference [53] assessed the effect of charging rate, distribution of EVs over a power network, and the location of EVCSs on the system loss. The results showed that both the rate of charge and the distribution of EVs over a power network are parameters that considerably effect the total system loss. The authors suggested applying an optimization problem to find optimal location of EVCSs in the network. Reference [54] evaluated the impact of different PEV penetration on distribution networks and on energy losses. A noteworthy finding of this work is that energy losses increased up to 40% in off-

peak hours for a case study where 60% of the vehicles in an area were PEVs in charging mode.

6.1.2 Proposed Solutions

In light of the foregoing, several studies were conducted in literature to offset all of the identified negative impacts that large penetration of EVs have on the power system. Those studies can be categorized into methods that are to be implemented in the planning phase and others during operation.

6.1.2.1 Solutions in the Planning Phase

Some of the methods in the planning phase include optimal allocation of EVCSs. In [55], for example, a multi-objective optimization problem (MOOP) was applied for the optimal allocation and sizing of EVCSs in a distribution power system. The objectives in this optimization problem were to maximize the profits of the EVCS investor and minimize the losses and voltage deviations for the distribution system operator. A similar study was applied in [56], where the objectives of the MOOP were to maximize the profits of the EVCS investor and the EV user satisfaction in terms of charging service efficiency. Beyond optimal allocation of EVCSs, other studies considered integrating distributed generation (DG) or ESSs at EVCSs to support the mitigation of EV-related stresses on the grid. An optimization model was presented in [57], for example, with the objective of maximizing the benefit of the EVCS owners without violating system constraints. The results determined the optimal mix of solar-based DG and storage units as well as the optimal charging prices for PEVs. In another study [58], energy storage devices were considered at the EVCSs and a scheme was presented to allocate power to them from the grid.

Forecasting factors were used in a 24-hour ahead planning method presented in [59] to perform load leveling, leading to lower total electricity cost.

6.1.2.2 Solutions in the Operation Phase

When looking at presented methods in literature that are designed for real-time settings, the results are also abundant. Several works like those in [60] and [61] used real-time smart charging control strategies to offset negative impacts caused by the large number of EV connections to the network. Reference [60] presented a charging control strategy integrated with utility demand response to mitigate the stresses on the residential distribution grid. The work in [61] comprised a real-time algorithm among several chargers at an EVCS to achieve charging coordination and power sharing among EVs for achieving peak-shaving. The results showed a reduction in the overall cost of charging as well as an improvement in the voltage profile and the losses in the system. The work in [62] assessed and utilized the potential of PEV storage in active distribution networks in the presence of photovoltaic panels. The results demonstrated the capability of PEV storage in offsetting the negative impacts of the increase in renewable energy penetration in the grid. The authors presented the management of EVs charging as an ancillary service that enables the system operator to deal with balancing issues arising because of the intermittency of the photovoltaic systems. Furthermore, an effective vehicle routing problem (VRP) was solved in real-time in [63] where the locational marginal prices (LMP)s were used at the EVCSs. One aim in [63] was to minimize the total cost of travel for the EV. Also, the others investigated the LMP at each EVCS by solving the optimal power flow.

6.1.2.3 Vehicle Routing Problems of EVs

In terms of the VRP of EVs, the work in [64], for example, proposed a mathematical model for route optimization of commercial and electric distribution vehicles to reflect the EV driving and charging characteristics and its interaction with the electricity market. Reference [58] applied a scenario where EVs are rerouted to individual EVCSs in a network of those.

Despite the variety of approaches and abundance of considerations including [52] - [64], literature falls short in terms of presenting the opportunity that lies in the collective redistribution of the EVs as an ancillary service that helps achieve a secure and optimal operation of the power system.

6.1.3 EVs as Enabling Technologies to Ancillary Services

Given the huge value and immense impact that energy storage systems (ESS)s can provide to the electricity grid at scale, it becomes necessary to put this mobile ES, the EV, on the ancillary services' center stage. Despite the extra degree of complexity in managing such an ESS from the power system point of view, the mobility feature which is unique to EVs among all ESSs brings along vast opportunities for the optimal and secure operation of power systems.

With the fast improvements in the charging technologies, and with the large charging infrastructure expansion [65], [66], the argument that several hurdles still face the wide EV adoption is now dematerializing. Also, in parallel with this expansion in the network of infrastructure, the number of EVs being produced by giant automakers is increasing exponentially as many are shifting towards an all-electric fleet.

With all of this happening, measures should be taken to embrace the multitude of introduced opportunities by this mobile and geo-distributed load. This would also control this rolling and overwhelmingly-growing snowball created because of the electrification of this sector.

Reference [47] provided perspective on the attributes of several products to assess ancillary compatibility, aligning technologies with defined ancillary services. Among the assessed products was the Plug-in EV (PEV). In a technology overview on the PEV, the report indicated that it has very low capital cost, very fast response, high power/low energy (per vehicle), and potential to supply energy back to the grid on demand. It also showed that it is capable of storing electricity from an intermittent generator such as PV or wind.

Given this technology overview, the compatibility of PEVs with the several ancillary services was assessed and classified to be technically feasible but not yet pursued. Exceptionally for the regulation ancillary service, the PEV was identified as an emerging capability in demonstration phase. Following that report, an overview of PEVs as providers of ancillary services was presented in [67].

In the studies assessing the compatibility of EVs with ancillary services, EVs are considered to be in the post-connection phase to the grid. The aspect of mobility that characterizes this energy storage technology has not been considered for this purpose. In this work, we propose a method that capitalizes on the mobility feature of the EVs to align it with ancillary services, helping achieve an optimal and secure operation of the power system.

6.1.4 The Proposed Method and its Ancillary Service Potential

“Collective distribution of the EVs” can be defined as follows: when overlooking all EVCSs in an area and all connected EVs, it is the number of EVs to be gathered at the individual EVCSs. In other words, considering a number of EVs requesting to charge around the same time, and EVCSs as nodes [x, y, z...] in the power system, the collective distribution is how many of those EVs would end up charging at node x in the power system, how many at node y, and how many at node z, etc. To this end, a hypothesis is raised in this work that the process of deliberately and optimally redistributing the EVs onto the public EVCSs could be used as a service that aids in the recovery of the power system after a contingency. This service also helps achieve a more economical operation of the power system. The Collective Distribution of Mobile Loads (CDML), is developed and presented in this work as an effective service with ancillary potential.

Despite the “collective” notion, the proposed method ensures that by being a participant in this system, the EV, on an individual level, will have the privilege of real-time navigation, being assured that it will be serviced. This is because the EV receives a confirmation before heading to the EVCS where a charging session will be reserved for it. Also, with the fair approach among all EVs, the energy criticality of the EV is considered by means of a prioritization approach. In the CDML, the price of charging at the EVCSs is not a variable but is considered during the EV on-board module logic.

Ancillary services vary in response time and in the conditions they are invoked at: normal or contingency conditions. In terms of response time, the anticipated outcome from one CDML round might take between 0 to 10 minutes. This period is the time needed for

the guided EVs to drive to the corresponding EVCSs that they are guided to. This time requirement for a round of the CDML aligns it with non-spinning reserves, that are expected to give full response within 10 minutes. The CDML is designed to be invoked under normal and contingency conditions, as will be discussed in section 6.3.

In summary, the work in this chapter achieves the following: a) introducing a service (CDML) with ancillary potential comprising a real-time system-level optimization for collective redistribution of EVs onto EVCSs, b) the BDSS, that was introduced in chapter 5 as a connectivity platform that is designed for industrial settings, is modified and utilized for the CDML purpose, c) the hypothesis is validated by means of several case studies in simulation on an IEEE 14-bus system, and an experiment is applied on an 8-bus system in a laboratory-scale power system testbed, d) the prospects for commercialization of the CDML are discussed.

The chapter is organized as follows: First, the connectivity platform that is presented in details in chapter 5 is outlined in section 6.2 and utilized here as the tool for achieving the optimization output. Then, the details of the optimization are presented in section 6.3. Next, case studies in section 6.4 are applied both in simulation on a modified IEEE 14-bus system, presenting the simulation results before and after the redistribution and in experiment on a laboratory-scale power system testbed. The prospects for commercialization of the CDML are discussed in section 6.5 and the chapter concluded in section 6.6.

6.2 Collective Distribution of Mobile Loads Using the Bilateral Decision Support System

In order to realize the traditional and established demand response programs, home energy management systems (HEMS) are usually used. This involves an advanced metering infrastructure. Similar to this, and in order to realize the CDML, a platform should be deployed that is designed for realizing its industrial settings and requirements.

In chapter 5, a connectivity platform that is designed for data-sharing among supervisory agents and geo-distributed EVs in a structured multi-agent system (MAS) was presented. The associated data-sharing scheme was given. The communication requirements were first analyzed and the appropriate communication resources were chosen for a practical system. An intelligent on-board module, which is a main participant of the system being the EV agent, was designed and tested. Finally, a setup was built and a successful test applied between roaming EVs and a datacenter where the supervisory agents reside. In that test, the EVs were successfully guided to EVCSs as a result of two-way communication with the datacenter and the logic implementation of the on-board module. In fact, the purpose of the presented MAS in chapter 5 is to serve as a bilateral decision support system (BDSS), the two sides being: the power system on one hand and the EV on the other. By means of the interaction between the EV and the supervisory agents, the system supports the decision of both. It helps the vehicle choose the alternative in favor of its benefit, and the supervisory agent to achieve any defined objective of its own. In other words, none of the participants is concerned chiefly with oneself and its advantage in exclusion of others.

The system comprised 4 types of agents in chapter 5 and a fifth agent is added in this chapter. Two agents are supervisory: The HLA and the VBA. Two are geo-distributed: The EVCS Agent, and the EV Agent. A VBA manages all requests for charging coming from a geographically defined area called a VB, and there is an individual VBA for each geographical area. Figure 6.1 presents a conceptual figure of the system and shows the added power system agent (PSA) in a red circle at the energy and power infrastructure layer. The layered system maps the EVCSs in the map layer to representative loads in the energy and power infrastructure layer.

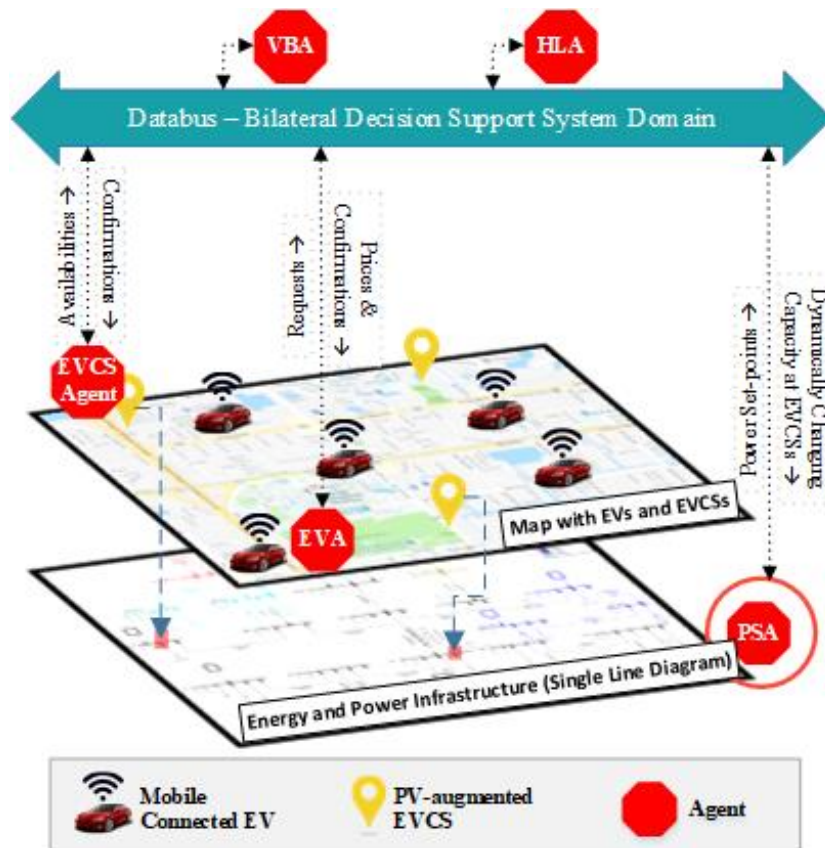


Figure 6.1 Conceptual figure of the platform showing the interaction of the power system optimizer agent

Furthermore, chapter 3 provided a thorough comparison among the features of several application protocols. Building on this comparison, it was found that the RTI Connex DDS middleware is the most suitable for the BDSS application, as it provides a variety of capabilities. It facilitates achieving a scalable, data-centric, and publish-subscribe, data-sharing scheme among the different agents of the system. For that, and using this middleware, the BDSS application is applied, where a global dataspace is set up. The agents contribute information to this dataspace as well as retrieve data addressed to them from it. The geo-distributed agents are HTTP client applications contributing to the global dataspace of the application by means of a translation capability. The latter is called the Web Integration Service (WIS), and it translates data from HTTP format to DDS format.

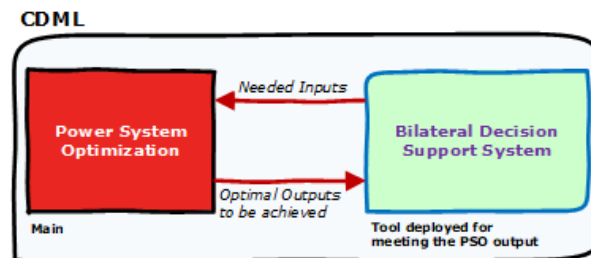


Figure 6.2 BDSS as a tool for achieving the CDML.

The work presented in chapter 5 was chiefly directed towards explaining the communication means to building this BDSS. The work in this chapter, however, uses the BDSS, to serve as an industrial apparatus to achieve the purpose of the proposed CDML and render it industrially viable. This interdependent mechanism is highlighted in Figure 6.2. The flow of information among the agents and the logic algorithm of the VBA are adjusted to go along with the CDML objectives. The CDML is explained here in three stages.

The price-based VBA logic in chapter 5 leads to improvements in attracting more EVs to some EVCSs and discouraging EVs from heading to others, which was formulated as a minimization of an objective function. However, in this work, the objective behind using the BDSS is to perfectly meet a power system optimization redistribution. For that, the VBA logic was modified to accurately meet the Particle Swarm Optimization (PSO) output despite the high unpredictability of the geo-distribution and the energy state criticality of the EVs that are participants in this system. The modified VBA logic is presented in detail in section 6.2.4.

6.2.1 CDML Stage 1

As depicted in Figure 6.3, the BDSS iteration starts when a number of EVAs each publish a request for charging at a public EVCS. The HLA collects the requests issued during a limited period of seconds and assigns the requests to the VBAs, depending on the GPS location of the requests. Each VBA sends out the charging price and the GPS coordinates corresponding to each EVCS within its VB. After receiving this information, the EVA/ On-board module runs it through its FLC and issues what is defined as a “Priority Vector.” This is a vector comprising indexes by decreasing order of how likely it is that heading to each EVCS would maximize its own benefit. For example, a Priority Vector [4,2,1,3] means that EVCS 4 is the most preferred to this EV, EVCS 2 is the second priority, EVCS 1 is its third priority, and EVCS 3 is the least likely among the 4 EVCSs that this EV would want to go charge at.

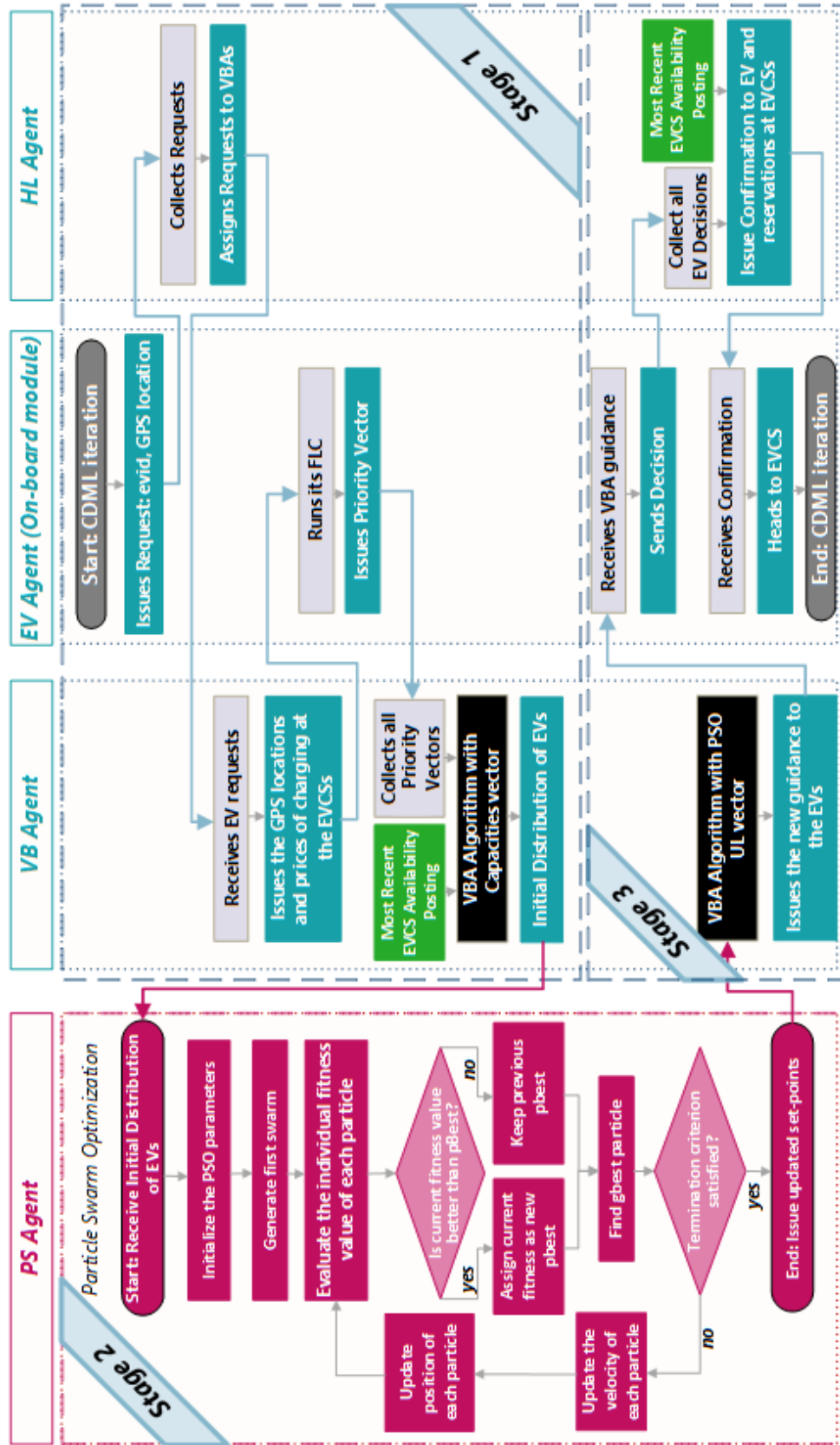


Figure 6.3 Flowchart highlighting the higher level power system optimization as it relates to the BDSS platform

After issuing its Priority Vector, the EVA then waits for guidance. The VBA collects the Priority Vector from each EV within its VB, and the most recent availability information issued by the EVCS. It then applies its logic, that is explained in section 6.2.4, for obtaining the initial distribution of the EVs onto the EVCSs.

6.2.2 CDML Stage 2

As depicted in Figure 6.3, after the initial distribution is obtained by the VBA logic in stage 1, it is communicated to the PSA. The PSA then runs the optimization algorithm, which is explained in section 6.3, and the resulting anticipated distribution (the set points) is communicated as the new upper limit (UL) vector to the VBA.

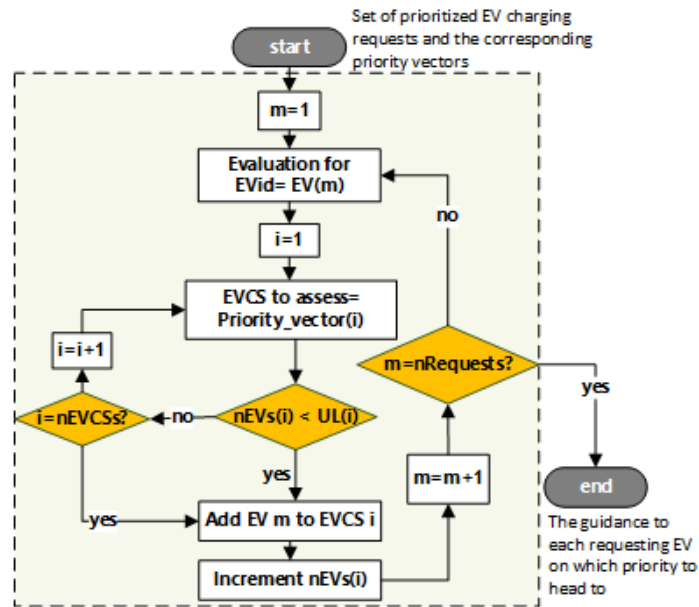


Figure 6.4 Flowchart of VBA algorithm, that is highlighted in black in Figure 6.3.

6.2.3 CDML Stage 3

The VBA now again applies its logic, that is presented in Figure 6.4. It is important to highlight that the UL vector is what changes between the VBA logic application in Stage

1 of the CDML and Stage 3. Upon applying the VBA logic at this level in order to meet the anticipated distribution obtained by means of the PSA, the VBA identifies which priority among each EV's Priority Vector would lead to the anticipated distribution. It then issues this guidance to each EVA, who in turn takes a decision, and sends it to the HLA to check the availability at the EVCSs before confirming to the EVAs and reserving charging sessions at the EVCSs' chargers.

6.2.4 VBA Logic

The application of the logic of the VBA in the CDML process is highlighted in two places in black in the flowchart of Figure 6.3 and is illustrated in detail in the flowchart of Figure 6.4. The VBA applies this process to get the distribution of the EVs while respecting what is defined here as the upper limit (UL) vector.

In stage 1, the UL vector comprises the availability at each EVCS. In other words, if EVCS 1 has 200 chargers, but only 100 are free for deployment, EVCS 2 has 30 deployable chargers, EVCS 3 has 40, and EVCS 4 has 75, the UL vector at this stage would be [100, 30, 40, 75]. Given this UL vector and the Priority Vectors of all EVs, the VBA then runs its logic, that is presented in Figure 6.4, and it identifies which priority among each EV's Priority Vector would ensure that their requests get fulfilled while not exceeding the constraints of availability of the EVCSs. The obtained distribution by the VBA at this stage will be referred to as the "initial distribution."

The number of requesting EVs is assumed to be $nRequests$, and the number of EVCSs in the corresponding VB of this VBA to be $nEVCSs$; hence the length of the *PriorityVector* is $nEVCSs$, and the length of the EV vector is $nRequests$. The number of EVs at any

iteration at one EVCS is assumed to be $nEVs$, the index of each evaluated EV to be m , and the index of each EVCS to be i . For each EV in the vector of EVs that are requesting charge, the corresponding Priority Vector is considered. The highest priority is accepted as long as the number of EVs at that EVCS is less than the upper limit obtained or set by the PSA output to that EVCS. If it is less, the number of EVs at that EVCS ($nEVs(i)$) is incremented and that EV is recorded as going to that EVCS. Otherwise, if the upper limit is reached, the next EVCS in the Priority Vector is considered and assessed for the same condition: whether the upper limit is reached or not. This evaluation is done sequentially for each EVCS in the Priority Vector until one is available to accommodate that EV, and is done for each EV in the array of requesting EVs.

6.2.5 Non-discriminatory Approach to fulfilling the EV requests

In following a nondiscriminatory approach among the EVs, the collected requests and corresponding Priority Vectors are first ordered by criticality of the state of charge (SoC) of their batteries. So the first Priority Vector being assessed is that of the EV with the least SoC. That would give it the highest chance at selecting its highest priority when the VBA applies its logic to obtain the distribution. An assumption taken is that being part of this ecosystem, some EVs would accept to go with a priority other than their highest priority when they are not critically in need of a charge, as they will be prioritized when they are. Incentives could be given to convince drivers of the EVs. This however is a behavioral oriented study and is out of scope of the work done in this dissertation.

6.3 The Optimization

The objective function, $OF(X)$, where X is the optimization variable vector, is defined

as in equation (6-1) as the system active power losses (P_{Loss}). If there are n EVCSs, vector X would be $[x_1, x_2, \dots, x_i, \dots, x_n]$, where x_i is the number of EVs at EVCS i .

$$OF(X) = \text{Min}(P_{Loss}(X)) = \text{Min}\left(\sum_{g=1}^{N_g} P_g - \sum_{l=1}^{N_l} P_l(X)\right) \quad (6-1)$$

such that

$$\sum_{j=1}^{N_{CS}} x_j = \sum_{j=1}^{N_{CS}} x_j^{init}, j = 1, 2, 3, \dots, N_{CS} \quad (6-2)$$

$$x_j^{min} \leq x_j \leq x_j^{max}, j = 1, 2, 3, \dots, N_{CS} \quad (6-3)$$

$$Q_g^{min} \leq Q_g \leq Q_g^{max}, g = 1, 2, 3, \dots, N_g \quad (6-4)$$

$$V_i^{min} \leq V_i \leq V_i^{max}, i = 1, 2, 3, \dots, N_b \quad (6-5)$$

$$S_k \leq S_k^{max}, k = 1, 2, 3, \dots, N_{TL} \quad (6-6)$$

$$P_i + jQ_i = V_i \sum_{k=1}^{N_b} Y_{ik} V_k e^{j(\delta_i - \delta_k - \theta_{ik})}, \quad (6-7)$$

$$i = 1, 2, 3, \dots, N_b$$

Where P_g and Q_g are the active and reactive powers of g -th generator, respectively. P_l is the active power of the l -th load.

x_j^{init} and x_j in equation (6-2) are the numbers of EVs at the j -th EVCS in the initial and each iteration of the optimization, respectively. The output of this optimization, X^{opt} , is an optimal vector of EV distributions on the EVCSs as in (6-8):

$$X^{opt} = [x_1^{opt}, x_2^{opt}, \dots, x_i^{opt}, \dots, x_n^{opt}] \quad (6-8)$$

The search space is represented by equation (6-3), where x_j^{min} and x_j^{max} are the lower bound and the upper bound of the range of parameters in the optimization variable vector X . They are the minimum and maximum number of EVs at the j-th EVCS, respectively. Equations (6-4) to (6-7) are the constraints of the optimization problem. V_i in equation (6-5) is the voltage magnitude at the i-th bus. S_k in equation (6-6) is the complex power of the k-th transmission line. P_i and Q_i are the pure active and reactive power injected at the i-th bus. In equation (6-7), Y_{ik} and θ_{ik} are the magnitude and phase of the admittance between buses i and k, respectively. δ_i , and δ_k are the voltage angle at the i-th and k-th bus, respectively. N_g , N_l , N_{CS} , N_b , and N_{TL} are the number of generators, loads, EVCSs, buses, and transmission lines, respectively.

6.3.1 Particle Swarm Optimization

In this work, the modified PSO algorithm is deployed to solve the optimization problem. PSO simulates the behaviors of bird flocking. In PSO [68], each single solution is a "bird" in the search space. It is called a "particle". All of the particles have fitness values which are evaluated by the objective function to be optimized, and have velocities which direct the flying of the particles. The particles fly through the problem space by following the current optimum particles. PSO is initialized with a group of random particles (solutions) and then searches for the optima by updating generations. In every iteration, each particle is updated by following two "best" values. The first one is the best solution (fitness) it has achieved so far. This value is called "pbest." Another "best" value that is tracked by the particle swarm optimizer is the best value obtained so far by any particle in the whole swarm. This best value is a global best and is called "gbest". As shown in the PS

Agent flowchart in Figure 6.3, after finding the two best values in the iteration, the particle updates its velocity and position. This is repeated while the condition of maximum iterations or minimum error criteria is not attained.

In this work, the number of iterations is 30 and the swarm size is 250 particles. If, during the PSO algorithm, a particle violates any of the constraints, it is ignored. The stopping criteria here is the maximum number of iterations. The PSO running time is recorded to be around 5.7 seconds.

The particle X here is 6 dimensional, each dimension being the number of EVs at the corresponding EVCS. In the power flow, this number is translated into MW for varying the load representing the EVCSs. N_j^{min} , the minimum number of EVs at the j -th EVCS, is set as 20% of the number of cars in the initial distribution of each round of optimization. N_j^{max} , the maximum number of EVs at the j -th EVCS, is set as 200.

6.3.2 Normal Conditions

In the normal operating state, the system is said to be secure, where all constraints like maximum capacities of transmission lines, minimum and maximum voltage limits at buses, and the minimum and maximum real and reactive power generation are satisfied. In this condition, collective distribution of EVs is performed to minimize the active power losses in the system while meeting all normal operation constraints.

In this study, the minimum and maximum voltage limits at each bus for normal conditions are set at the standard limits of 0.95 and 1.05 p.u, respectively as set by the NEC standard.

6.3.3 N-1 Contingencies

The failing of one or several components in the power system may lead to transmission congestion, a situation in which the power system cannot operate safely. This occurs when there is not enough transmission capability to perform the needed power flow and keep the generation-loading balance. In these cases, overloading in some transmission lines or voltage violation beyond acceptable ranges might occur. If the constraints defined in equations (6-4) and (6-7) are violated in any post-contingency scenario, the system's operating state is deemed insecure. This congestion may be alleviated by incorporating line capacity constraints in the real-time optimization.

The responsibility of the ISO is to maintain the system's security and manage the congestion through a real-time congestion management (RTCM) algorithm. Optimal operation of FACTS devices, generation rescheduling, load demand response and load shedding are some tools for RTCM.

In this chapter, the collective distribution of EVs is used as the tool for the RTCM problem, while simultaneously minimizing the losses in the system. For this purpose, the minimum and maximum voltage limits are considered as 0.90 and 1.05 p.u. for contingency conditions, while the maximum loading for transmission lines would be 90% for N-1 contingencies and 100% for contingencies with higher order. In the RTCM problem, the dynamic and quasi dynamic thermal ratings of transmission lines can be considered, as described in [50]. However, in this work, only the static rating of the transmission lines are considered.

In the contingency conditions, the optimization is run with the new limits for voltage and transmission line loading. Although the objective function aims at minimizing the losses in the system, huge penalty factors are added to the objective function if any constraint is violated. Therefore, the optimal collective distribution of EVs is obtained to manage the congestion while minimizing the active power losses in the system. Numerical results will demonstrate the effectiveness of this method in mitigating the congestion in power systems.

6.4 Case Studies and Results

To demonstrate the effectiveness of the proposed CDML, the optimization is applied in both normal and contingency conditions cases involving a modified version of the IEEE 14-bus system and a laboratory-scale 8-bus power system.

The CDML could be applied to both MV and LV systems. The high-capacity charging stations are usually considered to be connected to the MV system. The laboratory-scale 8-bus power system is a smart power system testbed facility at Florida International University that was reconfigured to run the experiment herein. The voltage level of this system is same as the distribution system voltage level in USA (208V).

As described in section 6.2, the initial distribution of the EVs onto the EVCSs, before the induced redistribution, is obtained by the VBA and fed to the PSA. The PSA also collects the most recent availability posted by the EVCSs during that period, runs the optimization, and obtains the optimum distribution of the EVs onto the EVCSs that would primarily secure the system against congestions in contingency conditions, and secondly minimize the losses.

The levels of congestion management are presented in the contingency condition case study. Also, in normal and contingency conditions, the percentage loss reduction, % LR , is calculated by equation (6-9) and presented.

$$\% LR = \frac{(P_{Loss}(X_{init}) - P_{Loss}(X_{opt}))}{P_{Loss}(X_{init})} \times 100 \quad (6-9)$$

where P_{Loss} is calculated by equation (6-1), X_{init} is the initial distribution vector, and X_{opt} is the optimal distribution vector, corresponding to the final gbest in the optimization.

6.4.1 Modified IEEE 14-bus System, Normal Conditions

A case study with a VB covering 6 EVCSs is considered. The standard IEEE 14-bus system is modified to include 6 EVCSs augmented with photovoltaic systems, at buses 5, 9, 11, 12, 13, and 14. A single line diagram of the system is shown in Figure 6.5. The

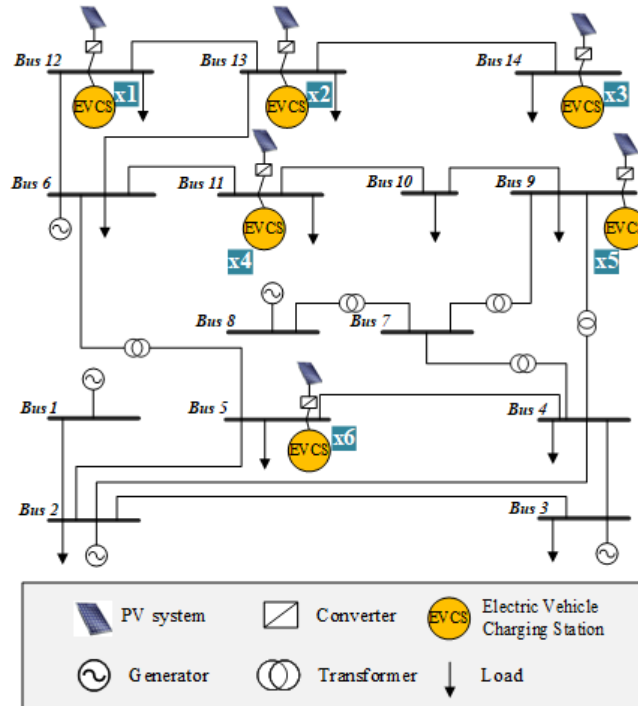


Figure 6.5 Single line diagram of the modified IEEE 14-bus system.

capacity of each EVCS is translated from the number of maximum dedicated EV chargers, here assumed to be 200, to power in MW, where each EV charger is assumed to be rated 72 kW [69].

The optimization variable vector is $X = [x_1, x_2, x_3, x_4, x_5, x_6]$, where $x_1, x_2, x_3, x_4, x_5, x_6$ are the number of EVs at EVCS 1, 2, 3, 4, 5, and 6, respectively, as labelled in Figure 6.5. The power flow is run at each optimization particle X and $OF(X)$, the losses, are calculated by equation (6-1).

The IEEE 14 bus system was modeled in DIgSILENT PowerFactory 2017 and simulated for 96 periods. The time assumed is 24 hours, and each period is assumed to be 15 minutes. At each period, a large number of EVs were considered to be geo-distributed in the VB and issuing request for public charging. The number of EVs is varied during the 24-hour period to be maximum at a peak hour. At any of the 96 periods, the initial distribution of the EVs onto the EVCSs, X_{init} , makes up the initial particle to be optimized by the PSO.

To calculate the fitness function of each particle X during the PSO process, the power flow is run to calculate the system losses. The particle with minimum OF in the whole swarm -that corresponds to the final gbest- is the optimal distribution vector for that period. The calculated losses for the particle X_{opt} , at each of the 96 periods, are recorded and compared to the losses in the initial distribution, X_{init} . The 24-hours results are depicted in Figure 6.6 (a1) vs. (a2) for the periods between hours 0 and 6, (b1) vs. (b2) between hours 6 and 12, (c1) vs. (c2) between hours 12 and 18, (d1) vs.(d2) between hours 18 and 24.

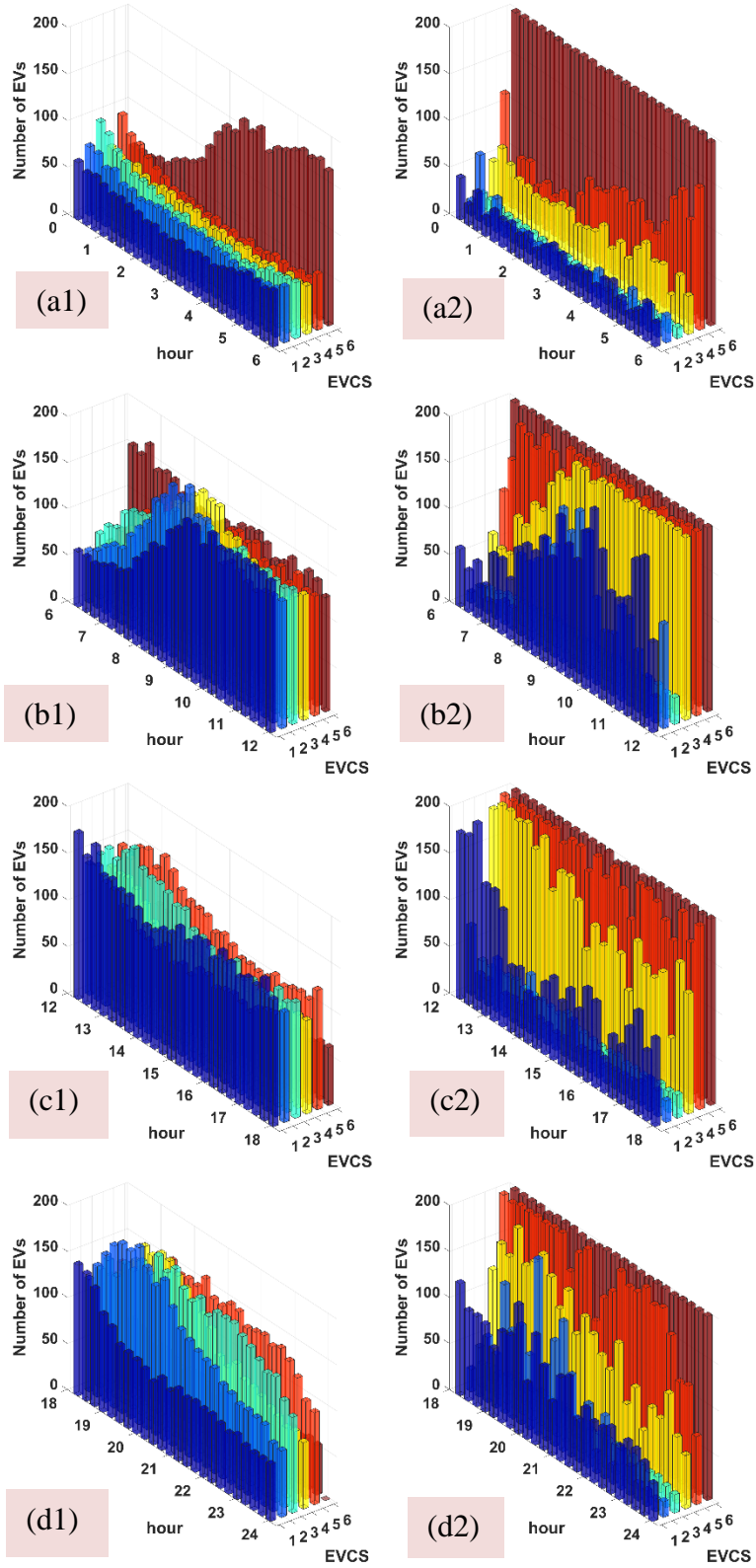


Figure 6.6 (a) Initial & (b) Optimal Distribution of the EVs onto the EVCSs, in all Periods between (a) hours 0 – 6, (b) hours 6 – 12, (c) hours 12 – 18, (d) hours 18 – 24

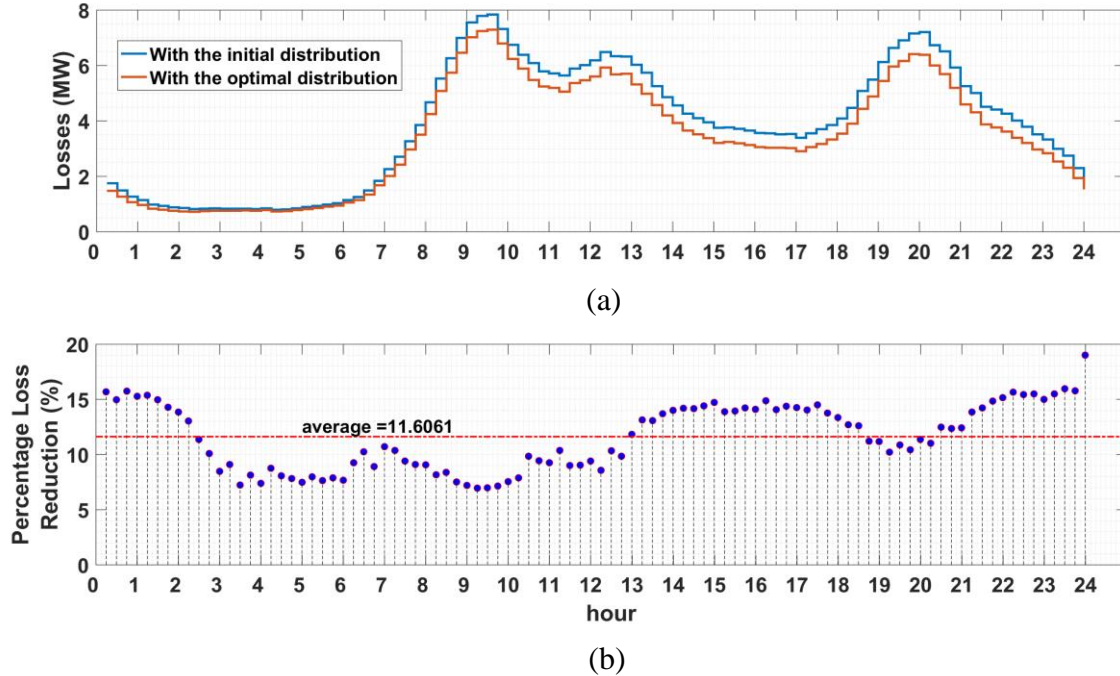


Figure 6.7 (a) Losses with the Initial Distribution vs with the Optimal Distribution, and (b) Percentage loss reduction in all Periods.

Also, for each of the 96 periods, the % *LR* is calculated as in (6-9). The results of the losses in MW and the % *LR* in all periods of the 24 hours are presented in Figure 6.7 (a) and (b), respectively. The CDML successfully achieved a percentage loss reduction varying at different times of the day between 8 and 18 %, with an average of 11.6 %.

6.4.2 Modified IEEE 14-bus System, Contingency Conditions

To demonstrate the effectiveness of the CDML in congestion conditions, two contingencies were applied and the results of the CDML recorded. In the first contingency situation, an N-1 contingency is simulated where line 6-12 is out of service. Table 6-1 shows that under this contingency, line 6-13 is congested at 98.57% loading level. The initial and optimal distributions of EVs as obtained by the VBA and the PSA, respectively,

are presented. The CDML was successful in redistributing the EVs in a way that reduced the congested line (CL) loading to below the set 90% loading limit.

Table 6-1 N-1 Contingency

Time	9:15 AM	
Out of service	Line 6-12	
Congested line (CL)	Line 6-13	
	EV distribution	
EVCS index	<i>Base</i>	<i>Optimal</i>
EVCS 1	144	17
EVCS 2	176	200
EVCS 3	30	133
EVCS 4	200	200
EVCS 5	200	200
EVCS 6	200	200
CL Loading (%)	98.57	88.26
Losses (MW)	9.292309	8.340039
% Loss Reduction	10.25	

Table 6-2 N-3 Contingency

Time	7:45 AM	
Out of service	Line 6-12. Line 6-11, bus 7	
Congested line (CL)	Line 6-13	
	EV distribution	
EVCS index	<i>Base</i>	<i>Optimal</i>
EVCS 1	104	18
EVCS 2	84	25
EVCS 3	28	106
EVCS 4	200	200
EVCS 5	170	200
EVCS 6	160	197
CL loading (%)	122.92	112.45
Losses (MW)	12.62885	13.77
% Loss Reduction	- 9.03 %	

Furthermore, the CDML was successful in reducing the active power losses in this case. The losses decreased from ~ 9.3 to 8.3 MW, constituting a % LR of 10.25 %. In a second case, an N-3 contingency was simulated, as described in Table 6-2. In this case, although the CDML increased the system losses by 9.03% from 12.63 to 13.77 MW, it managed the congestion by reducing the loading of the CL from

122.92% of loading in line 6-13 to 112.45%. To completely eliminate the congestion from the system, 7.3 MW of load shedding is needed in the optimal distribution compared to 13.1 MW in the initial distribution. This means that the CDML reduced the mandatory load shedding by around 6 MW.

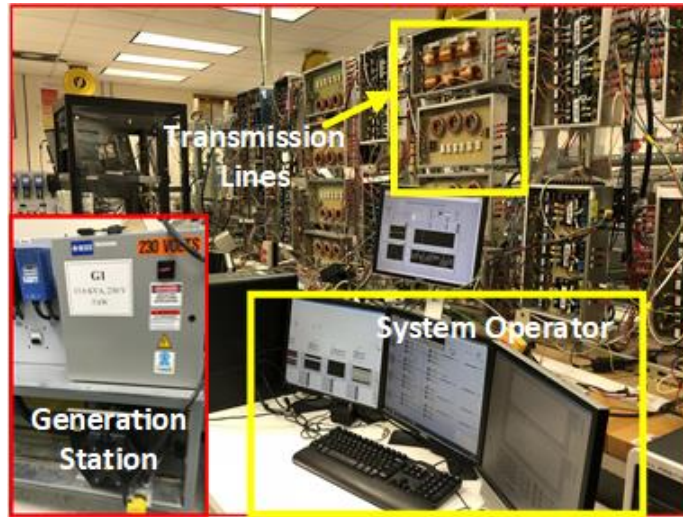
An efficient customer-side economic indicator for power system security is the Value of Lost Load (VoLL). It represents customers' willingness to pay for avoiding curtailment of electricity service, which might occur in response to targeted load shedding over discrete timeframes due to insufficient operating reserves [70]. The ERCOT-wide implied macroeconomic VOLL value in 2011, calculated based on a method referred to in [70] as the MSA ratio, is 6,468 \$/MWh. That is, the CDML-achieved 6 MW reduction in the mandatory load shedding can be translated into saving $6 \times 6,468 = 38,808$ \$ per hour of load shedding.

6.4.3 Experiment: 8 Bus System

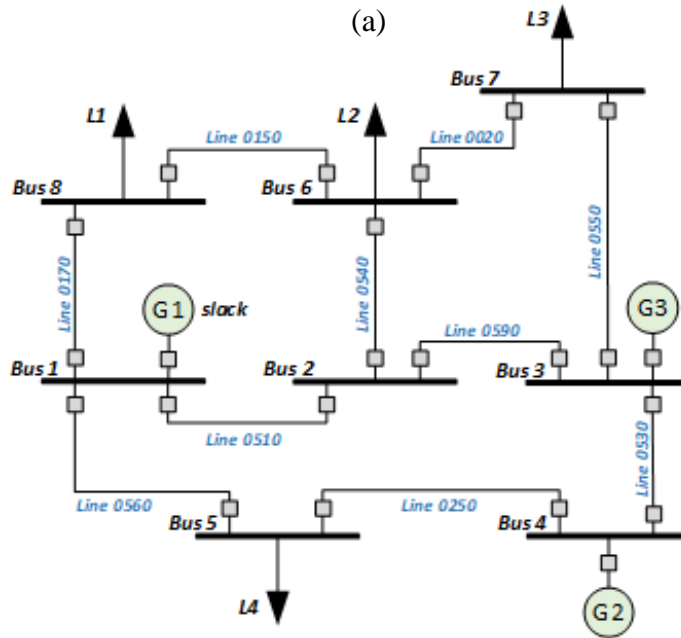
To experimentally demonstrate the effectiveness of the CDML concept in reducing active power losses in normal conditions, a case study was implemented where an initial distribution and the corresponding optimal distribution was applied on a hardware-based laboratory smart grid test-bed [71], [72] with experimental dynamic load emulator models. Figure 6.8 (a) shows a picture of the smart grid test-bed on which this experiment was applied. This test-bed is reconfigured in this work to construct the 8-bus system depicted in Figure 6.8 (b). The transmission lines and synchronous generators' parameters are given in [71], and the transmission lines are labelled here as in [72].

The system was first modeled in DIgSILENT given those parameters and simulated with an initial vector for load distribution $X_{init} = [L1_initial, L2_initial, L3_initial, L4_initial]$. The PSO is applied to this simulation and the optimal vector $X_{opt} = [L1_optimal, L2_optimal, L3_optimal, L4_optimal]$ obtained.

After the generators are synchronized, the dynamic loads are set to predefined values, making up the initial distribution vector X_{init} . This is applied for 6 periods, i.e. 6 different initial distributions, where the period is 30 seconds in experiment. Then, the loads are changed and the experiment run again for 6 periods to follow the optimal vectors, X_{opt} . In the initial and optimal distribution experiments, the generation and the load readings are collected using the real-time system's measurements inside of the LabVIEW and the data acquisition systems' (DAQs) in the real-time environment of the testbed [72]. The LabVIEW software was used as the junction for acquiring and interpreting the data from the test bed, as well as the junction to send control commands to the testbed itself. Figure 6.9 shows the Labview Interface used to conduct the experiment.



(a)



(b)

Figure 6.8 (a) FIU Smart Grid Testbed view (b) Single line diagram of the experimental 8-bus system

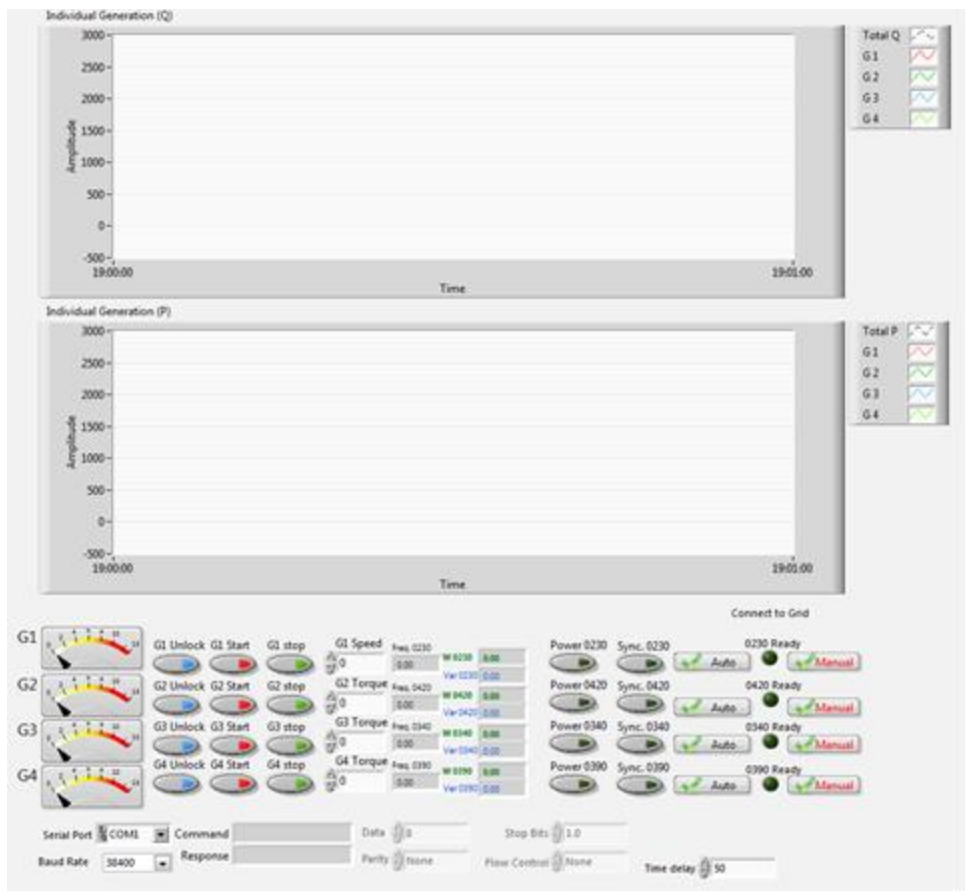
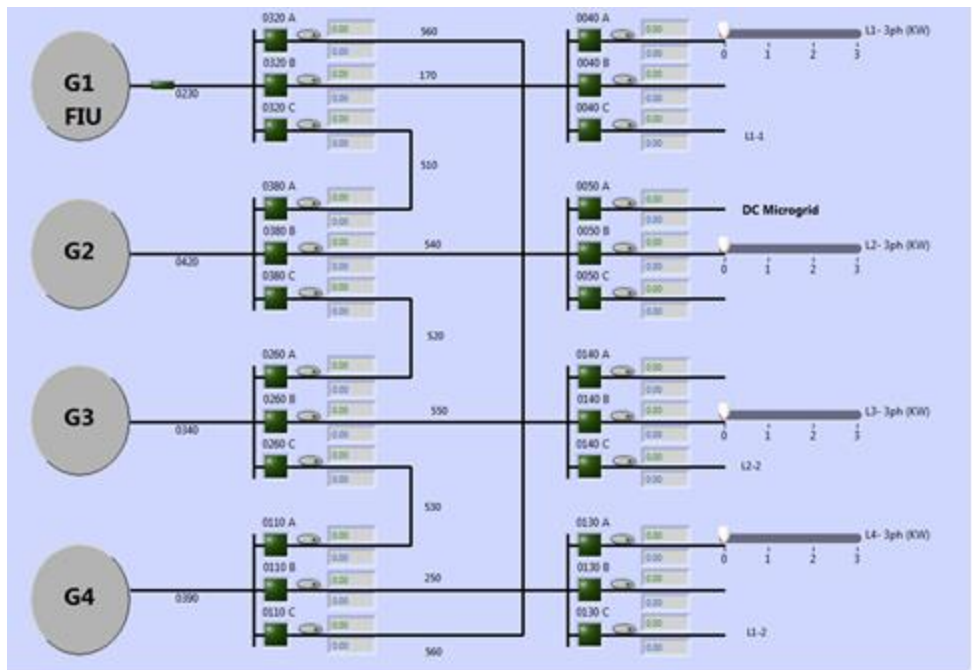


Figure 6.9 Labview Interface

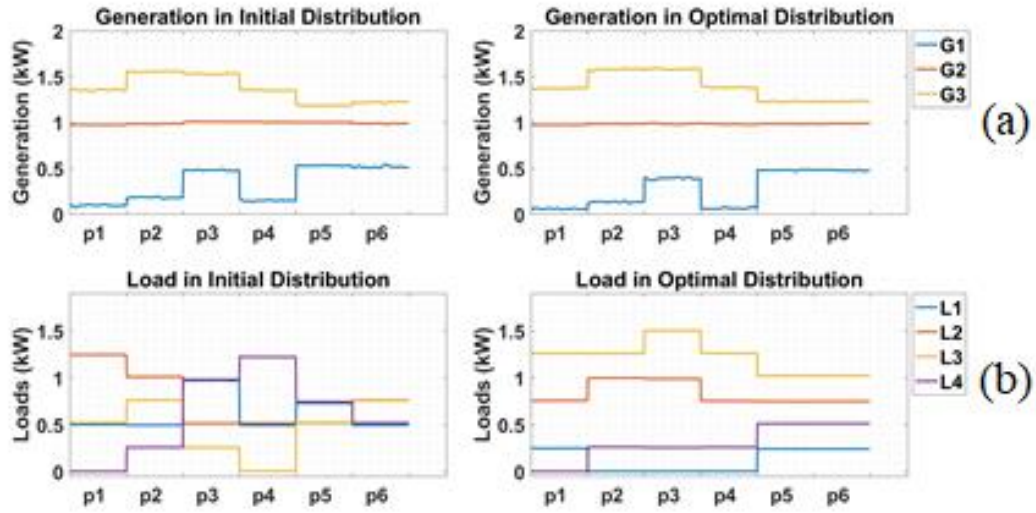


Figure 6.10 The different (a) Generation and (b) Load in Initial and Optimal Distributions, for all six periods.

The generation and the load readings are presented in Figure 6.10 (a) and (b), respectively. Figure 6.11 (a) presents the summation of the generation and the summation of the loads, in the initial and the optimal cases. The losses are then calculated by (3) and are presented in Figure 6.11 (b). The average % *LR* is calculated for each period and is presented in Table 6-3.

With an average % *LR* ranging from ~ 8% to ~ 43%, the results validate the hypothesis and prove the CDML promising.

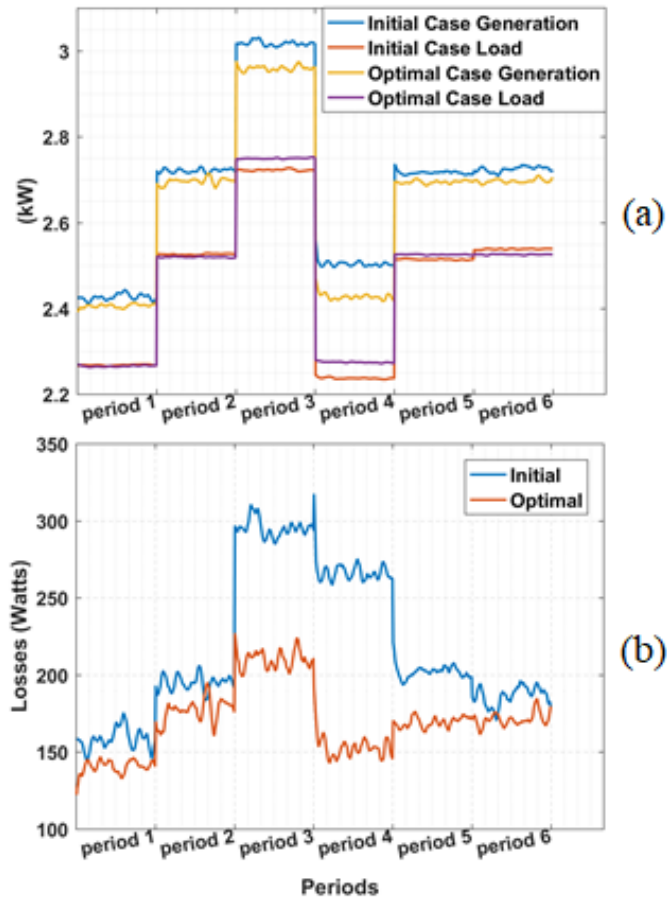


Figure 6.11 (a) Sum of generation and of load in initial and in optimal distribution, (b) Losses in the Initial vs Optimal distribution, for all six periods.

Table 6-3 Average Percentage Loss Reduction in Each Run Period

Period	p1	p2	p3	p4	p5	p6
Average LR (%)	11.06	9.16	28.8	42.62	16.2	8.11

6.5 Prospects for Commercialization of the CDML and Future Work

When considering the commercialization of the CDML as a service, it is imperative to consider the present players in the industry of public charging of EVs. There are two key stakeholders in this industry [73]: The Charging Point Operator (CPO) and the Electric Mobility Service Provider (EMSP). An EMSP is alternatively referred to as an Electric

Vehicle Service Provider (EVSP). A CPO is a company that operates a pool of charging points, whether it owns them or not. Its management includes technical and IT maintenance, payments for its electrical connection, and managing the energy supply. The EMSP/EVSP is user-oriented. It is a company that provides the EV owner with access and billing capability on charging infrastructure owned and operated by CPOs. It typically provides access charge cards, a mobile app or web interface, and a billing system. Hence, CPOs rely on EVSPs to provide access to their charging stations. Examples of CPOs are ABB for plug-in EVSE [74] and WiTricity for wireless EVSE [75]. Examples of EVSPs are EV Connect, Nextcharge network, and Greenlots [76]. In addition to the CPOs and EVSPs, there are companies that provide navigation systems. They help customers plan ahead their charging sessions by finding a public charger. Examples of navigation systems companies are Plugshare [77], Plugsurfing [78], and Zap-map [79]. Although those are 3 different categories, some companies provide the three services combined. For example, Tesla Motors is a CPO, an EVSP, and provides a navigation system.

For commercializing the CDML, a coalition could be formed among the EVSPs, where the VBA and the HLA would obtain the information from the EVSPs networks that operate EVCSs in a given geographical area, for obtaining real-time information on the status of the EVSEs, and for communicating reservations to them. An attempt for achieving interoperability among public EVSEs was made through an application protocol called the Open Charge Point Protocol (OCPP) [80]. The purpose of the OCPP is defining the communication language between EV charging stations and central management systems, like that of EVSPs. While the OCPP is still not a standard, it has been adopted by many

CPOs and EVSPs. The OCPP data types can be utilized or edited to incorporate the needed data to be communicated between the EVSE and the EVSP network. The use of application protocols like OCPP, capitalizing on the interoperability feature provided by the use of a middleware like that used in the BDSS, and the joint efforts of EVSPs and Energy Service Providers (ESP)s, are three steps needed to facilitate the commercialization of the CDML.

The on-board module can be an added service within the provided services to the customer by the EVSP. This can be looked at in analogy to usage-based auto-insurance [81], in which drivers choose to plug-in a device to their vehicles. This device monitors the driving behavior to reward safe drivers by discounted insurance rates or penalize aggressive drivers by increasing their rates.

Assessment survey studies on the socio-economic benefits to the EV owner from participating in the CDML can be done to identify the best incentive plan for the users' participation. Currently, the transmission and distribution system losses are passed on to the end user as volumetric cost or a percentage of their electricity bill. A decrease in the system loss in normal conditions can be reflected as a decrease in the participating customers' home electricity bills or as a reward by a discounted charging session. As for the ISO, maximizing revenue requires optimizing the joint operation of all available ancillary services. The CDML proves to provide great benefit, reducing the amount of load to be shed in contingencies and ensuring a more economic operation of the system in normal conditions.

6.6 Conclusion

In this chapter, an effective service with promising ancillary potential, the Collective Distribution of Mobile Loads, CDML, was presented. A real-time system-level PSO algorithm was applied to determine the optimal collective distribution of mobile loads. Afterwards, the optimization results were passed to the BDSS to guide the EVs to the appropriate EVCS. Studies were applied in a simulation of a modified version of the standard IEEE 14-bus system under normal and contingency operation conditions, as well as in an experiment comprising an 8-bus laboratory-scale power system, under normal conditions. The results of the applied case studies have proven the CDML a viable and effective service, achieving noteworthy levels of loss reduction and post-contingency congestion relief that minimize the need for load shedding.

Chapter 7 Advanced Computing for Real-time Handling of Big-Data that is associated with the Management of a Large Number of Electric Vehicles

7.1 Introduction

As part of the international environmental treaty, the United Nations Framework Convention on Climate Change (UNFCCC), global world leaders and policymakers have met annually since 1995 in the Conferences of the Parties (COP): COP1-COP23. The goal has always been to assess progress in dealing with climate change and to establish policy commitments. Furthermore, since the electrification of the transport sector offers a major step towards a clean energy transition, Sustainable Mobility has been an extensively discussed focus area in the most recent summits [82], the latest being COP23 in 2017. With such a global drive, many countries have set deadlines for automakers to end the sale of new Internal Combustion Engine (ICE) vehicles and have started a new policy of giving incentives to consumers for promoting EV ownership.

Barriers to the growth of EV adoption, including users' mileage range anxiety and the short availability of EVCSs, among others, are already being overcome. Technical solutions, such as fast and ultra-fast chargers, are being developed and deployed in many parts of the world.

At this stage, power system engineers and researchers are conducting extensive research to propose solutions that organize this underway expansion. The objective is to prepare the power system to optimally embrace this bulk load added and find ways to benefit from this coming shift. For example, several works have presented studies in which

the energy in the vehicle is used for purposes like peak shaving and improved energy management schemes, producing the Vehicle to Grid (V2G) concept. This notion and others became well-examined applications by researchers involved in system-level integration of EVs. Another interesting example for harnessing the benefits of using EVs as mobile energy storage devices could be found in the study conducted in [83] that assesses the feasibility of deploying a number of EVs in an adaptive protection technique to ride through cyber-attack threats in microgrids.

In the pursuit of a seamless transition, and as part of this power-system-level research drive in dealing with the issue, a data-sharing platform which involves connected EVs and supervisory management is presented in chapter 5. The work in that chapter presents a connectivity platform involving two-way communication on two levels: one among supervisory management agents, and the other between those agents and the EVs to guide them to the most appropriate public EVCSs at which to charge. This is while respecting their energy needs and their preferences. A brief on this system is given and the big data issue illustrated in section 7.2.

The need for organizing the connections of this large number of EVs for the welfare of the power system, without disregarding the benefits of all involved stakeholders, brings along large volumes of heterogeneous data sets to be analyzed and processed in real-time. This real-time requirement comes into picture because of several factors, essentially including the mobility aspect of the vehicles in this application.

On a parallel note, huge advancements in the area of processing power are taking place, presenting vast support for research of data scientists. The GPU, particularly, is gaining

popularity and has become the processor of choice in the data science environment [84]. Although it has been originally intended for offering speedups in the gaming graphics rendering and image processing applications [85], it is now being leveraged to many big data applications, like sequencing techniques in medical studies [86], computational finance, deep learning, oil and gas, and safety and security industries [87]. GPUs comprise hundreds and thousands of computational cores, scaling computing challenges in those different applications with the thread concurrency mechanism that it inherently features. GPU utilization facilitates using large data sets in orders of magnitude less time and using far less power and datacenter infrastructure.

An example of the issue of big data in platforms of supervisory management of EVs is highlighted and an overview of the CUDA GPU computing environment is presented. The CUDA GPU computing environment and its appropriateness for the application of supervisory management of EVs is presented in section 7.3. Then, the approach followed in terms of coordinated computing between the Central Processing Unit (CPU) and the Graphics Processing Unit (GPU) is illustrated in section 7.4. The case studies applied, with the data sets' preparation and the results comparing performance on CPU vs GPU, are presented in section 7.5. The chapter is concluded in section 7.6.

7.2 Supervisory Management of Large Electric Vehicle Fleet: A Big Data Issue

With the study of large scale energy management systems involving tens or hundreds of distributed power entities, those being microgrids, individual generation or load nodes, big data challenges unfold [88]. From a power system point of view, public EVCSs, that comprise several individual chargers at their premises, represent variable loads because of

vehicles connecting and disconnecting to the individual chargers. Each EV represents an increment or a decrement of that load because at any time of the day, it might decide to connect at any EVCS, which is a node in the power system.

As mentioned before, and in the pursuit of a seamless transition towards the domination of EVs and their infrastructure on the future or upgraded cities, a data-sharing platform which involves the communications with geo-distributed connected EVs and supervisory management was presented in chapter 5. As part of this system, a multistage cognitive price-based strategy is applied as the computational part of a supervisory agent and is further illustrated in [9]. This supervisory agent is called the VBA.

In short, the EV driver issues a request to charge at one of the public EVCSs. Concurrently, tens or hundreds of EV drivers will be issuing a similar request, while they are en-route to their destination. The EV would be equipped with an on-board module that receives a set of information related to the available EVCSs, and then performs its logic and guides the EV driver to the EVCS that has available chargers and that is most suitable for the vehicle's current energy-related status.

One of the parameters that the EV on-board module receives to perform its logic is the price at each EVCS. It receives this in the form of a price vector. For a supervisory agent like the VBA, in this example, to manage a large number of requests coming in in real-time and to send out the prices that would attract more vehicles to where the power system is ready to increase its load and discourage vehicles from heading towards the rest of the EVCSs, large sets of heterogeneous data need to be processed and analyzed.

The objective is to redistribute the EVs onto EVCSs in a way to maximize a predefined objective function related to power distribution, while respecting system constraints. Each vehicle communicates the following features to the VBA: the state of charge (SoC), the distance to each EVCS (DtCS), and the time to each EVCS (TtCS). The VBA also collects the availabilities and the prices at each of the EVCSs. It then forms a price vector of the prices at the individual EVCSs, and uses this vector's elements as the manipulated variable to achieve its objective. It stipulates the CPVs, evaluates the objective function (OF) at each of them, and then identifies the one that maximizes this OF. It is noteworthy that the EV driver has to wait after issuing the request to receive from the VBA the new redistribution prices that are changed dynamically.

When this strategy was presented in [9], an effort was presented to minimize this wait time by minimizing the processing time of the VBA's strategy. CPU parallel processing and a 3D lookup table (LUT) were used. Despite the immense time reduction (from hours to seconds) achieved by the 3D LUT, the time was still at 11 seconds for a case study of 21 EVs and 6 EVCSs. While this time is within an acceptable range for drivers to wait for a response from its on-board module on the preferred EVCS, the application of this strategy using GPU provides better handling of the big data by eliminating the need for complex mapping into a LUT. In addition, it provides a scalability feature by supporting far more data volume while using less power. Hence, the work in this chapter introduces a solution to the big data problem that arises when introducing the cognitive price-based strategy of the VBA, presented in chapter 5. It also lays the foundation for the application of GPU computing for the deployment of such large scale real-time management systems that

alternatively could have been confronted with the hurdle of the big data processing requirement.

To give an example to envisage the size of the data sets at hand, we assume an instance with 100 EVs (i.e. $nEVs=100$) issuing request for charging in a certain geographical area managed by a VBA, and 6 public EVCSs (i.e. $nEVCSs=6$) in that same area. A 1D array of SoCs at that instance collected by the VBA will be of length 100. Each of the 1D DtP and TtP arrays will be of length $nEVs \times nEVCSs = 100 \times 6 = 600$. For stipulating the CPVs, the VBA has to assume a “discretization level” of the acceptable price range, within the agreed-on limits with the EVCSs’ owners or service providers. If, for example, the discretization level is chosen to be 3, this means that when stipulating the price vectors, the VBA would consider 3 possible prices at each EVCS. Assuming that the discretization level for the price at each EVCS is 6, the number of CPVs, calculated by equation (7-1), would be:

$$n\ CPV\ s = (n\ EVCS\ s)^{discretization\ level} \quad (7-1)$$

that is $6^6=46,656$. Since they are 6 EVCSs, the CPV’s dataset will be a 2D array of size $6 \times 46,656$.

In the connectivity platform referred to in this work, the on-board module is fuzzy-logic based, and the VBA would need to perform similar FL evaluations to foresee the decisions of the EVs and accordingly aggregate those to foresee the distribution of the EVs onto the EVCSs. The number of FL evaluations to be performed by the VBA for this instance is calculated as in equation (7-2).

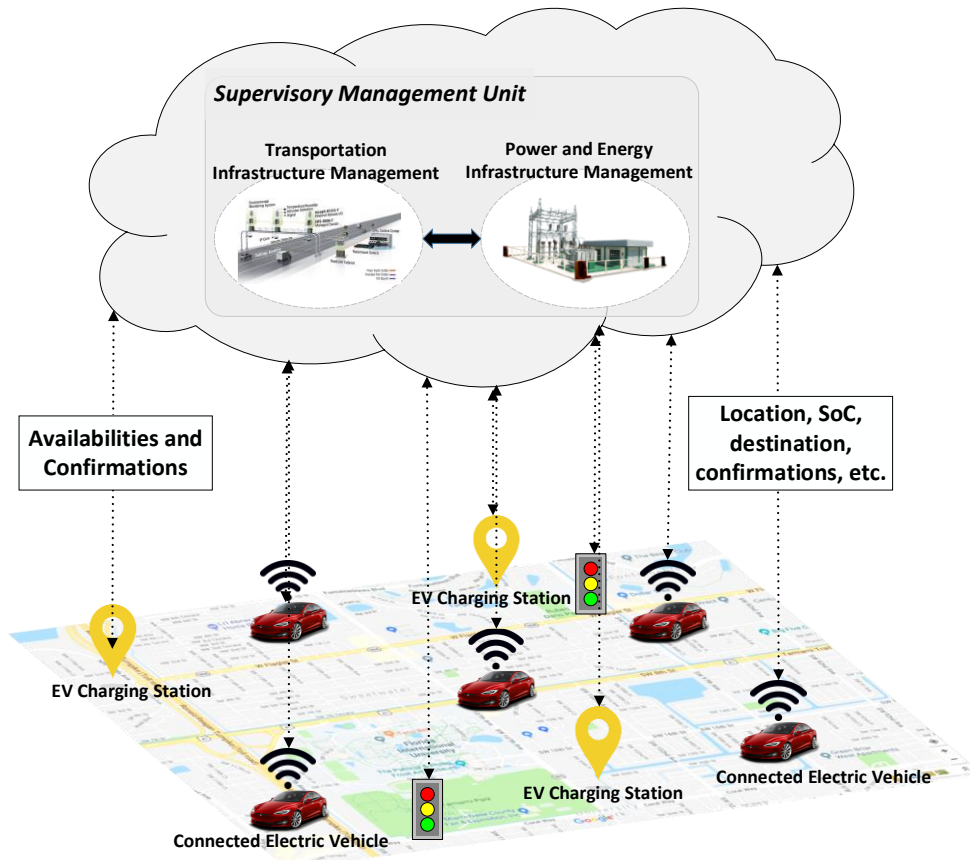


Figure 7.1 Supervisory Management of Large Number of EVs.

$$n \text{ FL evaluations} = n \text{ EVs} \times (n \text{ EVCSs})^{((discretization \ level) + 1)} \quad (7-2)$$

that is $100 \times 6^7 = 27,993,600$ FL evaluations for this instance.

Given this huge data volume indicated by the numbers presented, a decision might seem unfeasible with conventional computational means.

Although the work presented in this chapter involves a decision-making strategy for the management of a large number of EVs when considering the power and energy infrastructure; the real-time feature that the GPU has helped achieve could allow for augmenting the application to involve the interdependencies that arise in such applications

between the transportation infrastructure management and the power and energy infrastructure management, as can be seen in Figure 7.1. Considering the effects of the transportation, such as traffic levels at different links in the EV routes, would further expand the dimensions of the data at hand, highlighting the need for GPU processing.

7.3 GPU Parallelization Using CUDA Computing Environment

For data scientists, GPUs have become the processor of choice when dealing with big data. GPUs comprise hundreds and thousands of computational cores, scaling computing challenges in different data-parallel applications with the thread concurrency mechanism that it inherently features. GPU utilization facilitates using large data sets in orders of magnitude less time and using far less power and datacenter infrastructure. Furthermore, in many data-parallel applications, indexing is a very important feature that cannot be overlooked. Sorting data for prioritization purposes, in addition to iterated evaluations of the same function on a big data set, like the application at hand, are examples where

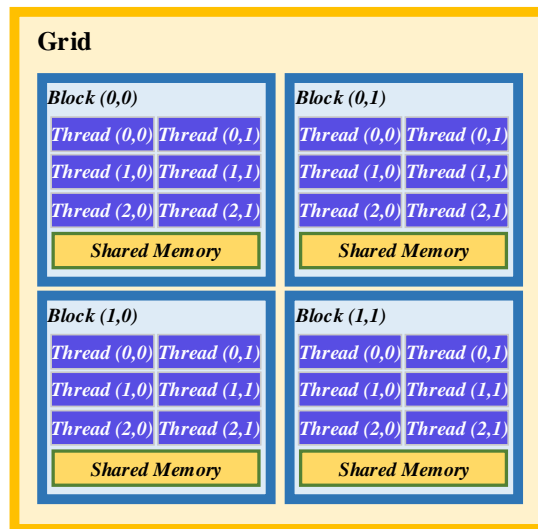


Figure 7.2 GPU Grid building blocks.

indexing is necessary. For that, the CUDA computing environment provides means to leverage the GPU parallelization feature.

In the CUDA computing environment, the GPU grid is organized into three layers of resources: Thread, Block, and Grid, as depicted in Figure 7.2. Also, in this computing platform, the CPU and its memory is referred to as “host” and the GPU and its memory is referred to as “device”. To run a function on the device and call it from the host side, this function is identified as a global one called “kernel.” This function is to be referred to in code by the identifier `__global__`.

The functions to be used in the scope of the host code only are host functions, with identifier `__host__`. Similarly, the functions to be used in the scope of the device code only are device functions, with identifier `__device__`.

The sequence of the operation of a CUDA C program is to declare and allocate the host and device memory, initialize host data, then transfer data from host to device, execute one

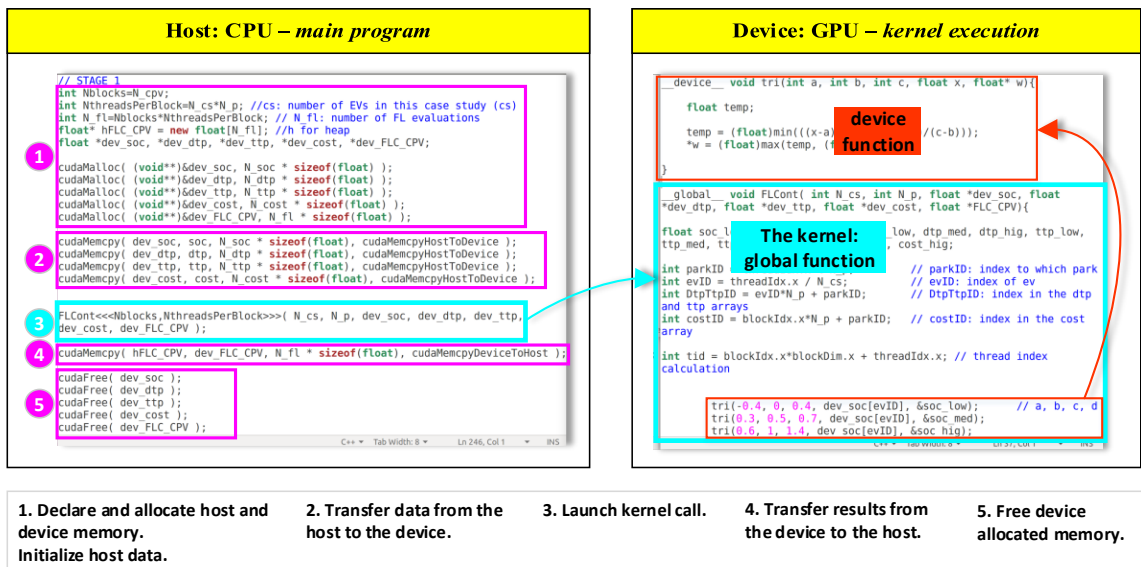


Figure 7.3 The sequence of steps on the host and device parts of the application code.

or more kernels, transfer results from the device to the host, and finally free the device allocated memory. Those steps are depicted in Figure 7.3, where the parts of the application's host code and device code are presented.

When a kernel call is launched, several copies of the kernel function are created and run in parallel. Each of these parallel invocations is called a thread block, or simply a block. Multiple blocks are combined to form a grid, and all the blocks in the same grid contain the same number of threads. Thread blocks execute independently, while threads within a block can cooperate by sharing data through shared memory and by synchronizing their execution to coordinate memory accesses. The grid of blocks and the thread blocks can be 1, 2, or 3-dimensional. A 2D grid made up of 2D thread blocks is shown in Figure 7.2. It is important to note that the extent of scalability regarding the instances of the kernel being run concurrently vary depending on device limits, but in all cases, the number of cores in any GPU is significantly more than the CPU, largely accelerating the application algorithm.

The block index within the grid is referred to in CUDA as *blockIdx*, the dimension of the block in terms of number of threads that make it up is referred to as *blockDim*, and the thread index within the block as *threadIdx*. Those are used for proper thread addressing, i.e. for distributing the device code's input data onto the threads with the appropriate indices and obtaining the output results from the concurrently running threads properly. The number of kernel copies and the grid dimensions are specified in the kernel call, in the host code. For example, calling `kernel<<gridDim, blockDim>>(input1,input2)` launches a grid with dimensions *gridDim* and the number of blocks in each dimension specified in *blockDim*.

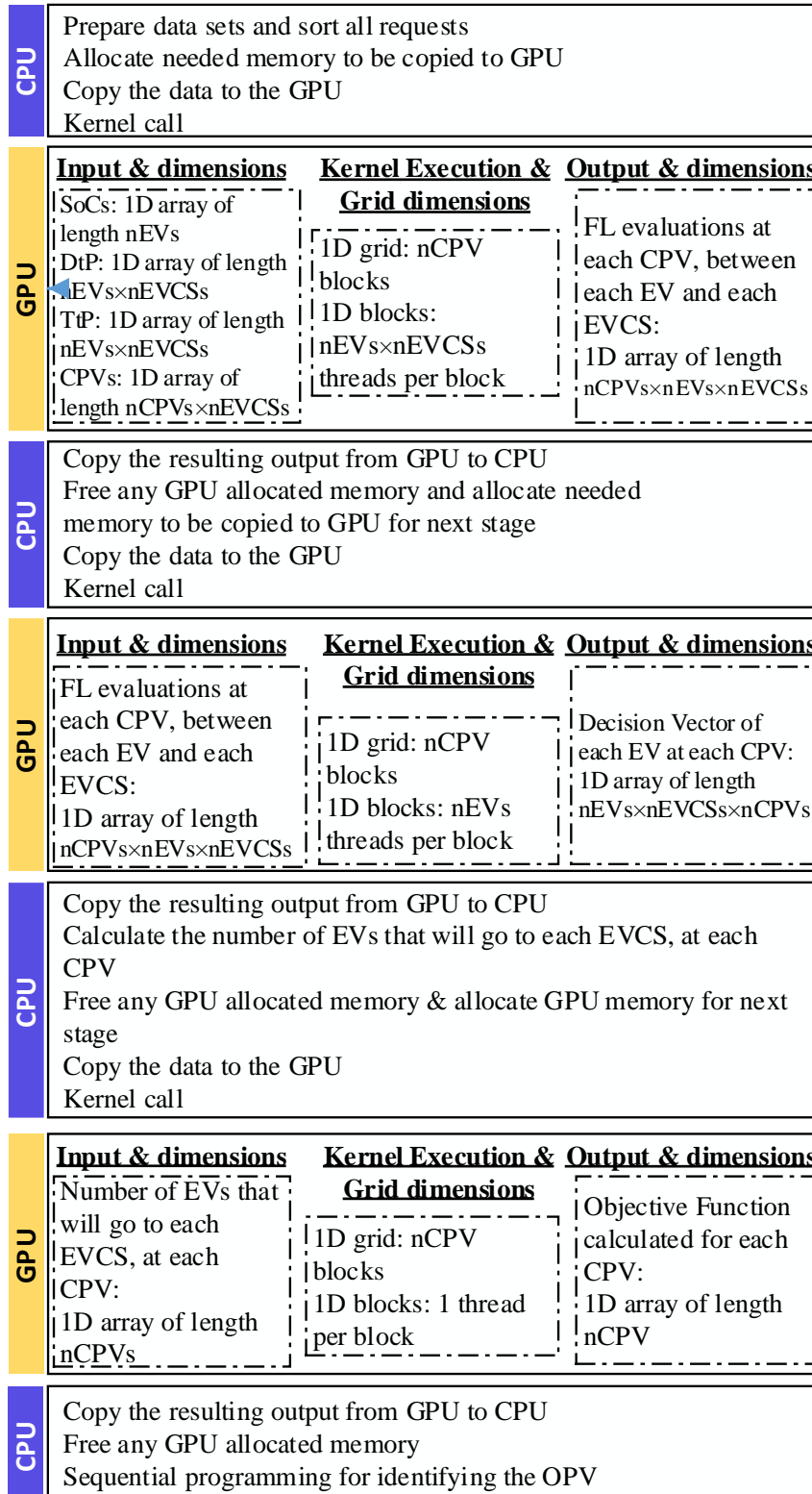


Figure 7.4 The three stage coordinated computing between CPU and GPU.

7.4 Three-Stage CPU-GPU Coordinated Computing

The CUDA computing environment provides a means for coordinated computing between CPUs and GPUs; i.e. the application code is prepared in a way to send the compute-intensive functions of the applied algorithm to the GPU, and the rest of the sequential code to perform on the CPU. The data is prepared on the CPU, passed over to the GPU to take advantage of the parallelization feature, and then the results copied back to the CPU for further sequential processing. This speeds up the code and is of maximum benefit in applications where parallelization is necessary.

In the algorithm followed in the work here, three functions are identified to be of need for parallelization. For this reason, the computing is coordinated between the CPU and the GPU in three stages, as shown in Figure 7.4. Also, the dimensions of the grid in each stage are indicated in Figure 7.5. First, the data is prepared on the CPU and the requests are sorted by criticality of state of charge (SoC). Then, the required device memory of the GPU for the inputs and the outputs of stage 1 is allocated. The input data is then copied from the host to device, and the kernel function is called.

As depicted in Figure 7.5 (a), the GPU grid in this stage is a 1D grid made up of n_{CPV} blocks, n_{CPV} being the number of CPV vectors that the VBA needs to assess and choose from. Each block is made up of $n_{EVs} \times n_{EVCSs}$ threads. The threads run in parallel and output the FL evaluations at each CPV, a 1D array of length $n_{CPVs} \times n_{EVs} \times n_{EVCSs}$. This array is then copied to the CPU.

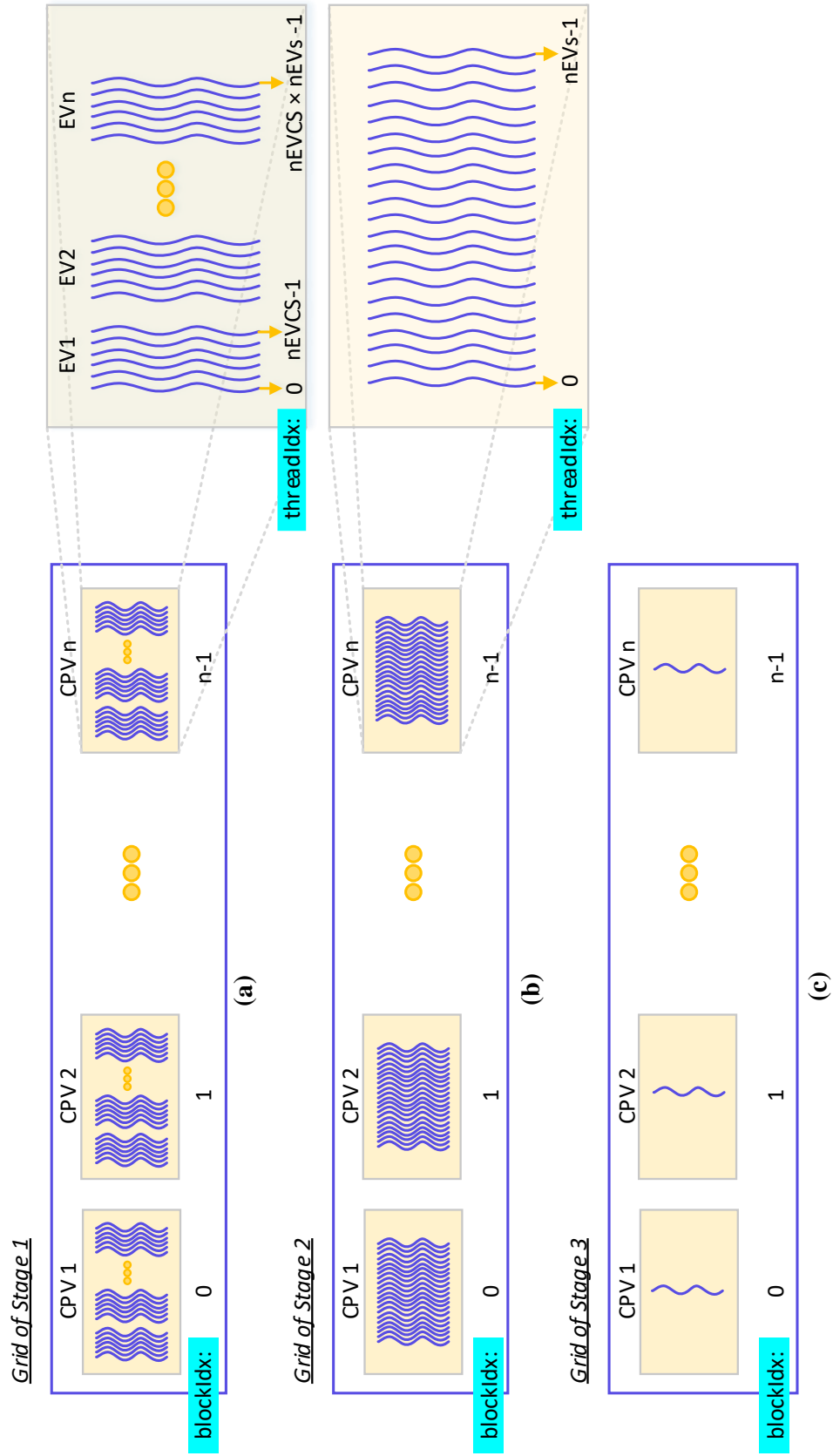


Figure 7.5 The grid dimensions in each stage.

The device allocated memory is freed and the device memory for the input and output of stage 2 is allocated. The output array of stage 1 is copied now to the GPU as an input to the kernel. The GPU grid in this stage as well is a 1D grid made up of n_{CPV} blocks, each running n_{EVs} threads in parallel, as depicted in Figure 7.5 (b). After the kernel execution, the output array is copied to the CPU, and the device allocated memory is freed.

On the CPU, the code is set to loop through the array to foresee the aggregated distribution of the EVs onto the EVCSs, labeled by the index of each CPV.

Then, the device memory for the input and output of stage 3 is allocated, and the 1D array with the length n_{CPVs} , comprising the number of vehicles going to each EVCS at each CPV, is copied to the GPU. As depicted in Figure 7.5 (c), the GPU grid in this stage is a 1D grid made up of n_{CPV} blocks, each made up of one thread that calculates the

Objective Function of the obtained distribution of vehicles given this CPV. The output is then copied to the CPU and the device memory freed.

On the CPU, the OPV is identified by finding the CPV that maximizes the objective function.

7.5 Data Sets and Results

For achieving the best strategic decision, the decision-making unit in a supervisory EV infrastructure management system collects this big volume of data needed. It then processes it on the GPU using the three-stage coordinated computing approach explained earlier in section 7.4. The collected data by the VBA, is prepared into the format of the allocated memory for the input to the kernel.

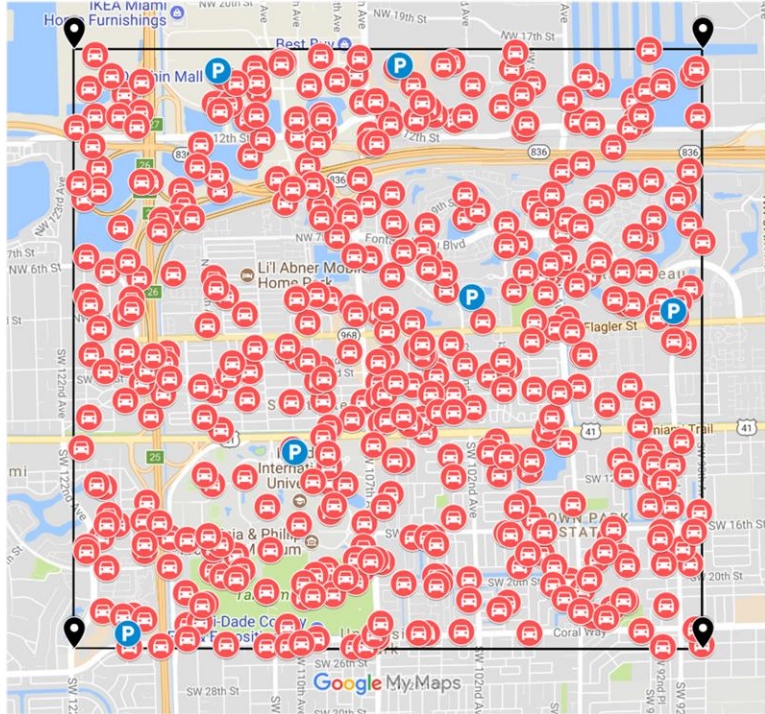


Figure 7.6 Geo-distributed EVs in a Virtual Block.

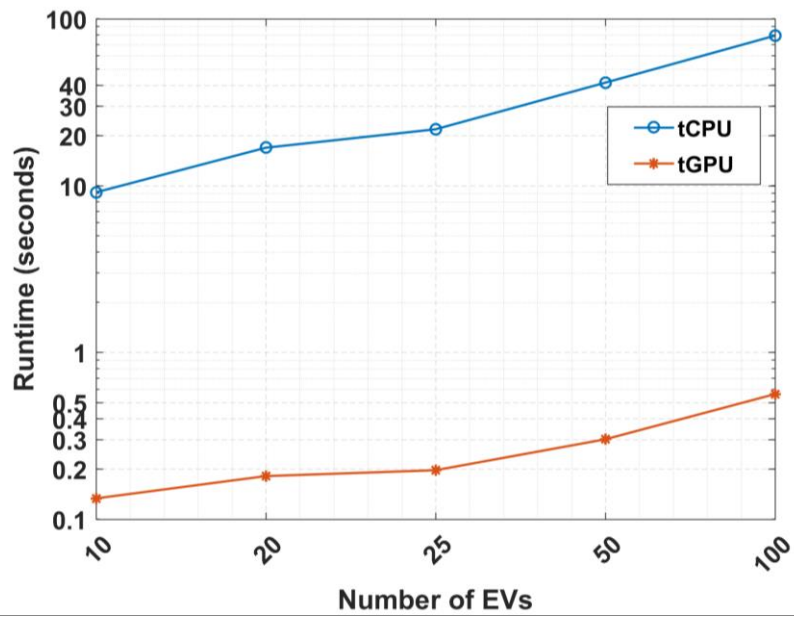


Figure 7.7 Runtime of application in CPU and GPU environments.

A number of EVs were assumed to be scattered within a geographical area, as seen in Figure 7.6. The SoCs were assumed to be between 20-80%. The Google Distance Matrix API was used to obtain the distance and time from each vehicle to each of the 6 EVCSs. In the MAS referred to in [9], the EVs will be sending those values as part of the data-sharing process between the agents. Five different cases were assumed as follows: 10, 20, 25, 50, and 100 EVs issuing requests at a time. A logarithmic graph in Figure 7.7 shows the runtime on both the GPU and the accelerated approach on the CPU, given these different number of EVs to be managed at a certain instance. As mentioned before, the accelerated approach presented in [9] is used here as the benchmark with which the presented GPU approach is being compared. A clear improvement and speedup is reflected by the numbers. The speedup factor and the percentage improvement in the runtime are evaluated by equations (7-3) and (7-4), respectively.

$$Speedup\ Factor = \frac{t_{CPU}}{t_{GPU}} \quad (7-3)$$

$$\% Improvement = \frac{|t_{GPU} - t_{CPU}|}{t_{CPU}} \times 100 \quad (7-4)$$

where t_{CPU} is the runtime of the CPU approach and t_{GPU} is the runtime of the three-stage GPU approach.

Table 7-1 Response time in CPU approach vs. GPU approach.

# of EVs	10	20	25	50	100
Runtime CPU	9.1133	16.866	21.757	41.3915	79.2167
Runtime GPU	0.1333	0.1813	0.1966	0.3013	0.5622
Speedup Factor	68.3715	93.0373	110.664	137.392	140.896
% Imp. in RT *	98.5374	98.9252	99.0964	99.272155	99.2903

* Imp. In RT: Improvement in Runtime

Table 7-1 presents the resulting speedup factor and percentage improvement in the response time in the two approaches. The results show huge speedup factors that increase as the number of managed nodes increase, which consequently scales up the data size. Almost 100% improvement in response time in the GPU approach, as compared to the CPU approach, is noted.

The GPU used in this work is the Nvidia GeForce GTX 950M on a computer featuring an Intel Core i7-7500U CPU.

7.6 Conclusion

Along with the large scale deployment of EVs comes challenges, such as the need for processing large sets of data in real-time. An example of such a system where this need arises was described in this chapter. A GPU computing environment was deployed with the hypothesis that it will cause significant acceleration to the application and meet the real-time requirement. The work presented a three stage coordinated algorithm between the CPU and the GPU, describing the grid dimensions and the kernel in each stage. The implementation of this algorithm resulted in a highly efficient, high-throughput computation, where the performance metrics showed more than 99% improvement in runtime in the GPU environment over that of the CPU-only environment.

Comprising a scalable algorithm, the effort presented in this chapter contributes towards the improvement of the performance of a structured message-sharing platform designed for the supervisory management of a large number of EVs. This GPU computing environment could be easily modified and customized to fit various big data applications in this area.

Chapter 8 Cyber Security Measures for Securing the developed System-Level Data Sharing Platform

8.1 Introduction

As the BDSS system scope expands, security becomes a concern. Without deployment of explicit security measures, a public charging platform of the presented BDSS will be susceptible to security attacks that could expose the EVs' and the utility's privacy, cause traffic and denial of service to disrupt the anticipated outcome of the service, fake requests from vehicles to interfere with the decisions taken by sending the recommendation to all vehicles to go to one EVCS for example, and possibly reveal utility-related information that outsiders should not have access to.

With the goals of controlling and restricting access to information to the intended recipients, and guaranteeing access to the information by the authorized users, several functional requirements can be defined. Those are Authentication, Confidentiality, Integrity, and Availability.

In this dissertation, Connex DDS Secure [89] is used to apply security measures to the developed application. This framework allows *DomainParticipants* to authenticate and authorize each other before initializing communication, and then encrypt and decrypt the communication traffic to achieve confidentiality, message authentication, and data integrity. The RTI Connex DDS and the RTI web-integration service used are of the 5.3.0 release version. The OpenSSL 1.0.2j is used, and the operating system is Linux Ubuntu version 14.04.

Before getting into the security configuration of the application, a discussion on cryptography and its security goals, examples of security attacks, and cyber security threat sources and risk management are presented. Then, possible threat scenarios in the application of the BDSS are elaborated, and the security measures taken are explained, providing details on the format and the content of the configuration files used.

8.1.1 Cryptography

Cryptography allows shared information to be kept secret by converting the data into a format that is unreadable, except for authorized users who have the appropriate keys for decoding it. This allows transmitting the information without unauthorized entities decoding it into a readable format, thus getting hold of the data.

Algorithms for encryption include Secret Key Cryptography (SKC), or what is known as symmetric encryption, and Public Key Cryptography (PKC), alternatively referred to as asymmetric encryption. SKC is referred to as symmetric encryption because a single key is employed for both encryption and decryption. The sender uses the key to encrypt plaintext and sends the encrypted text, known as ciphertext, to the receiver. Then, to recover the plaintext, the receiver uses the same key to decrypt the message. In PKC, a pair of keys, the public and the private keys, are required and that is why it is known as asymmetric encryption. The two keys are mathematically related, but the knowledge of one of them does not help conclude the other. PKC depends upon mathematical functions that are easy to compute, but their inverse function is not. The sender encrypts the information using the receiver's public key. The receiver decrypts the ciphertext using his/her private key. For the process to work, both keys are required. While the public key

can be shared with any participant of the system, the private key should never be revealed to another party.

Under this scheme, if for example Alice wants to send Bob a message, she encrypts the information using Bob's public key. Bob decrypts the ciphertext using his private key. This method could also be used to apply authentication and non-repudiation, proving to Bob that Alice sent the message. That is Alice could encrypt some plaintext with her private key; when Bob decrypts using Alice's public key, he knows that Alice sent the message and Alice cannot deny that she sent the message.

Although asymmetric encryption provides a safer communication of information, it cannot always be used alone. This is because encrypting and decrypting with private and public key takes a lot of processing power. Hence, they are only used during the SSL Handshake to create a symmetric session key. After the secure connection is made, the session key is used to encrypt all transmitted data. In other words, a hybrid cryptosystem is used, benefiting from using both types of encryption. For example, for establishing secure SSL communications between a browser and a website's server, the browser connects to the web server, secured with SSL (https), requesting that the server identifies itself. The server then sends a copy of its SSL Certificate, including the server's public key. The browser checks the certificate to validate the connection. If the browser trusts the certificate, it creates a symmetric session key and encrypts it using the server's public key. It then sends the encrypted symmetric key to the server, which in turn decrypts the symmetric session key using its private key and sends back an acknowledgement

encrypted with the session key to start the encrypted session. The browser and the web server now encrypt all the transmitted data with the symmetric session key.

8.1.2 Security Goals achieved by Cryptography

The three main goals towards which cyber security is oriented are protecting the confidentiality of the information, preserving its integrity, and promoting the availability of data. Those three goals are central to any Information Security study and are often looked at together and referred to as the CIA triad, as seen in Figure 8.1. While the CIA goals are the starting point in securing a system, they can also be viewed as prerequisites to other goals of information security, like authentication, authorization, and non-repudiation. In other words, starting with the CIA goals in mind would lay a solid ground for achieving a secure system that can repudiate different kinds of attacks.

8.1.2.1 Confidentiality

Protecting the confidentiality of the information being shared is ensuring that only authorized participants can view or access it. To prevent unauthorized participants from accessing information that they are not allowed to get hold of, data is often encrypted and access control measures are taken by the system architect.

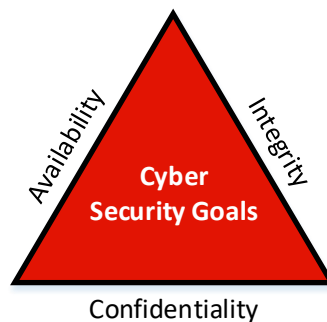


Figure 8.1 The CIA triad.

Encryption is applying mathematical algorithms to transform data so that it can only be read by the intended parties. For example, in SSL/TLS communications, the private and public keys that are part of the server's digital certificate and the symmetric session key secure the data sent to and from the web browser.

8.1.2.2 Integrity

Preserving the integrity of the data is ensuring that the information is correct, and no unauthorized person or malicious software can alter it over its entire lifecycle. In other words, integrity is the protection against unauthorized modification. A man-in-the-middle (MITM) attack, explained in section 8.1.3.1 can compromise data integrity. Encryption is the primary method for preserving integrity of the communicated data. In other words, if nobody except the intended parties can successfully read the data, the data cannot be modified in its lifecycle because modifying the encrypted data would render it useless, and the intended parties would then know that someone had tried to tamper with the data.

8.1.2.3 Availability

Availability means keeping the service running, and giving authorized users access to key networks and controls when needed. Information only has value if the authorized people can access it at the needed times. A downtime of a service usually proves to be very costly. Backups and redundancy are important measures to maintain service availability, and Denial of service and data deletion attacks threaten it.

8.1.2.4 Other Goals

Among the other goals of security are authentication, authorization, and non-repudiation. Authentication ensures that the individual is who (s)he claims to be.

Authorization is providing permission or approval to specific technology resources. After a participant is authenticated, (s)he may be authorized to access the system resources. Non-Repudiation is a mechanism by which the integrity and origin of data are proved, and the two communicating parties cannot claim that their communications came from a party other than themselves. That is to say that integrity and authenticity combine to establish non-repudiation. Furthermore, non-repudiation can be split into two concepts: Non-Repudiation of Origin (NRO) and Non-Repudiation of Emission (NRE). NRO provides evidence that a participant sent the message, and NRE provides legal evidence that the participant sent that specific message.

8.1.3 Example Security Attacks

Security attacks can be categorized into two groups: active and passive attacks. In active attacks, attackers attempt to alter system resources or affect their operation, directly compromising integrity and/or availability. A passive attacker, however, would attempt to learn or make use of information from the system, without affecting system resources, hence compromising confidentiality. Passive attacks are tricky to detect since data is unaffected.

Cyberattacks that have an adverse physical effect are known as cyber-physical attacks. At this point, it is useful to discuss some kinds of attacks that the presented application might be exposed to.

8.1.3.1 Man-in-the-middle (MITM) attack

A man-in-the-middle attack (MITM) involves three players: the victim, the participant with whom the victim believes they are communicating, and the attacker, here known as

the “man” in the middle, who intercepts the communication between the two. This attacker then decrypts the communicated information. There are several types of MITM attacks, some of which are passive, analyzing the decrypted data, and others that are active, taking further action of manipulating the decrypted data and retransmitting it by impersonating the legitimate participant with whom the victim is trying to communicate.

MITM attacks have two major forms: Eavesdropping (passive) and Manipulation (active). In Eavesdropping, the attacker is able to listen to, record, and analyze the conversation between the two participants. In Manipulation, the attacker not only intercepts all messages exchanged between the two participants, but also injects new ones to control the conversation. An example of this is reported to be indicated in one of the documents leaked by Edward Snowden, an ex-intelligence analyst employed by the National Security Agency (NSA), indicating that the NSA used MITM attacks in people’s interactions with Google servers, also spying on the French Ministry of Foreign Affairs, the Society for Worldwide Interbank Financial Telecommunications (SWIFT), and Brazilian oil company Petrobras [90]. It is as though a person is sending a package to a friend, but the NSA tells the postal carrier to bring it to their offices first. They look at it, repackage it, and send it on to its final destination. They were reported [91] to be able to do that through the use of secret servers, named Quantum, placed at key places on the Internet backbone. This privileged placement, which is inaccessible to organizations other than the NSA, allows them to react faster than other websites can. By exploiting that speed competency, the Quantum servers could impersonate a visited website to the target before the legitimate website can respond, thereby tricking the target's browser to visit a Foxacid server. The

Foxacid server is a previously revealed program that the NSA used to hack into targeted systems [92].

MITM attacks can be prevented or detected by means of trusted authentication and tamper detection. Authentication provides the user with some degree of certainty that a message has come from a legitimate source. Tamper detection shows evidence that a message may have been altered. In an article [93] discussing the reported NSA's MITM and how to prevent similar attacks, expert suggestions are made on the need for certificate tracking and inspection, and trusting highly trusted certificate authorities.

8.1.3.2 Denial-of-service (DoS) attack

A denial-of-service (DoS) attack is a cyber-attack in which the attacker targets the availability of the system by making network resources unavailable to the intended users or disrupting services by preventing requests from being fulfilled. Denial of service is usually accomplished by flooding the system resource with unessential requests to overload it with unneeded traffic. The most serious DoS attacks are distributed DoS (DDoS) attacks. In a DDoS attack, the traffic flooding the system originates from hundreds or thousands of distributed sources, making it almost impossible to stop the attack.

A massive web-outage occurred in October 2016 when Dyn, an Internet performance management and web application security company, was a victim of a large DDoS, bringing down major sites including Twitter, Reddit, GitHub, Amazon, Netflix, Airbnb, Spotify, Runescape, and Quora [94], [95]. The primary source of this attack was identified as the Mirai botnet, a malware that targets online consumer devices such as IP cameras and home routers, turning those networked devices running Linux into remotely controlled

devices, conscripted to contribute to a large-scale network attack, collectively called a botnet. In other words, a botnet is a collection of internet-connected devices, such as smartphones or IoT devices, whose security have been breached and control ceded to a third party, changing each one of them into a “bot.” In the 2016 DDoS attack, the Mirai malware was installed on a large number of IoT devices. The network flood was reported to be 1.2 Terabits per second (Tbps).

Another example of a DDoS is an even larger attack that occurred in February of 2018. This time, the victim was Github, a developer platform that offers distributed version control and source code management services. The attack lasted for about 10 minutes, in which Github used a DDoS mitigation service from Akamai, a content delivery network and cloud service provider [96]. Akamai used “scrubbing centers” to analyze the traffic to the website and remove the malicious packets. This DDoS attack was 1.35 Tbps.

In an article [97] on ways to mitigate and prevent DoS and DDoS attacks, a suggestion given is overprovisioning the system’s bandwidth to provide extra time to identify and deal with a DDoS attack and allow the server to accommodate unexpected spikes in traffic. Another suggestion is making the system’s architecture as resilient as possible by geographically spreading the resources to host the system’s services in separate data centers, ensuring available backups for emergencies. Other suggestions include continuous monitoring of traffic levels, using a Content Delivery Network (like Akamai), system hardening by reducing its surface of vulnerability, and regular updates for reducing the risk of attack.

8.1.4 Cyber Security Threat Sources and Risk Management

8.1.4.1 *Insiders*

An insider is anyone with physical or remote access to the network of the system providing the service. This could include trusted employees accidentally misplacing information, ex-employees intending to damage the business, malicious insiders with legitimate access to critical information, or even business clients with access to critical information and assets.

A compromised insider device can cause large-scale attacks like the ones discussed in section 8.1.3, if the information they can publish or can subscribe to is not limited by granular access control.

8.1.4.2 *Outsiders*

External cyber security threats originate from sources external to the company providing the service, and can be any actor that is not affiliated with the company directly. For example, they can be from organized criminal groups, professional hackers, or amateur hackers. The motives can be economic gain, political espionage, or even political or social change.

The best defense against security threats must consider the worst-case scenario: an attack by a user with legitimate access to the data. Focusing on securing the data itself is the key to addressing any kind of threat, whether by an insider or an outsider, and reducing the chances of success of several types of attacks.

8.1.4.3 Cyber Security Risk Management

Even the smallest security vulnerabilities in a network can lead to large cyber-attacks resulting in huge losses to the victim company. By analyzing and understanding potential risks, the chance of falling victim to a cybersecurity incident is reduced by far. Hence it is imperative for any company that provides a service to undergo a cyber-security risk assessment, prioritizing the network security enhancements, and setting up a clear plan on the steps to be taken to achieve an enhanced cyber-secure posture. This includes threat modeling and proactive incident response planning. Until recently, there was no specific model to follow in risk management. In response to this, the National Institute of Standards and Technology (NIST) developed the “Framework for Improving Critical Infrastructure Cybersecurity” [98] as a guide for businesses of all types and sizes.

The framework provides a common language for assessing cyber-security across businesses, providing a set of activities to achieve specific cybersecurity outcomes, and reference examples to guide the companies using it into achieving those outcomes. The core of the framework comprises four subsections: Functions, Categories, Subcategories, and Informative References. The main functions are Identify, Protect, Detect, Respond, and Recover. Categories are the subdivisions of a Function, and examples of those are “Asset Management,” “Access Control,” and “Detection Processes.” Subcategories divide a Category into specific outcomes of technical activities. Lastly, Informative References are sections of cross-sector standards, guidelines, and practices. They provide a method to achieve the outcomes specified in the Subcategories.

This NIST report provides steps for establishing or improving a cybersecurity program. The steps are listed as: prioritize and scope, orient, create a current profile, conduct a risk assessment, create a target profile, determine and prioritize gaps, and lastly implement an action plan.

8.2 Threat Scenarios in the proposed communication infrastructure for the EV public charging application

In order to counteract the risks facing the developed system, it is imperative to understand the different cyber threats and the ways attackers might interrupt the services presented. Any of those attacks can lead to the inability to meet contractual obligations and loss of trust among customers and suppliers, here the EVs and the service provider of the BDSS, respectively. Sections 8.2.1 through 8.2.3 below explain scenarios in which the system can be exposed to cyber security threats.

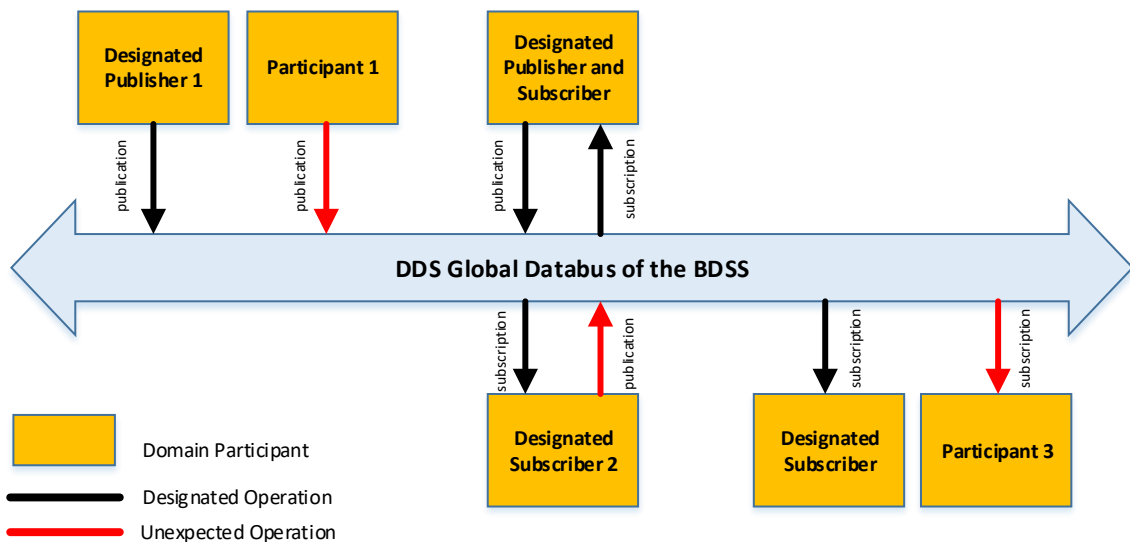


Figure 8.2 Threat Scenarios

8.2.1 Unauthorized subscription

Participant 3 in Figure 8.2 is connected to the DDS global databus of the application at hand, as are the rest of the participants. Although the messages are not intended to be sent to it, it is still able to observe the network packets. This situation can easily happen if participant 3 is connected to the same network where the application is running, if it could tap into the network switch, or if it could observe the communication channels. Where the Designated publisher and the Designated subscriber are communicating over multicast, participant 3 could simply subscribe to the same multicast address. To prevent this unauthorized subscription, two measures need to be taken. First, access to the system should be controlled by setting the permissions to each domain participant. Second, the data should be encrypted.

8.2.2 Unauthorized publication

Similar to participant 3, participant 1 is connected to the same network infrastructure as the rest of the agents. With this access, it is able to inject network packets with any content by publishing to the topics on the global databus. To prevent this from happening, the designated subscribers need to have a way to realize that the data is not originating from the designated publisher, but instead from an unauthorized participant, and therefore reject those malicious packets. This could be facilitated by having the designated publisher add a digital signature to the messages that are published to the topics on the global databus. A digital signature is based on PKC. To create a digital signature, the publisher encrypts part of its message using its private key. Since the designated subscribers have access to the publisher's public key, the recipients can use it to decrypt the messages and identify

that they originated from the legitimate publisher. Any digital signatures that participant 1 may use will be rejected by the recipients. In addition, granting permissions to specific participants to publish to the topics will provide access control and will limit malicious attempts as publications from participant 1.

8.2.3 Tampering and Replay

Designated subscriber 2 is designed to subscribe to some topics on the global dataspace of the application. Therefore, it is already a node in the system, with access to the global dataspace, and a deliberate attacker can control this subscriber, altering its functions by adding the ability to publish information to specific topics, and then exploiting this subscriber to inject wrong or unneeded information to the global dataspace. To prevent this, it is important to apply access control on not only the participant level, but also that of the topics.

8.3 Security measures taken to secure the BDSS

In this dissertation, Connex DDS Secure [89] is used to apply security measures to the developed application. This framework allows *DomainParticipants* to authenticate and authorize each other before initializing communication, and then encrypt and decrypt the communication traffic to achieve confidentiality, message authentication, and data integrity.

8.3.1 Configuring and Deploying Security Measures

For securing the data sharing in the different domains of the developed system, there is a need to cover several security policies, including Authentication, Access Control, Confidentiality, and Integrity. For that, DDS Security is used for: Topic-by-Topic security

configuration, while unchanging the system architecture, thus maintaining the key benefits of the use of DDS. By using the DTLS protocol, a mature variant of the SSL/TLS protocol, the information exchange between different sites is secured.

As an end user, several files need to be configured with the *DomainParticipants* for them to communicate in a secure DDS domain. These are set in the *DomainParticipant's PropertyQosPolicy*. The first step is to modify the USER_QOS_PROFILES.xml file of the DomainParticipant that the system designer intends to secure, and use the built-in QoS profile: "Generic.Security." The used profile then inherits from the built-in BuiltinQosLib::Generic.Security profile to enable RTI Security Plugins in the DomainParticipant. Then, several files, depicted in Figure 8.3, should be configured to

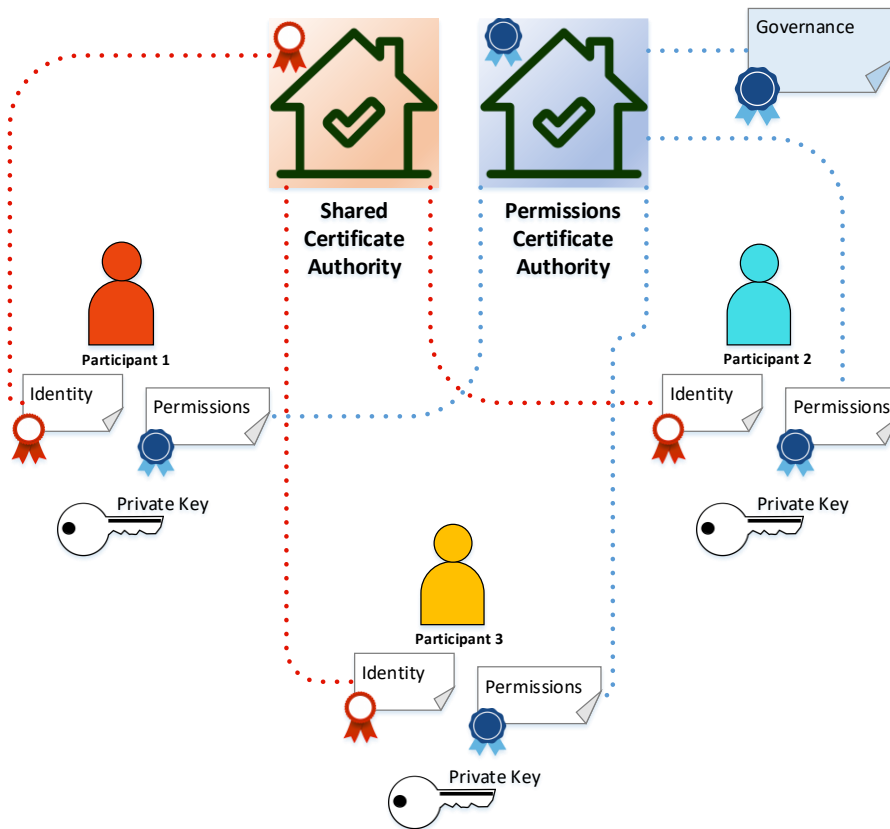


Figure 8.3 Configuring and Deploying DDS Secure.

achieve the needed security outcomes. With the use of those configured files, the security requirements of the system are defined in a data-centric approach. First of all, a certificate authority (CA) is used to issue digital certificates, called Identity Certificates, for the DomainParticipants. In this application, the used CA also issues a self-signed certificate, called the Identity CA Certificate, and a private key to each *DomainParticipant*. Those files are used for authentication and cryptography purposes. The CA is specified by using a PEM format file containing its public key. In order to successfully communicate with a peer, the CA key that is supplied must include the CA that has signed that peer's identifying certificate.

As for the purpose of applying access control to the application, a Domain Governance file is used in each domain of the application to define the control on the domain and topic levels, and a Permissions file is used with each DomainParticipant to define the control on the participant level. A Permissions CA is used to sign those two files. In addition, it generates a self-signed certificate, called the Permissions CA certificate. The Shared CA and the Permissions CA can be the same or two separate entities.

8.3.2 Authentication

Authentication is done via a series of inter-participant challenge and response messages. These messages perform mutual authentication, so the end result is that this participant authenticates the remote participant and vice-versa. Once authentication succeeds, the two participants start communicating.

For applying authentication, the *DomainParticipant* must be configured with two files: The certificate of the Shared Identity CA and the identity certificate of the *DomainParticipant*.

8.3.2.1 Identity CA Certificate

The Identity CA Certificate is the certificate of the Shared CA, the issuer of the Identity Certificates of the *DomainParticipants*. This certificate can be self-signed if the CA is the root CA. The Public Key in the Certificate, which is assumed to be distributed onto the *DomainParticipants* securely, should be trusted to sign *DomainParticipant* Identity Certificates.

8.3.2.2 Private Key

Every *DomainParticipant* has a private key associated with it. This is generated by the Shared CA.

8.3.2.3 Identity Certificate

Every *DomainParticipant* has an Identity Certificate associated with it, also generated and signed by the Shared CA.

8.3.3 Access Control

Access Control Permissions checking is done to ensure that *DomainParticipants*, *DataWriters*, and *DataReaders* have the appropriate permissions to exist and match with each other. Access Control is done in two phases: governance and permissions checking. Governance is the process of configuring locally created *DomainParticipants*, *Topics*, *DataWriters*, and *DataReaders* to perform the right amount of security for the right use case. Permissions checking is the process of making sure locally created and remotely discovered entities are allowed to do what they want to do. Those two phases are invoked

by the use of XML documents that are signed by the permissions CA. Domain governance is done during entity creation to ensure the right security attributes are applied to the right *DomainParticipants*, *DataWriters*, and *DataReaders*.

Examples files are used as a reference, with their content updated to match the system configuration of domains, topics, and used identity certificates. Then those files are signed. To indicate that these XML files are to be used, several properties are added and specified in the *DDS_DomainParticipantQos*.

8.3.3.1 Permissions CA certificate

The Permissions CA certificate is a certificate that contains the Public Key of the CA that will be used to sign the Domain Governance and Domain Permissions documents, which are explained in sections 8.3.3.2 and 8.3.3.3, respectively. In the application presented in this dissertation, the Permissions CA used is the same as the shared CA.

This certificate should be provided to the domain participants using the *PropertyQosPolicy* on the *DomainParticipantQos*.

8.3.3.2 The Domain governance signed by the Permissions CA

The domain governance document is an XML document that specifies how the domain should be secured, indicating which DDS domain IDs should be protected, and different properties of the protection.

Several aspects that apply to the whole domain are configured in this file. For example, the system designer uses the properties in this file to specify which of the discovery information, the liveliness messages, and the Real-Time Publish-Subscribe (RTPS) messages should be protected, and the level of their protection. It is also used to decide whether a discovered

domain participant that fails the authentication should be allowed to join the domain and see any discovery data and Topics that are configured as “unprotected”. It also gives the system designer the option to decide whether any discovered domain participant that authenticates successfully should be allowed to join the domain and see the discovery data without checking the access control policies.

Furthermore, the handling of the security of the information on the topics within the domain is detailed in this file. For example, a property is used that allows the system designer to decide whether publication and subscription access to the individual Topics should be open to all participants in this domain or restricted to specific domain participants. It also gives the option to decide whether the metadata information sent on the Topic like the sequence numbers, heartbeats, acknowledgment messages, and others should be protected. This document provides a means to decide the kind of protection of the different types of messages exchanged on the domain. There are three protection levels: NONE, SIGN, ENCRYPT. **NONE** indicates that no cryptographic transformation is wanted. **SIGN** indicates the cryptographic transformation shall be purely a message authentication code (MAC) and that no encryption of the message is needed. **ENCRYPT** indicates that an encryption of the message is needed.

This document should be signed by the Permissions CA, and the signed document should be provided to the domain participant to be secured using the latter’s *PropertyQosPolicy* on the *DomainParticipantQos*.

The following is the format of the Domain Governance document, in its XML Schema Definition, of the EVCS domain in the communication infrastructure explained in Chapter 5. It is presented here as an example of the Domain Governance document, for explaining its different sections and what they represent.

```

<?xml version="1.0" encoding="ISO-8859-1"?>
<dds
xsi:noNamespaceSchemaLocation="../schema/dds_security_governance.xsd"
xmlns:xsi="http://www.w3.org/2001/XMLSchema-instance">

  <domain_access_rules>
    <domain_rule>
      <domains>
        <id>4</id>
      </domains>

      <allow_unauthenticated_participants>false</allow_unauthent
        icated_participants>

      <enable_join_access_control>true</enable_join_access_contr
        ol>

      <discovery_protection_kind>ENCRYPT</discovery_protection_k
        ind>

      <liveliness_protection_kind>ENCRYPT</liveliness_protection
        _kind>

      <rtps_protection_kind>SIGN</rtps_protection_kind>
    <topic_access_rules>
      <topic_rule>

        <topic_expression>*</topic_expression>

        <enable_discovery_protection>true</enable_discover
          y_protection>

        <enable_read_access_control>true</enable_read_acce
          ss_control>

        <enable_write_access_control>true</enable_write_ac
          cess_control>

        <metadata_protection_kind>ENCRYPT</metadata_protect
          ion_kind>

        <data_protection_kind>ENCRYPT</data_protection_kin
          d>
      </topic_rule>
    </topic_access_rules>
  </domain_rule>
</domain_access_rules>
</dds>

```

The main delimiter in this document is the `<dds>` XML element tag. The document contains a single delimiter for the domain access rules section: this is the

`<domain_access_rules>` XML element tag. This section contains a set of domain rules, each delimited by the `<domain_rule>` XML element tag. Each domain rule contains the following elements:

- The domain to which the rules are being set. This is delimited by the `<domains>` and `<id>` XML element tag. It can specify a range of domain IDs, by setting the delimiter `<id_range>` instead of the `<id>` XML element tag, followed by `<min>` and `<max>` delimiters. It can also contain a list of domain IDs and domain ID ranges. For example:

```
<domains>
  <id>0</id>
  <id>25</id>
  <id>27</id>
  <id_range>
    <min>10</min>
    <max>20</max>
  </id_range>
  <id_range>
    <min>30</min>
    <max>50</max>
  </id_range>
</domains>
```

- Identifying whether to allow unauthenticated participants. This is delimited by the `<allow_unauthenticated_participants>` XML element, which takes the values TRUE or FALSE.
- Identifying whether the permissions file should be enforced. This is delimited by the `<enable_join_access_control>` XML element, which takes the values TRUE or FALSE.

- Specifying the protection kind used for the secure builtin *DataWriter* and *DataReader* entities used for discovery, delimited by the `<discovery_protection_kind>` XML element.

This element may take five possible values: NONE, SIGN, ENCRYPT, SIGN_WITH_ORIGIN_AUTHENTICATION, or ENCRYPT_WITH_ORIGIN_AUTHENTICATION.

- Specifying the protection kind used for the secure builtin *DataWriter* and *DataReader* entities used for discovery, delimited by the `<discovery_protection_kind>` and the `<liveliness_protection_kind>` XML elements. These elements may take five possible values: NONE, SIGN, ENCRYPT, SIGN_WITH_ORIGIN_AUTHENTICATION, or ENCRYPT_WITH_ORIGIN_AUTHENTICATION.

- Specifying the protection kind used for the whole RTPS message, delimited by the `<rtps_protection_kind>` XML element. It may take five possible values: NONE, SIGN, ENCRYPT, SIGN_WITH_ORIGIN_AUTHENTICATION, or ENCRYPT_WITH_ORIGIN_AUTHENTICATION.

In addition to those elements, the domain rule in the governance file, delimited by the `<domain_rule>` XML element tag, contains a section for defining the topic rules. It is delimited by the `<topic_access_rules>` XML delimiter. Those rules include elements on the set of DDS Topic names to which the rule applies, elements to determine whether topic endpoint information is sent through secure channels, others to decide whether to enable publication and subscription access control, and others to determine the kind of protection of the messages.

8.3.3.3 *The DomainParticipant permissions signed by the Permissions CA*

The DomainParticipant Permissions document is an XML document that specifies the access permissions for the DomainParticipant to which it is associated. The following is the format of DomainParticipant Permissions document, in its XML Schema Definition, of the Battery Energy Storage System participant in the communication infrastructure explained in Chapter 5. It is presented here as an example of the Permissions document, for explaining its different sections and what they represent.

```
<?xml version="1.0" encoding="UTF-8"?>
<dds xmlns:xsi="http://www.w3.org/2001/XMLSchema-instance"
xsi:noNamespaceSchemaLocation="../schema/dds_security_permissions.xsd">
  <permissions>
    <grant name="ParticipantEMU">
      <subject_name> C=US, ST=FL, O=Florida International
        University,
        CN=EMUECdsa/emailAddress=xxxxx@fiu.com</subject_name>
      <validity>
        <not_before>2013-06-01T13:00:00</not_before>
        <not_after>2023-06-01T13:00:00</not_after>
      </validity>
      <allow_rule>
        <domains>
          <id>4</id>
        </domains>
      </allow_rule>
      <publish>
        <topics>
          <topic>From BESS</topic>
        </topics>
      </publish>
      <subscribe>
        <topics>
          <topic>To BESS</topic>
        </topics>
      </subscribe>
      </allow_rule>
      <default>DENY</default>
    </grant>
  </permissions>
</dds>
```

The permissions section in this document, delimited by a <permissions> XML element tag, could contain several grant sections, each delimited by a <grant> XML element tag. Each grant section includes the following:

- A subject name element, delimited by the `<subject_name>` XML element tag. This element identifies the DomainParticipant to which the permissions apply.
- A section specifying the valid dates for the permissions, delimited by a `<validity>`, a `<not_before >`, and a `<not_after >` XML element tags.
- A section specifying the allow rules assigned to the DomainParticipant. The rules are applied in the same order that appear in the document. The “default” rule, delimited by the `<default>` XML element tag is applied if the operation being attempted by the DomainParticipant does not match any defined rule. Each rule contains a Domains Section that identifies the DDS domain_id values to which the rule applies. This is delimited by the `<domains>` and `<id>` XML element tags, and followed by a set of allowed actions. There are three kinds of allowed actions: publish, subscribe and relay, differentiated by the name of the XML element used to delimit the action: `<publish>`, `<subscribe>`, and `<relay>`, respectively. The `<topics>` delimiter defines a section in which the DDS Topic names must be matched for the allow rule to apply. Each topic name should be identified separately in a `<topic>` XML element tag within the `<topics>` element.

Deny rules appear inside a `<deny_rule>` XML element tag, and have the same format as the allow rules.

8.3.3.4 Vehicle Access Control with the Web Integration Service

An Access Control List (ACL) file is identified when starting the WIS. This ACL file is a Sqlite3 database with a single table that contains all the API keys, a message describing each API key, and the date when they were added to the file. Each vehicle communicating with the global dataspace will be allowed to publish and subscribe only if it has an API

key, and that is included in the ACL file. Figure 8.4 shows the creation and listing of an API key from the ACL file.

```

abla@abla-OptiPlex-9020: ~/rti_connex_t_dds-5.3.0/bin
abla@abla-OptiPlex-9020: ~/rti_connex_t_dds-5.3.0/bin$ $NDDSHOME/bin/rtiwebintegrate
tionservice -cfgName default -listeningPorts 8090s -sslCertificate server.pem -a
clFile acl file.db -createAPIKey "Abla"
Created API key "zXGfvnzJDKwfdjgLPqaQ9Kt03KwLl5Zbrl/21zw"
abla@abla-OptiPlex-9020:~/rti_connex_t_dds-5.3.0/bin$ $NDDSHOME/bin/rtiwebintegrate
tionservice -cfgName default -listeningPorts 8090s -sslCertificate server.pem -a
clFile acl file.db -listAPIKeys

```

API Key	Creation Date	Description
zXGfvnzJDKwfdjgLPqaQ9Kt03KwLl5Zbrl/21zw	2018-10-01 18:29:35	Abla

```

abla@abla-OptiPlex-9020:~/rti_connex_t_dds-5.3.0/bin$
abla@abla-OptiPlex-9020:~/rti_connex_t_dds-5.3.0/bin$

```

Figure 8.4 Creating and Listing the API keys for the Remote Client Applications

8.3.4 Penetration Testing

To test the system’s response to malicious activity, and the validity of the measures taken, several scenarios are simulated.

8.3.4.1 Authentication

A test was applied by changing one letter in the private key, to emulate an attacker trying to authenticate and tap into the system. The screenshot in Figure 8.5 shows that this participant failed to authenticate and could not access the system.

```

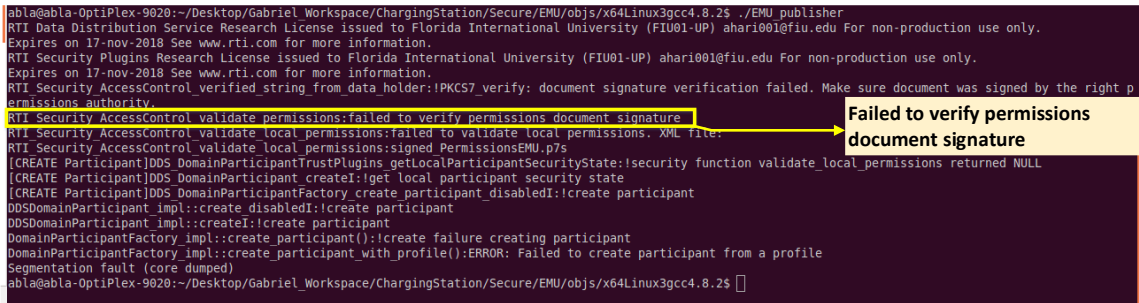
abla@abla-OptiPlex-9020:~/Desktop/Gabriel_Workspace/ChargingStation/Secure/EMU/objs/x64Linux3gcc4.8.2$ ./EMU_publisher
RTI Data Distribution Service Research License issued to Florida International University (FIU01-UP) ahari001@fiu.edu For non-production use only.
Expires on 17-nov-2018 See www.rti.com for more information.
RTI Security Plugins Research License issued to Florida International University (FIU01-UP) ahari001@fiu.edu For non-production use only.
Expires on 17-nov-2018 See www.rti.com for more information.
RTI Security Authentication create:failed to read authentication.private key file
RTI Security Authentication create:Failed to read authentication.private_key_file
RTI Security PluginsSuite create:Failed to read authentication.private_key_file
RTI Security PluginsSuite create:Failed to read authentication.private_key_file
[CREATE Participant]DDS DomainParticipantTrustPlugins_initialize:create security plugin
[CREATE Participant]DDS DomainParticipant createI:create builtin trust plugins support
[CREATE Participant]DDS DomainParticipantFactory_create participant disabledI:create participant
DDSDomainParticipant_impl::create disabledI:create participant
DDSDomainParticipant_impl::createI:create participant
DomainParticipantFactory_impl::create participant():create failure creating participant
DomainParticipantFactory_impl::create participant_with_profile():ERROR: Failed to create participant from a profile
Segmentation fault (core dumped)
abla@abla-OptiPlex-9020:~/Desktop/Gabriel_Workspace/ChargingStation/Secure/EMU/objs/x64Linux3gcc4.8.2$

```

Figure 8.5 System’s Response to Using a Wrong Private Key

8.3.4.2 Access control

In another test, one DomainParticipant's Permissions file was altered by changing the default allow rule from DENY to ALLOW. Since the permissions file is signed by the CA, the RTI Security Access Control plugin failed to verify the altered permissions file, as shown in Figure 8.6, and thus the attack failed.

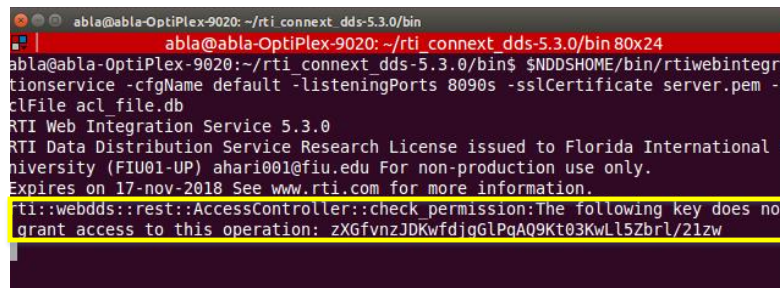


```
abla@abla-OptiPlex-9020:~/Desktop/Gabriel Workspace/ChargingStation/Secure/EMU/objs/x64Linux3gcc4.8.2$ ./EMU_publisher
RTI Data Distribution Service Research License issued to Florida International University (FIU01-UP) ahari001@fiu.edu For non-production use only.
Expires on 17-nov-2018 See www.rti.com for more information.
RTI Security Plugins Research license issued to Florida International University (FIU01-UP) ahari001@fiu.edu For non-production use only.
Expires on 17-nov-2018 See www.rti.com for more information.
RTI Security AccessControl_verified_string_from_data holder:PKCS7_verify: document signature verification failed. Make sure document was signed by the right p
permissions authority.
RTI Security AccessControl_validate_permissions:failed to verify permissions document signature
RTI Security AccessControl_validate_local_permissions:failed to validate local permissions. XML file.
RTI Security AccessControl_validate_local_permissions:signed PermissionsEMU.p7s
[CREATE Participant]DDS DomainParticipantTrustPlugins_getLocalParticipantSecurityState!security function validate_local_permissions returned NULL
[CREATE Participant]DDS DomainParticipant_createI:get local participant security state
[CREATE Participant]DDS DomainParticipantFactory_create_participant_disabledI:create participant
DDSDomainParticipant_impl::create_disabledI:create participant
DDSDomainParticipant_impl::createI:create participant
DomainParticipantFactory_impl::create_participant():create failure creating participant
DomainParticipantFactory_impl::create_participant_with_profile():ERROR: Failed to create participant from a profile
Segmentation fault (core dumped)
abla@abla-OptiPlex-9020:~/Desktop/Gabriel Workspace/ChargingStation/Secure/EMU/objs/x64Linux3gcc4.8.2$
```

Figure 8.6 System's Response to Using an Altered Permissions File

8.3.4.3 An EV using a wrong API Key

In the ACL file, an API key was generated for an EV DomainParticipant. Two vehicles were simulated: one with a generated and registered API key, and one with a made-up key. Figure 8.7 shows the response of the WIS when the EV with the wrong API key tried to publish to the global dataspace. It shows that since the used key by the vehicle was not registered in the ACL file, the EV was not granted access.



```
abla@abla-OptiPlex-9020:~/rti_connext_dds-5.3.0/bin
abla@abla-OptiPlex-9020:~/rti_connext_dds-5.3.0/bin 80x24
abla@abla-OptiPlex-9020:~/rti_connext_dds-5.3.0/bin$ $NDDSHOME/bin/rtiwebintegrate
tionservice -cfgName default -listeningPorts 8090s -sslCertificate server.pem -a
clFile acl_file.db
RTI Web Integration Service 5.3.0
RTI Data Distribution Service Research License issued to Florida International U
niversity (FIU01-UP) ahari001@fiu.edu For non-production use only.
Expires on 17-nov-2018 See www.rti.com for more information.
rti:webdds::rest::AccessController::check_permission:The following key does not
grant access to this operation: zXGfvnzJDKwfdjqG1PqAQ9Kt03KwL15ZbrL/21zw
```

Figure 8.7 Access Denied for Unregistered API key

8.4 Summary

In this chapter, the measures taken for securing the BDSS introduced in chapter 5 have been explained. Example files used for configuring authentication, access control, and revocation have been presented, and their format and content detailed. To test the applied measures, several scenarios were simulated, and screenshots from the relevant agents' terminals presented to show the response. The system successfully denied access to participants with a wrong private key and successfully detected a change in the digital signature of a Permissions file, thus strictly imposing the access control measures. In addition, an EV with an unregistered API key tried to connect to the system, and was denied access.

Chapter 9 Wireless Power Transfer for Electric Vehicle Charging Applications,

Part I

9.1 Performance Evaluation of a Wireless Power Transfer System using Coupled 3D Finite Element-Circuit Model

As more research is directed towards analyzing and developing wireless power transfer (WPT) systems, issues like electromagnetic resonance and inductive charging are being addressed. Various techniques can be utilized in the research on applications of WPT and can be categorized into analytical, numerical, and/or experimental techniques. Analytical methods include equivalent circuit modeling and scattering parameter (S-parameters) analysis. The second category include FEA for electromagnetic modeling, high-frequency structured simulation, and coupled field and lumped parameter analysis. The third category encompasses the experimental methods that include S-parameters measurements, field measurements, and power and energy emission tests [99].

The literature demonstrates several applications of 3DFEA models of WPT coupled resonators in comparative studies and performance analysis studies. FEA has been utilized to accurately obtain the characterizing parameters of the coupled coils, and use them to evaluate the performance of the WPT link based on derived analytical equations [100], [101].

In this study, the numerical technique involving coupled electromagnetic field analysis and electric circuit is used. This coupled model is utilized to evaluate the WPT system's efficiency and performance of different designs by varying a number of design variables.

A MATLAB-FEA routine is developed, serving as an interface from which the changes to the FEA model and the circuit parameters are applied. Then the results from the FEA model are compared with a mathematical model's results for validation.

9.1.1 Wireless Power Transfer Modeling

There are 3 different mechanisms for wireless energy transfer: inductive coupling, self-resonant coupling and modified resonant coupling [102]. The modeling for WPT using inductive resonant coupling mechanism can be done by: (1) the equivalent lumped parameter circuit model (ELPCM) and/or (2) a FEA model coupled with an electric circuit.

Here, the first approach is used for verifying the results, and the second is used for modeling the WPT. The ELPCM can be used since the characteristic wavelength (separation distance of the coils) of the system under study is smaller than $(1/10)^{th}$ of the relevant wavelength (wavelength of magnetic field) [103]. The details for the FEA model and the verification model are presented below.

9.1.1.1 Equivalent Lumped Parameter Circuit Modeling

The equivalent circuit model of the WPT system with a parallel-parallel compensation network, the basic T-model of two coupled inductors, is shown in Figure 9.1. L_{L1} and L_{L2} are the leakage inductances of the transmitting and receiving coils; M is the mutual inductance; R_1 and R_2 are the equivalent series resistances (ESR)s (parasitic resistances)

of the transmitting and receiving coils, C_1 and C_2 are the compensating capacitors to impose the resonance, and R_L is the load.

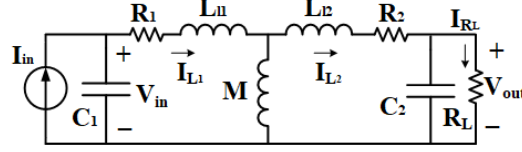


Figure 9.1 Electric Circuit of the WPT system

The power efficiency η can be derived from the circuit in Figure 9.1 as:

$$\eta = \frac{P_{R_L}}{P_{in}} = \frac{|I_{R_L}|^2 R_L}{|I_{L_1}|^2 R_1 + |I_{L_2}|^2 R_2 + |I_{R_L}|^2 R_L} \quad (9-1)$$

Where P_{R_L} is the output power, P_{in} is the input power, I_{R_L} is the load current and I_{L_1} and I_{L_2} are the resonant coil currents. Starting from (9-1), and using simple circuit analysis of the ELPCM, (9-2) can be derived.

$$\eta = \frac{1}{1 + A \frac{R_1}{R_L} + \frac{R_L}{\omega^2 L_2^2} R_2} \quad (9-2)$$

Where ω is the resonance frequency and A can be defined as:

$$A = \left(1 + \frac{L_{12} + R_L C_2 R_2}{M}\right)^2 + \left(\frac{-R_L - R_2}{\omega M} + \omega R_L C_2 \left(1 + \frac{L_{12}}{M}\right)\right)^2 \quad (9-3)$$

The resonance frequency is chosen to be compatible with the Qi standard [104] that was developed by the Wireless Power Consortium. The resonance is imposed by choosing the capacitance value, C , that will satisfy the resonance criteria in (9-4), where L is the value of the self-inductance of the coil.

$$C_1 = \frac{1}{L_1 \omega^2} \quad , \quad C_2 = \frac{1}{L_2 \omega^2} \quad (9-4)$$

9.1.1.2 3DFEA Modeling

The geometry used for the inductive resonant coupling WPT consists of two approximations of Litz coils. The use of these coils allow significant decrease of the undesirable AC resistance caused by the skin effect which is a usual consequence of high frequency level in the application at hand [105]. Figure 9.2 shows the circuit as modeled in the FEA program (Infolytica-Magnet). CoilT and CoilR represent the coils modeled in the FEA software. The current source and the capacitors (C_1 and C_2) are modeled as ideal components in this simulation; R_L is the load. Each of the coils are modeled as a copper ring with a cross-sectional area of $A_R = 0.785 \text{ cm}^2$. The geometric radius is defined as $R = 20 \text{ cm}$. The number of turns is defined as N .

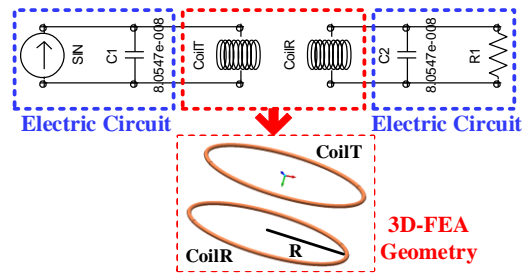


Figure 9.2 The 3DFE coils coupled with an electric circuit

9.1.2 The Finite Element and Matlab Script

In order to wirelessly transfer power across long distance and with high levels of efficiency, it is important to investigate the effect of different system parameters on the transmitted power and efficiency, and then apply a design technique that will provide the

optimum combination of these parameters to achieve the best system performance. The design parameters of WPT circuit can be classified as follows:

- *Electric Circuit Parameters:* the inductance value (L), the capacitance value (C) and the resonance frequency (ω).
- *Geometrical Parameters:* For the coil (to get the required L): number of turns (N), dimensions of the coils (radius R), gauge of the cable (g), type of the cable, and shape of the coil (circular, spiral, square, etc.). For the setup structure: distance between coils (d), alignment (angle of separation off the coaxial axis), and symmetry of the two coils (symmetry of shape, area, and turns ratio).

The selection of the best combination of these parameters for maximizing the power transfer efficiency is a complex problem due to the high number of parameters, some of which are electrical and others geometrical, thus making a simple circuit simulation insufficient for solving this problem. Therefore, a MATLAB-FEA routine, which serves as an interface from which the changes to the 3DFE model and the circuit parameters are applied, is developed. At each combination of two selected parameters (e.g: coil wire gauge, distance, etc.), a series of steps linking the MATLAB and the FEA model are made. The script allows for executing the FEA software to perform changes in the circuit or the 3DFEA model's parameters by passing an execution command. Following the changes made in the FEA model, the solver is invoked from MATLAB. The needed parameters, such as currents and voltages in the circuit components are passed back to the MATLAB script and are used to calculate the efficiency. The flowchart of this process is shown in Figure 9.3.

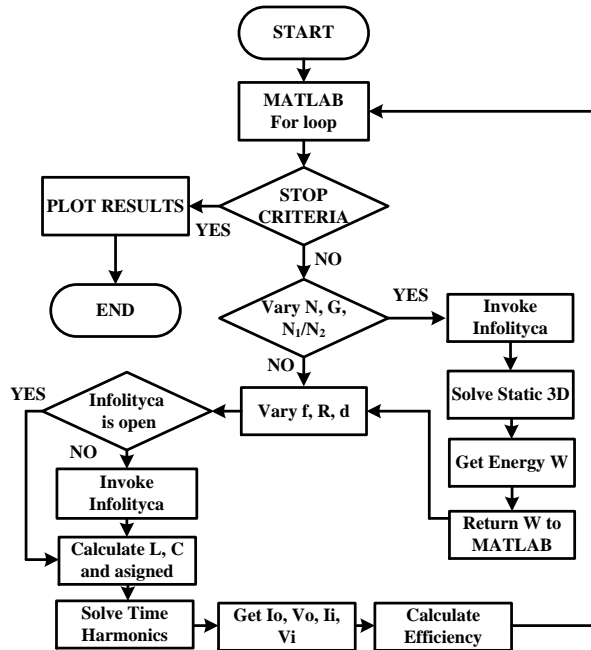


Figure 9.3 Platform interface methodology MATLAB and FEA.

9.1.3 Results and Verification

9.1.3.1 3DFE Model Results and Validation

Figure 9.4 shows the 3D model in the FEA software, Infolytica, showing the transmitting coil (CoilT), the receiving coil (CoilR), and the magnetic field density on 2 slices defined in the model. A zoom view on the transmitting coil, and how the generated field linking the two coils appears on the slices, is shown. Figure 9.5 shows the variation of the magnetic field density along the line P1 (line midway between the two coils (on the horizontal slice)), along P3 (coplanar with coilR), and along P2, (axial direction of the two coils (on the vertical slice)).

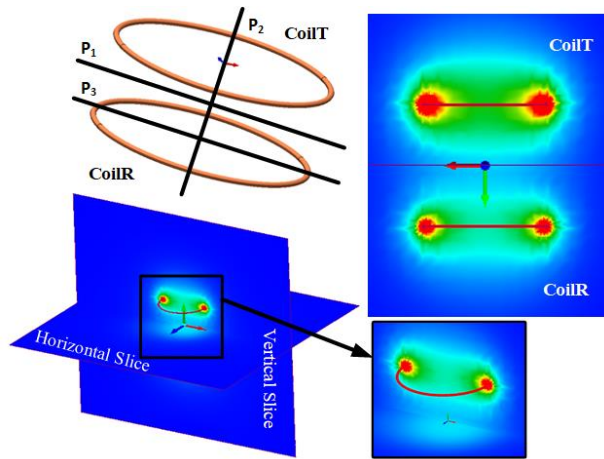


Figure 9.4 Magnetic Field Plots from 3DFEA Using Slices

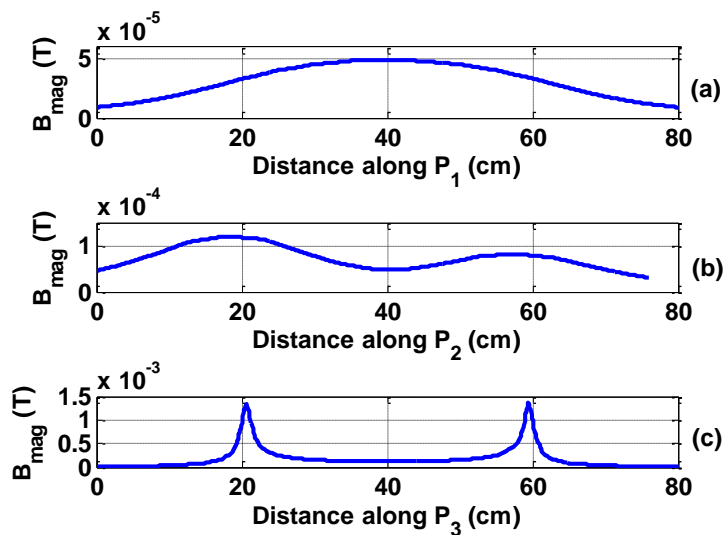


Figure 9.5 Magnetic field density magnitude (a) along line P₁ (b) along line P₂ (c) along line P₃

As can be seen, the magnetic field decreases as the distance increases away from the center (Figure 9.5(a)). Also, the field magnitude through CoilT is larger than through CoilR (Figure 9.5(b)). The two maxima that are depicted in (Figure 9.5(c)) correspond to the positions where the plane intersects the copper ring of the coil.

The electric variable waveforms, obtained from the FEA software and from the ELPCM simulated separately in Matlab Simulink, are compared in Figure 9.6, which verifies the results of the coupled FEA-circuit model.

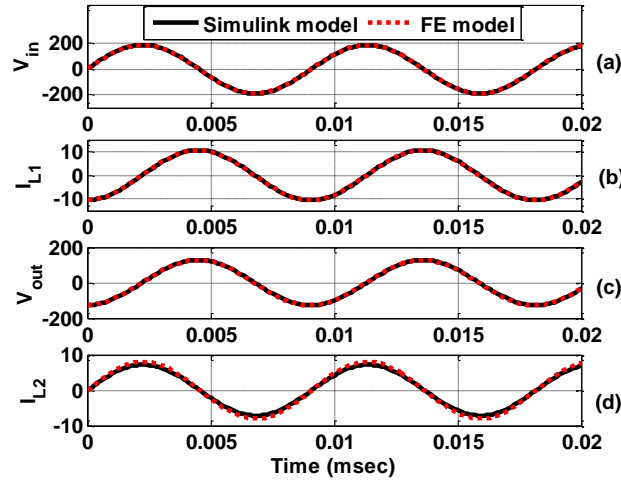


Figure 9.6 Simulink and FEA model results (a) input voltage (V) (b) primary coil current (A) (a) output voltage (V) (b) secondary coil current (A)

9.1.3.2 3DFEA-MatLab Script Results

The number of turns, turns ratio, and the coil wire gauge are the key design parameters which directly affect the ESR of the resonating coils. They were chosen for studying the effect of varying them on the power transfer efficiency, using the developed FEA-MATLAB script. The results are presented in Figure 9.7 (a) through (d). The influence that these parameters have on the efficiency is graphed at different designs. As the distance between the two coils is an important parameter that directly affects the coupling factor of the two resonators, the effect of the change of these parameters is expected to be attenuated with an increase of the distance. The simulation results in the figures show that, as expected, the efficiency decreases as the distance of separation between the coils increases. Examining the obtained graphs, Figure 9.7 (a) shows that as the number of turns are varied,

the efficiency reaches a maximum value at a specific number of turns. Therefore, for each specified separation distance, it is required to determine the number of turns that will give the maximum efficiency. The same figure also shows that as the distance increases, the number of turns that give maximum efficiency is not the same, but rather decreases as distance increases.

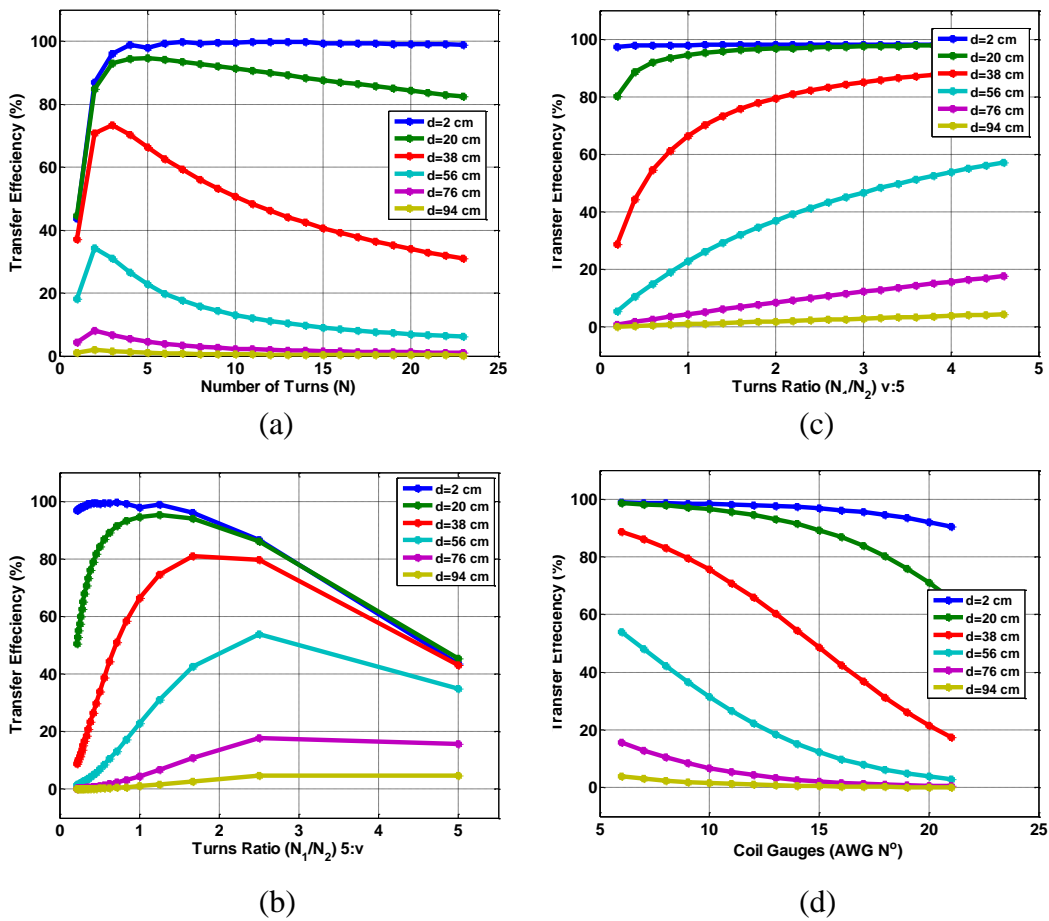


Figure 9.7 (a) Efficiency versus number of turns at different distances; (b) Efficiency versus Turns Ratio $N_1=5$ $N_2=$ variable at different distances; (c) Efficiency versus Turns Ratio $N_1=$ variable $N_2=5$ at different distances; (d) Efficiency versus Coil Gauges at different distances.

Figure 9.7 (b) shows the efficiency versus turns ratio, where the turns of the transmitting coil is fixed to 5, and the number of turns of the receiving coil is varied from 1 to 23. The behavior of this figure is similar to (a). Nevertheless, as the distance increases, in this case, the turns' ratio should be increased to get a more efficient link. Figure 9.7 (c) also shows the efficiency versus turns' ratio while fixing the number of turns of the receiving coil to 5, and varying the number of turns of the transmitting coil from 1 to 23. In this case, the efficiency increases with an increase of the turns ratio, but with a decreasing rate. Figure 9.7 (d) shows the efficiency versus coil gauge, which is varied from 6 to 21 AWG. As expected, increasing the coil wire gauge decreases the efficiency, as the coil ESR increases, increasing the losses.

9.1.3.3 Verification of the Script

Table 9-1 provides the verification of the developed script both by circuit simulation (Efficiency Circuit Simulation) and by equation (9-2) (Efficiency Equation), showing some of the simulated points. Each row in the table includes the parameters of one of the models and a comparison between: the efficiency obtained by using the circuit signals obtained from the FEA-MATLAB script (referred to as Efficiency Script), the efficiency obtained from simulating the T-model shown in Figure 9.1 (Efficiency Circuit Simulation), and the efficiency obtained by using equation (9-2) (Efficiency Equation).

The points shown in the table were chosen randomly from among the models presented in the graphs.

Table 9-1 Verification of Several of the Simulated Points

N1:N2	Distance	Gauge (cm^2)	Eff. Script	Eff. Cir. Sim.	Eff. Eqn.
5:5	38	0.034	66.49	65.64	66.44
20:20	56	0.034	7.004	6.605	6.996
5:20	76	0.034	0.298	0.288	0.298
5:5	38	0.00823	31.14	30.95	31.15
5:5	56	0.106	48.21	45.77	48.19

9.1.4 Concluding the study

A procedure using electromagnetic field analysis coupled with an electric circuit was developed for the performance evaluation of a WPT system. This coupled model was implemented as a 3DFE-MATLAB automated script which was utilized for the performance evaluation of the WPT coupled resonators link. The results obtained were verified using both circuit simulation and a mathematical equation.

9.2 An Iterative Design Approach for Shielding of WPT Systems in Electric Vehicle Charging Applications

EVs use electric motors for propulsion as opposed to fuel powered internal combustion engines. With the global trends shifting towards green energy to reduce greenhouse gas emissions, EVs are gaining considerable attention in the transportation industry. EVs run on battery power and need to be recharged on regular basis. Today, two types of EV battery recharging mechanisms are available: Cable charging and Wireless charging. In the former, power is transferred via an electric cable. In the latter, power is transferred between a pair of inductively coupled coils through a time-varying magnetic field.

Extensive research efforts are being made by researchers and car manufacturers to increase the efficiency of WPT systems for EVs [106]. The inevitable presence of time-varying magnetic field in WPT systems requires the study of the electromagnetic

interference of such systems alongside efficiency enhancement. The futuristic view of the transportation industry foresees a large penetration of EVs which will require EVCSs in close proximity to residential and commercial areas. It is therefore essential that these systems comply with safety standards for Electromagnetic Interference (EMI).

EMI is a very important consideration in the design phase of a WPT system because it is crucial to reduce the undesirable effects on the human body exposure which is caused by the interaction with the produced electromagnetic field signatures. The amplitude of the leakage field of any WPT system design should be controlled where a safe region should be defined. The magnetic flux density within this safe region should meet the safety standards or guidelines for EMI. An example of this is the application addressed in this work, when people are standing outside or sitting in an EV equipped with a WPT charger system. The most referenced international standards to ensure human safety in such applications are the guideline published by the ICNIRP 2010 [107] and the IEEE Std. C95.1-2005 standard [108]. Compared with the IEEE Std. C95.1-2005 whose maximum permissible exposure of head and torso for general public is $205\mu\text{T}$, the ICNIRP 2010 standard is still much more stringent, where the reference level for general public is $27.3\mu\text{T}$ at frequencies ranging between 3 KHz and 10 MHz [107]. In order to enable designers to achieve the compliance of their WPTL design with EMC standards at the early development stage, an FEA model is needed to predict and optimize the electromagnetic field signatures around the device.

Shielding the coils of a WPT system is critical for ensuring compliance with safety standards. However, several aspects need to be taken into consideration when selecting a

shield. Design parameters include the shield's radius and thickness which will directly affect the weight and cost of the system. Therefore, this study proposes an iterative approach for selecting a shield radius and thickness for a given WPT system, using Finite Elements Analysis, which ensures a safe level of EMI in compliance with the ICNIRP standard while minimizing the cost and weight of the system.

9.2.1 The WPT System Model

9.2.1.1 FEA Model

The proposed approach was applied on a sample WPT system for EV charging. This system is shown in Figure 9.8 and consists of a ground pad and an on-board-vehicle pad. Each pad consists of a spiral coil, a ferrite core that serves as a flux guide, and a shielding layer to be optimized. It is assumed that a positioning system that allows for exact alignment of the two pads is available in the EVCS, and thus misalignments are not considered in this study. Given the alignment of the two pads and the symmetry around their axes, a 2D axisymmetric model of the pads was developed.

The FEA model takes the excitation current I_T for the ground transmitting pad and I_R for the on-board receiving pad as inputs, solves the static finite elements field problem, and gives the magnetic field density (B) at the observation point I as an output. The calculation procedure of the excitation currents is discussed in the following section.

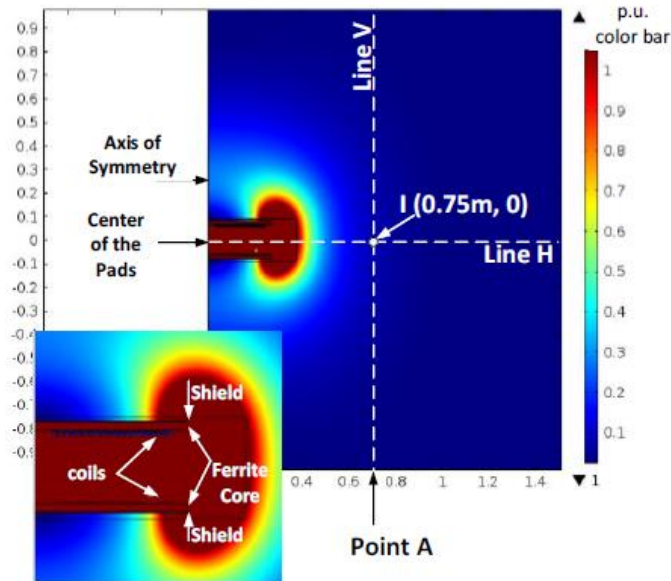


Figure 9.8 Color Map Showing the Magnetic Field Density B for the Initial WPT Pad Design

9.2.1.2 Equivalent Circuit and Current Calculation

In order to calculate the proper excitation currents for the coils in the FEA model, the following formulations for a series-series resonance topology of a typical WPT system, which was presented in [109], is utilized. Figure 9.9 shows the equivalent circuit model discussed in [109].

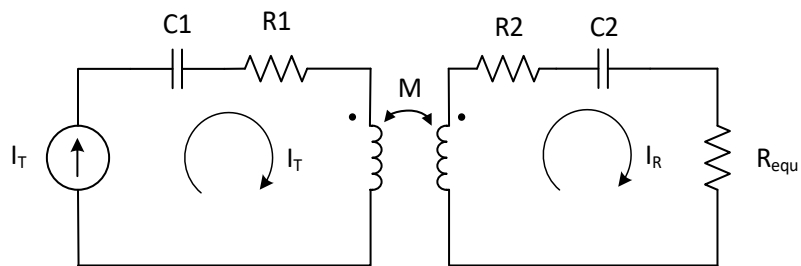


Figure 9.9 WPT Equivalent Circuit

$$|I_R| = \sqrt{\frac{2P_L}{R_{eq}}} = \left(\frac{\omega_0 M}{R_2 + R_{eq}} \right) |I_T| \quad (9-5)$$

$$|I_T| = \frac{R_2 + R_{eq}}{\omega_0 M} \sqrt{\frac{2P_L}{R_{eq}}} \quad (9-6)$$

The parameters in equations (9-5) and (9-6) are shown in Table 9-2 and Table 9-3. The capacitors C1 and C2 are the compensating capacitors of the series-series resonance topology at the resonance frequency, $\omega_0 = 2\pi f_0$.

Table 9-2 Operating Load Parameters

<i>Parameter</i>	<i>Value</i>
Frequency f_0	85 kHz
Equivalent Load Resistance R_L	2.3086 Ω
Load Power P_L	70 kW

Table 9-3 Equivalent Circuit Characteristics of the Initial Pad Design

<i>Parameter</i>	<i>Value</i>
L_t	455.69 μH
L_r	116.70 μH
R_t	1.87 Ω
R_r	1.39 Ω
M	89.38 μH
Efficiency	93.66 %

For interoperability purposes, the SAE agreed in their task force SAE-J2954 in November 2013 that the WPT low frequency band centers at 85 kHz, but ranges from 81.38–90 kHz. Therefore, 85 kHz have been used as the frequency in this study. Also, it is assumed that the load is a constant power load and its resistance is calculated at a typical EV battery bank terminal voltage.

9.2.2 Iterative Design Process

9.2.2.1 Process Description

This study proposes an iterative procedure for optimal design of shielding in EV wireless charging. This iterative procedure is outlined in the flowchart of Figure 9.10. As mentioned earlier, the ICNIRP had set the allowed level of magnetic field that a human being can be exposed to: $27.3 \mu\text{T}$. This is based on health considerations; however, in recent EVs, where the size of the battery stack has increased to extend the mileage range per a single charge (e.g. 70 kWh in Tesla model S), the required charging level may yield a

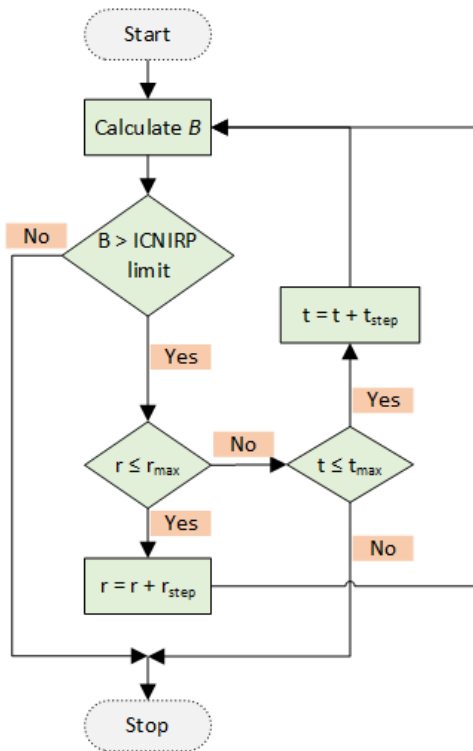


Figure 9.10 Flowchart for the iterative approach for optimal design of shielding layer.

magnetic field with a strength exceeding the specified limits by the standard. Moreover, it is of major importance for the EV manufactures to reduce the cost, as the cost was found

to be a serious impediment for purchasing an EV from the owner's point of view [110]. Also, the weight issue is important to be considered since any reduction in the weight of the vehicle will be desirable as it will reduce its energy consumption and, consequently, extend its range. Thus, a tradeoff between the dimensions of the shielding and the level of magnetic field should be carried out.

The iterative process starts with modeling the shield plate with a radius equal to the radius of the core. The self-inductance of the transmitting (CoilT) and receiving (CoilR) coils (L_t and L_r , respectively), the mutual inductance between the two coils M , and the ESR of the transmitting and receiving coils (R_t and R_r , respectively) are determined using superposition; The parameters of the transmitting (or receiving) coil are determined by exciting it with a unit current (1 Amp) while keeping the receiving (or transmitting) coil de-excited (setting the current=0).

The circuit parameters are obtained at each iteration because as the shielding changes, the effect on the circuit parameters change and should not be considered at constant values throughout the iterations.

After calculating the circuit parameters, equation (9-6) is used to calculate the current that will circulate in CoilT, I_T . The current circulating in CoilR, I_R , which is dependent on the assumed load parameters, is calculated from equation (9-5). Those two currents are then assigned to the coils modeled in the FEA software. The magnetic field B at the observation point I, which is labeled on Figure 9.8, is then collected. As a typical vehicle is 1.5 m wide, Point I was chosen at the edge of the car, which is 0.75 m away from the center of the pad. The obtained value of B at point I is then compared to the limit set by

the ICNIRP 2010 standard guidelines. If this value exceeds the limit, the radius of the shielding plate is incremented by a small value, r_{step} , as long as it is still less than a preset maximum constraint dimension. This constraint of the maximum allowed radius of the shielding layer is determined based on the allowed onboard space and dimensions, mainly the width. When this physical constraint is reached, the only option that the designer is left with is to allow for more shielding by increasing the thickness of the shielding layer. Similarly, and at each iteration, the thickness is compared to a preset maximum thickness, t_{max} . It is noteworthy that this other physical constraint (the maximum shielding layer thickness) is determined based on the maximum allowed weight for the shielding. If the thickness is less than t_{max} , it is incremented by a small value, t_{step} . Then B is collected again at the observation point I and the process continues until the magnetic field level is below the allowed limit by the standard. If the maximum radius and thickness are reached while the magnetic field value at point I is still higher than the permitted level, the process is stopped and a new material should be considered.

Following the calculation of the circuit parameters, equation (9-6) was used to calculate the current that will circulate in CoilT, I_T . The current circulating in CoilR, I_R , which is dependent on the assumed load parameters is calculated from equation (9-5). These two currents are then assigned to the coils modeled in the FEA software. The magnetic field B at the observation point I, as labeled on Figure 9.8, is then collected.

9.2.2.2 Levels of Charging

According to the National Electric Code (NEC), three levels of charging for EVs are defined [111]: 1) Regular household single phase AC plug that supports power of up to 2 kW, this may require charging time of several hours; 2) Dedicated three phase AC plug that supports power up to 19.2 kW and requires charging time of few hours; 3) Fast charging through dedicated DC plug with built-in charger that has virtually no limit on charging power, with currently available products ranging up to 120 kW [112]. Level one and two will generally be sufficient for owners who do not have the recharging duration as a priority. Fast charging (level 3) is considered when the minimization of the off-road time for charging is a priority for the driver, as the battery will be charged in one hour or less [113]. Level 3 charging is considered in this study in order to account for maximum output magnetic field.

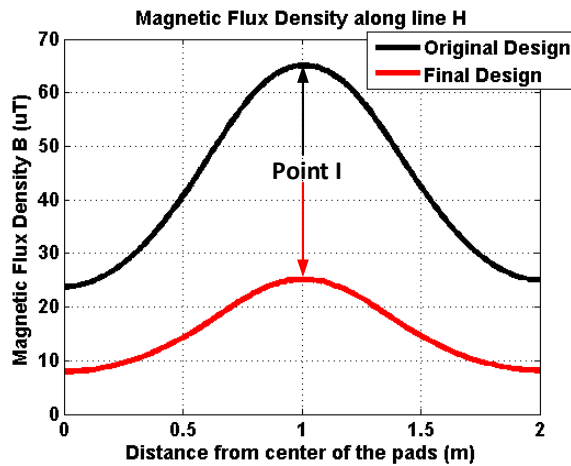


Figure 9.12 Magnetic Flux Density B in uT Along Line V in the Initial and the Final WPT Pads Design

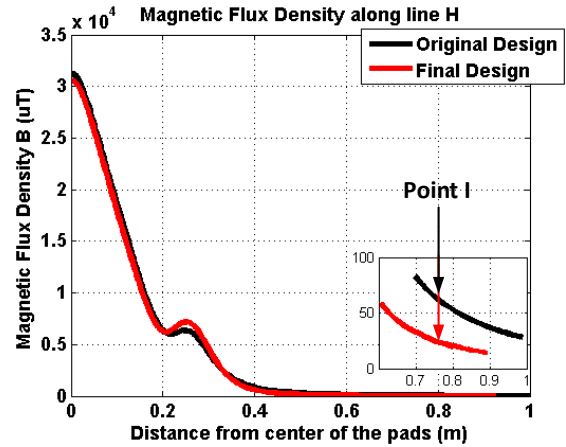


Figure 9.11 Magnetic Flux Density B in uT Along Line H in the Initial WPT Pads Design

9.2.2.3 Results

Figure 9.12 and Figure 9.11 show the magnetic field density B in μT along lines V and H, respectively, which are labeled in Figure 9.8, in both the initial and the final design. The values of the magnetic field B at the observation point I in the initial design and in the consecutive iterations of the proposed approach is shown in Table 9-4. Figure 9.12 shows the large minimization achieved in terms of the level of magnetic field density. Table 9-4 below shows this level at each iteration throughout the process when the radius was changed while keeping the thickness of the shield plate constant. In a parallel process, the thickness was changed while keeping the radius fixed, and the magnetic field level was recorded in the consecutive iterations. Table 9-5 shows the results of this process. By comparing Table 9-4 and Table 9-5, it can be concluded that the magnetic field is affected by varying the radius more than by varying the thickness. Also, in this design, Table 9-4 shows that varying the radius of the shield is sufficient for limiting the magnetic field level to abide by the standards.

Table 9-4 Recorded Magnetic Field Levels Through the Iterative Process of Changing the Shield Radius and Fixing the Shield Thickness

<i>Iteration</i>	<i>Shield Radius (mm)</i>	<i>Shield Thickness (mm)</i>	<i>B (uT)</i>
1	27	2	65.04
2	29	2	41.46
3	31	2	29.51
4	32	2	25.5

Table 9-5 Recorded Magnetic Field Levels Through the Iterative Process of Changing the Shield Thickness and Fixing the Shield Radius

<i>Iteration</i>	<i>Shield Radius (mm)</i>	<i>Shield Thickness (mm)</i>	<i>B (uT)</i>
1	27	2	65.04
2	27	2.5	64.556
3	27	3.5	63.795
4	27	5.5	62.37
5	29	5.5	40.41
6	31	5.5	28.71
7	32	5.5	24.506

9.2.3 Concluding the study

In this study, an iterative approach for the design of the shield for WPT pads for EV applications was presented. This effective approach helps achieve the optimal design of the shield considering the limits set forth by the ICNIRP 2010 standard reference level for general public exposure to time-varying electric and magnetic fields. The proposed iterative procedure was applied in a case study for a given design of WPT pads considering the 85 KHz frequency level set by SAE-J2954 TF. The approach starts with increasing the radius of the shield until a maximum radius is reached, then increasing the thickness of the shielding layer.

Based on a sensitivity analysis, it was observed that the magnetic field is affected by the radius more than the thickness. Therefore, priority was assigned to increase the radius. In this design, varying the radius of the shield was sufficient for limiting the magnetic field level to abide by the standards.

Chapter 10 Wireless Power Transfer for Electric Vehicle Charging Applications,

Part II

10.1 A Computational Approach for a Wireless Power Transfer Link Design Optimization Considering Electromagnetic Compatibility

WPT via inductive coupling is being extensively researched in numerous real-world applications such as biomedical implants and battery charging in consumer electronics and EVs. Studies on WPT could be very complex since it involves multiple areas including magnetics, power electronics, and communications. Among the well-known concerns in the initial design phase of any application is satisfying international EMC safety standards in regards to reducing the undesirable effects on the human body exposure which is caused by the interaction with the produced electromagnetic field signatures. The amplitude of the leakage field of any WPT system design should be controlled where a safe region should be defined for the application at hand. The magnetic flux density within this safe region should meet those guidelines. An example of this is when people are standing outside or sitting in an EV equipped with a WPT charger system. The most referenced international standards to ensure human safety in such applications are the guideline published by the ICNIRP 2010 [107] and the IEEE Std. C95.1-2005 standard [108]. Compared with the IEEE Std. C95.1-2005 whose maximum permissible exposure of head and torso for the general public is $205\mu\text{T}$, the ICNIRP 2010 standard is still much more stringent, where the reference level for the general public is $27\mu\text{T}$. In order to enable designers to achieve the compliance of their WPTL design with EMC standards at the early development stage, a

3DFE model is needed to predict and optimize the electromagnetic field signatures around the device.

Several approaches for the analysis of WPTL systems have been presented in literature. An example of an analytical approach was presented in [102], where the authors treat the WPT scheme as a two-port network and analyze the model using the coupled mode theory. In addition to this approach, there were many other approaches including experimental and numerical models. In [114], an FEM model was presented to estimate the efficiency of the power transfer, and the use of a magnetic shield was investigated for the reduction of the magnetic field signature. This and similar works ([115], [116]) identified the need for utilizing computational approaches for achieving EMC compatible systems at the early development stage. This study presents a new approach for WPTL design.

Electromagnetic emissions from the WPTL are the major aspect of interest in this study. The numerical approach of coupled 3DFE and circuit theory was used to provide an accurate solution for both efficiency calculations and minimizing the field signature around the WPTL.

As the presented design optimization process requires utilizing a large number of iterations, each of which requires 3DFE analysis, Artificial Neural Networks (NNs) were developed, trained and used to significantly reduce the computational effort. A GA based process was utilized to optimize the considered design parameters of the WPTL system. The objective is to maximize the WPTL efficiency and minimize the field signature around it. A constraint function was applied to the output power of the system.

10.1.1 Description and Modeling of the WPTL

The WPTL example used is shown in Figure 10.1 and is described in this section in addition to the modeling equations. The transmitting coil (CoilT) and the receiving coil (CoilR) each of which have N turns, are modeled in the magnetic domain and separated by a specific distance. CoilT and CoilR are lumped in a circuit that is composed of the two resonating coils with compensation networks, a source, and a load. The circuit, with the parallel-parallel compensation network, is shown in Figure 10.1, where the coils CoilT and CoilR represent the circuit parameters of the 3DFE modeled coils, and C_1 and C_2 represent the compensation network. The compensation circuit is utilized to simulate resonance, which increases the magnetic flux linking the receiving coil in the magnetic domain, and thus increases the induced voltage. The magnetic resonance WPT, which was first proposed by Tesla in the late 1800s, is based on the two fundamental laws of Ampere and Faraday.

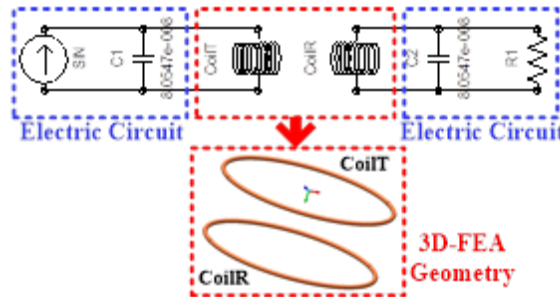


Figure 10.1 Electric circuit model and the 3DFE domain of the WPTL

CoilT is referred to as 1 and CoilR as 2 in the equations below. The AC current i_1 flowing through CoilT creates a time varying magnetic field with density B_1 . A magnetic flux $\Lambda_{21} = N\phi_{21}$ links CoilR, having area S_2 .

$$\Lambda_{21} = \int_{S_2} B_1 \cdot dS_2 = M. \quad (10-1)$$

where M is the mutual inductance between the transmitting coil and the receiving coil.

The electromotive force induced in the CoilR, e_2 , is the sum of e_{21} and e_{22} . e_{21} is the emf induced by the flux linking it, Λ_{21} , caused by the current flowing in CoilT. e_{22} is the emf induced in CoilR, caused by flux Λ_{22} linking itself.

$$e_2 = e_{21} + e_{22} = -M \frac{di_1}{dt} - L_2 \frac{di_2}{dt} \quad (10-2)$$

Taking into account the ESR, R , of each coil, the relationship between the input and output voltages and currents can be described as:

$$\begin{pmatrix} v_1 \\ v_2 \end{pmatrix} = \begin{pmatrix} R_1 + j\omega L_1 & -j\omega M \\ j\omega M & -R_2 - j\omega L_2 \end{pmatrix} \begin{pmatrix} i_1 \\ i_2 \end{pmatrix} \quad (10-3)$$

where $\omega = 2\pi f$, L_1 and L_2 are the values of the self-inductances of the transmitting and the receiving coils, respectively. In order to compute the values of the inductances (self and mutual) and the resistances, numerical 3DFE was utilized to solve the field problem. The current and voltage signals to evaluate the power and efficiency were also calculated. By applying a small current to one of the coils and performing static analysis, the self-inductances of both coils were obtained from the numerical model. This was done by dividing the obtained RMS values of the flux linking the coil by the applied current to this coil. A time harmonic analysis was performed and the mutual inductance, M , was evaluated by taking the ratio of the RMS values of the magnetic flux, through the second coil caused by the first current-carrying coil, and the current applied to the first coil.

Following the self-inductances calculation, the values of the capacitors of the compensating circuit, C_1 and C_2 , are obtained by:

$$C_1 = \frac{1}{L_1 \omega_0^2} \text{ and } C_2 = \frac{1}{L_2 \omega_0^2} \quad (10-4)$$

where $\omega_0 = 2\pi f_0$, f_0 being the desired resonant frequency. Then these parameters are then set in the circuit in order to impose f_0 . The efficiency, η , is calculated as:

$$\eta = \frac{P_{R_L}}{P_{in}} \times 100\% \quad (10-5)$$

where P_{R_L} and P_{in} are the output power and the input power, respectively.

10.1.2 The 3DFE Design and Lumped Circuit Model

The geometry used for the investigation consists of two stranded circular loop coils, resonating at the same frequency. The current source and the capacitors were modeled as ideal components in this electric circuit simulation. The model, developed in MagNet, Infolytica, is solved using the T- Ω formulation with a full structured 3D mesh with about 400,000 nodes. The size of the mesh, shown in Figure 10.2, was set to consider the skin depth of penetration in the conductors at the levels of frequency used, while conserving acceptable computing time, which is an essential consideration here when preparing the training data for a range of combinations of the optimization parameters. Moreover, since the problem at hand is a quasi-static one, the Time-Harmonic solver was used.

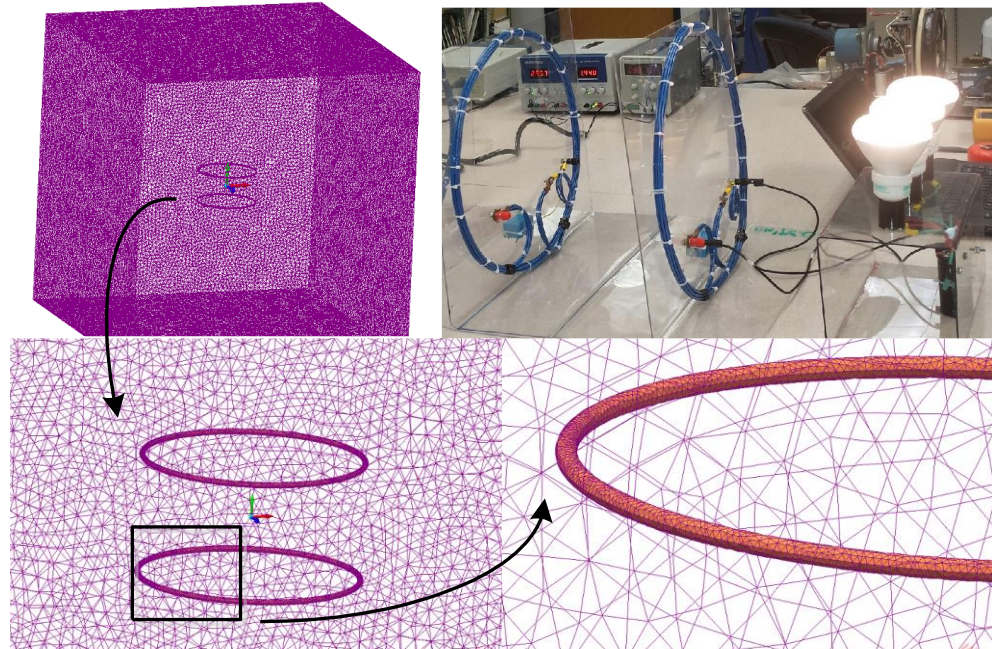


Figure 10.2 EM Model of the WPTL, top right: experimental platform.

Figure 10.3 (a) shows the field distribution of the WPTL, and (b) the locations at which the magnetic flux density will be evaluated. Figure 10.3 (c) illustrates the magnetic flux density along the lines 1 and 2 that are specified in (b) at 60 cm vertically above the two coils (along the y axis), and 60 cm horizontally next to the two coils (along the x axis). As can be seen from these plots, the magnetic field density for a non-optimum design disagrees with the ICNIRP standard, confirming the need to consider the magnetic field density in the design stage for any WPT system.

It should be noted that the modeled coil in the magnetic domain is an excellent approximation of a stranded coil (Litz coils) [117]. This allows significant decrease of the undesirable AC resistance caused by the skin effect which is a usual consequence of the frequency level in the application at hand. For this system geometry, the circular loop coil

diameter is 40 cm. The separation distance between the transmitting coil and the receiving coil is 20 cm.

Since the system under study is smaller than 1/10th of the dimension of the wavelength, it can be represented as a lumped-parameter system in which circuit theory can be used to analyze its behavior [103] for power and efficiency calculations.

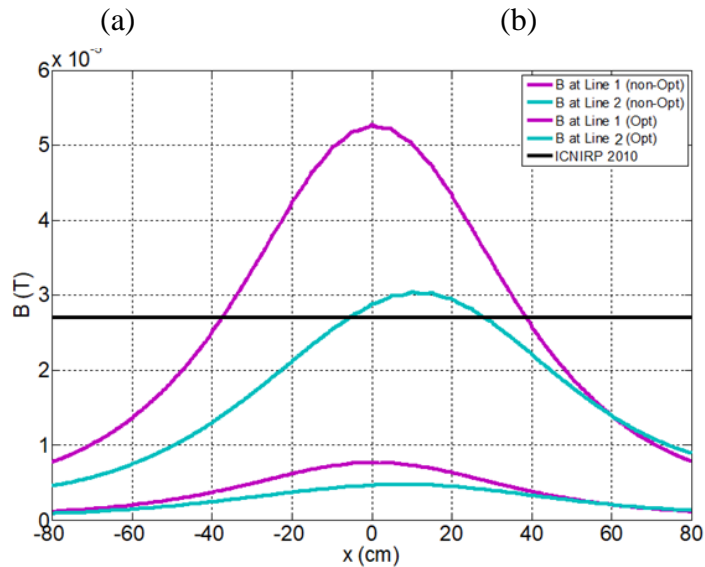
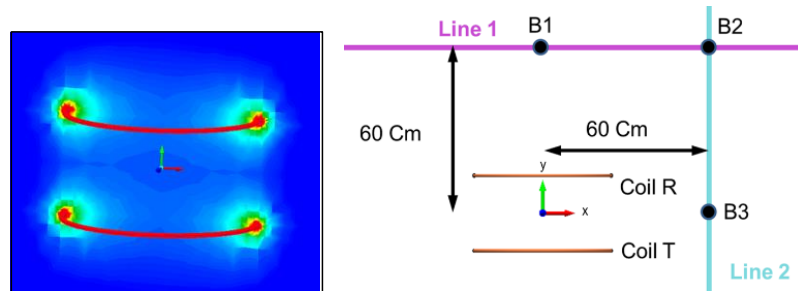


Figure 10.3 (a) Field Distribution of the WPTL; (b) Evaluation Locations; (c) Magnetic field density, B , in Tesla along lines 1 and 2, for both the optimum (Opt) and a non-optimum (non-Opt) combination of parameters, compared with the ICNIRP standard reference level.

In addition, with the resonance frequency ESR of the coils being a key design parameter [100], the two variables taken into account in this optimization are the resonance frequency and the number of turns which directly affects the ESR.

10.1.3 The EM-AI Optimization Approach

In order for the GA to determine the optimum design, it needs to evaluate the fitness for each candidate solution. This involves solving the 3DFE problem for a large number of combinations (~800 in our case), the thing which requires significant time and imposes a large computational burden.

In this study, the 3DFE problem is solved only 70 times. These 70 solution points were used to train five NNs that estimate the efficiency, the output power and the flux density at the three specified points in the 3D space of the computational model. The NN was able to obtain these parameters in a significantly reduced time with acceptable accuracy. A 3DFE-MATLAB script was developed and used to prepare the training data set for the NNs for use in the GA optimization.

10.1.3.1 The FE-MATLAB Script

For each combination of the two optimization parameters (Number of Turns and Resonance Frequency), a series of steps linking MATLAB and the 3DFE model were automated.

Other parameters can be taken as additional variables in the optimization. In fact, the use of 3DFE in the methodology presented here prove favorable in more complicated design problems, especially when shielding and layers of different materials are used above

the transmitting and below the receiving coils [118]. The developed process could also be favorable in studies of misalignments, where the 2D axisymmetric model cannot be utilized.

In the case of study presented here, the value of the magnetic field density at 3 points, indicated in Figure 10.3 in the 3D space around the coils, is obtained for each design. These points are located on the x axis, y axis, and on the diagonal direction of the x-y plane of the modeled geometry. It is worth noting that Biot-Savart law and the inversely proportional rule can be utilized to obtain the magnetic field density at the distances required, even if it is out of the boundary of the solution generated.

10.1.3.2 NNs and GA Optimization

The NNs are used to determine the efficiency of a WPTL, the output power, and the values of the magnetic field density of the design at the 3 points in the model. The NN approach was selected due to its ability to capture the nonlinear patterns observed in the data sets and re-estimate the outputs at different inputs. The used NNs are based on feed-forward architecture with the back propagation training algorithm [119]. The validation of the trained NN was performed. Table 10-1 shows 3 points validating the accuracy of the NNs. At each candidate solution of A, B, C, the values of the magnetic field, efficiencies, and power obtained from the 3DFE solution are compared with those from the NNs. The comparison shows excellent prediction ability of the developed NNs.

Table 10-1 NN prediction vs. FEA Solution

	Candidate A N=2 Freq=530 kHz	Candidate B N=3 Freq=340 kHz	Candidate C N=4 Freq=160 kHz	
B1 (μT)	4.86	3.62	6.98	FEA
	4.75	3.24	6.93	NN
B2 (μT)	1.31	0.996	1.9	FEA
	1.38	1.02	1.7	NN
B3 (μT)	2.97	2.44	4.47	FEA
	3.48	2.34	4.41	NN
Efficiency (%)	98.03	98.48	97.16	FEA
	98.26	98.95	96.5	NN
Output Power (W)	181.93	91.78	135.66	FEA
	168.33	80.46	148.08	NN

The flowchart of Figure 10.4 describes the full optimization process. The NNs are called by the GA in each iteration to estimate the values needed to evaluate the fitness function. The fitness function, F , given in (10-6) was formulated in such a way to minimize magnetic field densities at B1, B2, and B3, and maximize the efficiency:

$$F = \frac{B_1 * B_2 * B_3}{\eta} \tag{10-6}$$

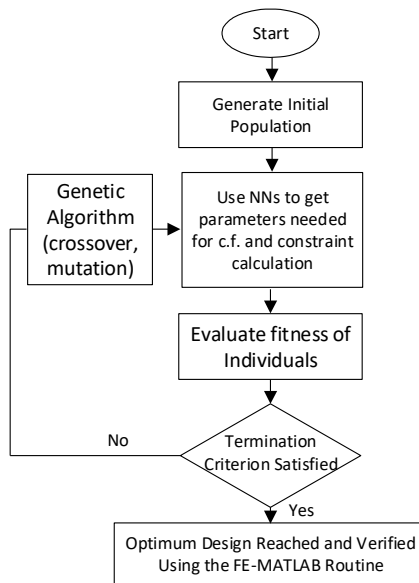


Figure 10.4 Optimization Procedure

The minimum output power is defined as a constraint for the GA. The effectiveness of using the NN in the EM-AI design optimization process presented in this study is demonstrated in Table 10-2, which shows an 89% decrease in the computational time needed for the optimization process. The 6.56 hours indicated in the table includes the time needed for preparing the training data set of the NNs, using the developed FE-MATLAB script.

Table 10-2 Comparison Of Computational Time For The EM-AI Design Optimization Approach With And Without NN Utilization

Number of Fitness Function Evaluations	Time Without NN	Time With NN
800	60 hours	6.56 hours

10.1.4 Optimization Results

In this section, the optimization algorithm is presented and verified. Six generations of GA were needed to solve the constrained optimization problem and satisfy the GA termination criterion. In other words, the average change in the fitness value and the violation constraint should be less than a tolerance value. The optimum design reached was verified using the FE-MATLAB script and is presented in Table 10-3.

The optimum design reached satisfies a high WPTL efficiency and power level around the specified constraint. In addition, the magnetic field levels (at the points considered in the 3D space around the 2 coils) are well below the ICNIRP 2010 reference level for general public exposure (27 μ T). In addition, the graph in Figure 10.3 shows that for the optimum design attained, the magnetic field density is well below the ICNIRP standard.

Table 10-3 GA result – Note that the output power is slightly less than the constraint (which was specified in our case of study to be 200 W). The reason for this is the small percentage error of the NN predicting the output power

	Number of Turns	Freq (kHz)	Eff (%)	B1 (μ T)	B2 (μ T)	B3 (μ T)	Pout (W)
Optimized Point	3	232	96.89	7.65	2.06	4.66	191

10.1.5 Concluding the study

An EM-AI design optimization environment was developed, presented and applied in a case-study to maximize the efficiency of and minimize the field density around the WPTL with the constraint applied on the output power. The use of NNs in the developed process presented in this study reduced the computational time required for the EM-AI optimization of the WPTL by 89% for a GA search space with 6 generations and 20 individuals. Also, the attained values of the magnetic field signature of the optimized design were well-below the EMC reference standard levels.

10.2 An Integrated Characterization Model and Multi-Objective Optimization for the Design of an EV Charger’s Circular Wireless Power Transfer Pads

The WPT EV charger system components can be sorted into the source, the converters, the resonant circuits, the magnetic pads, and the EV battery. As described in the literature, the power that an inductive power transfer system can produce is dependent on the circuit to which the primary pad is connected and the quality factor of each of the magnetic circuit and the circuit to which the secondary pad is connected [118].

A good approach for designing the system would start from decoupling the magnetic design from the primary and secondary circuits and focusing on achieving a design that has

high levels of coupling factor, k , and appropriate levels of quality factor of the primary and secondary coils, Q_1 and Q_2 , where $k = \frac{M}{\sqrt{L_1 L_2}}$ and $Q_L = \frac{\omega L}{R}$. Here, L , L_1 , and L_2 are the self-inductance of any coil, the primary coil, and the secondary coil, respectively; M is the mutual inductance between the two; ω is the frequency of operation, R is the unwanted wire resistance.

Designs of EV couplers in the literature have either been done numerically using FEA [120] or analytically. The design procedures done in FEA follow a trial and error method requiring numerous 3D trials because of the high number of parameters affecting the power transfer. This is both computationally expensive and time-consuming. Analytical designs of EV magnetic couplers have been performed but have not taken into consideration the effect that the presence of the magnetic core (flux guide) or the effect that the conductive layer shielding have on the parameters of the coils. These are critical considerations that should not be omitted because of the direct and considerable effect they have on k and Q_L .

Acero et al. have analyzed the coupling between two coils placed between two multilayered media in consecutive studies [121], [122], [123]. The analytical model presented in these references are used in this work for characterizing the circular WPT pads for the application of recharging EV batteries.

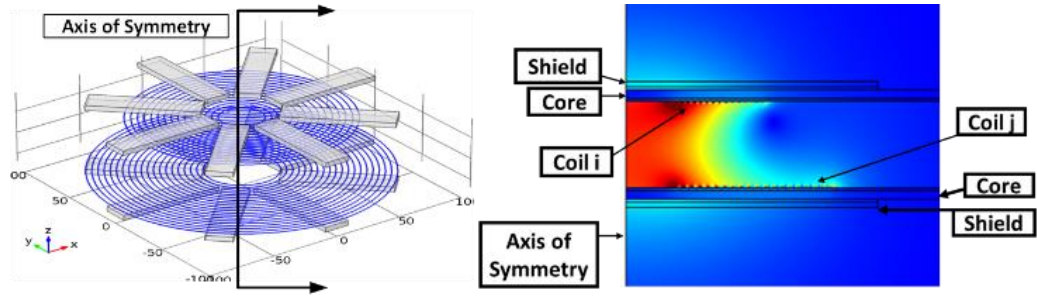


Figure 10.5 Left: 3D model of WPT Pads; Right: A 2D Axisymmetric Model showing the coils sandwiched between core and shielding layers.

10.2.1 The Analytical Model

The circular topology of the system under study is shown in Figure 10.5. The total self-inductance of coil j is calculated as the sum of the self-inductance of the coil in the air, $L_{v,j}$, and the contribution of the upper and lower media (u) and (l), $\Delta L_{ul,j}$, of the magnetic core (Ferrite Bars) that yields an increase to the inductance of the winding because of the current images. The characterization model utilized allows for the consideration of the effect of several layers simultaneously. However, this study is aimed towards obtaining the optimal design. Designing the shield that will ensure compliance with EMC standards for this topology of EV pads was presented in [124] and can be acquired further on, utilizing the optimum solutions obtained here. In a similar manner, the total resistance of a coil j is calculated as the sum of the resistance in the air, $R_{v,j}$, and the contribution of the media, $\Delta R_{ul,j}$. Also, the total coupling inductance between 2 coils, i and j is calculated as the sum of the mutual inductance of the coils in the air, $M_{v,ij}$, and the contribution of the media, $\Delta M_{ul,ij}$. $\Delta Z_{ul,j}$ and $\Delta Z_{ul,ij}$ are the contributions of the media to coil j 's impedance and the mutual impedance, respectively.

$$L_j = L_{v,j} + \Delta L_{ul,j} = L_{v,j} + \text{Im}(\Delta Z_{ul,j}/\omega) \quad (10-7)$$

$$R_j = R_{v,j} + \Delta R_{ul,j} = R_{v,j} + \text{Re}(\Delta Z_{ul,j}/\omega) \quad (10-8)$$

$$M_{ij} = M_{v,ij} + \Delta M_{ul,ij} = M_{v,ij} + \text{Im}(\Delta Z_{ul,ij}/\omega) \quad (10-9)$$

This model can accurately represent the magnetic solution that is obtained from a numerical model. The detailed equations used in this work for the characterization are presented in Appendix I. In this work, the resistance of the coil, due to the Joule effect by the driven current in the wire and associated with skin effect including dc losses, is considered. Another component of the power losses in the winding is due to eddy currents induced by the magnetic flux created by the rest of the turns on the winding, associated with the proximity effect and have been named as induction losses. The latter component is neglected in the self-resistance component characterization of this work, where the space between the turns is large compared to the radius of the wire. Also, in this work, the two WPT pads are assumed to be aligned. In literature, several topologies of the WPT pads have been proposed for the sake of enhancing the tolerance to misalignment. It can be concluded from [125], a study on driver's behavior and parking alignments, that even with the new topologies proposed, the implementation of an accurate positioning system is inevitable. From that point on, the misalignment will not be the main issue and therefore can be omitted in this study.

This analytical approach for the characterization of WPT systems provide much flexibility to the design process since the equations include the dependence on several parameters such as the number of turns, frequency of the currents, the physical properties

of the layers (core and shielding), and several geometrical parameters such as the diameter of the coils, inter-turn spacing, thickness of the layers, and misalignments.

The solution from a 2D axisymmetric model was obtained and compared against the results from an analytical model in Table 10-4. The results show the validity of the analytical model. The small error could be justified by the approximation in FEA.

Table 10-4 Comparison between Characterization Results from the Analytical and FEA Model

	Analytical Model	2D axisymmetric solution
L(μH)	29.85	30.86
M₁₂(μH)	6.11	5.58
R (Ω)	0.15	0.16

The equations used in this analytical model are developed in [121], [122], [123] based on the differential form of Maxwell's equations, and on the basis of cylindrical symmetry and follow a quasi-static approximation considering the dimension of the system with respect to the wavelengths at the involved frequency levels. The detailed equations are presented in this section. Sections 10.2.1.1, 10.2.1.2, and 10.2.1.3 present the equations used for the calculation of the self-inductance of the coil, the resistance of the coil, and the coupling inductance of the two coils, respectively.

10.2.1.1 Self-Inductance of the Coil

$$L_{v,j} = \sum_{p=1}^{n_j} \left(\mu_0 a_p \left[\ln \left(\frac{8a_p}{r_o} \right) - 1.75 \right] + 2 \times \sum_{q>p}^{n_j} M_{pq} \right) \quad (10-10)$$

Where

$$M_{pq} = \mu_0 \sqrt{a_p a_q} \frac{2}{\gamma} \left[\left(1 - \frac{\gamma^2}{2} \right) K(\gamma) - E(\gamma) \right] \quad (10-11)$$

$$\gamma = \sqrt{\frac{4a_p a_q}{(a_p + a_q)^2}} \quad (10-12)$$

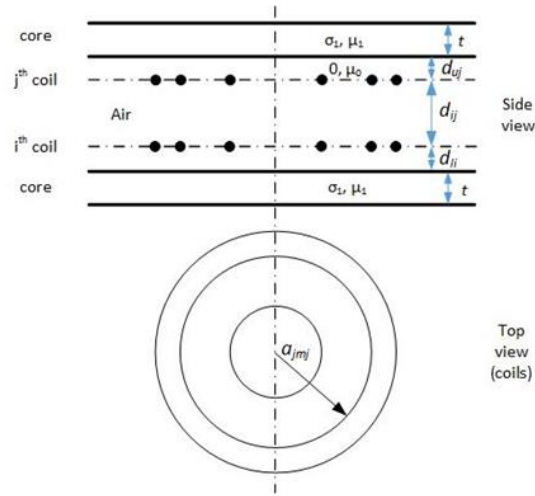


Figure 10.6 The spiral windings i and j between the two layers of the core

It is interesting to note that a 2D axisymmetric model is valid as the core layer can be modeled as a homogeneous layer with the obtained equivalent relative permeability, which is explained in Table 10-5.

Table 10-5 Nomenclature of the symbols used in the equations

Symbol	Explanation
a_{im_i} and a_{jm_j}	the radius of the individual turns in coils i and j respectively
r_o	the radius of the wire
$K(\gamma)$ and $E(\gamma)$	the elliptical integrals of the first and second kind, respectively
ω	the angular frequency of the current
a_p and a_q	the radii of turns p and q respectively, in any coil
μ_0	The permeability of free space
μ_1	The equivalent relative permeability of the layer in which the ferrite bars are placed. An experimental test is conducted for obtaining L_j and $L_{v,j}$. The difference of the two obtained values is the contribution of the media to the self-inductance of the coils. This is a function of the effective permeability of the layer, thus allowing to obtain the latter.
n_o	The number of strands in the wire used; in this work, a solid wire is used
ξ	The inverse of the skin depth
ber, bei, ber', bei'	Kelvin functions
d_{uj} & d_{ui}	the distance from layer u to coils j and i respectively
d_{lj} & d_{li}	the distance from layer l to coils j and i respectively

10.2.1.2 Resistance of the Coil

As mentioned before, the total resistance of a coil is calculated as the sum of the resistance in the air and the contribution of the media.

$$R_{v,j} = \frac{1}{n_o} \left[\frac{\xi}{r_o \sigma} \Phi_{cond} \sum_{i=1}^n a_i \right] - n_o \left[\frac{2\xi r_o}{3r_c^2 \sigma} \Phi_{ind} \sum_{i=1}^n a_i + \frac{2\pi^2 \xi r_o}{\sigma} \Phi_{ind} \sum_{i=1}^n [a_i \langle \mathcal{H}_{o,i}^2 \rangle] \right] \quad (10-13)$$

Where

$$\xi = \sqrt{\mu \sigma \omega} \quad (10-14)$$

$$\Phi_{cond} = \frac{\text{ber}(\xi r_o) \text{bei}'(\xi r_o) - \text{ber}'(\xi r_o) \text{bei}(\xi r_o)}{\text{ber}'^2(\xi r_o) + \text{bei}'^2(\xi r_o)} \quad (10-15)$$

$$\Phi_{ind} = \frac{\text{ber}_2(\xi r_o) \text{ber}'(\xi r_o) - \text{bei}_2(\xi r_o) \text{bei}'(\xi r_o)}{\text{ber}^2(\xi r_o) + \text{bei}^2(\xi r_o)} \quad (10-16)$$

$$\Delta Z_{ul,j} = j\omega \mu_0 \pi \int_0^\infty G(\beta, z_j, z_j) \times \left[\sum_{p=1}^{n_j} a_p J_1(\beta a_p) \right]^2 d\beta \quad (10-17)$$

$$G(\beta, z_j, z_j) = \frac{e^{-2\beta d_{uj}} \phi_u + 2\phi_u \phi_l e^{-2\beta(d_{uj} + d_{lj})} + e^{-2\beta d_{lj}} \phi_l}{1 - \phi_u \phi_l e^{-2\beta(d_{uj} + d_{lj})}} \quad (10-18)$$

10.2.1.3 Coupling Inductance of the Two Coils

$$M_{v,ij} = \mu_0 \pi \int_0^\infty e^{-\beta |d_{ij}|} \times \sum_{m_i=1}^{n_i} \sum_{m_j=1}^{n_j} a_{jm_j} a_{im_i} e^{-\beta |d_{ij}|} J_1(\beta a_{jm_j}) J_1(\beta a_{im_i}) J_0(\beta l) d\beta \quad (10-19)$$

$$\begin{aligned} \Delta Z_{ul,ij} &= j\omega\mu_0\pi \int_0^\infty G(\beta, z_i, z_j) \\ &\times \sum_{m_i=1}^{n_i} \sum_{m_j=1}^{n_j} a_{jm_j} a_{im_i} e^{-\beta|d_{ij}|} J_1(\beta a_{jm_j}) J_1(\beta a_{im_i}) J_0(\beta l) d\beta \end{aligned} \quad (10-20)$$

Where

$$\begin{aligned} G(\beta, z_i, z_j) &= \frac{e^{-\beta d_{uj}} + \phi_l e^{-\beta(d_{uj}+2d_{lj})}}{1 - \phi_u \phi_l e^{-2\beta(d_{uj}+d_{lj})}} \phi_u e^{-\beta d_{ui}} \\ &+ \frac{e^{-\beta d_{lj}} + \phi_u e^{-\beta(2d_{uj}+d_{lj})}}{1 - \phi_u \phi_l e^{-2\beta(d_{uj}+d_{lj})}} \phi_l e^{-\beta d_{li}} \end{aligned} \quad (10-21)$$

$$\phi_u = \frac{\mathbf{T}_{12}^u(\beta)}{\mathbf{T}_{22}^u(\beta)} \quad \text{and} \quad \phi_l = \frac{\mathbf{T}_{21}^l(\beta)}{\mathbf{T}_{11}^l(\beta)} \quad (10-22)$$

$$\mathbf{T}^u(\beta) = \prod_{k=s}^{N-1} \mathbf{R}_{k,k+1}(\beta) \quad \& \quad \mathbf{T}^l(\beta) = \prod_{k=1}^{s-1} \mathbf{R}_{k,k+1}(\beta) \quad (10-23)$$

$$\mathbf{R}_{k,k+1}(\beta) = \frac{1}{2} \begin{pmatrix} \left(1 + \frac{\lambda_{k+1}}{\lambda_k}\right) e^{-\eta_k t_k} & \left(1 - \frac{\lambda_{k+1}}{\lambda_k}\right) e^{-\eta_k t_k} \\ \left(1 - \frac{\lambda_{k+1}}{\lambda_k}\right) e^{\eta_k t_k} & \left(1 + \frac{\lambda_{k+1}}{\lambda_k}\right) e^{\eta_k t_k} \end{pmatrix} \quad (10-24)$$

$$\lambda_k = \eta_k / \mu_k \quad (10-25)$$

$$\eta_k = \sqrt{\beta^2 + j\omega\mu_k\sigma_k} \quad (10-26)$$

10.2.2 Multi-Objective Optimization Methodology

This problem is a multi-objective optimization problem (MOOP) with two objectives; maximizing the coupling factor and the quality factor for the coils of a WPT system for EV charging. In many studies, the Weighted Sum (WS) method is used to solve the MOOP. In this method, all the objective functions are expressed in one function with an assigned weight for each one. In other words, the MOOP is relaxed to be a single objective, and then

the problem is solved using one of the single objective techniques as in [126]. Despite the simplicity of this method, it suffers from major drawbacks including the difficulty of the appropriate assignment of the weights and its failure to generate feasible solutions on the nonconvex portions of the optimum solution front [127]. Furthermore, it generates only one solution which significantly limits the options in the decision making process [128]. Whereas in the Pareto Optimality (PO), a set of points that all fulfill the definition of an optimal solution and meet the problem constraints is defined. Thus, all the generated solutions in this set are considered optimal and satisfy the objective functions with varying degrees. This set of optimal solutions is known as the Pareto Front (PF) and is named after the economist Vilfredo Pareto.

Different methods were proposed in literature to generate the PF. The Non-Dominated Sorting Genetic Algorithm II (NSGA-II) has been one of the most successful techniques. It is an extension of the GA and uses an elitism approach and sorting algorithm to determine the PF [129]. The formulation of the MOOP is detailed as follows.

10.2.2.1 Objective Functions

- 1) Objective Function 1: it is required to maximize the coupling factor k .

$$\text{Maximize } k = \frac{M}{\sqrt{L_1 L_2}} = \frac{M}{L} \quad (10-27)$$

- 2) Objective Function 2: it is required to maximize the quality factor Q , which has the same value for the 2 coils since in this design, they are identical ($L_1 = L_2 = L$).

$$\text{Maximize } Q = \frac{\omega L}{R} \quad (10-28)$$

Based on the mathematical expressions, it can be concluded that both objectives are explicitly contradicting. That is in enhancing one objective, the other is expected to worsen.

This justifies the importance of adopting Pareto-based methods, where the different trade-offs between the objective functions can be realized.

10.2.2.2 Decision Variables

These variables are also called controlled variables. These are the variables manipulated by the optimization algorithm during the search process for the optimal solution. In this problem, three decision variables are considered; the number of turns of the coil, the inner radius of the coil and the distance between the coil and the core.

10.2.2.3 Constraints

In order to guarantee that the obtained solution is feasible and acceptable from the practical point of view, multiple constraints are considered. Constraints in equations (10-29) and (10-30) limit the current in coils i and j , respectively, to be less than the saturation current, calculated as explained in (10-38). (10-31) is a geometrical constraint that limits the outer radius of the coil. In order to select a design that is feasible to our application, the minimum amount of transferred power should be constrained, as expressed in (10-32).

$$I_i \leq I_{\text{sat}} \quad (10-29)$$

$$I_j \leq I_{\text{sat}} \quad (10-30)$$

$$r_{\text{out}} \leq r_{\text{out}}^{\text{max}} \quad (10-31)$$

$$P \geq P_{\text{min}} \quad (10-32)$$

While iterating through the individuals in the optimization algorithm, it is important to exclude those that cause the saturation of the core. To do this, the level of the current that causes saturation is calculated for each individual in the optimization. In this section, the evaluation of this current level is presented.

$$\text{Flux linkage: } \lambda = N \times \varphi = L \times I \quad (10-33)$$

$$\text{Therefore: } I_{sat} = \frac{N \times \varphi}{L} \quad (10-34)$$

But the maximum allowed magnetic field density is:

$$B_{max} = \frac{\varphi}{A} \text{ so } \varphi = B_{max} \times A \quad (10-35)$$

Substituting (10-35) in (10-34):

$$I_{sat} = \frac{N \times (B_{max} \times A)}{L} \quad (10-36)$$

$$\text{But: } A = (2\pi r_{in}) \times t \quad (10-37)$$

The surface area of (10-37) is highlighted in blue in Figure 10.7 because the most field will be concentrated in the center, where the highest percentage of ferrite is available. So, by ensuring that this part does not saturate, we ensure that the whole core does not as well.

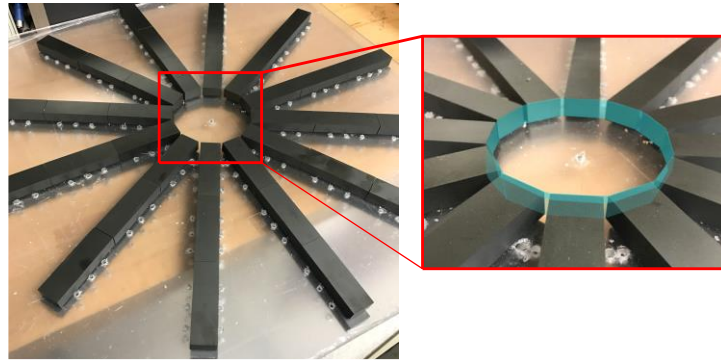


Figure 10.7 A zoom in view on the Ferrite core center area

Substituting (10-37) in (10-36):

$$I_{sat} = \frac{N \times B_{max} \times (2\pi r_{in}) \times t}{L} \quad (10-38)$$

In this work, N87 ferrite bars (I-cores) were used to create the magnetic core layer. The B_{sat} defined in the datasheet of the core ferrite bars is 0.49 T. However, $B_{max} = 0.32 T$ is used in this work to ensure that the magnetic field created by the current is well below the saturation.

The optimization problem is solved using NSGA-II, the number of generations is set to 100, and the population of each generation is set to 50 individuals. The transferred power is constrained in this optimization problem to a minimum of 1000 W. The obtained Pareto

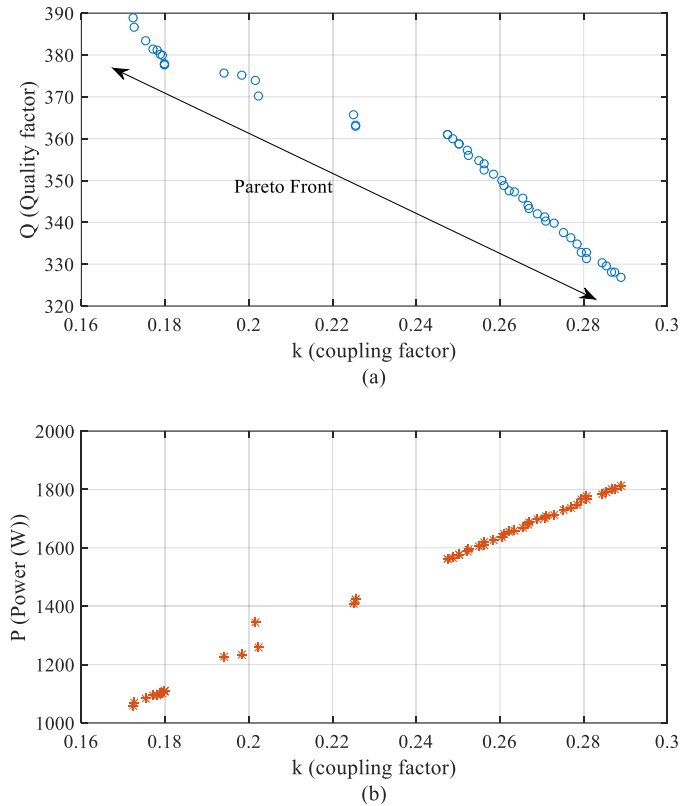


Figure 10.8 Optimization results (a) Pareto front (b) evaluated transferred power for each individual in the Pareto front.

Front is depicted in Figure 10.8 (a). Each point on the front represents a design for the pads. The values of the first objective function at each individual obtained are shown on the x-axis, while the values of the second objective are shown on the y-axis. It can be seen that when moving along the front, as one objective is improved, the other worsens. The corresponding values of the transferred power for each individual are evaluated and plotted as shown in Figure 10.8 (b).

10.2.3 Concluding the study

An MOOP with the objective of optimizing the design of two WPT EV charger pads has been applied using the Pareto Optimality Algorithm. To reduce the time of simulation required in FEA for iterating through the numerous combinations of solutions, an analytical model that takes into account the considerable effect of having the coils sandwiched between the two core (magnetic) layers is used. The reduction of the time for running the optimization problem at hand is the most significant contribution of this work; the optimization simulation for the 100 generations, 50 individuals problem took around 5 hours, whereas applying each combination of this huge number of individuals in FEA, together with the setup time of each geometry is much more expensive in terms of computation and time. The Pareto front with the set of optimal solutions obtained are presented in the results section.

Chapter 11 Conclusions and Future Works

11.1 Conclusions

The studies and solutions presented in this dissertation contribute to a seamless transition into the vision of cities dominated by EVs and their charging infrastructure.

Different aspects related to the real-time management of a large number of EVs in the application of public charging were presented in this dissertation. The accompanying challenges of communications means, big data, and cyber security were addressed. The dissertation started with an assessment of the communication links and the enabling technologies that are used in the management of EVs in the public charging category. In light of this assessment, linking all levels into one correlated connectivity platform became evident. The advantages of using a MAS with a clear message-sharing communication scheme to facilitate a designed system-level operation were then discussed. Then, a middleware-based MAS to facilitate the real-time management of en route EVs, using communication between the EVs and the control centers, was designed and tested in real-time, with real modules. The developed framework is referred to as the Bilateral Decision Support System, in which achieves the objectives of the EVs, EVCSs, and the power system are achieved in an integrated manner. The effectiveness of the proposed framework is demonstrated by presenting price-based case studies from two complementary perspectives: 1) The on-board decision support module to choose the optimal EVCS in favor of the EVs status, and 2) the electric power grid decision support by means of the logic of a higher-end agent to redistribute the EVs onto the EVCSs. The results proved that given a power distribution that could be provided by means of a higher-end optimization

or energy management system, the BDSS achieves the anticipated win-win situation for the EVs and the power grid. In this framework, the two are complementary in a way that the desired benefit to one cannot be achieved without attaining that of the other.

The design and rules of the intelligent FL based on-board module were explained in details, and case studies were presented for validating its operation. The case study results showed that the designed module gives trustworthy rerouting recommendations to the drivers.

The design of the BDSS in the form of middleware-based MAS was presented, with the individual agents, topics, and the messaging scheme followed in the MAS. In addition to the communication means and schemes used, the challenges that accompany the system were assessed. Among those were the issues of big data where GPU computing was deployed in a coordinated computing scheme between the CPU and the GPU to handle the large data sets in real-time, given the operational requirements of the framework. This computing environment was deployed to significantly accelerate the application and meet its real-time requirement. The work presented a three stage coordinated algorithm between the CPU and the GPU, describing the grid dimensions and the kernel in each stage. The implementation of this algorithm resulted in a highly efficient, high-throughput computation, where the performance metrics showed more than 99% improvement in runtime in the GPU environment over that of the CPU-only environment. Furthermore, the possible cyber security threat scenarios facing the BDSS are elaborated, and the taken security measures are explained. Example files used for configuring authentication, access control, and revocation have been presented, and their format and content detailed. To test

the applied measures, several scenarios were simulated, and screenshots from the relevant agents' terminals presented to show the response. The system successfully denied access to participants with a wrong private key and successfully detected a change in the digital signature of a Permissions file, thus strictly imposing the access control measures. In addition, an EV with an unregistered API key tried to connect to the system, and was denied access.

The management of en-route EVs in real-time is quite recent and not many research works can be found in the literature covering this topic comprehensively. For that, and using the developed BDSS is used to facilitate a service with ancillary potential. This introduced service in this dissertation is referred to as the Collective Distribution of Mobile Loads. A real-time system-level PSO algorithm was applied to determine the optimal collective distribution of the EVs onto the EVCSs. Afterwards, the optimization results were passed to the BDSS to guide the EVs to the appropriate EVCSs. Studies were applied in a simulation of a modified version of the standard IEEE 14-bus system under normal and contingency operation conditions, as well as in an experiment comprising an 8-bus laboratory-scale power system, under normal conditions. The results of the applied case studies have proven the CDML a viable and effective service, achieving noteworthy levels of loss reduction and post-contingency congestion relief that minimize the need for load shedding.

On a different scale, the component level, new and effective techniques that facilitate the optimization of the efficiency of the magnetic part of wireless EVSEs are presented.

Those methods consider international EMC standards. Four studies were applied, considering different aspects of the design of the WPT-based EVSEs.

One study presented the design of the shield of wireless charging pads for EV chargers in a way that considers the limits set forth by the ICNIRP 2010 standard reference level for general public exposure to time-varying electric and magnetic fields. The iterative proposed procedure was applied in a case study for a given design of WPT pads considering the 85 KHz frequency level set by SAE-J2954 TF.

In another study, a procedure using electromagnetic field analysis coupled with an electric circuit was developed for the performance evaluation of a WPT system. This coupled model was implemented as a 3DFE-MATLAB automated script which was utilized for varying several design parameters and evaluating the performance of the WPT coupled resonators link given various design vectors.

In terms of optimization techniques, two studies were applied, one using the FEA environment with NNs, and another using an analytical model for the characterization of the design. In the first, an EM-AI design optimization environment was developed, presented and applied in a case-study to maximize the efficiency of and minimize the field density around the WPTL with the constraint applied on the output power. The use of NNs in the developed process presented in this study reduced the computational time required for the EM-AI optimization of the WPTL by 89% for a GA search space with 6 generations and 20 individuals. Also, the attained values of the magnetic field signature of the optimized design were well-below the EMC reference standard levels. In the second optimization study applied, an MOOP with the objective of optimizing the design of two

WPT EV charger pads was applied using the Pareto Optimality Algorithm. To reduce the time of simulation required in FEA for iterating through the numerous combinations of solutions, an analytical model that takes into account the considerable effect of having the coils sandwiched between the two core (magnetic) layers is used. The reduction of the time for running the optimization problem at hand is the most significant contribution of this study; the optimization simulation for the 100 generations, 50 individuals' problem took around 5 hours, whereas applying each combination of this huge number of individuals in FEA, together with the setup time of each geometry is much more expensive in terms of computation and time.

11.2 Future Works

EVs are being looked at as an important component of emerging transportation system that will involve a growing market penetration of automated, connected, electric, and shared (ACES) vehicles. Providing an infrastructure and associated system operations and management (SO&M) strategies for optimal support of these vehicles will be critical to achieve the mobility, safety, and environmental benefits of these technologies. It is obvious that the current energy and transportation infrastructure are not able to provide this required support and that there is a need to retrofit them to support the new technologies. Solutions are needed at this stage not only to overcome the barriers of the growth of EVs, but also to set rules that organize this anticipated expansion once it is underway and determine the required management, operations, pricing, and incentives.

The work in this dissertation opens up opportunity for many interdisciplinary research studies. For example, combined efforts from interdisciplinary teams could be deployed to

model the interdependent operation of transportation, communication, and electric infrastructures. In light of this, the optimization problem applied in the CDML could be extended to a multi-objective optimization problem to include parameters from the transportation network for simultaneously reducing transportation system congestions.

The integration of the EV charging, power generation and transportation system modeling will also allow for the assessment of the interdependencies between the power and transportation infrastructures and the need for modifications to the transportation system to support charging.

Other approaches to the design of the on-board module could be assessed, considering modeling and analyzing the social behavior of the EVs owners and how they react to different incentives to abide by the recommendations. The model of the on-board module could be further extended to simulate the energy consumption of the vehicle as the traffic conditions and traffic management parameters change dynamically as the vehicles move in the network. The real-time simulation will be integrated with the dynamic multi-objective optimization for smart EV control of the project.

The guidance provided to the EVs and the associated SO&M will compensate for the range-anxiety dilemma resulting in an increase in the EV market penetrations, while reducing any impacts from the routings on the transportation system.

On a parallel note, the BDSS provides a great source of data for studies in transportation systems and others that support the developments in the quest towards smart cities. The data collected from this developed MAS could be used as one of the emerging data sources

that have the ability to complement conventional data of surveys and diaries used in transportation studies by improving data quality and accuracy. These data sources have a level of detail that offer researchers opportunities to create real-time representations of congestions and emissions throughout the transportation network. Eventually this kind of data helps produce more accurate transportation measures and representative models of human behavior. Examples of those data sources, data-processing algorithms that have been used to derive travel information, and applications that have been conducted on the basis of these data are reviewed in [130]. This comprehensive review shows the importance of the collection of such transportation-related data. Some identified data sources are personal or vehicle GPS devices, mobile phone network data, and smartphone GPS data.

The authors in [131] use Google location history data of a group of participants and apply a dataprocessing algorithm to derive travel information. They discuss the potential applications of this data to understand travel patterns. Studies like this in [131] demonstrate the potential of data sources like those reviewed in [130]. Examples of potential uses are studying daily variations in travel behavior and investigating human mobility patterns on a large spatiotemporal scale. This further supports the worth of data that can be collected from the BDSS developed in this dissertation.

Information from this research will identify solutions to the different barriers of EV adoption and data on the power system side can be logged for helping the power system cope with the expected rise in demand from EVs, considering the needed updates to the infrastructure and SO&M associated with ACES in recurrent and emergency conditions.

The BDSS could also be utilized in evacuation and recovery stages related to a disaster, where a guiding service like this will be of most importance both to EV owners and to power systems. This type of analysis has not been addressed in existing evacuation studies. User choices are modeled at the individual household level, recognizing that each household may have different choices and behavioral responses due to varying household characteristics and constraints. Collectively, the individual choices will represent the demand for transportation and energy infrastructures, which serve as the inputs for networks simulations and optimization.

**Appendix 1 – Fuzzy logic rules of the on-board module for recommending EVCSs in
response to public charging requests**

Rules	Input Variables				Output Variable
	SoC	dtCS	ttCS	price	Recommendation Level
1	low	low	low	low	highly recommend
2	low	low	low	medium	highly recommend
3	low	low	low	high	highly recommend
4	low	low	medium	low	poorly recommend
5	low	low	medium	medium	do not recommend
6	low	low	medium	high	do not recommend
7	low	low	high	low	do not recommend
8	low	low	high	medium	do not recommend
9	low	low	high	high	do not recommend
10	low	medium	low	low	poorly recommend
11	low	medium	low	medium	do not recommend
12	low	medium	low	high	do not recommend
13	low	high	medium	low	do not recommend
14	low	high	medium	medium	do not recommend
15	low	high	medium	high	do not recommend
16	low	high	high	low	do not recommend
17	low	high	high	medium	do not recommend
18	low	high	high	high	do not recommend
19	medium	low	low	low	highly recommend
20	medium	low	low	medium	recommend
21	medium	low	low	high	ok
22	medium	low	medium	low	recommend
23	medium	low	medium	medium	recommend
24	medium	low	medium	high	ok
25	medium	low	high	low	ok
26	medium	low	high	medium	poorly recommend
27	medium	low	high	high	poorly recommend
28	medium	medium	low	low	highly recommend
29	medium	medium	low	medium	recommend
30	medium	medium	low	high	do not recommend
31	medium	medium	medium	low	ok
32	medium	medium	medium	medium	poorly recommend
33	medium	medium	medium	high	do not recommend
34	medium	medium	high	low	poorly recommend
35	medium	medium	high	medium	do not recommend
36	medium	medium	high	high	do not recommend

37	medium	high	low	low	poorly recommend
38	medium	high	low	medium	poorly recommend
39	medium	high	low	high	do not recommend
40	medium	high	medium	low	poorly recommend
41	medium	high	medium	medium	do not recommend
42	medium	high	medium	high	do not recommend
43	medium	high	high	low	do not recommend
44	medium	high	high	medium	do not recommend
45	medium	high	high	high	do not recommend
46	high	low	low	low	highly recommend
47	high	low	low	medium	recommend
48	high	low	low	high	poorly recommend
49	high	low	medium	low	highly recommend
50	high	low	medium	medium	recommend
51	high	low	medium	high	poorly recommend
52	high	low	high	low	highly recommend
53	high	low	high	medium	recommend
54	high	low	high	high	do not recommend
55	high	medium	low	low	highly recommend
56	high	medium	low	medium	recommend
57	high	medium	low	high	ok
58	high	medium	medium	low	recommend
59	high	medium	medium	medium	ok
60	high	medium	medium	high	poorly recommend
61	high	medium	high	low	recommend
62	high	medium	high	medium	ok
63	high	medium	high	high	poorly recommend
64	high	high	low	low	highly recommend
65	high	high	low	medium	recommend
66	high	high	low	high	ok
67	high	high	medium	low	recommend
68	high	high	medium	medium	ok
69	high	high	medium	high	poorly recommend
70	high	high	high	low	ok
71	high	high	high	medium	poorly recommend
72	high	high	high	high	poorly recommend

LIST OF REFERENCES

- [1] "The History of the Electric Car | Department of Energy," 2014. [Online]. Available: <https://www.energy.gov/articles/history-electric-car>.

- [2] A. Brecher and D. Arthur, "Review and Evaluation of Wireless Power Transfer (WPT) for Electric Transit Applications, FTA Report Number 0060," Washington, 2014.

- [3] T. W. Ching and Y. S. Wong, "Review of wireless charging technologies for electric vehicles," in *2013 5th International Conference on Power Electronics Systems and Applications (PESA)*, Hong Kong, 2013.

- [4] D. Anair and A. Mahmassani, "State of CHARGE Electric Vehicles' Global Warming Emissions and Fuel-Cost Savings across the United States," Cambridge, 2012.

- [5] D. Anair and A. Mahmassani, "State of Charge: Technical Appendix," Cambridge, 2012.

- [6] F. Lambert, "Tesla aims to release more powerful Supercharger V3 for quicker charging this summer - Electrek," 2018. [Online]. Available: <https://electrek.co/2018/05/21/tesla-supercharger-v3-quicker-charging-summer/>.

- [7] V. M. Iyer, S. Guler, G. Gohil and S. Bhattacharya, "Extreme fast charging station architecture for electric vehicles with partial power processing," in *2018 IEEE Applied Power Electronics Conference and Exposition (APEC)*, 2018.

- [8] "First look at Tesla's new kind of Supercharger station with design refresh - Electrek," 2017. [Online]. Available: <https://electrek.co/2017/09/11/first-look-tesla-new-supercharger-station/>.

- [9] D. Hall and N. Lutsey, "EMERGING BEST PRACTICES FOR ELECTRIC VEHICLE CHARGING INFRASTRUCTURE Dale Hall, Nic Lutsey," Washington, 2017.
- [10] "Super charging lines | Tesla," 2017. [Online]. Available: <https://forums.tesla.com/forum/forums/super-charging-lines>.
- [11] "Tesla unveils its largest Supercharger station in the US — and it kind of looks like a truck stop - The Verge," 2017. [Online]. Available: <https://www.theverge.com/2017/11/16/16665504/tesla-supercharger-largest-us-kettlemen-truck>.
- [12] A. Colmenar-Santos, C. de Palacio, D. Borge-Diez and O. Monzón-Alejandro, "Planning minimum interurban fast charging infrastructure for electric vehicles: Methodology and application to Spain," *Energies*, 2014.
- [13] J. Motavalli, "For E.V. Drivers, a Stretch of Oregon Interstate to Relieve Range Anxiety," 2012. [Online]. Available: <https://wheels.blogs.nytimes.com/2012/03/19/for-e-v-drivers-a-stretch-of-oregon-interstate-to-relieve-range-anxiety/>.
- [14] "Tracking Clean Energy Progress," 2018. [Online]. Available: <https://www.iea.org/tcep/>.
- [15] "Electric Vehicles | Tracking Clean Energy Progress," 2018. [Online]. Available: <https://www.iea.org/tcep/transport/evs/>.
- [16] I. S. Bayram and I. Papapanagiotou, "A survey on communication technologies and requirements for internet of electric vehicles," *EURASIP Journal on Wireless Communications and Networking*, vol. 2014, no. 1, p. 223, 16 12 2014.
- [17] IEEE Std 2030-2011, "IEEE Guide for Smart Grid Interoperability of Energy Technology and Information Technology Operation with the Electric Power System (EPS), End-Use Applications, and Loads," 2011.

- [18] "5gamericas :: Global LTE Connections Hit 2.5 Billion Milestone," 2018. [Online]. Available: <http://www.5gamericas.org/en/newsroom/press-releases/global-lte-connections-hit-25-billion-milestone/>.
- [19] "International Standard IEC 60870-6-503," Geneva, 2002.
- [20] A. Al-Fuqaha, M. Guizani, M. Mohammadi, M. Aledhari and M. Ayyash, "Internet of Things: A Survey on Enabling Technologies, Protocols, and Applications," *IEEE Communications Surveys & Tutorials*, vol. 17, no. 4, pp. 2347-2376, 24 2015.
- [21] T. A. Youssef, M. E. Hariri, A. T. Elsayed and O. A. Mohammed, "A DDS-Based Energy Management Framework for Small Microgrid Operation and Control," *IEEE Transactions on Industrial Informatics*, vol. 14, no. 3, pp. 958-968, 3 2018.
- [22] M. Mahmoudian Esfahani, A. Hariri and O. A. Mohammed, "A Multiagent-based Game-Theoretic and Optimization Approach for Market Operation of Multi-Microgrid Systems," *IEEE Transactions on Industrial Informatics*, pp. 1-1, 2018.
- [23] "PlugShare - EV Charging Station Map," [Online]. Available: <https://www.plugshare.com/>.
- [24] "Open Charge Map - The global public registry of electric vehicle charging locations," [Online]. Available: <https://openchargemap.org/site>.
- [25] "Find every public charging stations for electric cars | ChargeHub," [Online]. Available: <https://chargehub.com/en/charging-stations-map.html>.
- [26] "Chargemap - charging stations for electric cars," [Online]. Available: <https://chargemap.com/>.
- [27] Y. Bai and D. Wang, "Fundamentals of Fuzzy Logic Control-Fuzzy Sets, Fuzzy Rules and Defuzzifications," in *Advanced Fuzzy Logic Technologies in Industrial Applications*, Springer, 2006, pp. 17-36.

- [28] "Distance Matrix API | Google Developers," [Online]. Available: <https://developers.google.com/maps/documentation/distance-matrix/start>.
- [29] F. Lambert, "Tesla is about to bring online its biggest Supercharger stations in the US – first look at new lounge," 2017. [Online]. Available: <https://electrek.co/2017/11/15/tesla-online-biggest-supercharger-stations-us-first-look-new-lounge/>.
- [30] "Tesla Gigafactory | Tesla," 2018. [Online]. Available: <https://www.tesla.com/gigafactory>.
- [31] D. Howell, S. Boyd, B. Cunningham, S. Gillard, L. Slezak, S. Ahmed, I. Bloom, A. Burnham, K. Hardy, A. N. Jansen, P. A. Nelson, D. C. Robertson, T. Stephens, R. Vijayagopal, R. B. Carlson, F. Dias, E. J. Dufek, C. J. Michelbacher, M. Mohanpurkar, D. Scoffield, M. Shirk, T. Tanim, M. Keyser, C. Kreuzer, O. Li, A. Markel, A. Meintz, A. Pesaran, S. Santhanagopalan, K. Smith, E. Wood and J. Zhang, "Enabling Fast Charging: A Technology Gap Assessment," 2017.
- [32] J. Tan and L. Wang, "Real-time charging navigation of electric vehicles to fast charging stations: A hierarchical game approach," *IEEE Transactions on Smart Grid*, vol. 8, no. 2, pp. 846-856, 2017.
- [33] H. Yang, S. Yang, Y. Xu, E. Cao, M. Lai and Z. Dong, "Electric vehicle route optimization considering time-of-use electricity price by learnable partheno-genetic algorithm," *IEEE Transactions on Smart Grid*, vol. 6, no. 2, pp. 657-666, 2015.
- [34] J. Barco, A. Guerra, L. Muñoz and N. Quijano, "Optimal Routing and Scheduling of Charge for Electric Vehicles: A Case Study," vol. 2017, 2017.
- [35] I. S. Bayram, G. Michailidis, M. Devetsikiotis and F. Granelli, "Electric power allocation in a network of fast charging stations," *IEEE Journal on Selected Areas in Communications*, vol. 31, no. 7, pp. 1235-1246, 2013.
- [36] M. Amini and O. Karabasoglu, "Optimal Operation of Interdependent Power Systems and Electrified Transportation Networks," *Energies*, vol. 11, no. 2, 2018.

- [37] M. M. De Weerd, E. H. Gerding, S. Stein, V. Robu and N. R. Jennings, "Intention-aware routing to minimize delays at electric vehicle charging stations," in *Proceedings of the Twenty-Third international joint conference on Artificial Intelligence*, 2013.
- [38] M. Alizadeh, H. T. Wai, A. Scaglione, A. Goldsmith, Y. Y. Fan and T. Javidi, "Optimized path planning for electric vehicle routing and charging," in *2014 52nd Annual Allerton Conference on Communication, Control, and Computing, Allerton 2014*, 2014.
- [39] S. Vandael, T. Holvoet and G. Deconinck, "A decentralized approach for public fast charging of electric vehicles using delegate multi-agent systems .," in *Proceedings of the Third International Workshop on Agent Technologies for Energy Systems (ATES 2012)*, 2012.
- [40] R. A. Kordkheili, S. A. Pourmousavi, M. Savaghebi, J. M. Guerrero and M. H. Nehrir, "Assessing the potential of plug-in electric vehicles in active distribution networks," *Energies*, vol. 9, no. 1, pp. 1-17, 2016.
- [41] L. Pieltain Fernández, T. Gómez San Román, R. Cossent, C. Mateo Domingo and P. Frías, "Assessment of the impact of plug-in electric vehicles on distribution networks," *IEEE Transactions on Power Systems*, vol. 26, no. 1, pp. 206-213, 2011.
- [42] M. H. Amini, K. G. Boroojeni, C. Jian Wang, A. Nejadpak, S. S. Iyengar and O. Karabasoglu, "Effect of electric vehicle parking lots' charging demand as dispatchable loads on power systems loss," *IEEE International Conference on Electro Information Technology*, Vols. 2016-Augus, pp. 499-503, 2016.
- [43] A. Hariri, M. Esfahani and O. Mohammed, "A Cognitive Price-Based Approach For Real-Time Management Of En-Route Electric Vehicles," in *Proceedings of the IEEE ITEC 2018*, Long Beach, 2018.
- [44] "Supercharging | Tesla," 2018. [Online]. Available: <https://www.tesla.com/support/supercharging>.
- [45] "Wireshark," [Online]. Available: <https://www.wireshark.org/>.

- [46] H. H. Eldeeb, S. Faddel and O. A. Mohammed, "Multi-Objective Optimization Technique for the Operation of Grid tied PV Powered EV Charging Station," *Electric Power Systems Research*, vol. 164, pp. 201-211, 11 2018.
- [47] "Ancillary Services Definitions and Capability Study Prepared for the," Hawai'i, 2012.
- [48] K. Bhattacharya and J. Zhong, "Reactive power as an ancillary service," *IEEE Transactions on Power Systems*, vol. 16, no. 2, pp. 294-300, 2001.
- [49] G. Fitzgerald, J. Mandel, J. Morris and H. Touati, "The Economics of Battery Energy Storage: how multi-use, customer-sted batteries deliver the most services and value to customers and the grid," Boulder, 2015.
- [50] M. Esfahani and G. Yousefi, "Real Time Congestion Management in Power Systems Considering Quasi-Dynamic Thermal Rating and Congestion Clearing Time," *IEEE Transactions on Industrial Informatics*, vol. 12, no. 2, pp. 745-754, 2016.
- [51] M. Esfahani, A. Sheikh and O. Mohammed, "Adaptive real-time congestion management in smart power systems using a real-time hybrid optimization algorithm," *Electric Power Systems Research*, vol. 150, pp. 118-128, 2017.
- [52] A. Bosovic, M. Music and S. Sadovic, "Analysis of the impacts of plug-in electric vehicle charging on the part of a real medium voltage distribution network," in *IEEE PES Innovative Smart Grid Technologies*, Istanbul, 2014.
- [53] M. H. Amini, K. G. Boroojeni, C. Jian Wang, A. Nejadpak, S. S. Iyengar and O. Karabasoglu, "Effect of electric vehicle parking lots' charging demand as dispatchable loads on power systems loss," in *IEEE International Conference on Electro Information Technology*, 2016.
- [54] L. Pieltain Fernández, T. Gómez San Román, R. Cossent, C. Mateo Domingo and P. Frías, "Assessment of the impact of plug-in electric vehicles on distribution networks," *IEEE Transactions on Power Systems*, vol. 26, no. 1, pp. 206-213, 2011.

- [55] S. Faddel, A. Elsayed and O. Mohammed, "Bi-layer multi-objective optimal allocation and sizing of electric vehicle parking garage," *IEEE Transactions on Industry Applications*, vol. 54, no. 3, pp. 1992-2001, 2018.
- [56] Y. Liu, Y. Xiang, Y. Tan, B. Wang, J. Liu and Z. Yang, "Optimal Allocation Model for EV Charging Stations Coordinating Investor and User Benefits," *IEEE Access*, vol. 6, pp. 36039-36049, 2018.
- [57] A. S. Awad, M. F. Shaaban, T. H. El-Fouly, E. F. El-Saadany and M. M. Salama, "Optimal Resource Allocation and Charging Prices for Benefit Maximization in Smart PEV-Parking Lots," *IEEE Transactions on Sustainable Energy*, vol. 8, no. 3, pp. 906-915, 2017.
- [58] I. S. Bayram, G. Michailidis, M. Devetsikiotis and F. Granelli, "Electric power allocation in a network of fast charging stations," *IEEE Journal on Selected Areas in Communications*, vol. 31, no. 7, pp. 1235-1246, 2013.
- [59] M. Aziz, T. Oda, T. Mitani, Y. Watanabe and T. Kashiwagi, "Utilization of electric vehicles and their used batteries for peak-load shifting," *Energies*, vol. 8, no. 5, pp. 3720-3738, 2015.
- [60] C. Cao, L. Wang and B. Chen, "Mitigation of the impact of high plug-in electric vehicle penetration on residential distribution grid using smart charging strategies," *Energies*, vol. 9, no. 12, p. 1024, 2016.
- [61] A. Mohamed, V. Salehi, T. Ma and O. Mohammed, "Real-time energy management algorithm for plug-in hybrid electric vehicle charging parks involving sustainable energy," *IEEE Transactions on Sustainable Energy*, vol. 5, no. 2, pp. 577-586, 2014.
- [62] R. A. Kordkheili, S. A. Pourmousavi, M. Savaghebi, J. M. Guerrero and M. H. Nehrir, "Assessing the potential of plug-in electric vehicles in active distribution networks," *Energies*, vol. 9, no. 1, p. 34, 2016.
- [63] M. Amini and O. Karabasoglu, "Optimal Operation of Interdependent Power Systems and Electrified Transportation Networks," *Energies*, vol. 11, no. 2, 2018.

- [64] H. Yang, S. Yang, Y. Xu, E. Cao, M. Lai and Z. Dong, "Electric vehicle route optimization considering time-of-use electricity price by learnable partheno-genetic algorithm," *IEEE Transactions on Smart Grid*, vol. 6, no. 2, pp. 657-666, 2015.
- [65] "Tesla unveils its largest Supercharger station in the US — and it kind of looks like a truck stop," 2018. [Online]. Available: <https://www.theverge.com/2017/11/16/16665504/tesla-supercharger-largest-us-kettlemen-truck>.
- [66] M. Harris, "Tesla Launches an Electric Semi Truck—and a New Sports Car," 2017. [Online]. Available: <https://spectrum.ieee.org/cars-that-think/transportation/advanced-cars/tesla-launches-an-electric-semi-truckand-a-new-sports-car..>
- [67] E. Gonzalez-Romera, F. Barrero-Gonzalez, E. Romero-Cadaval and M. I. Milanés-Montero, "Overview of plug-in electric vehicles as providers of ancillary services," in *2015 9th International Conference on Compatibility and Power Electronics (CPE)*, 2015.
- [68] J. Kennedy and R. Eberhart, "Particle Swarm Optimization," in *IEEE International Conference on Neural Networks*, Perth, 1995.
- [69] "First look at Tesla's new kind of Supercharger station with design refresh," 2017. [Online]. Available: <https://electrek.co/2017/09/11/first-look-tesla-new-supercharger-station/>.
- [70] J. Frayer, S. Keane and J. Ng, "Estimating the Value of Lost Load," Boston, 2013.
- [71] V. Salehi, A. Mohamed, A. Mazloomzadeh and O. A. Mohammed, "Laboratory-based smart power system, part I: Design and system development," *IEEE Transactions on Smart Grid*, vol. 3, no. 3, pp. 1394-1404, 2012.
- [72] V. Salehi, A. Mohamed, A. Mazloomzadeh and O. A. Mohammed, "Laboratory-based smart power system, part II: Control, monitoring, and protection," *IEEE Transactions on Smart Grid*, vol. 3, no. 3, pp. 1405-1417, 2012.

- [73] "The two sides of EV charging network operators," 2018. [Online]. Available: <https://www.virta.global/news/the-two-sides-of-ev-charging-network-operators>.
- [74] "EV Charging Infrastructure | ABB," 2018. [Online]. Available: <https://new.abb.com/ev-charging/>.
- [75] "Automotive Solutions • WiTricity," 2018. [Online]. Available: <http://witricity.com/products/automotive/>.
- [76] "EV Charge Network approved vendors," 2018. [Online]. Available: https://www.pge.com/en_US/business/solar-and-vehicles/your-options/clean-vehicles/charging-stations/program-participants/approved-program-vendors.page.
- [77] "PlugShare - EV Charging Station Map - Find a place to charge your car!," 2018. [Online]. Available: <https://www.plugshare.com/>.
- [78] "Plugsurfing - Charge your EV and find Charging Stations," 2018. [Online]. Available: <https://www.plugsurfing.com/en/>.
- [79] "Charging points and electric vehicles UK 2018 - Zap Map," 2018. [Online]. Available: <https://www.zap-map.com/>.
- [80] "Home - Open Charge Alliance," 2018. [Online]. Available: <https://www.openchargealliance.org/>.
- [81] "Snapshot Frequently Asked Questions | Progressive," 2018. [Online]. Available: <https://www.progressive.com/auto/discounts/snapshot/snapshot-common-questions/>.
- [82] "COP23: tackling climate change and the future of urban mobility," 2017. [Online]. Available: <http://www.uitp.org/COP23-tackling-climate-change-and-future-urban-mobility>. [Accessed 29 03 2018].

- [83] H. F. Habib, A. O. Hariri, A. Elsayed and O. A. Mohammed, "Deployment of electric vehicles in an adaptive protection technique for riding through cyber attack threats in microgrids," in *Conference Proceedings - 2017 17th IEEE International Conference on Environment and Electrical Engineering and 2017 1st IEEE Industrial and Commercial Power Systems Europe, IEEEIC / I and CPS Europe 2017*, 2017.
- [84] Z. Chen, J. Xu, J. Tang, K. Kwiat, C. Kamhoua and C. Wang, "GPU-accelerated High-throughput Online Stream Data Processing," *IEEE Transactions on Big Data*, vol. 5, no. 2, pp. 191-202, 2016.
- [85] "The History of the Modern Graphics Processor - TechSpot," [Online]. Available: <https://www.techspot.com/article/650-history-of-the-gpu/>. [Accessed 21 05 2018].
- [86] M. A. Rahman and R. C. Muniyandi, "Review of GPU implementation to process of RNA sequence on cancer," *Informatics in Medicine Unlocked*, vol. 10, pp. 17-26, 2018.
- [87] "GPU-Accelerated Applications," Nvidia.
- [88] A. Al-Ali, I. A. Zualkernan, M. Rashid, R. Gupta and M. Alikarar, "A smart home energy management system using IoT and big data analytics approach," *IEEE Transactions on Consumer Electronics*, vol. 63, no. 4, 2017.
- [89] "RTI Connex DDS Secure | Datasheet," Sunnyvale, 2018.
- [90] P. Szoldra, "This is everything Edward Snowden revealed in one year of unprecedented top-secret leaks | Business Insider India," 2016. [Online]. Available: <https://www.businessinsider.in/This-is-everything-Edward-Snowden-revealed-in-one-year-of-unprecedented-top-secret-leaks/articleshow/54367926.cms>.
- [91] B. Schneier, "Attacking Tor: how the NSA targets users' online anonymity | US news | The Guardian," 2013. [Online]. Available: <https://www.theguardian.com/world/2013/oct/04/tor-attacks-nsa-users-online-anonymity>.

- [92] A. Peterson, "Look at this amazing drawing the NSA made for its hacking system - The Washington Post," 2013. [Online]. Available: https://www.washingtonpost.com/news/the-switch/wp/2013/12/30/look-at-this-amazing-drawing-the-nsa-made-for-its-hacking-system/?noredirect=on&utm_term=.0fd84007d10a.
- [93] P. Bump, "How to Keep the NSA from Getting Between You and Your Googling - The Atlantic," 2013. [Online]. Available: <https://www.theatlantic.com/politics/archive/2013/09/how-keep-nsa-getting-between-you-and-your-googling/311108/>.
- [94] B. Solomon, "Hacked Cameras Were Behind Friday's Massive Web Outage," 2016. [Online]. Available: <https://www.forbes.com/sites/briansolomon/2016/10/21/hacked-cameras-cyber-attack-hacking-ddos-dyn-twitter-netflix/#581d24474fb7>.
- [95] N. Woolf, "DDoS attack that disrupted internet was largest of its kind in history, experts say | Technology | The Guardian," 2016. [Online]. Available: <https://www.theguardian.com/technology/2016/oct/26/ddos-attack-dyn-mirai-botnet>.
- [96] P. Nohe, "The Largest DDoS Attack in history just happened," 2018. [Online]. Available: <https://www.thesslstore.com/blog/largest-ddos-attack-in-history/>.
- [97] A. Bennett, "20 Ways to Prevent a Deadly DDoS Attack," 2017. [Online]. Available: <https://techspective.net/2017/05/11/20-ways-prevent-deadly-ddos-attack/>.
- [98] NIST, "Framework for Improving Critical Infrastructure Cybersecurity," 2014.
- [99] C. Mi, S. Bhattacharya and M. K. Mallela, "Study Methods of Wireless Power Transfer Technology in Electric Vehicle Charging," 2014. [Online]. Available: <https://tec.ieee.org/newsletter/july-august-2014/study-methods-of-wireless-power-transfer-technology-in-electric-vehicle-charging>.

- [100] S.-H. Lee and R. D. Lorenz, "Development and Validation of Model for 95%-Efficiency 220-W Wireless Power Transfer Over a 30-cm Air Gap," *IEEE Transactions on Industry Applications*, vol. 47, no. 6, pp. 2495-2504, 11 2011.
- [101] H. Fujibe and K. Kesamaru, "Magnetic field analysis of wireless power transfer via magnetic resonant coupling for electric vehicle," in *2013 International Conference on Electrical Machines and Systems (ICEMS)*, 2013.
- [102] K. Y. Kim, *Wireless Power Transfer - Principles and Engineering Explorations*, K. Y. Kim, Ed., InTech, 2012.
- [103] U. S. Inan, A. S. Inan and R. K. Said, *Engineering electromagnetics and waves*, 2nd ed., Pearson, 2015, p. 984.
- [104] "Wireless Power Consortium," [Online]. Available: <https://www.wirelesspowerconsortium.com/>.
- [105] Chen Deqing, Wang Lifang, Liao Chenling and Guo Yanjie, "The power loss analysis for resonant wireless power transfer," in *2014 IEEE Conference and Expo Transportation Electrification Asia-Pacific (ITEC Asia-Pacific)*, 2014.
- [106] A. O. Hariri, T. Youssef, A. Elsayed and O. Mohammed, "A Computational Approach for a Wireless Power Transfer Link Design Optimization Considering Electromagnetic Compatibility," *IEEE Transactions on Magnetics*, vol. 52, no. 3, pp. 1-4, 3 2016.
- [107] "ICNIRP Guidelines | Guidelines for limiting exposure to time-varying electric and magnetic fields (1 Hz TO 100 kHz)," *Health Physics*, vol. 99, no. 6, pp. 818-836, 2010.
- [108] "IEEE C95.1-2005 - IEEE Standard for Safety Levels with Respect to Human Exposure to Radio Frequency Electromagnetic Fields, 3 kHz to 300 GHz," 2005. [Online]. Available: https://standards.ieee.org/standard/C95_1-2005.html.

- [109] Hongseok Kim, Chiuk Song, Jonghoon Kim, D. H. Jung, Eunseok Song, Sukjin Kim and Jiseong Kim, "Design of magnetic shielding for reduction of magnetic near field from wireless power transfer system for electric vehicle," in *2014 International Symposium on Electromagnetic Compatibility*, 2014.
- [110] G. Haddadian, M. Khodayar and M. Shahidehpour, "Accelerating the Global Adoption of Electric Vehicles: Barriers and Drivers," *The Electricity Journal*, vol. 28, no. 10, pp. 53-68, 1 12 2015.
- [111] M. W. Earley, J. S. Sargent, C. D. Coache and R. J. Roux, "National electrical code handbook," 2011.
- [112] T. Dragicevic, S. Sucic, J. C. Vasquez and J. M. Guerrero, "Flywheel-Based Distributed Bus Signalling Strategy for the Public Fast Charging Station," *IEEE Transactions on Smart Grid*, vol. 5, no. 6, pp. 2825-2835, 11 2014.
- [113] M. Yilmaz and P. T. Krein, "Review of Battery Charger Topologies, Charging Power Levels, and Infrastructure for Plug-In Electric and Hybrid Vehicles," *IEEE Transactions on Power Electronics*, vol. 28, no. 5, pp. 2151-2169, 5 2013.
- [114] S. Cruciani, T. Campi, F. Maradei and M. Feliziani, "Numerical simulation of Wireless Power Transfer system to recharge the battery of an implanted cardiac pacemaker," in *2014 International Symposium on Electromagnetic Compatibility*, 2014.
- [115] W.-G. Kang, Z. Alexander, H.-Y. Jjun, Y.-H. Park and J.-K. Pack, "Exposure assessment for a wireless multi-phone charger," in *2014 International Symposium on Electromagnetic Compatibility, Tokyo*, Tokyo, 2014.
- [116] Y. Kitano, H. Omori, T. Morizane, N. Kimura and M. Nakaoka, "A new shielding method for magnetic fields of a wireless EV charger with regard to human exposure by eddy current and magnetic path," in *2014 International Power Electronics and Application Conference and Exposition*, Shanghai, 2014.
- [117] "Infolytica Live Docs," 2015. [Online].

- [118] M. Budhia, G. A. Covic and J. T. Boys, "Design and Optimization of Circular Magnetic Structures for Lumped Inductive Power Transfer Systems," *IEEE Transactions on Power Electronics*, vol. 26, no. 11, pp. 3096-3108, 11 2011.
- [119] O. Mohammed, D. Park, R. Merchant, T. Dinh, C. Tong, A. Azeem, J. Farah and C. Drake, "Practical experiences with an adaptive neural network short-term load forecasting system," *IEEE Transactions on Power Systems*, vol. 10, no. 1, pp. 254-265, 1995.
- [120] F. Y. Lin, C. Carretero, G. A. Covic and J. T. Boys, "A Reduced Order Model to Determine the Coupling Factor Between Magnetic Pads Used in Wireless Power Transfer," *IEEE Transactions on Transportation Electrification*, vol. 3, no. 2, pp. 321-331, 6 2017.
- [121] J. Acero, R. Alonso, L. Barragan and J. Burdio, "Modeling of Planar Spiral Inductors Between Two Multilayer Media for Induction Heating Applications," *IEEE Transactions on Magnetics*, vol. 42, no. 11, pp. 3719-3729, 11 2006.
- [122] J. Acero, C. Carretero, I. Lope, R. Alonso, O. Lucia and J. M. Burdio, "Analysis of the Mutual Inductance of Planar-Lumped Inductive Power Transfer Systems," *IEEE Transactions on Industrial Electronics*, vol. 60, no. 1, pp. 410-420, 1 2013.
- [123] C. Carretero, R. Alonso, J. Acero, J. M. Burdío and C. Carretero, "COUPLING IMPEDANCE BETWEEN PLANAR COILS INSIDE A LAYERED MEDIA," 2011.
- [124] A. Hariri, M. El Hariri, A. El Sayyed and O. A. Mohammed, "An Iterative Design Approach for Shielding of WPT Systems in Electric Vehicle Charging Applications," in *2016 IEEE Vehicle Power and Propulsion Conference (VPPC)*, 2016.
- [125] S. A. Birrell, D. Wilson, C. P. Yang, G. Dhadyalla and P. Jennings, "How driver behaviour and parking alignment affects inductive charging systems for electric vehicles," *Transportation Research Part C: Emerging Technologies*, vol. 58, pp. 721-731, 1 9 2015.

- [126] S. Conti, R. Nicolosi, S. A. Rizzo and H. H. Zeineldin, "Optimal Dispatching of Distributed Generators and Storage Systems for MV Islanded Microgrids," *IEEE Transactions on Power Delivery*, vol. 27, no. 3, pp. 1243-1251, 7 2012.
- [127] W. Jakob, C. Blume, W. Jakob and C. Blume, "Pareto Optimization or Cascaded Weighted Sum: A Comparison of Concepts," *Algorithms*, vol. 7, no. 1, pp. 166-185, 21 3 2014.
- [128] R. Baños, F. Manzano-Agugliaro, F. Montoya, C. Gil, A. Alcayde and J. Gómez, "Optimization methods applied to renewable and sustainable energy: A review," *Renewable and Sustainable Energy Reviews*, vol. 15, no. 4, pp. 1753-1766, 1 5 2011.
- [129] K. Deb, A. Pratap, S. Agarwal and T. Meyarivan, "A fast and elitist multiobjective genetic algorithm: NSGA-II," *IEEE Transactions on Evolutionary Computation*, vol. 6, no. 2, pp. 182-197, 4 2002.
- [130] M. Rojas, E. Sadeghvaziri and X. Jin, "Comprehensive Review of Travel Behavior and Mobility Pattern Studies That Used Mobile Phone Data," *Transportation Research Record: Journal of the Transportation Research Board*, no. 2563, pp. 71-79, 2016.
- [131] E. Sadeghvaziri, M. B. Rojas and X. Jin, "Exploring the Potential of Mobile Phone Data in Travel Pattern Analysis," *Transportation Research Record: Journal of the Transportation Research Board*, no. 2594, pp. 27-34, 2016.
- [132] O. Yousefi, G. Mahmoudian, M. Amanifar and A. Maghami, "A new approach for pricing of primary frequency control in deregulated environments," in *2011 19th Iranian Conference on Electrical Engineering*, Tehran, 2011.
- [133] H. Yang, S. Yang, Y. Xu, E. Cao, M. Lai and Z. Dong, "Electric vehicle route optimization considering time-of-use electricity price by learnable partheno-genetic algorithm," *IEEE Transactions on Smart Grid*, vol. 6, no. 2, pp. 657-666, 2015.

- [134] A. Wood, B. Wollenberg and G. Sheble, "Power System Security," in *Power Generation Operation and Control*, Third ed., Hoboken, John Wiley & Sons Inc., 2014, p. 296–300.
- [135] "Supercharger | Tesla," 2018. [Online]. Available: <https://www.tesla.com/supercharger>.
- [136] "Porsche Mission E - Porsche USA," 2018. [Online]. Available: <https://www.porsche.com/usa/aboutporsche/christophorusmagazine/archive/374/articleoverview/article01/>.
- [137] A. Hariri, M. Esfahani and O. Mohammed, "A Cognitive Price-Based Approach For Real-Time Management Of En-Route Electric Vehicles," in *Proceedings of the IEEE ITEC 2018*, Long Beach, 2018.
- [138] A. Hariri, M. El Hariri, T. Youssef and O. Mohammed, "Bilateral Decision Support Platform for Public Charging of Connected Electric Vehicles," *IEEE Transactions on Vehicular Technology*, 2018.
- [139] "First look at Tesla's new kind of Supercharger station with design refresh," 2017. [Online]. Available: <https://electrek.co/2017/09/11/first-look-tesla-new-supercharger-station/>.
- [140] "Porsche Mission E - Porsche USA," 2018. [Online]. Available: <https://www.porsche.com/usa/aboutporsche/christophorusmagazine/archive/374/articleoverview/article01/>.
- [141] "Supercharger | Tesla," 2018. [Online]. Available: <https://www.tesla.com/supercharger>.
- [142] O. Yousefi, G. Mahmoudian, M. Amanifar and A. Maghami, "A new approach for pricing of primary frequency control in deregulated environments," in *2011 19th Iranian Conference on Electrical Engineering*, Tehran, 2011.

- [143] L. Igualada, C. Corchero, M. Cruz-Zambrano and F. J. Heredia, "Optimal energy management for a residential microgrid including a vehicle-to-grid system," *IEEE Transactions on Smart Grid*, vol. 5, no. 4, pp. 2163-2172, 2014.
- [144] B. Potter and B. Fleck, 802.11 Security, 1st ed., Sebastopol: O'Reilly Media, Inc., 2002.
- [145] "What is a man-in-the-middle attack?," 2018. [Online]. Available: <https://us.norton.com/internetsecurity-wifi-what-is-a-man-in-the-middle-attack.html>.

VITA

ABLA HARIRI

1991	Born Saida, Lebanon
2009-2012	B.Sc., Electrical Engineering Hariri Canadian University, Mechref, Lebanon
2012-2014	M.Sc., Electrical Engineering Rafik Hariri University, Mechref, Lebanon
2014-2018	Graduate Assistant Florida International University, Miami, FL, USA
2018	Dissertation Year Fellowship Florida International University, Miami, FL, USA

SELECTED PUBLICATIONS AND PRESENTATIONS

Format: Journal [J-*n*], Conference [C-*n*]

- [J-1] Abla Hariri, Mohamed El Hariri, Tarek Youssef, and O. A. Mohammed, "A Bilateral Decision Support Platform for Public Charging of Connected Electric Vehicles," IEEE Transactions on Vehicular Technology, October 2018.
- [J-2] A. O. Hariri, T. Youssef, A. Elsayed and O. Mohammed, "A Computational Approach for a Wireless Power Transfer Link Design Optimization Considering Electromagnetic Compatibility," in IEEE Transactions on Magnetics, vol. 52, no. 3, March 2016.
- [J-3] Abla Hariri, A. Elsayed and O. A. Mohammed, "An Integrated Characterization Model and Multiobjective Optimization for the Design of an EV Charger's Circular Wireless Power Transfer Pads," in IEEE Transactions on Magnetics, vol. 53, no. 6, June 2017.
- [J-4] Mohammad Mahmoudian Esfahani, Abla Hariri, Osama A. Mohammed, "A Multiagent-based Game-Theoretic and Optimization Approach for Market Operation of Multi-Microgrid Systems," in IEEE Transactions on Industrial Informatics, February 2018.
- [J-5] Abla Hariri, Mohammad Mahmoudian Esfahani, and O. A. Mohammed, "Collective Distribution of Mobile Loads for Optimal and Secure Operation of Power Systems", submitted to IEEE Transactions on Industrial Informatics, September 2018.

- [C-1] Abla O. Hariri, M. Mahmoudian Esfahani, and Osama Mohammed, "A Cognitive Price-Based Approach for Real-time Management of En-route Electric Vehicles," 2018 IEEE (ITEC), Long Beach, CA, 2018.
- [C-2] Abla O. Hariri, Mohamad El Hariri, Tarek Youssef, and Osama Mohammed, "A Decentralized Multi-Agent System for Management of En Route Electric Vehicles," IEEE SoutheastCon 2018, Tampa, FL, 2018.
- [C-3] M. Mahmoudian Esfahani, Abla Hariri, and Osama Mohammed, "Game-theory-based Real-Time Inter-Microgrid Market Design Using Hierarchical Optimization Algorithm," IEEE PES General Meeting, Portland, OR, 2018.
- [C-4] A. O. Hariri, M. El Hariri, A. El Sayyed and O. A. Mohammed, "An Iterative Design Approach for Shielding of WPT Systems in Electric Vehicle Charging Applications," 2016 IEEE VPPC, Hangzhou, China, 2016.
- [C-5] A. Hariri, A. ElSayed and O. A. Mohammad, "An integrated characterization model for the magnetic design of an EV charger's circular wireless power transfer pads," 2016 IEEE CEFC, Miami, FL, 2016.
- [C-6] A. O. Hariri, A. Berzoy, A. A. S. Mohamed and O. A. Mohammed, "Performance evaluation of a wireless power transfer system using coupled 3D finite element-circuit model," 2015 IEEE WPTC, Boulder, CO, 2015.
- [C-7] A. Hariri, A. ElSayed, T. Youssef, and O. A. Mohammed, "Design Optimization of a Wireless Power Transfer Link Considering Electromagnetic Compatibility", IEEE COMPUMAG, Montreal, Canada, 2015.
- [C-8] H. H. Eldeeb, A. O. Hariri, C. R. Lashway and O. A. Mohammed, "Optimal sizing of inverters and energy storage for power oscillation limiting in grid connected large scale Electric Vehicle park with renewable energy," 2017 IEEE ITEC, Chicago, IL, 2017.
- [C-9] H. H. Eldeeb, A. O. Hariri and O. A. Mohammed, "Coordinated control for the integration of a large scale electric vehicle park with PV into the MV grid," 2017 IEEE IEEEIIC / I&CPS Europe, Milan, 2017.
- [C-10] H. F. Habib, A. O. Hariri, A. ElSayed and O. A. Mohammed, "Deployment of electric vehicles in an adaptive protection technique for riding through cyber attack threats in microgrids," 2017 IEEE International Conference on Environment and Electrical Engineering and 2017 IEEE IEEEIIC / I&CPS Europe, Milan, 2017.